THE UNIVERSITY *of* EDINBURGH

Characterisation of time-dependent mechanical behaviour of trabecular bone and its constituents

Shuqiao Xie

THE UNIVERSITY *of* EDINBURGH

Doctor of Philosophy

The University of Edinburgh

2018

Declaration

I declare that the thesis has been composed by myself and that the work has not be submitted for any other degree or professional qualification. I confirm that the work submitted is my own, except where work which has formed part of jointly-authored publications has been included. My contribution and those of the other authors to this work have been explicitly indicated below. I confirm that appropriate credit has been given within this thesis where reference has been made to the work of others. I am an author of the publications which are included in the appendix.

The work presented in Chapter 5 was previously published in *Journal of Biomechanics and Modeling in Mechanobiology* as 'Linear viscoelasticity - bone volume fraction relationships of bovine trabecular bone' by Krishnagoud Manda, **Shuqiao Xie**, Robert J. Wallace, Francesc Levrero-Florencio, Pankaj Pankaj (supervisor). This study was conceived by all of the authors. I carried out the entire mechanic tests and conducted part of data analysis. Any contribution from colleagues, such as diagrams and data, are explicitly referenced in the text.

The work presented in Chapter 5 was previously published in *Journal of Biomechanics and Modeling in Mechanobiology* as 'Nonlinear viscoelastic characterization of bovine trabecular bone' by Krishnagoud Manda, Robert J Wallace, **Shuqiao Xie**, Francesc Levrero-Florencio, Pankaj Pankaj (supervisor).

This study was conceived by all of the authors. I carried out the entire mechanic tests and conducted part of data analysis. Any contribution from colleagues, such as diagrams and data, are explicitly referenced in the text.

Shuqiao Xie

2018

Lay summary

The skeletal system is important to the body both biomechanically and metabolically. It is made up of individual bones and the connective tissue that joins them. It is the main loading bearing part of the body and protects major organs. The focus of this study is trabecular bone, which is typically found at the ends of long bones and within the interior of vetebrae. Trabecular bone has an open, honeycomb structure.

The trabecular bone's deformation is time-dependent rather than instantaneous when it is subjected to a load, this implies that it undergoes creep, i.e. its deformation increases with time, even when the load is constant. This study conducted multiple-load-creep-unload-recovery experiments on trabecular bone and the results show that the time-dependent response is related to porosity. Using the experimental data, computational models were developed that can be used to account for the nonlinear response of bone with load level and its irrecoverable deformation on load removal. These can be applied in the modelling of mechanical behaviour of bone and bone-implant systems.

Trabecular bone is a composite material which consists of a mineral phase, organic phase and water assembly into a complex, hierarchical structure. This study examined the contribution of the individual constituents, mineral and organic phases, to its mechanical behaviour. The organic phase of bone stiffens with increased load levels in tension, while experienced softening in compression. It presents time-dependent response which is nonlinearly related to load

levels. The strength and stiffness of the mineral phase increases with decreasing porosity of bone.

The developed time-dependent constitutive model was implemented in a bone-screw finite element model. This thesis shows that clinically observed loosening of implants is not simply caused by high strains but accentuated by deformations at the bone-screw interface. The interface deformations increase with increasing number of cycles of loading that result from normal physiological loading. The results also show that higher loading frequency and higher porosity increase the risk of implant loosening.

Abstract

Trabecular bone is a porous composite material which consists of a mineral phase (mainly hydroxyapatite), organic phase (mostly type I collagen) and water assembled into a complex, hierarchical structure. In biomechanical modelling, its mechanical response to loads is generally assumed to be instantaneous, i.e. it is treated as a time-independent material. It is, however, recognised that the response of trabecular bone to loads is time-dependent. Study of this time-dependent behaviour is important in several contexts such as: to understand energy dissipation ability of bone; to understand the age-related non-traumatic fractures; to predict implant loosening due to cyclic loading; to understand progressive vertebral deformity; and for pre-clinical evaluation of total joint replacement.

To investigate time-dependent behaviour, bovine trabecular bone samples were subjected to compressive loading, creep, unloading and recovery at multiple load levels (corresponding to apparent strain of 2,000-25,000 $\mu\varepsilon$). The results show that: the time-dependent behaviour of trabecular bone comprises of both recoverable and irrecoverable strains; the strain response is nonlinearly related to applied load levels; and the response is associated with bone volume fraction. It was found that bone with low porosity demonstrates elastic stiffening followed by elastic softening, while elastic softening is demonstrated by porous bone at relatively low loads. Linear, nonlinear viscoelastic and nonlinear viscoelastic-viscoplastic constitutive models were developed to predict trabecular bone's time-dependent behaviour. Nonlinear viscoelastic constitu-

tive model was found to predict the recovery behaviour well, while nonlinear viscoelastic-viscoplastic model predicts the full creep-recovery behaviour reasonably well. Depending on the requirements all these models can be used to incorporate time-dependent behaviour in finite element models.

To evaluate the contribution of the key constituents of trabecular bone and its microstructure, tests were conducted on demineralised and deproteinised samples. Reversed cyclic loading experiments (tension to compression) were conducted on demineralised trabecular bone samples. It was found that demineralised bone exhibits asymmetric mechanical response - elastic stiffening in tension and softening in compression. This tension to compression transition was found to be smooth. Tensile multiple-load-creep-unload-recovery experiments on demineralised trabecular samples show irrecoverable strain (or residual strain) even at the low stress levels. Demineralised trabecular bone samples demonstrate elastic stiffening with increasing load levels in tension, and their time-dependent behaviour is nonlinear with respect to applied loads . Nonlinear viscoelastic constitutive model was developed which can predict its recovery behaviour well. Experiments on deproteinised samples showed that their modulus and strength are reasonably well related to bone volume fraction.

The study considers an application of time-dependent behaviour of trabecular bone. Time-dependent properties are assigned to trabecular bone in a bone-screw system, in which the screw is subjected to cyclic loading. It is found that separation between bone and the screw at the interface can increase with increasing number of cycles which can accentuate loosening. The relative larger deformation occurs when this system to be loaded at the higher loading frequency. The deformation at the bone-screw interface is related to trabecular bone's bone volume fraction; screws in a more porous bone are at a higher risk of loosening.

I dedicate this thesis to my beloved family.

Acknowledgements

There are many people who have helped me during the PhD. There is not enough space, nor time, to acknowledge everyone to the extend they deserve. Besides the individuals mentioned below, I hope people understand the brevity of this part.

Firstly, I would like to express my sincere gratitude to my supervisor Prof. Pankaj Pankaj for the continuous support of my Ph.D study and related research, for his patience, motivation, and immense knowledge. His guidance helped me in all the time of research and writing of this thesis. Under his guidance, I greatly appreciate the freedom was given to pursue the research in my own way. It was a great pleasure to work and discuss with him. I could not have imagined having a better advisor and mentor for my Ph.D study.

Besides my advisor, I would like to thank the rest of my thesis committee: Dr. Krishnagoud Manda and Dr. Robert J. Wallace, for their insightful comments and encouragement, but also for the hard questions which invented me to widen my research from various perspectives.

I am also appreciate of all the help from colleagues in our research group, Dr. Francesc Levrero-Florencio, Dr. Erika Sales, Dr. Noel Conlisk and Adib Hamdani, for their support and encouragement, personal and academic, over many years and for numerous conversations. I am also grateful to Dr. Natalia Harasymowicz and laboratory manager Ms Stephanie Collishaw for helping in using the medical equipment located at the Royal Infirmary of Edinburgh.

This research would not be possible without the support from Engineering

and Physical Sciences Research Council [Grant EP/K036939/1] and therefore I would like to thank EPSRC for the financial support.

Last, but certainly not least, I must express my very profound gratitude to my parents and to Baozai for providing me with unfailing support and continuous encouragement throughout my years of study and the process of researching and writing this thesis. This accomplishment would not have been possible without them. Thank you.

Contents

List of Figures

List of Tables

List of abbreviations and nomenclatures

Abbreviation

BMD bone mineral density

BV/TV bone volume fraction

DM demineralised

DOA degree of anisotropy

DP deproteinised

EDTA ethylenediaminetetraacetic acid

FE finite element

FEA finite element analysis

HA hydroxyapatite

HCl hydrochloric acid

MLCUR multiple-load-creep-unload-recovery

NaOCl sodium hypochlorite

PBS phosphate-buffered saline

SMI structure model index

Tb.N trabecular number

Tb.Sp trabecular separation

Tb.Th trabecular thickness

μ**CT** micro-computed tomography

Nomenclature

σ	stress
ε	strain
σ_f	stress at failure
ε_f	strain at failure
σ_y	yield stress
ε_y	yield strain
E	elastic modulus
W	toughness
ε_l	instantaneous loading strain
ε_{cre}	creep strain
ε_{ul}	instantaneous unloading strain
ε_{rec}	recovery strain
ε_{res}	residual strain
$\varepsilon_{cre}(t)$	time varying creep strain
$\varepsilon_{rec}(t)$	time varying recovery strain
ε_{tot}	total strain
ε_{ve}	viscoelastic strain
ε_{nve}	nonlinear viscoleastic strain
ε_{vp}	viscoplastic strain
ρ	apparent density
D_g	instantaneous compliance
D_n	transient compliance
τ_n	retardation time
λ_n	recipricol of retardation time
$\mathbf{C}_{cre}(t)$	time-varying creep compliance
$\mathbf{C}_{rec}(t)$	time-varying recovery compliance
$\dot{\varepsilon}_{cre}$	steady state creep rate
ϕ	BV/TV

“Failing to plan is planning to fail”

Alan Lakein

1 Introduction

1.1 Motivation for current research

Superficially, bones look fairly solid, but looks are deceptive. Most bones are an elaborate construction, made up of an outer shell of dense cortical bone, and enclose a core of porous trabecular bone (Gibson and Ashby, 1999). In some instances (as at joints between vertebrae or at the end of long bones) this configuration minimises the weight of bone while still providing large bearing area, a design which reduces the bearing stresses at the joint. In others (as in the vault of the skull or the iliac crest) it forms a low weight sandwich shell-like structure. In either case the presence of trabecular bone reduces the weight while still complying with its primary mechanical function (Gibson and Ashby, 1999).

Researchers have long sought to understand the mechanical behaviour of bone. Bones are the main loading bearing members in the body and protect major organs, it is important to understand how they response when subjected to loads. Most previous researches have focused on the time-independent response, for both cortical and trabecular bone in which bone deforms instantaneously after load application. The most commonly reported and employed relationship is between apparent density (ρ) or its bone volume fraction (BV/TV) of bone with its elastic modulus (E) (Helgason et al., 2008). Experimental tests and computer simulations have also shown that the yield strain of trabecular bone is largely independent of BV/TV or its ρ (Bayraktar et al., 2004; Levrero-Florencio et al., 2016). Obvious nonlinearity in the stress-strain curve has been observed (Hansen et al., 2008; Keaveny et al., 1994a,b; Kopperdahl and Keaveny, 1998; Li and Aspden, 1997; Matsuura et al., 2008).

It has been demonstrated that trabecular bone's time-dependent behaviour is qualitatively similar to that of other materials such as ceramic and rubber (Schoenfeld et al., 1974; Zilch et al., 1980). The importance of this time-dependent behaviour has been pointed by a number of investigators for: understanding the energy dissipation ability of bone (Linde and Sørensen, 1993; Wang and Nyman, 2007); understanding the cause of age-related non-traumatic fracture (Rapillard et al., 2006); predicting implant loosening due to cyclic loading (Taylor et al., 2002); understanding progressive vetebral deformity (Pollintine et al., 2009); and pre-clinical evaluation of total joint replacement (Taylor et al., 2002).

The time-dependent properties of trabecular bone have been experimentally measured using long-term creep test (Bowman et al., 1998, 1994), relaxation test (Bredbenner and Davy, 2006; Deligianni et al., 1994; Quaglini et al., 2009; Schoenfeld et al., 1974; Zilch et al., 1980) and dynamic mechanical experiments (Bowman et al., 1998, 1996; Guedes et al., 2006). The long-term creep had been investigated for bone samples in which time-varying strain due

to applied constant load is measured over time until failure (the last part is denoted as tertiary creep). Limited information can be obtained from long-term creep experiments, such as relationship between normalised stress level, steady state creep rate, time-to-failure (Bowman et al., 1998, 1994), which are difficult to implement in a constitutive model to predict the bone's biomechanical behaviour. Some later studies employed load-creep-unload-recovery experiments to examine the time-dependent behaviour of bone (Kim et al., 2012, 2011; Yamamoto et al., 2006), which is allowed to evaluate the recovery (or viscoelasticity) response of bone after creep for a designated time, and to quantify the irrecoverable strain by evaluating the differences in strain between creep (which might include irrecoverable strain) and recovery phases. Yamamoto et al. (2006) reported that trabecular bone behaves nonlinearly after conduction of creep-recovery experiment to different samples at various corresponding strain levels. To the best of author's knowledge, there have been no studies that investigate the time-dependent behaviour of bone at the multiple stress levels for a given bone specimen. Also, while there have been a number of studies that have related bone density (or BV/TV) to its time-independent elastic modulus (Morgan et al., 2003; Odgaard et al., 1997; Zysset, 2003), similar relationships between bone volume fraction and time-dependent properties remain unknown.

With increasing ageing population, which is known to cause deteriorated bone quality, understanding the mechanical response of bone to loads has assumed increased importance. Bone is a composite material which comprises of a mineral phase (mainly carbonated hydroxyapatite), organic phase (mostly type I collagen) and water assembled into a complex, hierarchical structure (Chen et al., 2011; Wang et al., 2002). Mechanically, collagen and mineral play very different roles – the elastic modulus of collagen is much lower than that of the hydroxyapatite, but the former is three orders of magnitude tougher (Ruffoni and van Lenthe, 2017); while the mineral provides the stiffness, it is

much more brittle than the collagen. Consequently the effect of the contribution of bone constituents is important to understand this composite material, for both time-independent and time-dependent properties.

Bone fracture fixations, either external or internal, require bone screw that traverses bone and allows load being transferred (MacLeod and Pankaj, 2014). There are several failure mechanisms, such as plate failure, screw breakage and screw loosening. Loosening of connective screw is a typically reported complication in implant usage. Local bone yielding at the interface, due to high stresses/ strains, can initiate loosening and result in infection and further loosening (Donaldson et al., 2012). However, the role of time-dependent behaviour on loosening has not been investigated.

1.2 Scope of the thesis

1.2.1 Untreated trabecular bone

- To investigate trabecular bone's creep and recovery behaviour through compressive multiple-load-creep-unload-recovery (MLCUR) experiment.
- To examine its nonlinear behaviour with increased stress levels, and establish if this nonlinear behaviour is related to its bone volume fraction (BV/TV).
- To develop a simple linear viscoelastic constitutive model based on BV/TV, which can be readily applied in finite element simulations.
- To develop a more complex nonlinear viscoelastic constitutive model which fits the elastic response at multiple load levels better.
- To further develop the nonlinear viscoelastic-viscoplastic constitutive model, which incorporates the irrecoverable strain response.

1.2.2 Demineralised and deproteinised trabecular bone

- To isolate bone's main constituents (mineral and type I collagen) from trabecular bone.
- To investigate both tensile and compressive behaviour of demineralised trabecular bone (mainly type I collagen) through fully-reversed cyclic experiment.
- To examine the nonlinear behaviour of demineralised trabecular bone through tensile MLCUR on demineralised samples, and their possible relationship with BV/TV.
- To develop the linear viscoelastic constitutive model for demineralised bone and further develop a nonlinear viscoelastic constitutive model.
- To investigate the mechanical properties of deproteinised trabecular bone (mineral) through monotonic loading.
- To examine the material properties (e.g. strain at failure (ε_f), stress at failure (σ_f), etc.) of deproteinised trabecular bone with its BV/TV.

1.2.3 Application of the developed models

- To implement time-dependent behaviour of trabecular bone in the referential bone-screw system in Abaqus, which is subjected to triangular cyclic loading at designated loading frequencies.
- To investigate the effect of loading frequency at bone-screw interface by assigning trabecular bone modelled with BV/TV-based linear viscoelastic material.
- To investigate the possibility of irrecoverable deformation generated at the bone-screw interface if trabecular bone is assigned nonlinear viscoelastic-viscoplastic material.

- To examine how trabecular bone's BV/TV influences its deformations at the bone-screw interface.

1.3 Structure of thesis

This thesis is divided into ten chapters. Chapters 2 and 3 review the literature on this topic and the relevant theory. Chapter 4 to 9 constitute the main research under taken in this thesis and this is summarised in Fig. 1.1. Chapter 10 discusses the conclusions and future research directions. A brief description of the content of each chapter is provided below.

Chapter 2 reviews the literature that is relevant to this topic. It focuses on the morphology, mechanical behaviour of trabecular bone and its main constituents (type I collagen and mineral), including time-independent and time-dependent properties. The current status of researches on bone-screw interface are also discussed.

Chapter 3 briefly discusses theory on time-dependent behaviour. It starts from phenomenological aspects of time-dependent behaviour to rheological models. It consists of linear viscoelastic, nonlinear viscoelastic and also viscoplastic constitutive models. The methods of parameters fitting from MLCUR experiment are discussed.

Part I Experimental Investigation and Constitutive Models Development for Trabecular Bone

Chapter 4 describes the details of the experimental protocol and conduct of compressive MLCUR tests. The nonlinear BV/TV-related viscoelastic behaviour of trabecular bone is discussed in terms of experimental observations.

Chapter 5 describes the development of time-dependent constitutive models with increasing complexity: BV/TV-based viscoelastic model from bone's creep response to the first cycle; nonlinear viscoelastic model developed from the un-

loading phase by considering all loading cycles; and the viscoplastic model is developed by taking the strain differences between the loading and unloading phases.

Chapter 6 describes the two types of experiments conducted on demineralised trabecular bone (mainly type I collagen), which are (a) fully-reversed cyclic loading from tension to compression and (b) tensile MLCUR. The nonlinear time-dependent behaviour is investigated from experimental observation and its nonlinear viscoelastic constitutive model is developed.

Chapter 7 investigates the mechanical properties of deproteinised trabecular bone (mineral) through monotonic loading. Its failure stress, failure strain, elastic modulus and toughness are discussed with respect to BV/TV. The relative modulus and compressive strength are modelled using cellular solids' constitutive equations for open-cell cellular solids as a function of relative density.

Part II Application of the Developed Models

Chapter 8 employs the developed BV/TV-based linear viscoelastic constitutive model (from Chapter 5, Sec. 5.2) for trabecular bone in am idealised two-dimensional bone-screw system. The displacement at the bone-screw interface with loading cycles and loading frequencies is investigated.

Chapter 9 employs the developed nonlinear viscoelastic-viscoplastic constitutive model (from Chapter 5, Sec. 5.3 and 5.4) for trabecular bone in an idealised three-dimensional bone-screw system. The displacement at the interface with increasing cycles, the deformation trend with BV/TV are investigated. From these conclusions with regard to screw loosening are drawn.

Chapter 10 summaries the conclusions from this study, with a special emphasis on BV/TV related time-dependent response of trabecular bone and the possible application of its time-dependent behaviour. Future work which could be performed is also outlined.

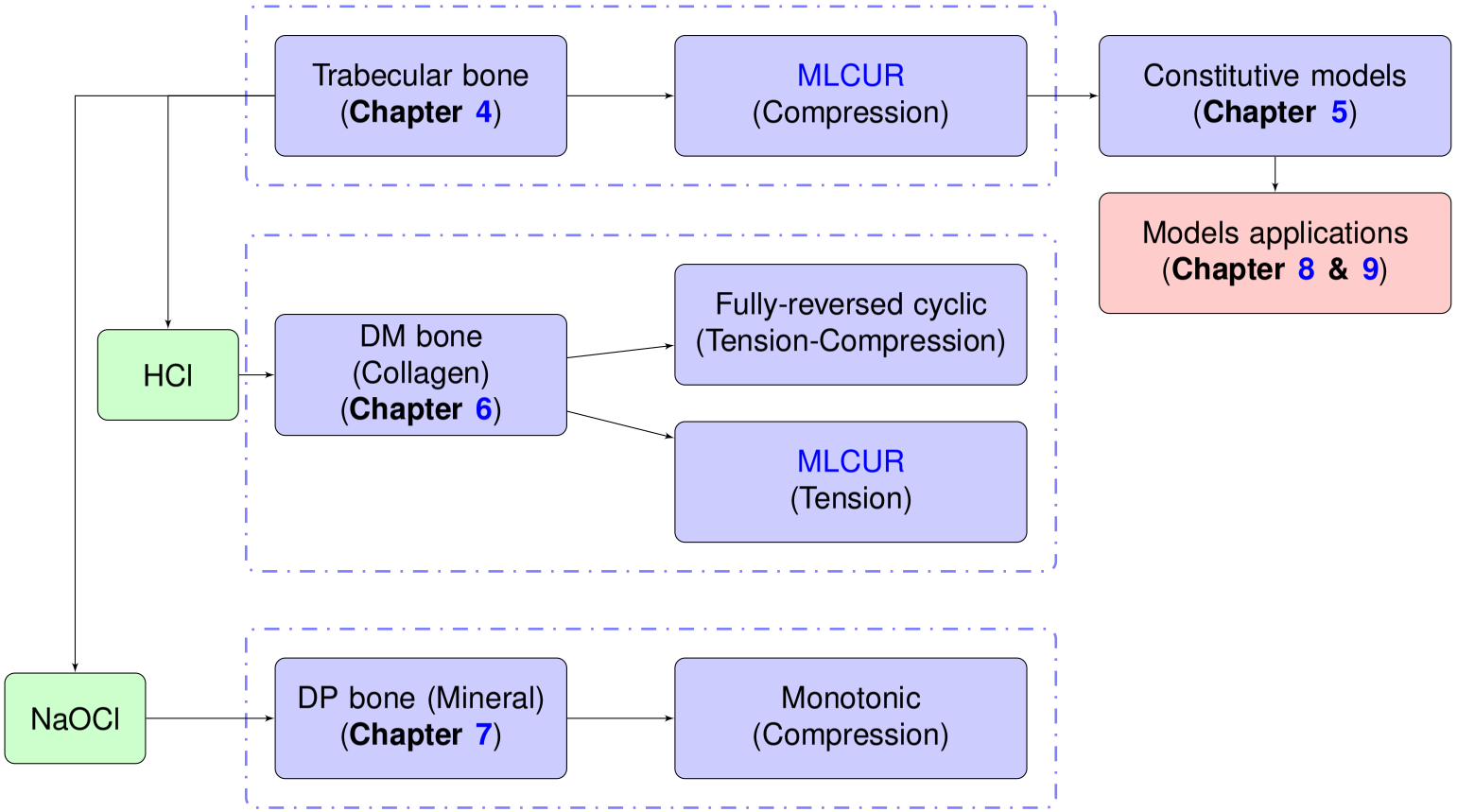

Figure 1.1: The structure of Chapter 4 to 9.

"The reading of all good books is like conversation with the finest men of past centuries."

Rene Descartes

2

Bone structures and mechanics

The skeletal system is important to the body both biomechanically and metabolically. Bones are the main load bearing members in the body and protector of major organs, it is important to understand their mechanical behaviour.

Here, this Chapter starts with morphology, microstructure of bone, and the literatures on bone's time-independent and time-dependent properties are summarised in Sec. 2.2.1 and 2.2.2. Bone mainly consists of mineral, type I collagen and water. As a living material, its mineral and collagen content and/or mineral-collagen ratio changes with age, and it also suffers from bone disease, such as osteoporosis with age (Sec. 2.3). Therefore, the mechanics on collagen and mineral are particularly important but only a few studies are currently available (Sec. 2.4). Some experimental considerations are discussed in Sec. 2.5. The available studies on loosening of connecting screws in a bone-screw system are summarised in Sec. 2.6.

2.1 Morphology

2.1.1 Cortical and trabecular bone

There are two main types of bones, cortical bone (also known as compact bone) and trabecular bone (also known as cancellous or spongy bone). Cortical bone is a dense, solid mass with only microscopic channels. Approximately 80% of the skeletal mass in the adult human skeleton is cortical bone, which forms the outer wall of all bones and is largely responsible for the supportive and protective function of the skeleton (Cowin, 2001). It has a much lower surface area than trabecular bone due to its lower porosity.

The remaining 20% of the bone mass is trabecular bone, a lattice of large plates and rods known as the trabeculae, found within flat and irregular bones (*e.g.* vertebral bodies) and at the ends of long bones, and it has an open, porous structure (Cowin, 2001). Here, in this thesis, only trabecular bone's mechanical properties are investigated.

2.1.2 Composition and hierarchical structure of bone

A critical issue that distinguishes trabecular bone from many other biological tissues is its substantial heterogeneity, which leads to wide variations in mechanical properties (Keaveny et al., 2001). The trabecular bone enclose a three-dimensional, interconnected, open porous space, resulting in a porous material (Gibson, 2003). The pores are filled with bone marrows and cell in-vivo.

Bone is a complex, hierarchical material. It is essentially a multi-phase composite consisting of organic phase (32–44% bone volume (BV)), inorganic phase (33–43% BV) and water (15–25% BV) (Olszta et al., 2007). The organic phase is composed of collagen type I (approx. 90%) and non-collagenous proteins (NCPs) (approx. 10%) (Olszta et al., 2007). The composition of the

inorganic (mineral) component can be approximated as hydroxyapatite (HA), with the chemical formula $Ca_{10}(PO4)_6(OH)_2$.

It can be described in terms of 5 hierarchical levels of organisation (Hamed et al., 2012a), as shown in Fig. 2.1:

Level 1: Elementary components of mineralised tissue (sub-nanoscale)

The sub-nanostructures of the three main materials are HA, collagen molecules and water (Hellmich et al., 2004).

- Needle (not mature) or plate-shaped (mature) mineral crystals consisting of impure hydroxyapatite with typical 1 to 5 nm thickness, and 25 to 50 nm length.
- Long cylindrical shaped collagen molecules with a diameter of about 1.2 nm and a length of about 300 nm, which are self-assembled in staggered organisation schemes (fibril) with characteristic diameters of 50 to 500 nm.
- Water plays an important role in the bio-mineralisation process and serves as a plasticiser, enhancing the toughness of bone.

These components have very different mechanical properties: the mineral is stiff but brittle while the (wet) protein is much softer but also much tougher than mineral. Remarkably, the composite combines the optimal properties of both components, the stiffness and toughness (Fratzl et al., 2004).

Level 2: Mineralised collagen fibrils (nanoscale)

Cross-linked collagen molecules are triple helical protein chains with 40 nm gaps between ends (Hamed et al., 2012a). Neighbouring collagen molecules are offset 67 nm resulting in a banded structure have been suggested by Weiner and Wagner (1998) and Fratzl et al. (2004). Collagen is formed first,

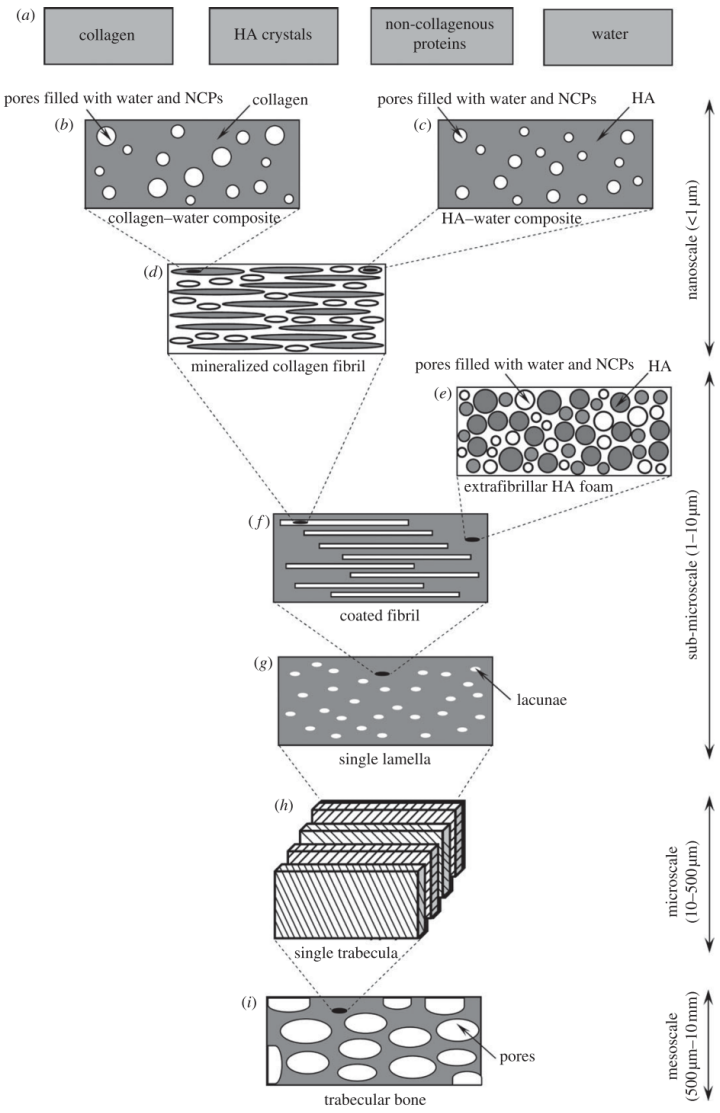

Figure 2.1: A schematic showing hierarchical structure of trabecular bone: Basic constituents of bone (a), a collagen water composite formed by cross-linked collagen matrix containing some pores filled with water and NCPs (b), a HA water composite built up by an HA crystal containing some intercrystalline pores within filled with water and NCPs (c), a mineralised collagen fibril made up from collagen-water and interfibrillar HA-water minerals (d), an extrafibrillar HA foam made up from HA minerals and some pores in-between them hosting water and NCPs (e), a coated fibril formed through the interaction of mineralised collagen fibrils and extrafibrillar HA foam (f), a single lamella built up from the coated fibrils matrix perforated by lacunar cavities (g), several lamellae with different fibril orientation stacked together to form a single trabeculae (h) and a trabecular bone as a porous network of trabeculae (i). Adapted from Hamed et al. (2012a)

followed by mineralisation, which involves the filling up of gaps and spaces in-between collagen molecules as well as those outside with HA nanocrystals (Hamed et al., 2012a). Such mineralised collagen fibrils are the basic building blocks of both cortical and trabecular bone types (Fratzl et al., 2004; Weiner and Wagner, 1998).

Level 3: Single lamellae (sub-microscale)

Spanning from one to few micrometres, single lamellae contains mineralised collagen fibrils which are aligned preferentially to form a single lamellae of thickness approximately 3 to 7 μm. Spaces between the fibrils are filled with randomly arranged minerals forming a porous foam-like structure.

Level 4: Single trabeculae (microscale)

Ranging from tens to hundreds micrometres, single trabeculae represents a trabecular bone tissue. It is made of trabecular bone packets (Cowin, 2001) (consisting of layers of lamellae oriented in different directions) and cement lines, which form trabeculae, and an interstitial bone at interconnects of trabeculae.

Level 5: Whole bone (mesoscale)

In trabecular bone, the pores typically in the order of 1 mm are filled with bone marrow, fat and bone cells. In cortical bone, this level represents randomly arranged osteons embedded in an interstitial lamella, with some resorption cavities, all surrounded by circumferential bone.

2.1.3 Micro-architecture indices

Micro-computed tomography (μCT) allows direct qualitative morphology analysis on 3D reconstructed images from scanning (Hildebrand et al., 1999).

This technique allows the non-invasive evaluation of morphological parameters such as bone volume fraction (BV/TV), trabecular thickness (Tb.Th), trabecular separation (Tb.Sp), trabecular number (Tb.N), and degree of anisotropy (DOA). Figure 2.2 shows trabecular bone sample's 3D reconstructed images with significantly different BV/TV.

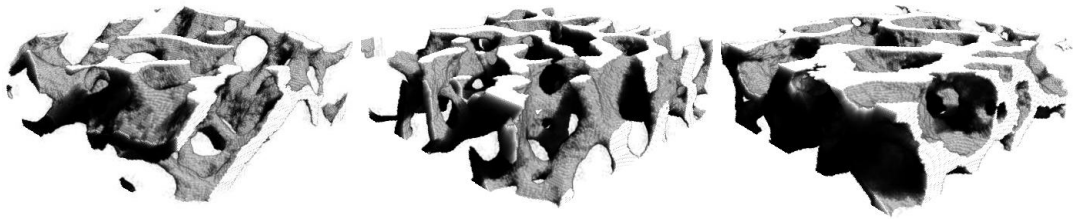

(a) (b) (c)

Figure 2.2: 3D μCT images (17.22 μm voxels resolution) of trabecular bone samples with three different BV/TV. Samples taken from (a) the bovine trochanter (BV/TV = 15%); (b) proximal tibia (BV/TV = 25%); (c) femoral head (BV/TV = 35%). All samples have the same bulk dimensions (3x3x1 mm^3).

2.2 Mechanical properties of bone

Studying on the mechanical behaviour of trabecular bone is important as it is the main loading bearing bone in vertebral bodies (Pollintine et al., 2009) and also transfers the load from the joints to the cortical bone in long bones (Cowin, 2001). Bone must be stiff and able to resist deformation, thereby permitting the skeleton to maintain shape, while also be flexible, able to absorb energy by deforming, to shorten and widen when compressed, and to lengthen and narrow in tension without cracking (Seeman and Delmas, 2006).

2.2.1 Time-independent behaviour

Bone mechanical properties can be obtained by performing experiments in which bone is subjected to tension, compression, bending, torsion, shear or a combination of these. Other approaches such as testing using ultrasound

(Alves et al., 1996; Turner and Burr, 1993) or numerical homogenisation (Hollister et al., 1991; Levrero-Florencio et al., 2016) have been used to determine the mechanical properties of bone. There are a number of parameters that can be used to characterise the elastic and post-elastic behaviour of bone. The key relationship is that between load applied to bone and its deformation in response to the applied load. The simplest characterisation comprises converting load-displacement curve to uniaxial stress (σ) - strain (ε) curve by simply divided them by effective loading area and effective length of testing sample, respectively (Fig. 2.3). In these, the elastic and post-elastic regimes are distinguished using 0.2% strain (ε) offset approach as shown in Fig. 2.3. It is also well recognised that bone is not an isotropic material (Dempster and Liddicoat, 1952; Turner et al., 1995); consequently its properties are strongly direction dependent. Trabecular bone has been often treated as an orthotropic material with orthogonal planes of symmetry (Ciarelli et al., 1991; Goulet et al., 1994).

Modulus-density

The slope of the most linear portion of σ - ε curve represents the intrinsic Young's or elastic modulus (E) of bone (Fig. 2.3). The reported modulus for trabecular bone falls in a range of few hundred MPa to few GPa, and the modulus of bone is also anatomic site dependent and direction dependent (Morgan and Keaveny, 2001).

The best-established relationship is that between trabecular bone's elastic modulus and its apparent density (ρ). Investigation on the relationships between bone morphology and mechanical properties has become more accessible in the past years. Hence, some of the empirical models related the time-independent properties with trabecular bone morphology (e.g. BV/TV). Figure 2.4 shows some established empirical relationships between modulus and ρ or BV/TV for both cortical and trabecular bone (adapted from Helgason

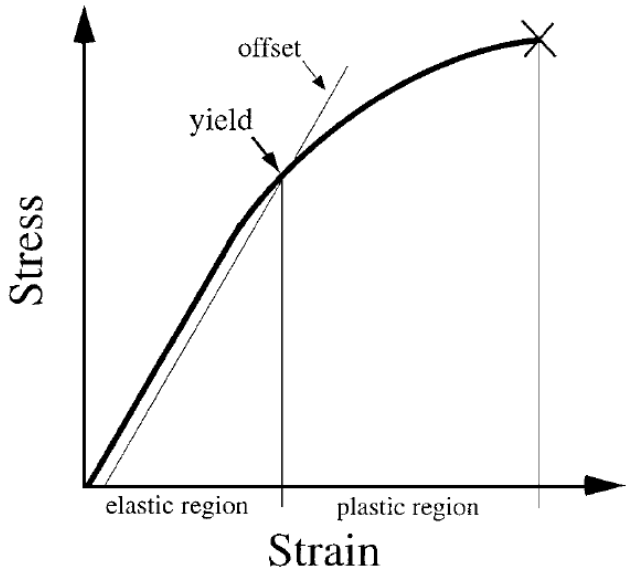

Figure 2.3: Typical $\sigma - \varepsilon$ curve for a bone sample under monotonic loading. It is divided into elastic and plastic regions by the yield point (the stress above which permanent damage occurs in the bone matrix). The yield point is often estimated using the 0.2% strain offset method - a line, parallel to but offset from the linear portion of the curve, is constructed and the intersection point of the $\sigma - \varepsilon$ curve called yield stress (σ_y) and yield strain (ε_y), and the slope denoted as elastic modulus (E) (Cowin, 2001).

et al. (2008)). It is also recognised that BV/TV in conjunction with additional bone micro-architecture parameters can provide anisotropic elastic properties of bone (Maquer et al., 2015).

Yielding

Aforementioned, the slope of the linear portion of σ - ε curve gives its modulus (E), by offset this line with 0.2% strain (ε), the intersection point with σ - ε curve called yield stress (σ_y) and yield strain (ε_y), respectively (Keaveny et al., 1994b). Strong linear correlation between stress at which trabecular bone yields and the corresponding elastic modulus for both tension and compression have been found as shown in Fig. 2.5. It has been demonstrated that σ_y in both tension and compression increases in a linear fashion with increasing modulus (Keaveny et al., 1994b). Slope of the line represents the strain at yielding (ε_y), this correlation suggests that yield strain (ε_y) for trabecular bone

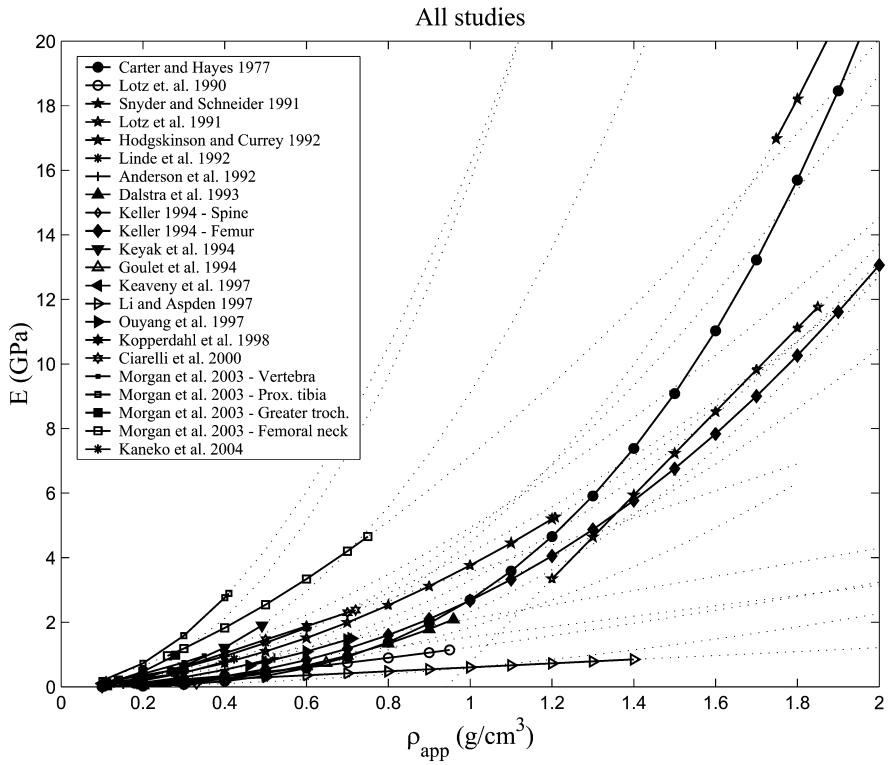

Figure 2.4: Some published empirical relationship between ρ and E. It is important to note that the relationship shown in figure include both human cortical and trabecular bone (Dotted lines are predictions). Adapted from Helgason et al. (2008)

are relatively constant (i.e. $\varepsilon_y \approx 0.96$ % for compression and $\varepsilon_y \approx 0.56$ % for tension as per Keaveny et al. (1994b)). It is now generally accepted that the ε_y of trabecular bone is independent of BV/TV; this has been shown experimentally (Bayraktar and Keaveny, 2004) and computationally (Levrero-Florencio et al., 2016). Further yielding of bone in strain space is isotropic, i.e. it does not dependent on the direction of loading (Levrero-Florencio et al., 2016).

During normal daily activities, strain in bone usually does not exceed 3,000 $\mu\epsilon$ (Cowin, 2001), the elastic properties determine its mechanical behaviour during such activities as experiments have shown that its constitutive behaviour can be approximated as linear in this range (Keaveny et al., 1994b; Moore and Gibson, 2002).

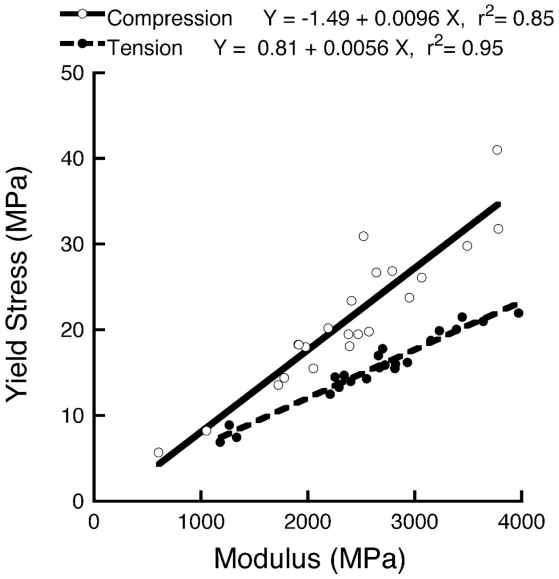

Figure 2.5: Yield stress (σ_y) vs. elastic modulus (E) for bovine tibia trabecular bone. Samples loaded in an on-axis configuration in either compression or tension. Adapted from Keaveny et al. (1994b)

Nonlinear behaviour

Obvious nonlinearity in the stress-strain curve has been observed (Hansen et al., 2008; Keaveny et al., 1994a,b; Kopperdahl and Keaveny, 1998; Li and Aspden, 1997; Matsuura et al., 2008). After an initial linear phase, the slope of the load-deformation curve reduces. Further straining in compression can lead to increased load carrying capacity at very high strain levels due to densification (Charlebois, 2008). Typical nonlinear compression and tension stress-strain curves from a monotonic uniaxial loading are shown in Fig. 2.6.

Morgan et al. (2001) conducted monotonic loading on trabecular bone samples at strain rate of 0.005 ε/s, a clear concave downward nonlinearity in the initial stress-strain curve was found for all anatomic sites in both compression and tension. The authors also suggested that viscoelasticity is a potential cause of this nonlinearity at strains below yield point when samples to be loaded at such slow strain rate.

2.2.2 Time-dependent behaviour

Following preliminary reports on time-dependent behaviour of trabecular bone (Schoenfeld et al., 1974; Zilch et al., 1980), it has been shown that trabecu-

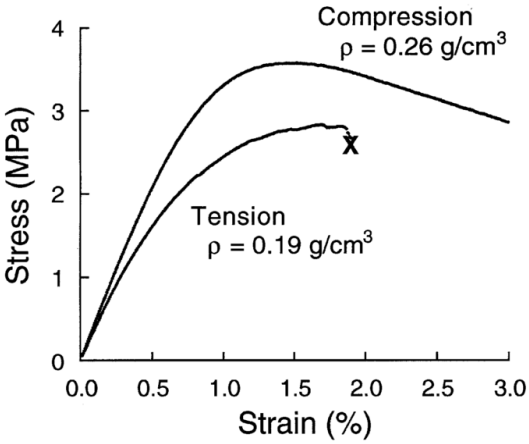

Figure 2.6: Typical nonlinear compression and tension stress-strain curves from a monotonic loading for two human vertebral samples. Adapted from Kopperdahl and Keaveny (1998).

lar bone has similar time-dependent behaviour to those of demonstrated by materials such as rubber.

Study of this time-dependent behaviour is important in several contexts such as: to understand energy dissipation ability of bone (Linde and Sørensen, 1993; Wang and Nyman, 2007); to understand the age-related non-traumatic fracture (Rapillard et al., 2006), to predict implant loosening due to cyclic load (Taylor et al., 2002), to understand progressive vertebral deformity (Pollintine et al., 2009), and pre-clinical evaluation of total joint replacement (Taylor et al., 2002). Consequently, trabecular bone's time-dependent behaviour has great clinical relevance, but it has received relatively little attention.

The time-dependent properties of trabecular bone have been measured experimentally using creep tests (Bowman et al., 1998, 1994; Kim et al., 2012, 2011; Novitskaya et al., 2014; Yamamoto et al., 2006) in which time-varying strain due to applied constant load is measured over time; relaxation tests (Bredbenner and Davy, 2006; Deligianni et al., 1994; Quaglini et al., 2009; Schoenfeld et al., 1974; Zilch et al., 1980) in which time-varying force due to applied constant deformation is measured over time; and dynamic mechanical analysis (Bowman et al., 1998, 1996; Guedes et al., 2006) in which the lag between sinusoidal stress and strain is measured over a frequency range. The detailed theory and acquisition on parameters of time-dependent material will be discussed in Chapter 3.

Creep

Some authors attempt to understand the time-dependent behaviour of trabecular bone by conducting prolonged creep test in which the applied force is kept constant until bone sample failure. Similar to other time-dependent material (ceramic, rubber, cortical bone, etc.), trabecular bone exhibits three classic phases of creep when subjected to a step load: an initial rapid response, followed by a steady-state creep at an almost constant creep rate and finally a rapid increase in strain just before fracture, which are called primary, secondary and tertiary creep, respectively (Bowman et al., 1998, 1994) (Fig. 2.7).

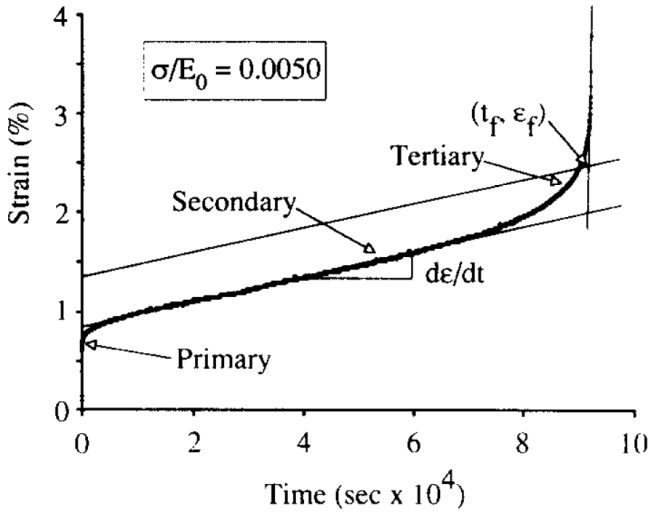

Figure 2.7: Typical long-term creep strain vs. time curve for trabecular bone. Adapted from Bowman et al. (1994).

There are number of terms can be defined from the typical three-stage creep curve. Normalised stress (σ/E_0) is defined as the ratio between applied stress level and its intact modulus, which can reduce scatter of data due to inter-sample variation of density and microstructure (Caler and Carter, 1989). The steady state creep rate ($\dot{\varepsilon}_{cre} = d\varepsilon/dt$) is defined as the slope of the creep strain vs. time curve in the central portion of the secondary regime. The time-to-failure (t_f) is defined as the time at the intersection of the straight line of secondary - offset by 0.5% strain to increase reproducibility - and the later part of the tertiary creep regimes (Fig. 2.7).

A strong power law relationships of the type $t_f = a(\sigma/E_0)^b$ and $\dot{\varepsilon} = a(\sigma/E_0)^b$ have been reported between the normalised stress (σ/E_0) and both time-to-failure (t_f) and steady state creep rate, $\dot{\varepsilon}_{cre}$, with $r^2 > 0.82$ and the power term not equal to unity (Bowman et al., 1994), which implies that the trabecular bone's creep behaviour is not in linear. Some published data are shown in Table 2.1. The negative power terms relating t_f to σ/E_0 indicated that with increased normalised stress levels, the shorter time is needed for fracture to occur. Bowman et al. (1998) pointed out that repetitive, low-intensity loading from daily activities can generate damage in trabecular bone, and the damage accumulation in the bone due to creep load may play a role in clinical problems by reducing the strength of bone.

Later, the load-creep-unload-recovery experiments were employed to examine the time-dependent behaviour of bone (Fig. 2.8), which had been used successfully previously for other time-dependent material, such as rubber. These novel experiments allowed examination of the recovery behaviour of bone, to quantify the residual strain and the differences between creep (when load is constant) and recovery (after load is removed) behaviour. This creep-recovery experiment have been conducted on cadaveric vertebral trabecular bone sample (Kim et al., 2011; Yamamoto et al., 2006), rat vertebral bodies (Kim et al., 2012) and human proximal tibia samples (Novitskaya et al., 2014).

A clear nonlinear time-dependent behaviour of trabecular bone was observed by Yamamoto et al. (2006), when the samples were subjected to different static strain levels. In this cited study, samples were held at a constant stress for almost 35 h, and considerable residual strain was observed although they were allowed 35 h of recovery. The authors also suggested that this irrecoverable strain is possibly related to age-related vertebral morphology fractures. Specifically, Kim et al. (2011) found that the unloading modulus is significantly higher than its loading modulus, which implies that a reorganisation of micro or ultrastructural components of bone caused by creep may happen.

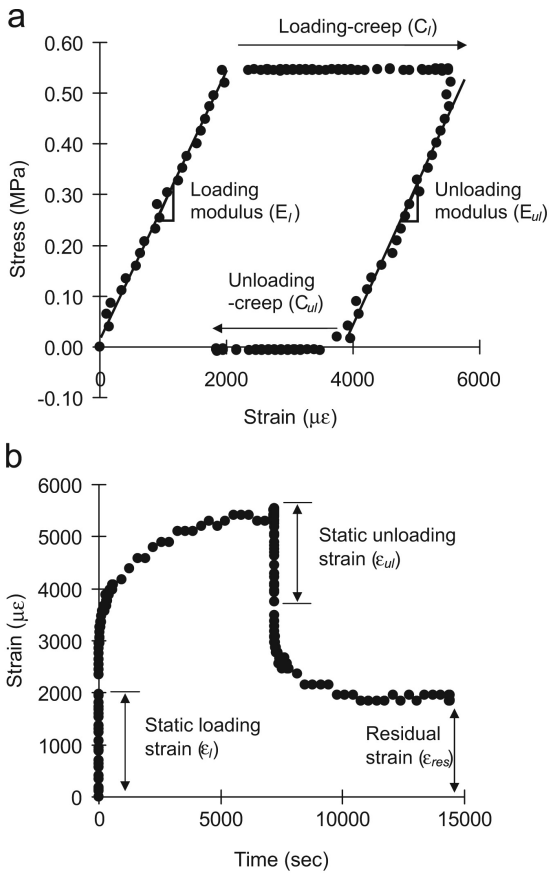

Figure 2.8: Typical stress and strain response from a load-creep-unload-recovery experiment. Stress vs. strain (a) and strain development with time during loading and unloading periods (b). Adapted from Kim et al. (2011).

Kim et al. (2012, 2011) reported that the trabecular bone with thinner trabeculae and greater connectivity were associated with increased logarithmic creep rate. In another words, the microarchitecture of trabecular bone is an important factor in its mechanical behaviour. Novitskaya et al. (2014) observed the changes in micro-architectural indices evaluated from micro-computed tomography (μCT) before and after the creep; the study found that creep induced changes in trabecular separation and structural model index. Novitskaya et al. (2014) also found that the steady state creep rate was higher and the final creep strain was larger for samples with low BV/TV (or apparent density).

Relaxation

Zilch et al. (1980) observed that the stress decreases with time if the trabecular bone is held at a constant deformation, the authors also reported that the relaxation function of trabecular bone is anatomic location dependent (e.g. re-

laxation is greater in the femoral head than in the condyles). Later, Deligianni et al. (1994) examined the time-dependent behaviour of trabecular bone from human femoral head in compression through a series of stress relaxation tests at three strain levels and in three different directions for each cubic samples. They found that the trabecular bone from human femoral head was nonlinear viscoelastic and displayed anisotropic behaviour. Through a number of relaxation tests, Quaglini et al. (2009) also reported that the viscoelastic behaviour of trabecular bone is nonlinear with respect to its initial applied stress, i.e. higher stress will result in slower relaxation rate and the smaller the decrease in stress at the steady regime.

Bredbenner and Davy (2006) examined the viscoelastic behaviour of trabecular bone at low strains and the effects of damage in this viscoelastic behaviour through a relaxation test, suggested that modelling the observed change in relaxation times with damage accumulation is necessary to successfully predict the post-damage viscoelastic response.

Cyclic loading

Michel et al. (1993) reported that fatigue of trabecular bone was accompanied by increased nonlinearity and hysteresis, and distinctly different patterns of fatigue for high- and low-stress fatigue. In the early stages of fatigue, the modulus increases slightly for low stress levels and progressively decreases for high stress levels; in the final stages of fatigue, there is a rapid drop in modulus for both cases.

It has been suggested that cyclic loading results in cumulative creep deformations in addition to loss of stiffness and failure has been defined as 10% reduction in the secant modulus from its initial value (Bowman et al., 1998). Bowman et al. (1998) conducted fatigue tests on bovine proximal tibiae, and a strong and significant power-law relationship was found between cycle-to-failure (N_f), time-to-failure (t_f), steady-state creep rate ($d\varepsilon/dt$) and the applied

loads. The creep strain included two components: creep damage and viscous creep, where creep damage was possibly due to breakage of collagen-links was permanent; while viscous creep, possibly due to sliding of collagen fibrils or fluid flow, was recoverable.

Moore et al. (2004) reported that different densities of trabecular bone lead to different fatigue behaviour. By conducting cyclic (1 Hz) compressive stepwise increasing loads to trabecular bone samples, Topoliński et al. (2011) found a strong relationship between fatigue life and the BV/TV. They also found that the size of the hysteresis loops is also dependent on the levels of loading.

2.3 Ageing and disease of bone

The preliminary researches in human vertebrae indicate that both trabecular and cortical bone tissue from young adults (age 20-40) have significantly higher moduli than the older one. In addition, trabecular bone has a lower moduli than cortical bone. It is of great importance to determine the underlying microstructure and compositional alterations that result in these tissue property changes (Cowin, 2001, Chapter 10). Researchers have begun to address the age-related change in bone tissue properties, which may have profound importance in understanding bone biomechanics with ageing and disease.

Loss of bone mass has been considered as the major cause of age-related change in bone mechanics. A recent study reported that the risk of bone fracture for older women ($\sim$ 75 years old) is about 7%, whereas risk is 1% for younger individuals ($\sim$ 45 years old) even when they have a similar bone density level (Wang et al., 2002). Burr et al. (1997) reported that for the same bone mass, the risk of fracture in older people is greater than that for younger ones, thus, factors other than the loss of bone mass may be of crucial importance to the understanding of age-related change in bone's load carrying capabilities.

Table 2.1: Some published relationships from prolonged creep and fatigue experimental studies

Author	Animal	Site	Bone	Test*	$Y = aX^b$						Strain Rate	n
					Y	X	X range	a	b	r^2		
Caler and Carter (1989)	Human	Femur	Cortical	Creep(T)	t_f	σ/E_0	-	1.45×10^{-36}	-15.81	0.95	0.002-0.009	11
				Creep(C)	t_f	σ/E_0		4.07×10^{-37}	-17.76	0.87		13
Mauch et al. (1992)	Bovine	Ulna	Cortical		t_f	σ/E_0	-	9.41×10^{16}	-16.7	0.51		
Rimnac et al. (1993)	Bovine	Femur	Cortical	Creep(T)	t_f	$d\varepsilon/dt$	-	4.2×10^{3}	-1.03	0.87		
Bowman et al. (1994)	Bovine	PT	Trabecular	Creep(C)	$d\varepsilon/dt$	σ/E_0	0.005-0.01	2.21×10^{33}	17.75	0.82	0.005	24
					t_f	σ/E_0		9.96×10^{-33}	-16.18	0.83		
					t_f	$d\varepsilon/dt$		3.5×10^{-2}	-0.92	0.98		
Bowman et al. (1998)	Bovine	PT	Trabecular	Creep(C)	t_f	$d\varepsilon/dt$	-	2.18×10^{2}	-0.95	0.99	-	39
Fondrk et al. (1988)	Human		Cortical	Creep(T)	$d\varepsilon/dt$	σ/E_0	-	1.66×10^{37}	18.9	0.57	0.005	31
Abdel-Wahab et al. (2011)	Bovine	Femur	Cortical	Creep(T)	$d\varepsilon/dt$	σ	17-21	3.75×10^{11}	2.7		0.0004	3
Caler and Carter (1989)	Human	Femur	Cortical	Fatigue(T)	t_f	σ/E_0	-	1.91×10^{-33}	-14.97	0.94	0.02-2Hz	15
				Fatigue(C)	t_f	σ/E_0		4.79×10^{-25}	-11.18	0.97		16
Michel et al. (1993)	Bovine	DF	Trabecular	Fatigue	N_f	ε_{Max}	0.008-0.021	3.37×10^{-23}	13.89	0.78	0.005	24
Bowman et al. (1998)	Bovine	PT	Trabecular	Fatigue	$d\varepsilon/dt$	σ/E_0	0.029-0.01	8.47×10^{16}	9.94	0.82	0.012-0.04	20
					t_f	σ/E_0		1.71×10^{24}	-11.56	0.77		
					t_f	$d\varepsilon/dt$		4.2×10^{-3}	-0.9	0.96		
					N_f	$d\varepsilon/dt$		1.77×10^{23}	-11.19	0.85		
Moore et al. (2004)	Bovine	PT	Trabecular	Fatigue	N_f	σ/E_0	0.0065-0.0095	2.7×10^{-27}	-13.0	0.86	2Hz	21
Bowman et al. (1999)	Human	Humeri	DM Cortical	Creep(T)	$d\varepsilon/dt$	σ/E_0	-	6.74×10^{12}	15.52	0.84	0.005	8
					t_f	σ/E_0		2.56×10^{15}	-15.58	0.79		8
					t_f	$d\varepsilon/dt$		2.93×10^{02}	-0.91	0.93		24

PT: proximal tibia
DF: distal femur
DM: demineralised
*T: tension; C: Compression

Although a number of studies have determined the influence of mineralisation, osteon morphology, and porosity (Currey et al., 1996; Wang et al., 1998), but the age-related alterations in quality of collagen matrix and their relationship with bone mechanics remain poorly understood. Bailey et al. (1999) reported that there is an age-related decrease in bone collagen content, and it might indicate an increase in the mineralisation degree. However, they found that there were no biochemical modifications of bone collagen during ageing.

This has motivated researches to explore the role of collagen modifications in promoting change in bone biomechanics. Thus, understanding the mechanical properties of bone's constituents is of great interest and importance.

2.4 Mechanical properties of bone's constituents

Bone is a composite material which comprises of the mineral phase, organic phase and water assembled into complex, hierarchical structure (Chen et al., 2011; Hellmich et al., 2004; Wang et al., 2002), as shown in Fig. 2.9 (also discussed in Sec 2.1.2). Understanding of main constituents' (mineral and organic phases) biomechanical properties and their contribution will help understanding the mechanics of this composite material, therefore, some researchers have attempted to isolate the constituents from whole bone and conducted mechanical experiments on each of them.

The study of demineralised and deproteinised bone is considered to be important from two perspectives. From a biological point of view, osteoclasts and osteoblasts maintain a balance, which if lost can cause osteoporosis (Castro-Ceseña et al., 2011). From materials science perspectives, this composite material formed from mineral and organic phases is able to resist deformation therefore making load carrying possible without excessive deformation, while also being sufficiently flexible to enable absorption of shocks and optimised for stiffness and toughness.

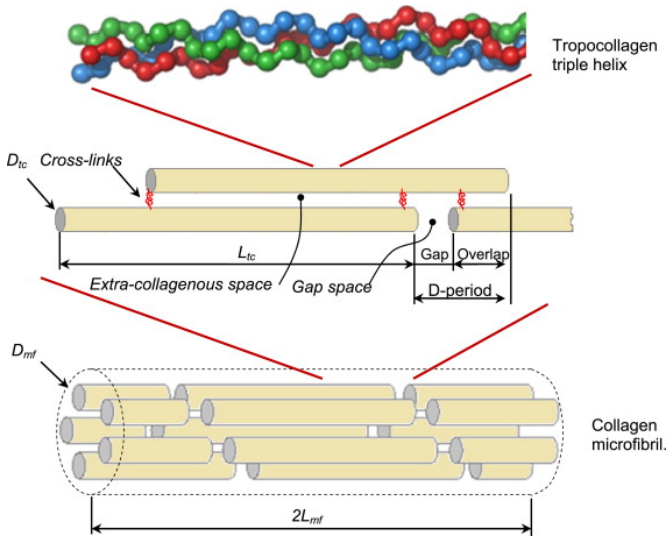

Figure 2.9: Double period model of cylindrical microfibril. It composed of (i) five TC molecules shifted by the interval D forming a cylindrical shape with, (ii) mineral phase filling the gap space (GM model) and the extra-collagenous space (EM model) and (iii) cross-links joining two TC molecules end (adapted from Hambli and Barkaoui (2012)).

Mechanically, collagen and mineral play very different roles - the elastic modulus of collagen is much lower than that of the hydroxyapatite, but the former is three orders of magnitude tougher (Ruffoni and van Lenthe, 2017); while the mineral provides the stiffness, it is much more brittle than the collagen. The mechanical properties of mineral and collagen phases is considered in the following sections.

2.4.1 Mechanical properties of demineralised bone

Acquisition

Organic phase of bone can be obtained by submerge bone into chemical solution (e.g. ethylenediaminetetraacetic acid (EDTA), hydrochloric acid (HCl)), this process is called demineralisation. Although EDTA solutions have been used to demineralise bone, use of HCl solutions speed up the process and it has been used successfully in previous studies (Burstein et al., 1975; Castro-Ceseña et al., 2013; Chen and McKittrick, 2011; Chen et al., 2011).

Time-independent behaviour

To evaluate the time-independent mechanical behaviour of the organic phase of bone, a number of previous studies have undertaken mechanical test on demineralised bone, almost all of which have been on cortical bone (Bowman et al., 1996; Burstein et al., 1975; Catanese III et al., 1999; Novitskaya et al., 2011, 2013), and the author could find only one study on trabecular bone (Chen and McKittrick, 2011). These studies are summarised in Table 2.2, and include values of E, ε_f and σ_f.

A preliminary study on mechanical properties of demineralised bone was performed by Burstein et al. (1975), who examined the tensile mechanical behaviour of progressively demineralised bovine tibia cortical bone by using HCl solution showed that the ultimate stress σ_f, yield stress (σ_y) and elastic modulus (E) decreased with the degree of demineralisation. Later, Bowman et al. (1996) investigated tensile behaviour on completely demineralised bovine humeri and tibiae cortical bone samples by immersing them into EDTA solution and found that the average modulus was much lower than the modulus of untreated bone. Bowman et al. (1996) also noted an initial non-linear 'toe' region at strain less than 4%, where the Young's modulus was very small, and the authors attributed it to the straightening of coiled collagen structure. At higher strains, the Young's modulus was found to remain constant, attributed to stretching of the collagen molecules. Catanese III et al. (1999) compared the mechanical properties of bovine and human demineralised bone by conducting uniaxial tension tests. The authors reported that both elastic modulus and ultimate strength of demineralised bone were heterogeneous among different sites. Possible source of this heterogeneity were identified to include microstructural factors, such as organic weight fraction and porosity (Catanese III et al., 1999). Further investigation by Novitskaya et al. (2013) found a strong nonlinear loading response by conducting cyclic loading-unloading compres-

sion test up to 2% strain on demineralised bovine cortical femur bone.

Chen and McKittrick (2011) tested the fully demineralised bovine proximal femur trabecular bone under monotonic compression and found that the elastic modulus and compressive strength for demineralised bone was far lower than that of untreated bone, plastic buckling was observed in demineralised samples with assistance of scanning electron microscope.

The different pattern of stress-strain loading curve for tension (stiffening) (Bowman et al., 1996) and compression (softening) (Novitskaya et al., 2013) are of great importance to gain an insight into understanding the mechanics for this two-phase composite material.

Time-dependent behaviour

Creep tests were conducted on demineralised cortical bone at various normalised stresses and temperature by Bowman et al. (1999) and three stages of creep behaviour, primary, secondary and tertiary creep were clearly observed. The nonlinear creep behaviour was observed as the experiments were conducted at the various normalised stresses (σ/E_0), a strong power law relationship was found between normalised stress (σ/E_0) and steady state creep rate ($\dot{\varepsilon}_{cre}$) (as shown in Table 2.2). Bowman et al. (1999) also reported that the creep behaviour was also a function of temperature.

2.4.2 Mechanical properties of deproteinised bone

Mineral phase of bone can be obtained by submerging bone into chemical solution (e.g. sodium hypochlorite (NaOCl), sodium hydroxide (NaOH)) and this process is called deproteinisation. Castro-Ceseña et al. (2013) also reported that the deproteinisation process faster at the relatively higher temperature, but the higher temperature may damage collagen. Therefore, to maintain 37 $^{\circ}C$ (body temperature) during deproteinisation process is necessary.

Table 2.2: Some published data on demineralised bone

Author	Animal	Site	Bone	Test*	Strain rate $(\%/s)$	$E\ (MPa)$	$\sigma_f\ (MPa)$	$\varepsilon_f\ (\%)$	n
Burstein et al. (1975)	Bovine	Tibia	Cortical	Monotonic (T)	-	750	39.5	6.1	4
Bowman et al. (1996)	Bovine	Humeri	Cortical	Monotonic (T)	-	618	61.5	12.3	6
Catanese III et al. (1999)	Human	Femur	Cortical	Monotonic (T)	0.30	275	14.7	8.7	10
		Tibia			0.30	351	18.2	7.8	13
	Bovine	Tibia			0.30	450	25.5	8.4	8
		Humerus			0.30	313	21.3	8.9	8
Novitskaya et al. (2011)	Bovine	Femur	Cortical	Monotonic (C)	0.1	232	14	-	-
Novitskaya et al. (2013)	Bovine	Femur	Cortical	Cyclic (C)	0.1	5.1^{+}	-	-	-
Chen and McKittrick (2011)	Bovine	Femur	Trabecular	Monotonic (C)	0.1	84	3	-	15

σ_u: ultimate stress
ε_u: ultimate strain
*T: tension; C: Compression
$^{+}$: it is the initial tangent modulus and taken from its first loading cycle.

Experimental data showed that the deproteinised samples can be modelled as cellular solids, with strong dependence of mechanical properties on the relative density (Chen and McKittrick, 2011). Chen and McKittrick (2011) also reported that deproteinised samples with fracture strain less than 1% and brittle crushing failure mechanism were observed in a monotonic compression test. The decrease in elastic modulus was reported by a number of studies for cortical (Manilay et al., 2013; Novitskaya et al., 2011; Wright et al., 1981), and trabecular bone (Chen and McKittrick, 2011), i.e. mineral phase of bone has lower modulus than untreated bone.

2.4.3 Bone as a composite material

Composite models of bone help to illustrate the complex interrelationship between bone microstructure and material properties. In particular, bone is frequently modelled as two-phase composite hydroxyapatite mineral crystals dispersed throughout an organic collagen matrix. Currey (1964) was first to use this modelling approach to explain the mechanical properties of bone on the basis of its constituent materials. However, it is surprising that even after some 50 years, there is little reliable data on the mechanical properties of demineralised bone. In fact, most models of bone as a two-phase composite material have been based on collagen modulus values obtained from the mechanical tests of ox skin performed by Hall (1951).

Hamed et al. (2012a) developed a new theoretical model that predicts the experimentally measured elastic modulus of cortical bovine femur bone. This model assumes that cortical bone has a hierarchical structure, which comprises an interpenetrating composite of bio-polymers and hydroxyapatite minerals, and consists of porosity at different hierarchical levels. Although in this model the demineralised bone properties was also based on Hall (1951), but Hamed et al. (2012a) moved a step further and found a close agreement be-

tween the model and experimental results of deproteinised and demineralised bone. By employing the volume fraction, Hamed et al. (2012b) also successfully predicted the elastic behaviour of trabecular bone.

The elastic modulus of trabecular bone has been derived based on the measured elastic properties of separate mineral and protein phases by Lubarda et al. (2012). By adopting the mechanics of cellular solids approach, the moduli of elasticity of deproteinised and demineralised bone were expressed in terms of the trabecular moduli of elasticity and the corresponding density ratios using the power law expressions. Then by incorporating an appropriate weight function to account for the mineral/protein interaction effects the departure from the ideal mixture rule was explained. The elasticity of osteoporotic bone was predicted by modifying the rate of loss of the mineral content and the protein. These available composite models are limited to predict time-independent behaviour of bone.

2.5 Experiment considerations

Bone biomechanical properties vary with anatomic site and are affected by the age and general health of the donor. In addition, the preparation of bone sample and experiment set-up can affect the mechanical properties of the tissue. Important factors include sample hydration, testing temperature and experiment artefacts.

Water loss significantly affects the moduli, strength and toughness of bone. Nyman et al. (2006) showed bone strength increased with a 5% loss of water by weight, and the toughness significantly decreased through a loss of plasticity; with water loss exceeding 9%, strength actually decreased, and it caused toughness to decrease through decreases in strength and fracture strain. For accurate testing, therefore, it is best to test bone in its hydrated condition.

This can be done by keeping samples in physiological saline or wrapped with saline-soaked gauze during the test.

The mechanical properties of bone are influenced by the surrounding temperature. For accurate measurement of mechanical properties, bone sample should be tested at 37 $^{\circ}C$ (physiological temperature), however, this is not always practical. Testing at room temperature (23 $^{\circ}C$) increases the Young's modulus of bone about 2 to 4% compared with a test at 37 $^{\circ}C$ (Cowin, 2001, pp 7-2). Thus, the error caused by testing at the room temperature is not large.

Keaveny et al. (1997) reported that a systematic underestimation error when using platens for measurement and direct compression of samples; the error to be in the range of 20-40%. Stress-strain curves from each anatomic site illustrate that the end-artefacts in the platens compression test not only introduce an initial nonlinear region but also reduce the modulus, whereas there is no indication of any initial nonlinear region with end-cap technique. Therefore, for testing on bone samples use of end-caps has been recommended to reduce artefacts.

2.6 Bone-screw system

Bone screws can be used alone or in conjunction with plates to connect fragments of a fractured bone, such as hip fracture (Born et al., 2011), distal femoral condyle (Wähnert et al., 2010) and tibial plateau fractures (Tschegg et al., 2008), etc. The typical complications reported in a number of studies is loosening of the connecting screws, and higher loosening rate for osteoporotic patients (Galbusera et al., 2015). Loosening also causes patient discomfort. Clinical findings of screw loosening and failure probably result from bone-screw separation events and from elevated strains (Sakaguchi and Borgersen, 1993).

This stability of bone-screw system can mainly vary depending on both screw design variables (size, length, threads) (Bianco et al., 2014; Gorczyca

et al., 2002), patient variables (bone quality, bone defects) (Conlisk et al., 2016; Liu et al., 2014) and surgical variations (Taylor and Prendergast, 2015).

2.6.1 Classification of stability

A common pattern of implant or screw stability is typically divided into two consecutive phases: primary (or initial) and secondary (Taylor and Tanner, 1997). Primary stability happens right after operation and before any biologically driven bone remodelling takes place, it relies on interlocking and frictional bone-screw contact phenomena, while secondary stability is accompanied by a biological process (Steiner et al., 2015).

Primary stability is recognised as an important determinant in the aseptic loosening (Viceconti et al., 2000). This stability, or the lack of it, is commonly measured as the amount of relative motion at the interface between the bone and the screw under load. Large interfacial relative movements reduce the chance that bone will osseointegrate with the screw, and may cause the formation of a fibrous tissue layer around the screw or implants (Kadir, 2013), which will exhibit bone remodelling. An accurate evaluation, prediction of the bone-screw relative micromotion is becoming important in both pre-clinical and clinical contexts.

2.6.2 Current experimental investigations

Experimental investigations suggested that a common pattern of migration had an initial phase and this is followed by a slower continuous phase. Numerous experimental studies have reported similar two phases of migration or loosening from pedicle screw (Bianco et al., 2016; Johnston et al., 2006), dynamic hip screw (Basler et al., 2013), distal tibia fracture fixation (Schüller et al., 2008; Tschegg et al., 2008) and distal radius fracture fixation(Schüller et al., 2009). All above cited studies observed two clear phases of loosening.

Apart from bone damage during surgery, some studies (Bowman et al., 1998; Moore et al., 2004; Rapillard et al., 2006) also report that accumulation of permanent damage increased with increasing cycles, which may create a screw fixation weakness and cause loosening. It has become clear that these implants have a decreased performances, particularly in low density bone.

The nature of both phases of migration suggests that this is a mechanical phenomenon or at least mechanically triggered, rather than a completely biological process (Taylor and Tanner, 1997). Experimental investigations give sufficient information on the whole image of implant history, but it is difficult to establish a priori location of the maximum bone-implant micromotion. Thus, finite element analysis (FEA) provides an opportunity to report the relative micro-motion at each point of the bone-screw interface.

2.6.3 Current status of FE analysis

In computational modelling loosening at the interface has, in the past, been examined by evaluating strain level after employing time-independent elastic (MacLeod et al., 2016) or elastoplastic (Bianco et al., 2014; Donaldson et al., 2012) constitutive models for bone. It is recognised that bones' response to loads is time-dependent (Bowman et al., 1994) and some permanent deformation arises even at low strain levels ($<$ 3,000 $\mu\varepsilon$) (Kim et al., 2011; Yamamoto et al., 2006).

The high inter-sample variability in morphology between dense and porous trabecular bone encouraged some researches to include the microstructure of trabecular bone for peri-implant investigations (Wirth et al., 2012, 2010). Wirth et al. (2012) reported that the load transfer from the screw to the surrounding bone differed strongly between the continuum and discrete (including microstructure) models, especially for low-density bone. They also pointed out significant differences in strain distribution at the peri-implant surface.

It is important to note that, the above cited studies were able to provide the peri-implant stress and strain conditions (both peaks and locations) only, but it couldn't provide any information on the effects of time and walking cycles. In an ideal scenario, an implant or screw will be well-fixed in the bone, stay at the same location and fulfil its task over entire life time (Wirth et al., 2010). However, since bone has a recognised time-dependent behaviour, cyclic loading induced damage accumulation is also reported to weaken vertebrae (Burr et al., 1997) and is often associated with loosening of implants (Taylor and Tanner, 1997). None of above finite element (FE) studies reported the fatigue-like two-phase implant/screw migration, as the time-independent material models were employed in FEA.

There appears to be only one study which reported that due to the viscoelastic response of cortical bone, the bone-implant contact pressure decreased with time and suggested that increased the interference (0.1 mm) is of little help (Shultz et al., 2006). The deformation and interface micromotion for bone-implant interface with time or walking cycles remains unknown and it is extremely important to understand the mechanically triggered implant or screw loosening.

“Give me six hours to chop down a tree and I will spend the first four sharpening the axe.”

Abraham Lincoln

3

Modelling of time-dependent behaviour

Characterisation of trabecular bone’s time-dependent mechanical behaviour is one of the main aims of this thesis, therefore, relevant theories and constitutive models are presented in this chapter.

The phenomenological aspects of three approaches, creep, relaxation and dynamic loading, are first discussed. Then, from simple rheological models to more complex time-dependent constitutive models are discussed. Both linear and nonlinear viscoelasticity are considered and this is followed by discussion on viscoplasticity. The aspects of experimental observations, including time-varying creep compliance, steady state creep rate and strain components, are discussed in Sec. 3.4. Lastly, the methodologies of parameters fitting are discussed in Sec. 3.5.

3.1 Phenomenological aspects

Experimentally, one seeks to characterise materials by performing simple laboratory tests. In the case of viscoelastic materials, mechanical characterisation often consists of performing uniaxial tensile or compressive tests similar to those used for time-independent elastic solids, but with modifications to enable observation of the time dependency of the material response. The simplest tests in this respect are: creep, relaxation and dynamic loading (Roylance, 2001).

3.1.1 Creep

The creep test consists of measuring the time dependent strain $\varepsilon(t)$ resulting from the application of uniaxial stress σ_0 as a step function as illustrated in Fig. 3.1a (Roylance, 2001). There are several stages of creep development that can occur in a material, which may eventually lead to failure of the material. There are three stages of creep response: primary creep (rapid strain rate), secondary creep (constant strain rate) and tertiary creep (leading to failure).

3.1.2 Relaxation

Stress relaxation is another test which the stress in the material will decrease over time while being subjected to a constant strain or deformations (Fig. 3.1b) (Roylance, 2001).

3.1.3 Dynamic loading

Creep and relaxation tests are convenient for studying material response for long durations (typically in minutes or more), but they are less accurate for short duration response time. When a time dependent material is subjected to a sinusoidally varying stress (or strain), a steady state will eventually be

reached, in which the resulting strain (or stress) is also sinusoidal, having the same angular frequency but with a phase lag (Roylance, 2001).

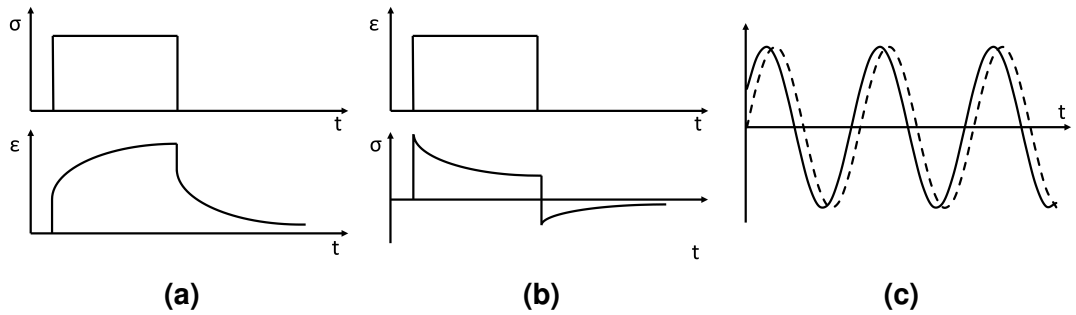

Figure 3.1: Typical time dependent behaviour: creep (a), relaxation (b) and dynamic loading (c).

3.2 Simple rheological models

The expression 'visco-elastic' signifies the dual natures of a material: on the one hand it behaves in a viscous way, as a liquid, on the other hand elastically, as a solid. The behaviour of viscoelastic materials under uniaxial loading may be represented by means of conceptual models composed of elastic and viscous elements which provide physical insights.

For an ideal solid, Hooke's law holds: the stress, σ, applied is proportional to the strain, ε, and the proportionality constant is the modulus of elasticity E, so $\sigma = E\varepsilon$. As a simple model, one considers a helical spring with stiffness E. The response ε of such a spring to a stress σ is schematically indicated in Fig. 3.2a. Noticeably, the response of loading and unloading both are instantaneous without any time dependency, and the strain is fully recovered upon unloading (Roylance, 2001).

For an ideal liquid, Newton's law holds: the stress (σ) is proportional to the rate of deformation $d\varepsilon/dt = \dot{\varepsilon}$, the proportional constant is the viscosity η, so $\sigma = \eta\dot{\varepsilon}$, as a model, a dashpot is used. Noticeable, there is no instantaneous response and no recovery takes place when compared with the spring (Roylance, 2001) (Fig. 3.2b).

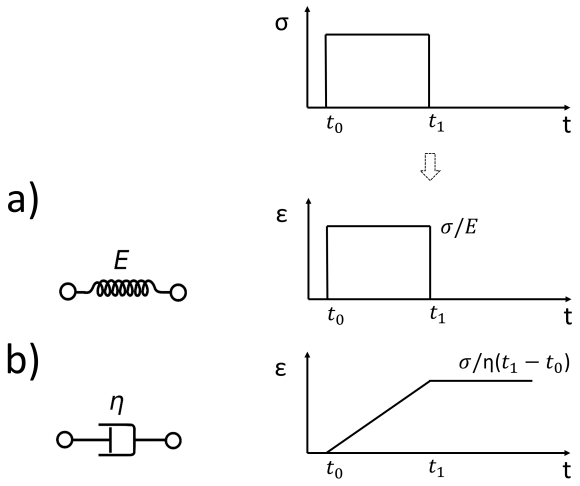

Figure 3.2: Schematic drawing for rheological model elements. Ideal solid is represented by a spring (a) and ideal liquid can be represented as a dashpot (b).

For a viscoelasic material, combinations of these two elements provide a variety of models. For example, a spring and a dashpot in series and parallel are called Maxwell and Kelvin-Voigt models, respectively.

3.2.1 Maxwell model

As shown in Fig. 3.3a, the Maxwell model is constructed by connecting a spring and a dashpot in a series. In this case, a stress σ applied to the entire system is applied equally on the spring and the dashpot $\sigma = \sigma_s = \sigma_d$, and the total strain response can be divided into strain from the spring (ε_s) and the strain from the dashpot(ε_d). Thus, total strain is given by

$$\varepsilon = \varepsilon_s + \varepsilon_d \tag{3.1}$$

with

$$\varepsilon_s = \frac{\sigma}{E}, \qquad \dot{\varepsilon_d} = \frac{\sigma}{\eta} \tag{3.2}$$

Differentiating ε and ε_d and using Eq. 3.1 gives

$$\dot{\sigma} + \frac{\sigma}{\tau} = E\dot{\varepsilon} \tag{3.3}$$

where $\tau = \eta/E$ and $\dot{\sigma} = d\sigma/dt$. This expression is a governing equation for Maxwell model. Note that it contains time derivatives, so that simple constant of proportionality between stress and strain does not exist. Eq. 3.3 can be solved for stress, $\sigma(t)$, once $\varepsilon(t)$ is specified, or for the $\varepsilon(t)$ if the $\sigma(t)$ is specified.

In a stress relaxation test, a constant strain ε_0 acts as the 'input' to the material, and the stress response can be obtained through integration as (Roylance, 2001):

$$\sigma(t) = \varepsilon_0 E \exp(-t/\tau) \tag{3.4}$$

In a creep test, a constant stress σ_0 acts as the 'input' to the material and gives strain response as:

$$\varepsilon(t) = \sigma_0(\frac{t}{\eta} + \frac{1}{E}) \tag{3.5}$$

The Maxwell model, handles creep-recovery badly, but it accounts fairly well for relaxation (Fig. 3.3a).

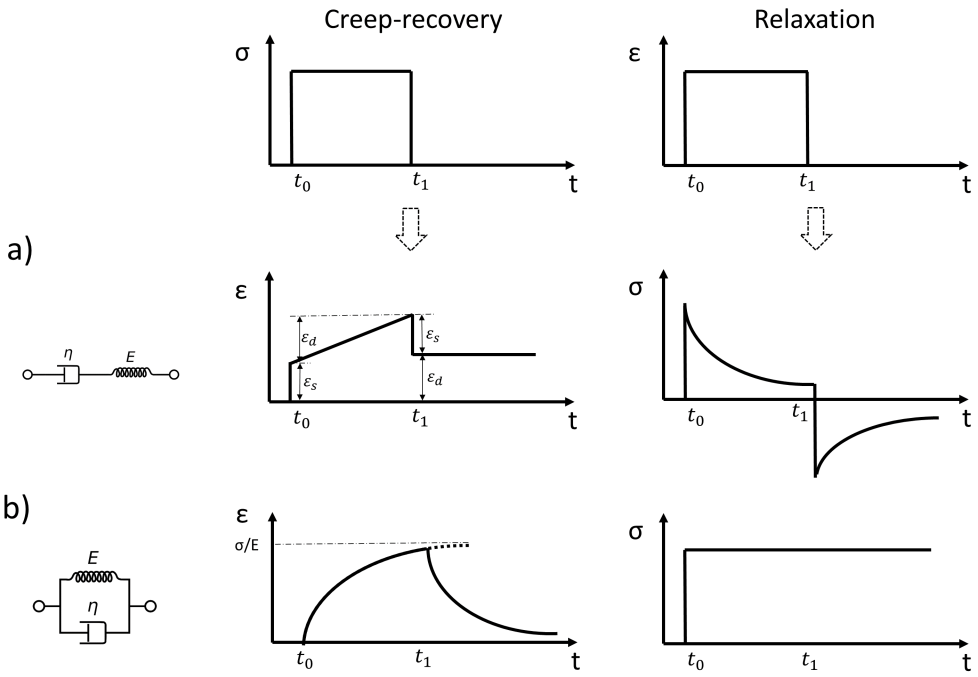

Figure 3.3: Schematic drawing of simple rheological models for viscoelastic material: Maxwell (a) and Kelvin-Voigt (b) model.

3.2.2 Kelvin-Voigt model

Consider next the other two-element model, the Kelvin-Voigt model (Fig. 3.3b), which consists of a spring and a dashpot connected in a parallel arrangement (Marques and Creus, 2012). The total stress σ applied to the system will be shared by the spring (σ_s) and the dashpot (σ_d), while the strain ε of the system will be equal to the strains occurring in the spring (ε_s) and the dashpot (ε_d):

$$\sigma = \sigma_s + \sigma_d \tag{3.6}$$

with

$$\sigma_s = E\varepsilon \qquad \sigma_d = \eta\dot{\varepsilon} \tag{3.7}$$

Consequently (Kelly, 2013, Chapter 10),

$$\sigma = E\varepsilon + \eta\dot{\varepsilon} \tag{3.8}$$

Thus stress relaxation and creep tests give

$$\sigma(t) = E\varepsilon_0 + \eta\dot{\varepsilon} \tag{3.9}$$

and

$$\varepsilon(t) = \frac{\sigma_0}{E}[1 - exp(-t/\tau)] \tag{3.10}$$

respectively. Clearly, the Kelvin-Voigt model handles creep and recovery fairly well, but it does not account for relaxation.

3.3 More complex constitutive models

This study employs creep-recovery behaviour of trabecular bone, so the theory discussed in this Chapter will largely focus on creep behaviour.

3.3.1 Linear viscoelastic model

Both model, Maxwell and Kelvin-Voigt, are generally poor and limited in their quantitative representation of the actual viscoelastic response. In order to improve the representation, number of parameters need to be increased by combining a number of springs and dashpots, so called Boltzmann superposition principle (Park and Schapery, 1999). In this the viscoelastic strain is given by

$$\varepsilon_{ve}(t) = D_g\sigma + \int_0^t \Delta D(t-\tau)\frac{d\sigma(\tau)}{d\tau}d\tau \tag{3.11}$$

where D_g is instantaneous compliance that describes the elastic response at time t=0, $\Delta D(t)$ is the transient creep compliance that evolves with time, and σ is the applied stress. For a creep-recovery experiment, the plateau stress (σ) is applied at $t = 0$ and removed at $t = t_a$, by substituting this step input of stress into equation, for the loading phase ($0 < t < t_a$) the creep strain is obtained as:

$$\varepsilon_{cre}(t) = D_g\sigma + \Delta D(t)\sigma \tag{3.12}$$

and for unloading phase ($t > t_a$) the recovery strain is given by

$$\begin{aligned}\varepsilon_{rec}(t) &= \varepsilon_{cre}(t) - \varepsilon_{rec}(t-t_a)\\ &= [\Delta D(t) - \Delta D(t-t_a)]\sigma\end{aligned} \tag{3.13}$$

The transient compliance $\Delta D(t)$ is well described by using generalised Kelvin-Voigt model (Fig. 3.4a), which comprises of n Kelvin units in series. It is also referred to as Prony series,

$$\Delta D(t) = \sum_{i=1}^{n} D_i[1 - exp(-\lambda_i t)] \tag{3.14}$$

so, for a linear viscoelastic material the strain variation under the constant stress can be expressed as

$$\varepsilon_{ve}(t) = D_g\sigma + \sum_{i=1}^{n} D_i[1 - exp(-\lambda_i t)]\sigma \tag{3.15}$$

where D_i, the retardation strengths, λ_i, reciprocal of retardation times ($1/\tau_i$, where τ_i is retardation times) and n, the number of Prony terms or number of Kelvin units, are positive constants. These parameters can be determined by minimising the error between experimental curve and Eq. 3.15 by using a nonlinear least-squares fit method under prescribed number of Prony terms.

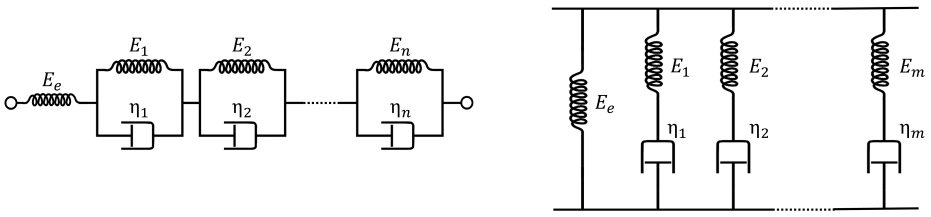

(a) **(b)**

Figure 3.4: Schematic drawing of generalised model for viscoelastic material: Generalised Kelvin-Voigt model (a) and generalised Maxwell model (b).

Creep compliance functions obtained from experiments can be easily converted to relaxation functions, by using interconversion methods proposed by Park and Schapery (1999), the relaxation modulus function can be expressed as:

$$E(t) = E_e + \sum_{i=1}^{m} E_i \ \exp(-t/\rho_i) \tag{3.16}$$

where E_e is the equilibrium modulus, E_i and ρ_i are the relaxation strengths and relaxation times, respectively. It can be described by generalised Maxwell model (Fig. 3.4b), which comprises of $m + 1$ constituent elements in parallel, with m Maxwell models and an isolated spring (to represent solid behaviour).

The creep compliance function can also be converted to complex modulus, as proposed by Park and Schapery (1999):

$$D'(\omega) = D_g + \sum_{j=1}^{n} \frac{D_j}{\omega^2 \tau_j^2 + 1} \tag{3.17}$$

$$D''(\omega) = D_g + \sum_{j=1}^{n} \frac{\omega \tau_j D_j}{\omega^2 \tau_j^2 + 1} \tag{3.18}$$

where $D'(\omega)$, $D''(\omega)$ and ω are storage compliance, loss compliance and loading frequency, respectively. Loss tangent, $tan(\delta)$, is defined as the ratio of loss compliance to storage compliance:

$$tan(\delta) = \frac{D''(\omega)}{D'(\omega)} \tag{3.19}$$

3.3.2 Nonlinear viscoelastic model

A linear viscoelastic material must meet the following criteria,

- The Boltzmann superposition principle is applicable
- Creep compliance is stress level independent

If any of the conditions for linear viscoelasticity is not satisfied, the viscoelastic behaviour is considered to be nonlinear. The nonlinearity can be influenced by number of factors, such as applied stress level, strain rate and temperature.

The Schapery single integral constitutive equation of nonlinear viscoelasticity (Schapery, 1969) was derived from fundamental principles by utilising the concepts of irreversible thermodynamics in a small strain context. In this model the nonlinear viscoelastic strain is given by

$$\varepsilon_{nve}(t) = g_g D_0 \sigma + g_1 \int_0^t \Delta D(\psi^t - \psi^\tau) \frac{d(g_2 \sigma(\tau))}{d\tau} \tau \tag{3.20}$$

where g_0, g_1 and g_2 are stress-dependent nonlinear viscoelastic parameters.

The parameter g_0 is a nonlinear instantaneous compliance parameter, the transient nonlinear parameter g_1 measures the effect of nonlinearity in the transient compliance, and the g_2 describes the effects of loading rate on the transient creep response, and ψ, called reduced time, is given by

$$\psi^t = \int_0^t \frac{d_{\tau'}}{\alpha_{\sigma(\tau')}\alpha_{T(\tau')}\alpha_{e(\tau')}} \tag{3.21}$$

where τ' is a time variable, α_σ, α_T and α_e are stress, temperature and other environment time-shift factors, respectively. The temperature and environment time-shift factors were not considered in this study, therefore, reduction time function is reduced to $\psi^t = t/\alpha_\sigma$. For a linear viscoelastic material, g_0, g_1, g_2, α_σ and α_T are unity and, therefore, Eq. 3.20 is reduced to Eq. 3.11. Similar to the linear equation, the strain response during loading and unloading phases in a typical creep-recovery test are given by:

$$\varepsilon_{cre}(t) = g_0 D_g \sigma + g_1 g_2 \Delta D(\frac{t}{\alpha_\sigma})\sigma \tag{3.22}$$

$$\varepsilon_{rec}(t) = [g_2 \Delta D(\frac{t}{\alpha_\sigma}) - g_2 \Delta D(\frac{t - t_a}{\alpha_\sigma})]\sigma \tag{3.23}$$

respectively.

3.3.3 Viscoplastic model

The time-dependent response to an applied constant stress is decomposed into recoverable (nonlinear viscoelastic) and irrecoverable (viscoplastic) components as

$$\varepsilon_{total} = \varepsilon_{nve} + \varepsilon_{vp} \tag{3.24}$$

where, ε_{total} , ε_{nve} and ε_{vp} are the total strain, nonlinear viscoelastic strain and viscoplastic strain responses, respectively at a given time t.

The total strain rate $\dot{\varepsilon}_{total}$, obtained by taking the derivative of Eq. 3.24, is given by

$$\dot{\varepsilon}_{total} = \dot{\varepsilon}_{nve} + \dot{\varepsilon}_{vp} \tag{3.25}$$

The viscoplastic strain rate based on Perzyna model is given by (Perzyna, 1971)

$$\dot{\varepsilon}_{vp} = \Gamma\langle\phi(F)\rangle\frac{\partial G}{\partial\sigma} \tag{3.26}$$

and

$$\langle\phi(F)\rangle = \begin{cases} 0 & \phi(F) \leq 0 \\ (\frac{F}{\sigma_y^0})^N & \phi(F) > 0 \end{cases}$$

where Γ is the viscosity parameter, G is the viscoplastic potential function and ϕ is the overstress function expressed in terms of the rate-independent yield surface F; and σ_y^0 and N are material parameters. Trabecular bone has been previously modelled using time-independent Drucker-Prager yield criterion (Mullins et al., 2009). The yield surface F based on extended Drucker-Prager yield criterion is given by

$$F = \tau - \alpha p - \kappa(\varepsilon_e^{vp}) \tag{3.27}$$

where $p = -\frac{1}{3}tr(\boldsymbol{\sigma})$ is the equivalent pressure stress, $\boldsymbol{\sigma}$ is the stress tensor, $\alpha = tan(\theta)$ is a pressure-sensitivity parameter related to friction angle, θ, and $\kappa(\varepsilon_e^{vp})$ is viscoplastic hardening function which is a function of effective viscoplastic strain ε_e^{vp}. The parameter τ is deviatoric effective shear stress, and is given by (Hibbitt et al., 2012)

$$\tau = \frac{\sqrt{J_2}}{2}\left[1 + \frac{1}{d} - (1 - \frac{1}{d})\frac{J_3}{\sqrt{J_2^3}}\right] \tag{3.28}$$

where $J_2 = \frac{3}{2}\boldsymbol{S} : \boldsymbol{S}$ and $J_3 = \frac{9}{2}\boldsymbol{S}\cdot\boldsymbol{S} : \boldsymbol{S}$ are the second and third deviatoric stress invariants, respectively, $\boldsymbol{S} = \boldsymbol{\sigma} - \frac{1}{3}tr(\boldsymbol{\sigma})\boldsymbol{I}$ is the deviatoric stress tensor,

and d is a material parameter which is the ratio of the yield stress in uniaxial tension to the yield stress in uniaxial compression. For uniaxial tension, the deviatoric effective shear stress $\tau = \sqrt{J_2}/d$ whereas for uniaxial compression $\tau = \sqrt{J_2}$. The dependence of τ on the third deviatoric stress invariant J_3 is removed when $d = 1$, and to ensure the convexity of the yield surface d must be in the range of $0.778 \leq d \leq 1$ (Hibbitt et al., 2012). The viscoplastic flow potential is given by

$$G = \tau - \beta p \tag{3.29}$$

where $\beta = \tan(\theta')$ is a parameter related to the dilation angle (θ'). Associated flow results if $\alpha = \beta$, whereas non-associated flow results if $\alpha \neq \beta$. In this study, the viscoplastic hardening function (κ) in Eq. 3.27 was assumed to be an exponential function of the effective viscoplastic strain (ε_e^{vp}) (Huang et al., 2011) as

$$\kappa = \kappa_0 + \kappa_1[1 - exp(-\kappa_2(\varepsilon_e^{vp}))] \tag{3.30}$$

where κ_0 defines the initial yield stress, κ_1 describes the saturated stress for the fully-hardened material, κ_2 describes the transition rate between κ_0 and $\kappa_0 + \kappa_1$, and

$$\varepsilon_e^{vp} = \int_0^t \dot{\varepsilon}_{eff}^{vp} t \tag{3.31}$$

where $\dot{\varepsilon}_{eff}^{vp}$ is the effective viscoplastic strain rate and is expressed as (Huang et al., 2011)

$$\dot{\varepsilon}_{eff}^{vp} = \frac{1}{\sqrt{1 + 2(\frac{0.5+\beta/3}{1-\beta/3})^2}} \sqrt{\dot{\varepsilon}_j^{vp} \dot{\varepsilon}_j^{vp}} \tag{3.32}$$

3.4 Aspects of creep-recovery experiment

As mentioned before, the creep behaviour can be classified into three stages (Fig 3.5). Primary creep in which the curve is concave down, secondary creep in which deformation is proportional to time, and tertiary creep in which de-

formation accelerates until creep rupture. Although secondary creep is represented by a straight line in a plot of strain versus time (constant strain rate, also called steady state creep rate ($\dot{\varepsilon}_{cre}$)), this straight line has nothing whatsoever to do with linear viscoelasticity.

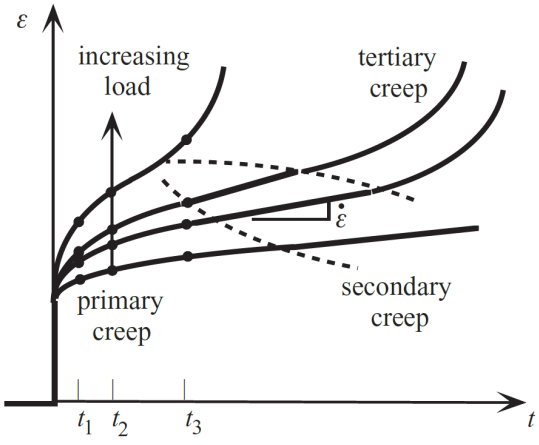

Figure 3.5: Classification of regions of creep behaviour. It shows the plot of strain versus time for different load levels. Adapted from Lakes (2009).

3.4.1 Time-varying creep compliance

The time-varying creep compliance ($\mathbf{C}_{cre}(t)$) is the ratio between creep strain and the stress level, given by

$$\begin{aligned}\mathbf{C}_{cre}(t) &= \frac{\varepsilon_{cre}(t)}{\sigma_0} \\ &= g_0 D_g + g_1 g_2 \sum_{i=1}^{n} D_n (1 - exp(-\lambda_n \frac{t}{\alpha_\sigma}))\end{aligned} \tag{3.33}$$

where σ_0 is the stress level which results creep strain $\varepsilon_{cre}(t)$. As discussed earlier, the nonlinear parameters (g_0, g_1, g_2, α_σ) are stress level dependent parameters and for a linear viscoelastic material, these four parameters are unity. In other words, for a linear viscoelastic the time-varying creep compliance is a stress level independent function. If compliance is higher than its linear viscoelastic prediction then the material is exhibiting softening and if the compliance is lower than its linear viscoelastic prediction then the material is stiffening (Fig. 3.6).

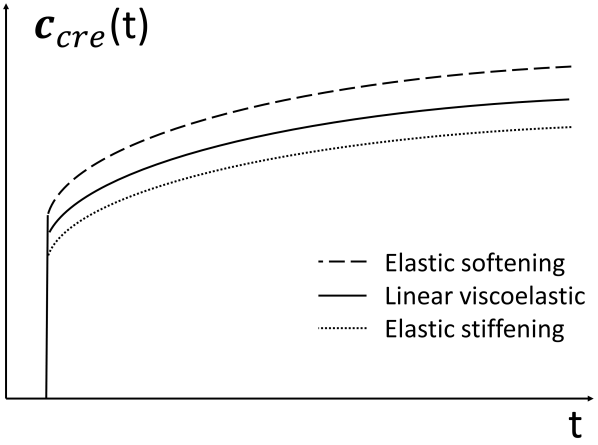

Figure 3.6: Time-varying creep compliance. It is defined as the ratio of strain response to its corresponding stress levels. For a linear viscoelastic material, the time-varying creep compliance ($\mathbf{C}_{cre}(t)$) is a parameter independent to its stress levels. With increased stress level, elastic softening occurs if compliance above its linear viscoelastic response; while elastic stiffening occurs if compliance is below its linear viscoelastic response.

3.4.2 Steady state creep rate

Steady state creep rate ($\dot{\varepsilon}_{cre}$) is defined as the slope of the linear portion of the secondary creep curve, it can be expressed as

$$\begin{aligned}\dot{\varepsilon}_{cre} &= d\frac{\varepsilon_{cre}(t)}{dt} \\ &= d\frac{g_1 g_2 \sum_{i=1}^{n} D_n(1-exp(-\lambda_n \frac{t}{\alpha_\sigma}))}{dt}\sigma_0 \\ &= \frac{g_1 g_2}{\alpha_\sigma}\sum_{i=1}^{n} D_n \lambda_n exp(-\lambda_n \frac{t}{\alpha_\sigma})\sigma_0\end{aligned} \tag{3.34}$$

Figure 3.7 shows the plot of steady state creep rate ($\dot{\varepsilon}_{cre}$) versus normalised effective stress (σ/σ_0); a straight line response indicates linear viscoelasticity. For a nonlinear material the steady-state creep rate is stress dependent, in which the $\dot{\varepsilon}_{cre}$ is lower than the linear extrapolation for elastic stiffening material, higher than linear extrapolation for elastic softening material.

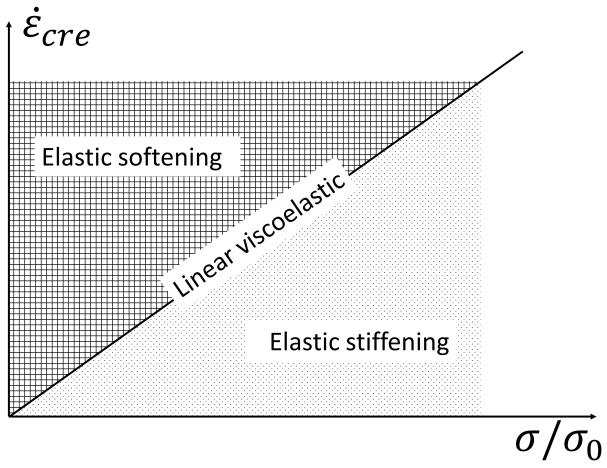

Figure 3.7: Steady state creep rate vs. normalised effective stress. It is defined as the slope of the curve from strain-time plot, indicates how fast of creep strain generation. For a linear viscoelastic material, the $\dot{\varepsilon}_{cre}$ linearly increase with increasing normalised stress level. The $\dot{\varepsilon}_{cre}$ lower than linear estimation indicates elastic stiffening; while elastic softening occurs if $\dot{\varepsilon}_{cre}$ is higher than linear estimation.

3.4.3 Strain components

For a multiple-load-creep-unload-recovery (MLCUR) experiment comprises of a loading phase, a load holding phase, an unloading and a recovery phase. The typical load application and its strain response are shown in Fig. 3.8a, 3.8b, respectively. The following strain responses were defined (see Fig. 3.8c, 3.8d):

- ε_l: instantaneous loading strain
- ε_{ul}: instantaneous unloading strain
- ε_{cre}: amount of creep strain accumulated during plateau loading phase
- ε_{rec}: amount of creep strain relaxed during recovery phase
- ε_{res}: strain that remains at the end of each cycle

For a linear viscoelastic material, the ratio, $\varepsilon_{cre}/\varepsilon_l$, is always constant with increasing stress levels, and the ratio, $\varepsilon_{ul}/\varepsilon_l$, is constant as well. If sufficient time is allowed the material recovers fully for any viscoelastic material, i.e, ε_{rec} = ε_{cre}.

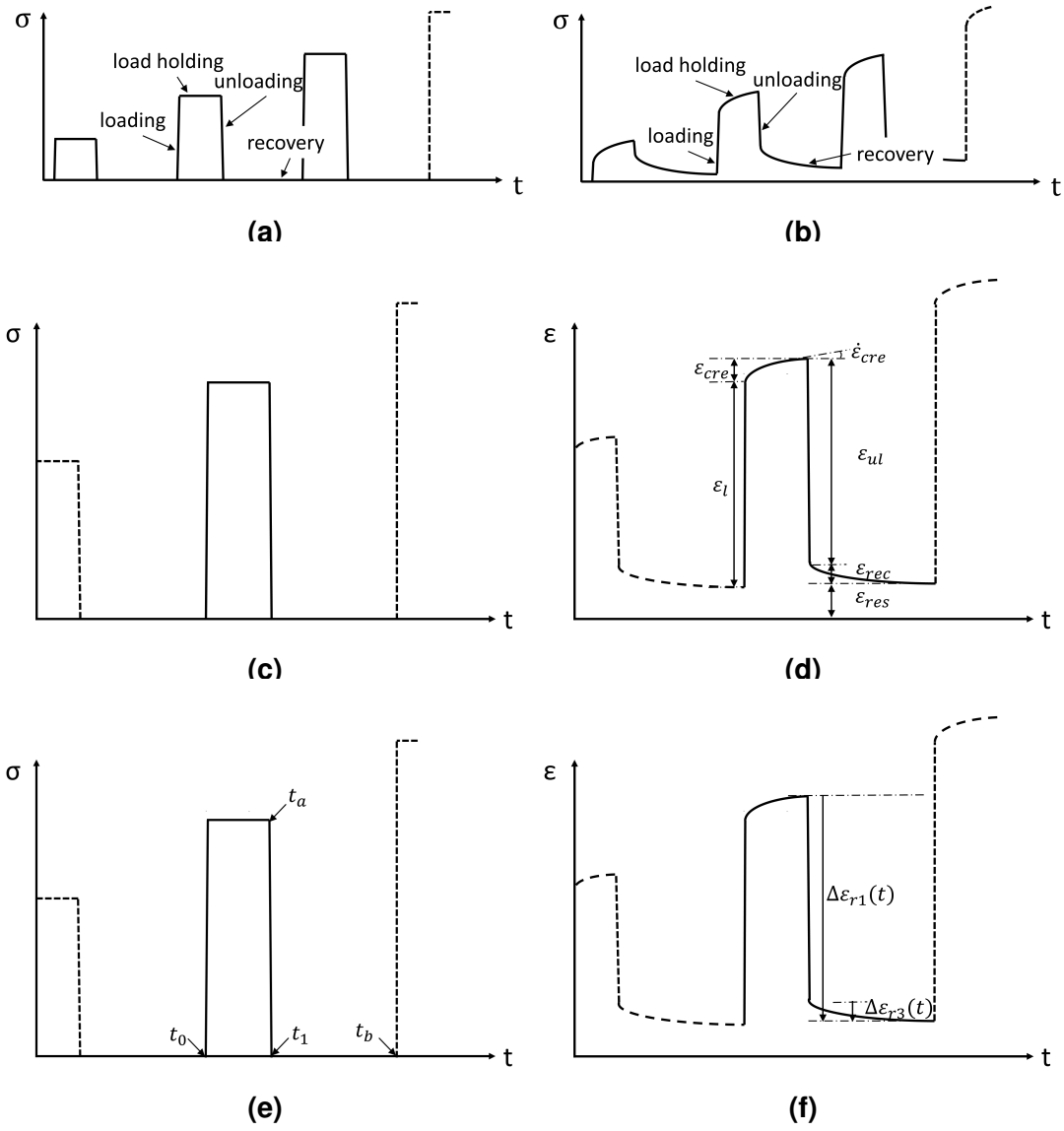

Figure 3.8: Strain components definition for creep-recovery experiment: Typical load application for MLCUR experiment (a) and its strain response (a); load application and strain components used for experimental observations (c,d); load application and strain components used for parameters fitting and computational models (e,f).

3.5 Parameter fitting

The processes to obtain all the parameters can be classified into three steps, including parameters for linear viscoelastic, nonlinear viscoelastic and viscoplastic model as shown in Fig. 3.9. If the recovery behaviour from lowest stress cycle is assumed to be linear viscoelastic, and the nonlinear viscoelastic parameters can be obtained from recovery part of higher load cycles. Further, the differences between creep and recovery strain responses allow for evaluation of viscoplastic parameters.

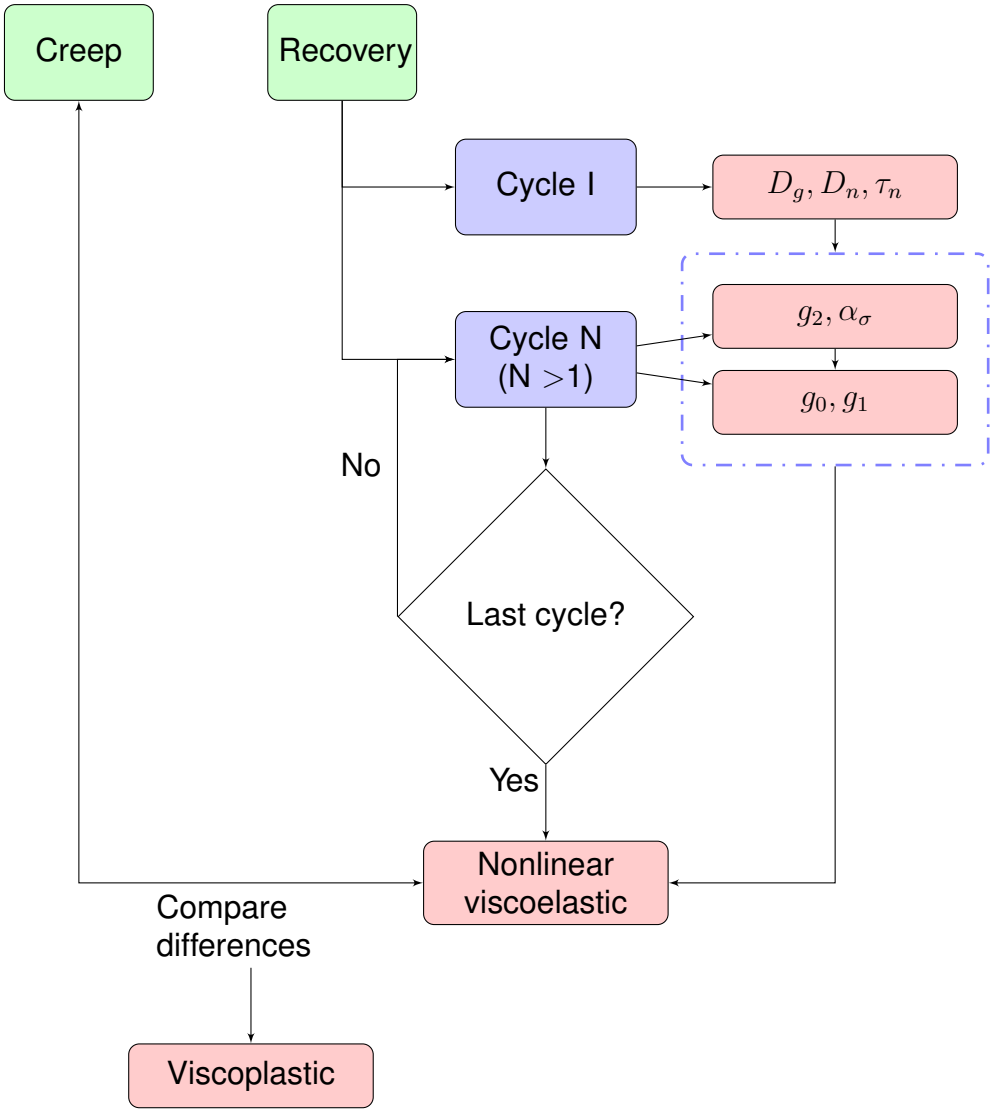

Figure 3.9: Fitting procedure for viscoelastic, nonlinear viscoelastic and viscoplastic parameters.

3.5.1 Linear viscoelastic parameters

The first step of the fitting procedure is to obtain the Prony series coefficients D_g, D_n and λ_n from a linear viscoelastic response at the lowest stress level (Cycle I). In this thesis, it is assumed that the unloading response at first cycle is linear viscoelastic ($g_0 = g_1 = g_2 = \alpha_\sigma = 1$). The expression for $\Delta\varepsilon_{r1}(t)$ (Fig. 3.8f), which represents recovered strain between t_a and t_b is given by

$$\begin{aligned}\Delta\varepsilon_{r1}(t) &= \varepsilon_{cre}(t_a) - \varepsilon_{rec}(t) \\ &= D_g\sigma + \sigma \left\{ \begin{array}{l} \sum_{n=1}^{N} D_n[1 - exp(-\lambda_n t_a)] \\ - \sum_{n=1}^{N} D_n[1 - exp(-\lambda_n t)] \\ + \sum_{n=1}^{N} D_n[1 - exp(-\lambda_n (t - t_a))] \end{array} \right\}\end{aligned} \tag{3.35}$$

Then the Prony series coefficients are determined by minimising error between the experimental curve and equation for $\Delta\varepsilon_{r1}(t)$.

3.5.2 Nonlinear viscoelastic parameters

Then linear viscoelastic coefficients from cycle I can now be used to determine the nonlinear viscoelastic parameters at higher cycles. The recoverable strain $\Delta\varepsilon_{r3}$ (Fig. 3.8f), from t_1 to t_b, can be evaluated and used to determine the nonlinear parameters g_2 and α_σ:

$$\begin{aligned}\Delta\varepsilon_{r3}(t) &= \varepsilon_{rec}(t_1) - \varepsilon_{rec}(t) \\ &= g_2\sigma \left\{ \begin{array}{l} \sum_{n=1}^{N} D_n[1 - exp(-\lambda_n(\frac{t_1}{\alpha_\sigma}))] \\ - \sum_{n=1}^{N} D_n[1 - exp(-\lambda_n(\frac{t_1 - t_a}{\alpha_\sigma}))] \\ - \sum_{n=1}^{N} D_n[1 - exp(-\lambda_n\frac{t}{\alpha_\sigma})] \\ + \sum_{n=1}^{N} D_n[1 - exp(-\lambda_n(\frac{t - t_a}{\alpha_\sigma}))] \end{array} \right\}\end{aligned} \tag{3.36}$$

Once the nonlinear parameters g_2 and α_σ are obtained, the remaining two parameters g_0 and g_1 are obtained by minimising error between the experiment measurement and $\Delta\varepsilon_{r1}(t)$ (Fig. 3.8f):

$$\begin{aligned}\Delta\varepsilon_{r1}(t) &= \varepsilon_{cre}(t_a) - \varepsilon_{rec}(t) \\ &= g_0 D_g \sigma + g_1 g_2 \sigma \left\{ \begin{array}{l} \sum_{n=1}^{N} D_n[1 - exp(-\lambda_n(\frac{t_a}{\alpha_\sigma}))] \\ -\sum_{n=1}^{N} D_n[1 - exp(-\lambda_n \frac{t}{\alpha_\sigma})] \\ +\sum_{n=1}^{N} D_n[1 - exp(-\lambda_n(\frac{t-t_a}{\alpha_\sigma}))] \end{array} \right\}\end{aligned} \tag{3.37}$$

The nonlinear viscoelastic parameters are assumed to be general polynomial functions of the effective stress, these functions then can be expressed as

$$\begin{aligned} g_0 &= 1 + \sum_{i=1}^{n} \alpha_i \langle \frac{\sigma_{eff}}{\sigma_0} - 1 \rangle^i \\ g_1 &= 1 + \sum_{i=1}^{n} \beta_i \langle \frac{\sigma_{eff}}{\sigma_0} - 1 \rangle^i \\ g_3 &= 1 + \sum_{i=1}^{n} \gamma_i \langle \frac{\sigma_{eff}}{\sigma_0} - 1 \rangle^i \\ \alpha_\sigma &= 1 + \sum_{i=1}^{n} \delta_i \langle \frac{\sigma_{eff}}{\sigma_0} - 1 \rangle^i \end{aligned} \tag{3.38}$$

where

$$\langle x \rangle = \begin{cases} x & x > 0 \\ 0 & x \leq 0 \end{cases}$$

the coefficients (α_i, β_i, γ_i, δ_i) can be calibrated from nonlinear parameters at multiple effective stress level, σ_{eff} (which is also the applied stress level). The σ_0 is the corresponding stress level from cycle I, which is considered to behave in linear viscoelastic manner.

3.5.3 Viscoplastic parameters

The viscoplastic strain response is extracted by subtracting the nonlinear viscoelastic strain from total experimental strain at each stress level. The Eq. 3.26 can be rearranged as

$$\frac{\Delta\gamma^{vp}}{\Delta_t} = \Gamma\left[\frac{\tau - \alpha p - [\kappa_0 + \kappa_1(1 - exp(-\kappa_2\varepsilon_e^{vp}))]}{\sigma_y^0}\right]^N \tag{3.39}$$

where τ and p, for a uniaxial compressive multiple-load-creep-unload-recovery (MLCUR) test with a plateau stress of σ_1, are equal to σ_1 and $\sigma_1/3$ in that cycle, respectively. The experimental $\Delta\gamma^{vp}$ can be obtained from

$$\Delta\gamma^{vp} = \frac{\Delta\varepsilon_1^{vp}}{\partial G/\partial\sigma_1} = \frac{\Delta\varepsilon_1^{vp}}{1 - \beta/3} \tag{3.40}$$

where ε_1^{vp} and $\Delta\varepsilon_1^{vp}$ are the measure uniaxial viscoplastic strain and its increment, respectively, in a chosen cycle of the MLCUR experiment data. The effective viscoplastic strain ε_e^{vp} can be calculated for uniaxial compression as (Huang et al., 2011)

$$\varepsilon_e^{vp} = \frac{1}{\sqrt{1 + 2(\frac{1/2+\beta/3}{1-\beta/3})^2}}\sqrt{(\varepsilon_1^{vp})^2 + 2(\varepsilon_2^{vp})^2} \tag{3.41}$$

where ε_2^{vp} is the viscoplastic strain in the radial direction, which can be calculated as (Huang et al., 2011)

$$\varepsilon_2^{vp} = \frac{0.5 + \beta/3}{1 - \beta/3}\varepsilon_1^{vp} \tag{3.42}$$

Part I

Experimental Investigation and Constitutive Models Development for Trabecular Bone

"Success depends upon previous preparation, and without such preparation there is sure to be failure"

Confucius

4

Untreated trabecular bone

Previous studies have shown that under static conditions (or very slow strain rates), the strain in trabecular bone increases non-linearly with applied loads (Keaveny et al., 1994b; Li and Aspden, 1997; Linde and Hvid, 1989; Morgan et al., 2001). However, time dependent behaviour with changing load levels has received limited attention. A few previous studies have considered multiple load levels but different loads were applied to different specimens i.e., each specimen was subjected to a single load level (Bowman et al., 1998, 1994; Moore et al., 2004). Bowman et al. (1994) found a strong power law relationship between the steady state creep rate ($\dot{\varepsilon}_{cre}$) and the applied stress level (σ), but when they included apparent density (ρ) into the relation, the fit did not improve, in fact the r^2 value decreased. Also, Moore et al. (2004) related $\dot{\varepsilon}_{cre}$ to σ, but this study also conducted cyclic loading tests on each sample at a single stress level.

In summary, previous studies have shown that under static loading trabecular bone has a nonlinear stress-strain behaviour and its time-independent elastic modulus (E) can be related to BV/TV. Therefore, the hypothesis of this Chapter is that time-dependent behaviour of trabecular bone can also be related to BV/TV and it is not linearly viscoelastic. The aims of this Chapter are to determine how creep-recovery response varies with load levels and how it can be related to BV/TV.

4.1 Sample preparation

The sample preparation process is summarised in Fig. 4.1. Bovine proximal femurs, female, under 30 months old, were obtained from a local butcher and stored in a freezer at -20 $^{\circ}C$ before further preparation. Femoral heads and greater trochanters were removed using a hacksaw after permitting the bone to thaw at room temperature. Transmission radiographs were taken to identify principal trabecular directions to ensure that samples cored in the following step were aligned along the principal direction. Cylindrical trabecular bone specimens were cored in a hydrated condition, to mitigate against temperature damage, using a 10.7 mm inner diameter diamond-coated coring tool (Starlite, Rosemont, USA). A low-speed saw (Buehler, Germany) was used to trim off growth plate if present and to cut the edges parallel. Fifteen femoral head trabecular bone specimens were obtained from 3 femoral heads and other five from 2 bovine trochanters (length: 24.8 $\pm$ 2.8 mm), where one sample was found to behave poorly and was excluded from the analysis. The specimens' dimensions were measured before being glued into brass end-caps using bone cement (Simplex, Stryker, UK) with assistance of a custom made alignment tool. Effective length for each specimen was calculated as the length between end-caps plus half the length of bone embedded within the end-caps from each side (Keaveny et al., 1997). Mean effective length was 21.9 $\pm$ 2.7 mm. Each

specimen was placed in an epoxy tube filled with phosphate-buffered saline (PBS), as shown in Fig. 4.2, to ensure that the specimens remain hydrated at all stages of testing. The samples were stored in a freezer at -20 $^{\circ}C$ until utilised.

4.2 μCT scanning

All the specimens were scanned with high voxel resolution (17.22 μm) before mechanical testing using μCT scanner (Skyscan 1172, Bruker, Kontich, Belgium). The following scan parameters were used: source voltage 100 kV, current 100 μA, exposure 1771 ms with a 0.5 mm aluminium filter between X-ray source and the specimen. Image quality was improved by using two-frame averaging. The images were reconstructed with no further reduction in resolution using nRecon (V1.6.9.4, Bruker, Kontich, Belgium). Morphometric analysis was performed using CTan software (Bruker, Kontich, Belgium). By considering the whole volume of each specimen, the BV/TV was found in the range 15-54% (mean $\pm$ SD: 37% $\pm$ 11%). DOA and Tb.Th were also evaluated and found in the range of 2.04-16.95 and 168.3-277.3 μm, respectively.

4.3 Mechanical testing (compressive MLCUR)

Mechanical tests were performed at room temperature using Zwick material testing machine (5 kN Load Cell, Model Z005/TH2A, Zwick Roell, Herefordshire, UK). Each specimen was first preconditioned by subjecting it to 10 cycles of compressive loading with an amplitude of 0.1% of apparent strain (Bowman et al., 1994). After preconditioning, the specimen was unloaded, removed from the testing machine and allowed to recover for half an hour. Each specimen was then subjected to compressive multiple-load-creep-unload-recovery (MLCUR) cycles. Loading cycles comprised of applying 2,000 $\mu\varepsilon$, 4,000 $\mu\varepsilon$,

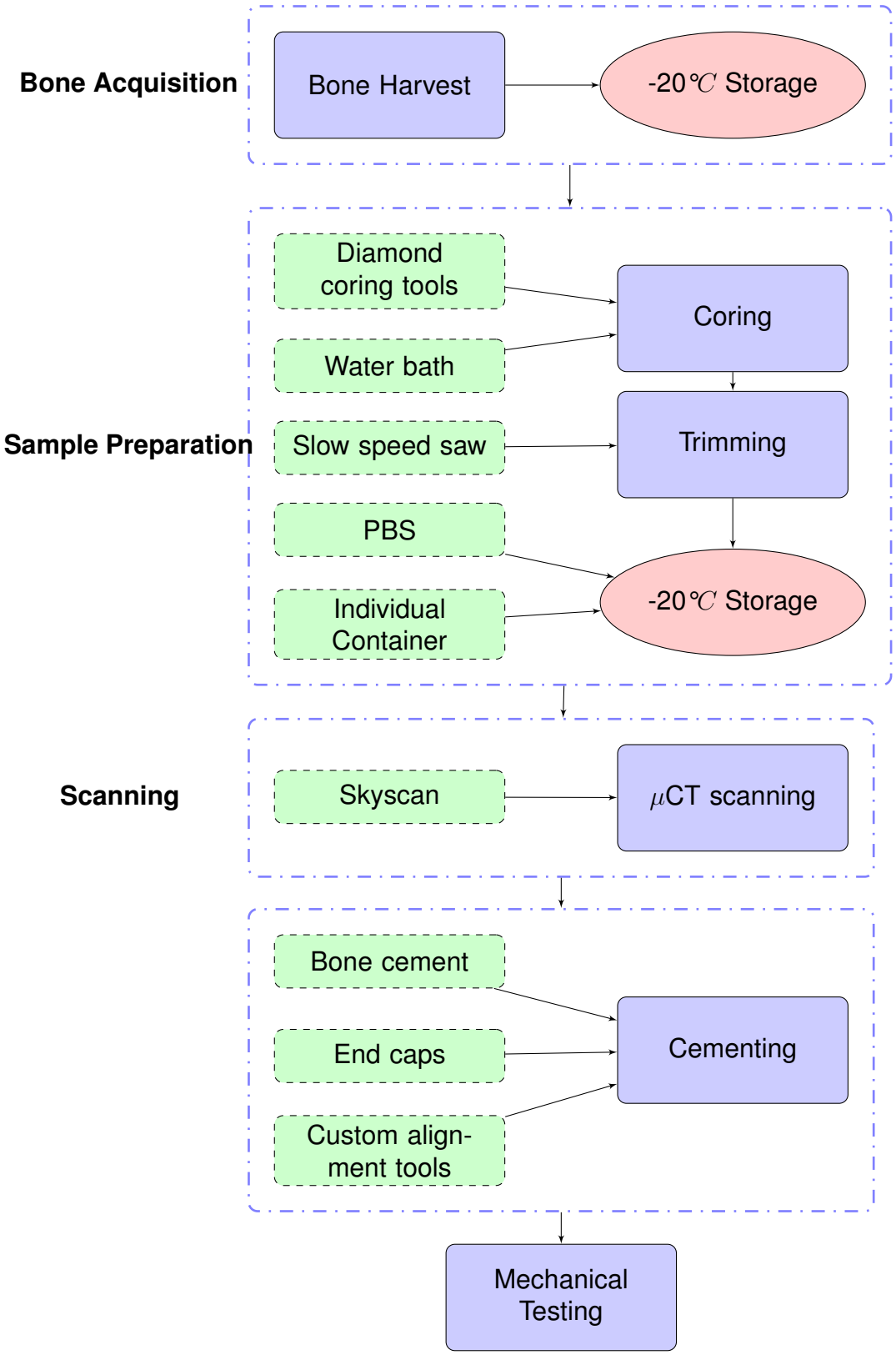

Figure 4.1: Flowchart for experiment process.

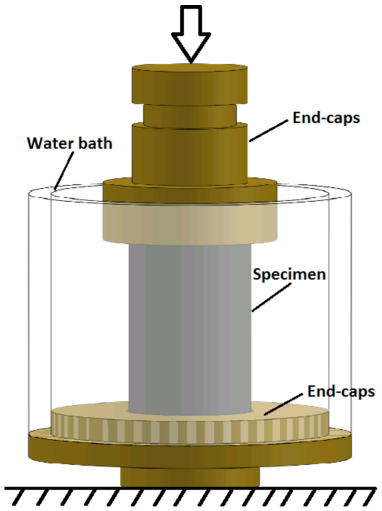

Figure 4.2: A schematic representation of loading set-up. Epoxy tube filled with PBS is used to keep specimen hydrated.

6,000 $\mu\varepsilon$, 8,000 $\mu\varepsilon$, 10,000 $\mu\varepsilon$, 15,000 $\mu\varepsilon$, 20,000 $\mu\varepsilon$ and 25,000 $\mu\varepsilon$ apparent strain at a rate of 10,000 $\mu\varepsilon/s$, denoted as cycle I, II, III, IV, V, VI, VII and VIII, respectively. When the target strain was achieved the corresponding load was maintained for 200 s thereby permitting the specimen to undergo creep. Each loading step was followed by an unloading step to an almost zero force (2 N) and this force was maintained for 600 s before the application of the next load cycle. In other words, this was a load-controlled experiment for creep and recovery while instantaneous loading and unloading were displacement controlled. These durations were selected after a number of preliminary tests which showed that the creep rate becomes constant in less than 200 s upon loading and the recovery curves reach a plateau in less than 600 s. Typical strain response to a MLCUR experiment is shown in Fig. 4.3 with the corresponding loading sequence as an inset in the figure (here, only two cycles are shown, for clarity). The experiment was stopped immediately, if creep strain increased rapidly to beyond 5% in any loading cycle.

Data related to this Chapter can be found at Edinburgh DataShare. It includes μCT images and experiment results and it entitled 'Characterisation of time-dependent mechanical behaviour of trabecular bone samples' (http://dx.doi.org/10.7488/ds/2339).

4.4 Analysis method

In each loading cycle, a number of strain responses were measured, including instantaneous loading strain (ε_l), instantaneous unloading strain (ε_{ul}), creep strain (ε_{cre}), recovery strain (ε_{rec}), residual strain (ε_{res}), steady state creep rate ($\dot{\varepsilon}_{cre}$) and time-varying creep compliance ($\mathbf{C}_{cre}(t)$) (as shown in Fig. 4.3. Detailed definitions of these were provided in Sec. 3.4).

It is important to note that for a linear viscoelastic material, the ratio $\varepsilon_{cre}/\varepsilon_l$ will be constant for different load levels and $\dot{\varepsilon}_{cre}$ will vary linearly with stress level. Also for a viscoelastic material, strain will recover fully if sufficient time is allowed. Strain response ε_l and ε_{cre} may include both recoverable and any irrecoverable components, while ε_{ul} and ε_{rec} only include the recoverable parts.

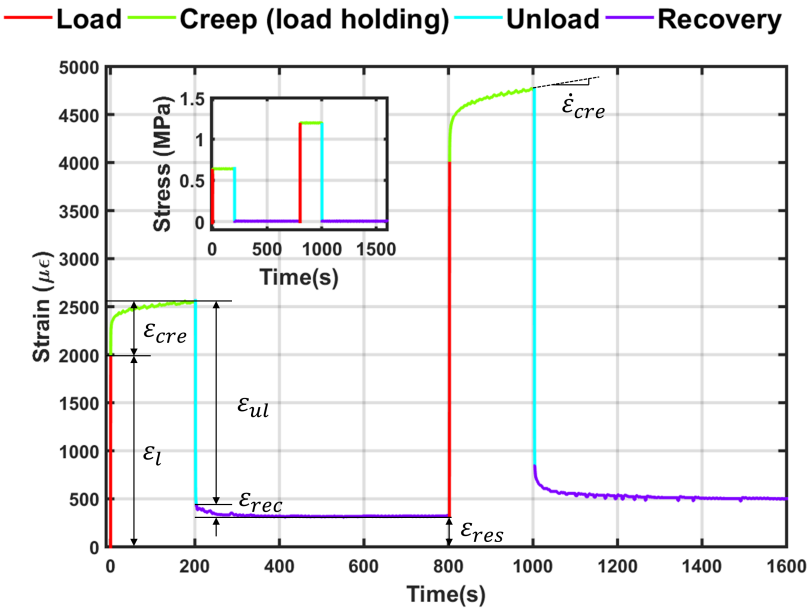

Figure 4.3: Strain response during MLCUR experiment. Load application is shown in the inset. Only two cycles are shown for clarity.

4.5 Results

Without exception, each specimen exhibited classical rapid primary and slow secondary regimes of creep behaviour (Fig. 3.5) across all stress levels. Sixteen samples (thirteen from femoral heads and other 3 from trochanters) are considered in this Chapter and they all could be subjected to cycle V. Four specimens demonstrated tertiary creep on application of cycle VI, and only three specimens could be subjected to cycle VII without tertiary creep. For sake of completeness only the first 5 cycles were considered for most of the analysis in this section.

4.5.1 Time-varying creep compliance

The $\mathbf{C}_{cre}(t)$ is given by Eq. 3.33. Fig. 4.4a, 4.4c and 4.4e show $\mathbf{C}_{cre}(t)$ at different stress levels for 3 typical samples which have significantly different BV/TV (42.8, 25.1 and 18.6%). It can be seen that for the dense sample (Fig. 4.4a) the $\mathbf{C}_{cre}(t)$ initially becomes smaller with increasing load levels (the curves at lower stress levels are above those at higher stress levels) and then increases with the load level, at the largest applied stress (20.55 MPa). For the medium BV/TV sample (Fig. 4.4c), $\mathbf{C}_{cre}(t)$ decreases as the stress level is increased from 0.64 to 1.89 MPa but then increases when stress levels are increased to 2.44 MPa and then to 2.74 MPa. This decrease followed by an increase in $\mathbf{C}_{cre}(t)$ indicates elastic stiffening followed by elastic softening. For the dense sample, softening occurs at a stress level corresponding to a much higher strain in comparison to the medium BV/TV sample. The trend is followed by the low BV/TV sample (Fig. 4.4e), which demonstrates softening with increasing load levels right from the beginning.

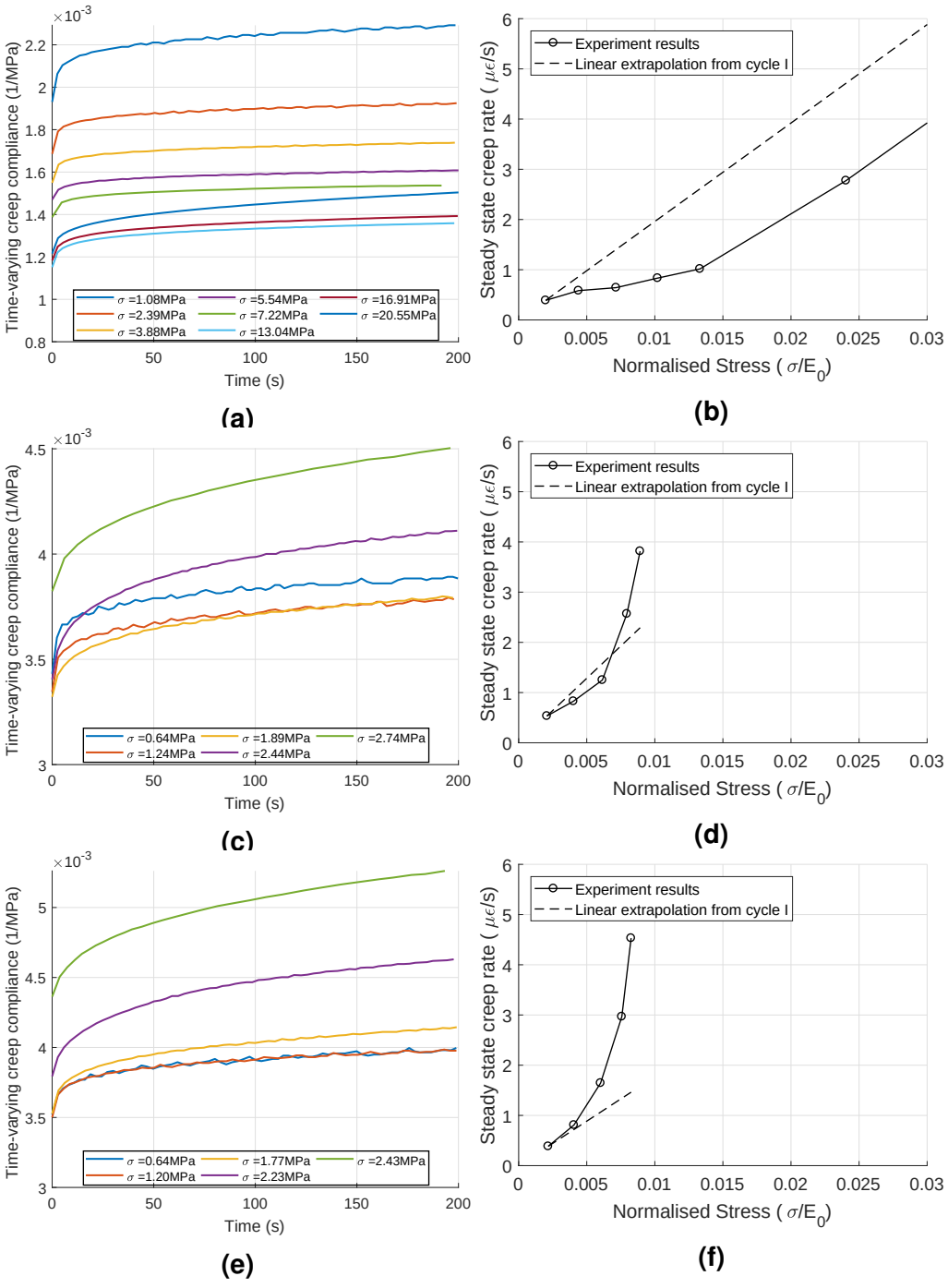

Figure 4.4: Time-varying creep compliance (a, c, e) and steady state creep rate (b, d, f) plots of three typical samples. BV/TV = 42.8% (a , b), BV/TV = 25.1% (c , d), BV/TV = 18.6% (e , f). Dashed line shows extrapolation from the response at the lowest load cycle which is assumed to be linear viscoelastic.

4.5.2 Steady state creep rate

This stiffening-softening phenomenon can also be seen from the steady state creep rate ($\dot{\varepsilon}_{cre}$) variation with normalised stress level (stress in each cycle divided by the modulus obtained from the first cycle) (Figs. 4.4b, 4.4d, and 4.4f), where the experimentally measured $\dot{\varepsilon}_{cre}$ were compared with the linear extrapolation from the cycle I are compared. If the trabecular bone's creep behaviour is linear viscoelastic, then the $\dot{\varepsilon}_{cre}$ will be proportional to the normalised stress levels. Therefore, the $\dot{\varepsilon}_{cre}$ were extrapolated using the response from the first loading cycle (assumed linear), to predict the linear viscoelastic behaviour of trabecular bone. For a high BV/TV specimen (Fig. 4.4b), $\dot{\varepsilon}_{cre}$ is lower than the linear viscoelastic prediction for the first few cycles but higher than the linear viscoelastic prediction at the highest load level applied. For a low BV/TV specimen (Fig. 4.4f), $\dot{\varepsilon}_{cre}$ is higher than linear viscoelastic prediction even at lower stress levels while for the medium BV/TV specimen (Fig. 4.4d) $\dot{\varepsilon}_{cre}$ is lower than the linear viscoelastic prediction for cycles II and III and higher than the linear viscoelastic prediction for cycles IV and V.

Considering all the specimens tested, the steady state creep rate ($\dot{\varepsilon}_{cre}$) was found to vary from 0.07 to 4.51 $\mu\varepsilon/s$. The mean $\dot{\varepsilon}_{cre}$ for load levels corresponding to 2,000 $\mu\varepsilon$ and 10,000 $\mu\varepsilon$ were 0.30 $\mu\varepsilon/s$ ($\pm$0.12) and 1.84 $\mu\varepsilon/s$ ($\pm$1.42), respectively. Regression analysis of the experimental results showed that $\dot{\varepsilon}_{cre}$ had strong nonlinear (power law) relation with normalised stress level as defined by Bowman et al. (1998). The steady state creep rate, $\dot{\varepsilon}_{cre}$, was also found to have a strong relationship with BV/TV. The best fit equation was found to be

$$\dot{\varepsilon}_{cre} = 0.003103\sigma^{1.256}(BV/TV)^{-3.469} \tag{4.1}$$

where $\dot{\varepsilon}_{cre}$ is in $\mu\varepsilon/s$ and σ is in MPa ($r^2 = 0.74, p < 0.001$). Figure 4.5 shows the relationship along with actual data points.

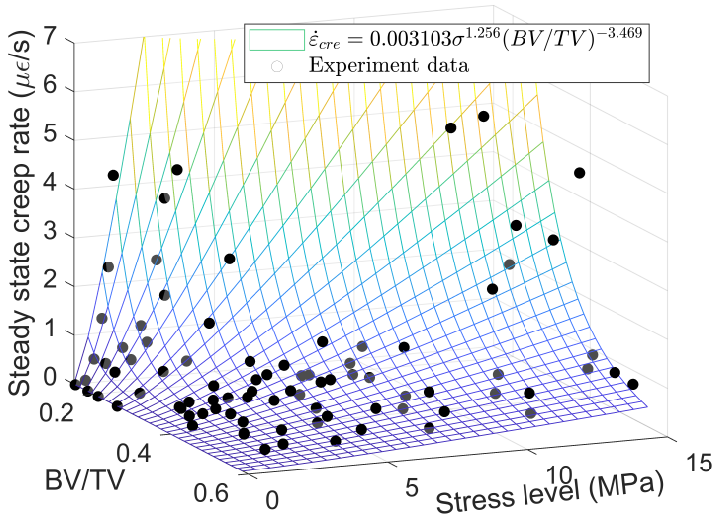

Figure 4.5: Curve fit of $\dot{\varepsilon}_{cre}$ with applied stress level (σ) and bone volume fraction (BV/TV).

4.5.3 Mean strain responses

Figure 4.6a shows a bar plot of the measured mean strain responses for different load cycles for all samples tested. Figure 4.6b shows the ratios of different strain responses against load cycles.

The ratio of $\varepsilon_{ul}/\varepsilon_l$ increased with increasing corresponding strain level for all the specimens (Fig. 4.6b). The majority of instantaneous strain was recovered immediately upon unloading (average 86.5% for pooled data, r^2 = 0.99).

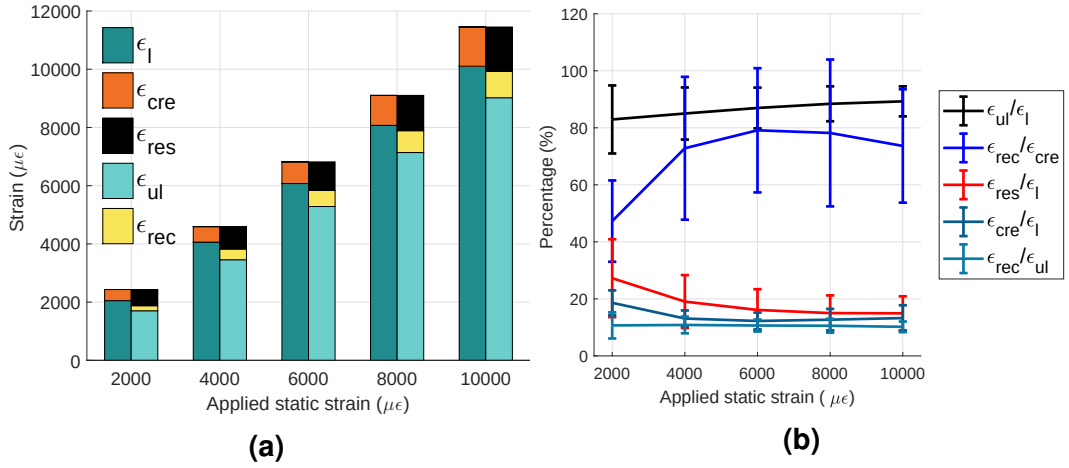

Figure 4.6: Measured strain response during MLCUR experiments. Mean strain response for the 16 samples tested for the five creep-recovery cycles (a); Strain ratio and their variation for different creep-recovery cycles (b). (Large BV/TV variation results in large variation for some of the ratios).

Creep strain during stress holding cycle, ε_{cre}, was found to increase with increasing load level (Fig. 4.6a). From cycle I to cycle V it increased from 377 $\mu\varepsilon$ ($\pm$84) to 1,365 $\mu\varepsilon$ ($\pm$498), however, the ratio $\varepsilon_{cre}/\varepsilon_l$ was found to decrease after the first load cycle after which it remained almost constant (Fig. 4.6b).

As expected, ε_{ul} and ε_{rec} both increased with increasing load level (Fig. 4.6a), from 1718 $\mu\varepsilon$ ($\pm$266) and 180 $\mu\varepsilon$ ($\pm$45) to 9048 $\mu\varepsilon$ ($\pm$544) and 928 $\mu\varepsilon$ ($\pm$157), respectively, and had relatively constant ratio of $\varepsilon_{rec}/\varepsilon_{ul}$ (Fig. 4.6b) indicating that, as would be expected, the unloading phase is viscoelastic.

As mentioned above both ε_{cre} and ε_{rec} increased with increasing load levels (Fig. 4.6a), however, the ratio, $\varepsilon_{rec}/\varepsilon_{cre}$, had a very interesting trend $-$ it first increased with load level and then decreased at higher load level (Fig. 4.6b). This trend again indicates elastic stiffening is followed by elastic softening with increasing load levels as demonstrated earlier by individual samples.

4.5.4 Residual strain

The results showed that some residual strain, ε_{res}, always exists at the end of 600 s of recovery after every unloading cycle and for all the specimens tested. The mean residual strain (Fig. 4.6a) ($\pm$SD) at the lowest load level corresponding to instantaneous loading strain of 2,000 $\mu\varepsilon$ was 542 $\mu\varepsilon$ ($\pm$255) and for higher load level corresponding to instantaneous loading strain of 10,000 $\mu\varepsilon$ was 1,523 $\mu\varepsilon$ ($\pm$604). The ratio of $\varepsilon_{res}/\varepsilon_l$ was found to decrease with increasing load level (Fig. 4.6b) indicating that residual strain does not increase proportionally with load level.

4.6 Discussion

The results show that residual strain arises even at low load levels, trabecular bone response is not linear viscoelastic and that bone demonstrates stiffen-

ing followed by softening with increasing load levels. It is now recognised that the yield strain of trabecular bone is independent of BV/TV (Bayraktar and Keaveny, 2004; Levrero-Florencio et al., 2016). The trabecular bone macroscopically yields below 0.8% strain in compression (Morgan and Keaveny, 2001). Therefore, this study considered compression force equivalent to different strain levels (from 2,000 $\mu\varepsilon$ to 25,000 $\mu\varepsilon$), to examine the time-dependent behaviour of trabecular bone in pre- and post-yield regimes.

4.6.1 Time-varying creep compliance

Examination of creep compliance curves for different samples shows that they vary with load levels. The samples with medium BV/TV show an initially decreasing and then increasing creep compliance with increasing stress. This indicates that the samples first becomes stiffer and then experience softening (stiffness degradation). High BV/TV samples demonstrate decreasing creep compliance with stress indicating stiffening and an increase is observed only at much higher stress levels. For low BV/TV samples compliance increased with stress levels indicating softening from the start. This behaviour was also demonstrated by steady state creep rate comparison with creep rate linearly extrapolated from the first cycle: for low BV/TV samples the steady state creep rate is higher than linear extrapolation throughout; for high BV/TV samples it is below the linearly extrapolated values for most stress levels; and for medium BV/TV samples it is initially below the linear extrapolation and then above at higher stress levels. On an average the ratio initially increases and then decreases with stress level again demonstrating stiffening and softening behaviour. It is, however, not apparent why this occurs; it could be due to the reorganisation of ultrastructural components (i.e. mineral and collagen) in the bone matrix that make it stiffer initially followed by damage and buckling of trabeculae causing softening. Although the movement of collagen is constrained

by mineral (Bonar and Glimcher, 1970), sliding of collagen fibrils plays an important role in the time-dependent properties of bone (Bowman et al., 1998; Sasaki and Odajima, 1996; Yamashita et al., 2001). It is likely that collagen fibrils initially reorganise when the load levels are increased to resist deformation and maintain network integrity, and at larger loads micro-damage breaks this integrity. For specimen with lower BV/TV, it starts softening at the lower stress levels, possibly because it has less ability of reorganisation of collagen, the damage dominate the mechanics. On the other hand, for specimen with higher BV/TV, it shows stiffening at lower stress levels, which indicates it has better capability of collagen reorganisation, it only softens at relative larger stress level where damage dominates the mechanics.

4.6.2 Steady state creep rate

Kim et al. (2011) reported mean $\dot{\varepsilon}_{cre}$ of 0.22 $\mu\varepsilon/s$ when the specimens were compressed at force equivalent to 2,000 $\mu\varepsilon$ (Cycle I in this case). This compares well with the mean value (0.30 $\mu\varepsilon/s$) found in this study. This study also found that at cycle V the steady state creep rate (1.84 $\mu\varepsilon/s$) was more than five times the value at cycle I and increased stress level does not result in a linear increase, which would be expected from a linear viscoelastic material. The steady state creep rate can be reasonably well related to stress level and BV/TV.

4.6.3 Mean strain responses

Ratio of $\varepsilon_{ul}/\varepsilon_l$, was found to be high ($>$80%) and increase slightly with increasing load level. For a viscoelastic material in a creep-recovery experiment (instantaneous loading and unloading) this ratio is unity. The ratio $\varepsilon_{ul}/\varepsilon_l$ $<$1 possibly indicates presence of irrecoverable strains arising during the loading phase. Yamamoto et al. (2006) found little difference between instantaneous

loading and unloading strains. Kim et al. (2011) considered a single load level and found that 92.3% of strain was recovered immediately upon unloading. Kim et al. (2011) suggested that the difference between ε_{ul} and ε_{l} implies a re-organisation of micro- or ultra-structural components of the bone matrix caused by compressive creep and this reorganised state is not fully released upon unloading. Smallest $\varepsilon_{ul}/\varepsilon_{l}$ ratio at the low load level indicates that most reorganisation of the bone matrix happens at its first loading experience. The fact that the majority of the strain was recovered upon unloading and the recovery was found to be true for all specimens and for all load cases.

This ratio $\varepsilon_{rec}/\varepsilon_{ul}$ was found to be approximately constant in this study indicating that the unloading and recovery phase is viscoelastic. The ratio $\varepsilon_{cre}/\varepsilon_{l}$ was found to decrease with increasing applied stress level initially and then become almost constant (it slightly increased at higher stress levels in samples which were tested beyond the 5 cycles). This study found $\varepsilon_{rec}/\varepsilon_{ul} > \varepsilon_{rec}/\varepsilon_{ul}$ for all stress levels indicating presence of irrecoverable strains arising in the loading and load holding phases.

4.6.4 Residual strain

Strain, ε_{res}, always exists even at low load levels, which implies that certain amount of irrecoverable strain is generated during loading and load holding. This study found that the average ratio of residual strain to loading strain ($\varepsilon_{res}/\varepsilon_{l}$) varied from 26% in the cycle I to 15% in the cycle V. Yamamoto et al. (2006) measured of human L3 vertebral trabecular bone and reported mean values of 515 $\mu\varepsilon$ and 1,565 $\mu\varepsilon$ for load levels corresponding to 750 $\mu\varepsilon$ and 1,500 $\mu\varepsilon$, respectively i.e. $\varepsilon_{res}/\varepsilon_{l}$ ratios of 69% and 104%. Similarly, Kim et al. (2011) reported an average $\varepsilon_{res}/\varepsilon_{l}$ value of 90% at load level corresponding to 2,000 $\mu\varepsilon$. In both these studies the load holding time was much longer – Yamamoto et al. (2006) held the load for around 35 hours while Kim et al. (2011)

held it for 2 hrs. Yamamoto et al. (2006) extrapolated that the residual strain may fully recover in sufficiently long time (20 times the load holding time). Tests conducted in this study showed that the decrease in beyond 600 s was negligible i.e. these residual strains were largely irrecoverable. Large $\varepsilon_{res}/\varepsilon_l$ ratios in the above cited studies in comparison to this indicate that irrecoverable strains accumulate during load holding.

4.6.5 Clinical implications

An important clinical implication of the present study relates to the possible role of creep mechanisms and deformations in non-traumatic bone fractures. Non-traumatic vertebral fracture presents as shortening or height loss of bone without obvious trauma, and the progression is very slow and occurs gradually over a long period (Nicholson et al., 1993; Pollintine et al., 2009). Results from this study show that residual strain always exists even at low stress level, and it is accumulated with increasing stress levels. Trabecular bone with relative low BV/TV has larger value of steady state creep rate, and it starts softening at low stress level. Schaffler et al. (1995) suggested that creep deformity could accumulate over time in elderly human bones due to their reduced ability to remodel. These findings from current study show that elderly people who suffer from osteoporosis and consequently have low BV/TV are at greater risk of non-traumatic fractures even under normal physiological loads.

4.7 Limitations

This work suffers from a few limitations. Firstly, all the tests were conducted at room temperature; creep behaviour has been reported to be temperature dependent (Bonfield and Li, 1968; Bowman et al., 1998). Secondly, the identification of instantaneous (loading and unloading) strain responses from the

time-dependent strain response in MLCUR experimental curves was done using the loading platens of the machine rather than an extensometer attached to the central region with a more homogeneous mechanical environment, which may result-in small errors in the analysis of the results. Thirdly, a small force of 2 N was used during recovery phase to make sure that the end-caps were in contact with the load applicator to facilitate the measurement of the strain response. The effect of this small load is likely to be small on the measured response. Lastly, it is not possible in practice to perform ideal creep-recovery experiments. Small viscoelastic deformations are likely to occur during the ramp loading (1 s to reach 1.0% strain with strain rate 0.01 s^{-1} employed). The amount of viscoelastic deformation is likely to be small compared with instantaneous deformation and the total creep deformation during stress holding.

4.8 Conclusions

- Majority of strain is recovered after unloading phase, but some residual strain always exists even at the low load level (corresponding to 2,000 $\mu\varepsilon$, which is below physiological strain level, 3,000 $\mu\varepsilon$).
- Time-dependent response of trabecular bone comprises of both recoverable and irrecoverable strain.
- The strain response is nonlinearly related to applied load levels.
- The time-dependent response is BV/TV dependent; elastic stiffening followed by elastic softening is observed for relatively denser bone, while elastic softening may start at a very low load level for porous bone.
- Steady state creep rate is related to both applied stress level and BV/TV, a best fit equation was found (Eq. 4.1).

"Study without desire spoils the memory, and it retains nothing that it takes in."

Leonardo da Vinci

5

Constitutive models for untreated trabecular bone

The characterisation of time-dependent properties of bone is not well documented, and only a few studies are available, which related the steady state creep rate ($\dot{\varepsilon}_{cre}$) with normalised stress level (σ/E_0) (Bowman et al., 1994), but they do not fully describe the constitutive behaviour of trabecular bone and as such cannot be incorporated in FE codes. At the same time many constitutive equations have been developed for characterising nonlinear viscoelastic behaviour of different materials and these include single (Christensen, 1980; Knauss and Emri, 1981; Schapery, 1969) and multiple (Findley et al., 1976) integral formulations. The single integral representations have been the most wildly applied theories for different viscoelastic materials and are relatively easy to implement in a numerical scheme (Schapery, 1969). Previous studies

have developed methodologies to determine the nonlinear viscoelastic parameters based on single integral formulations for materials with power law time dependence (Lou and Schapery, 1971) and with Prony series time dependence (Huang et al., 2011). These formulations have been used for material like asphalt concrete and polymers (Huang et al., 2011). This Chapter employs the Prony series to describe time-dependent behaviour for trabecular bone; the background for this development was considered in Chapter 3.

BV/TV or apparent density (ρ) have been extensively employed to evaluate the time-independent stiffness of bone (Morgan et al., 2003), which is then used in subject-specific models (Pankaj, 2013). Similar relationships between BV/TV and time-dependent response will permit their application in computational simulations where modelling time dependent behaviour is important (*e.g.* implant loosening). These relationships need to be considered at multiple loads to incorporate any load-level dependence.

The data used in this Chapter is identical to that obtained from experiments described in last Chapter. The development of constitutive models is discussed in Chapter 3 (Sec. 3.5)

5.1 Sensitivity to the number of Prony terms

Prony series (discussed in Chapter 3) was chosen as the function to represent the time-dependent behaviour of trabecular bone, so the sensitivity of the response on number of Prony terms needs to be considered. A random typical sample's first cycle is shown in Fig. 5.1a, which is compared using 1 to 6 terms of the Prony series. Figure 5.1b shows the residual sum of squares *vs.* number of Prony terms, it is clear that the residual sum squares are decreased with increasing number of terms, and 3 terms of Prony series are enough to predict the creep behaviour and it give an error of less than 0.3%. This was found to be the case with a number of other samples considered.

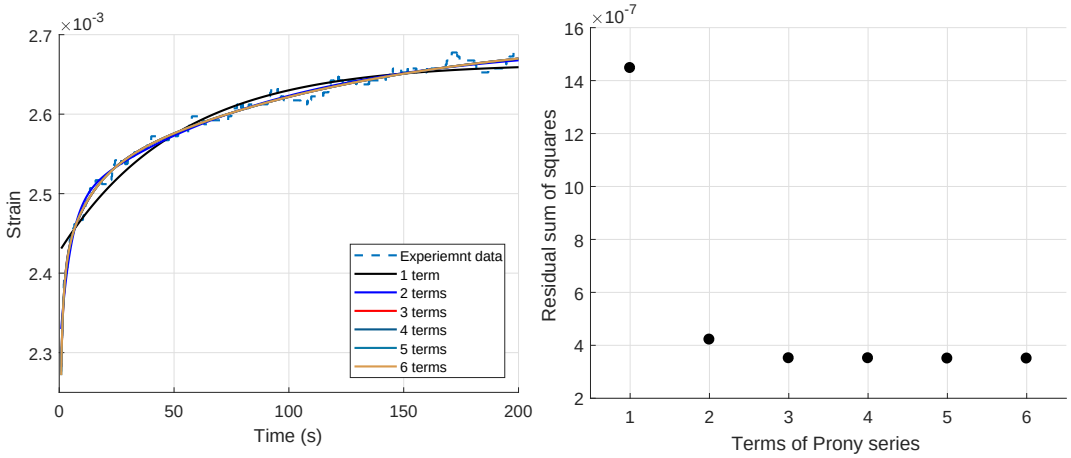

Figure 5.1: Sensitivities study on number of Prony terms in constitutive model. It conducted by fitting the experimental strain response with Prony series for one random sample's first cycle's creep strain response. Creep strain response along with Prony series fitting (a), residual sum of squares with respect to number of Prony terms (b).

5.2 BV/TV-viscoelastic relationship (creep part)

The experimental creep curves and $\mathbf{C}_{cre}(t)$ corresponding to cycle I for 13 selected samples are shown in Fig. 5.2, their compliance after 200 s constant load was in the range of 1.08×10^{-3} - 4.17×10^{-3} MPa^{-1}. The trabecular bone was loaded at small stress level (corresponding to 2,000 $\mu\varepsilon$). The linear viscoelastic parameters based on 3-term Prony series were evaluated by minimising experimental measurements with Eq. 3.15 and all the evaluated parameters are listed in Table 5.1, which include the instantaneous compliance (D_g), transient compliance (D_n) and retardation time (τ_n). The evaluated D_g for all the samples was in the range of $9.40 \times 10^{-4} - 34.36 \times 10^{-4}$ MPa^{-1}.

5.2.1 BV/TV-creep function

BV/TV or ρ have been extensively employed to evaluate the time-independent stiffness of bone, which is then used in subjected-specific models. As discussed in Chapter 4 this time-dependent behaviour was found to be associated to bone's BV/TV from experimental observation (Sec. 4.5). Also a strong power

Table 5.1: The value of linear viscoelastic properties of bovine trabecular bone from first cycle's creep behaviour (Manda et al., 2016b)

BV/TV	$\sigma(MPa)$	D_g	$D_n \times 10^{-4}$			$\tau_n(s)$			E_e	E_i			ρ_n		
		$\times 10^{-4}$	D_1	D_2	D_3	τ_1	τ_2	τ_3		E_1	E_2	E_3	ρ_1	ρ_2	ρ_3
0.19	0.64	34.36	1.84	1.25	2.48	1.54	24.42	284.12	250.43	14.94	9.15	16.53	1.46	23.59	266.41
0.21	0.60	34.38	3.17	1.64	3.40	0.42	8.95	161.57	234.83	24.64	11.16	20.24	0.39	8.57	148.71
0.25	0.64	35.24	1.30	1.31	2.63	1.76	13.21	155.22	247.06	10.20	9.49	17.04	1.69	12.74	145.13
0.26	0.80	26.80	1.65	1.33	1.75	0.95	8.74	128.76	317.18	21.83	15.54	18.51	0.90	8.35	121.60
0.33	1.19	17.54	1.10	0.67	0.75	0.98	8.26	101.45	498.53	34.09	18.24	19.13	0.92	7.97	97.67
0.35	1.31	15.99	0.83	0.65	1.14	1.41	10.59	130.74	537.18	31.30	21.99	34.79	1.34	10.20	122.73
0.35	0.94	21.70	1.38	1.10	1.41	0.75	8.31	157.54	390.70	27.90	19.49	22.71	0.71	7.93	148.85
0.39	1.33	15.36	1.06	0.84	1.07	0.79	8.15	157.22	545.65	42.47	29.54	33.56	0.74	7.75	148.03
0.40	0.77	26.93	1.26	0.92	1.02	0.87	6.39	103.02	332.01	16.73	11.08	11.58	0.83	6.19	99.53
0.42	1.37	14.76	1.06	0.79	0.87	0.35	5.68	115.70	572.05	45.69	30.06	29.85	0.33	5.41	109.94
0.43	1.08	19.43	1.19	0.93	1.75	1.28	10.45	135.57	429.24	30.05	20.79	34.48	1.21	10.00	125.41
0.43	2.13	9.40	0.64	0.37	0.65	1.06	9.47	148.63	904.68	68.15	34.72	55.87	0.99	9.13	139.94
0.46	1.75	11.59	0.89	0.42	0.58	1.50	14.46	156.06	741.75	61.76	25.77	33.23	1.39	13.99	149.33

BV/TV is the bone volume fraction, σ (MPa) is the applied stress, D_g is the instantaneous compliance in $1/MPa$, D_n are transient compliance coefficients in $1/MPa$ and τ_n (s) are retardation time in Prony series in s^{-1} (see also Eq. 3.15)

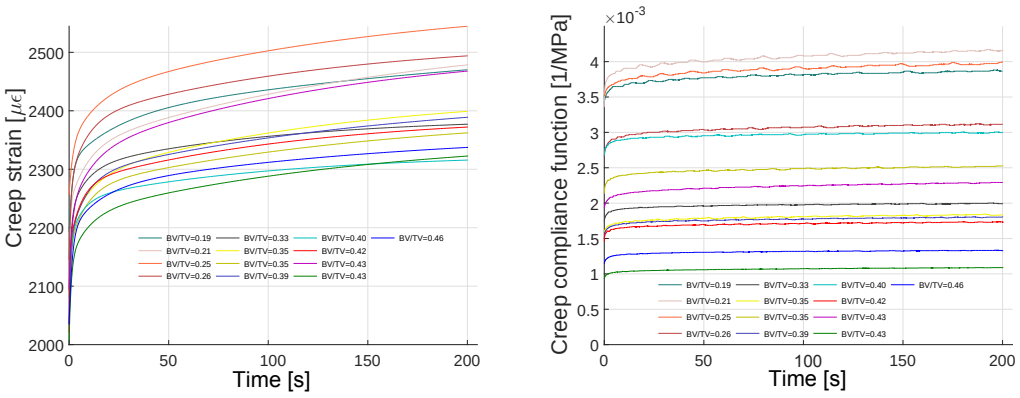

(a) **(b)**

Figure 5.2: Experimental creep responses with varying BV/TV. Creep strain (a) and time-varying creep compliance (creep strain/applied stress) curves (b) for 13 samples (Manda et al., 2016b).

law relationship was found between D_g and BV/TV (Manda et al., 2016b),

$$D_g = 6.6 \times 10^{-4}(\text{BV/TV})^{-1.043}(r^2 = 0.72, p < 0.001) \tag{5.1}$$

as shown in Fig. 5.3. Consequently, the relationship between time-dependent behaviour and BV/TV was considered, assuming that the BV/TV (ϕ) can be the lone predictor for time-dependent response of trabecular bone. By minimising the error using nonlinear least squares, the relationship between $D(t)$ and BV/TV was found to be ($r^2 = 0.73, p < 0.001$) (Manda et al., 2016b)

$$D(t) = A\phi^m + A[\sum_{n=1}^{N} \tilde{D}_n(1 - exp(-t/\tilde{\tau}_n))\phi^{m_t}] \tag{5.2}$$

This is a BV/TV-based Prony series expanded from the original equation (Eq. 3.15), which makes BV/TV the only variable in this equation. $\tilde{D}_n$ represent the dimensionless transient compliance coefficient, $\tilde{\tau}_n$ are time coefficients, ϕ is the BV/TV of trabecular bone, and A, m, m_t are constant. All the evaluated constant parameters are reported in Table 5.2. Three typical samples with BV/TV of 26%, 35% and 46% were chosen to show the representative behaviour of the samples. The predicted viscoelastic response for those three

typical samples are shown in Fig. 5.4. The maximum error between the measured and the predicted value from Eq. 5.2 were -1.8, -11.6 and 28.8% for BV/TV of 26%, 35% and 46%, respectively. The negative error value indicates the under-prediction of the power law model, whereas positive error indicates the over-prediction of the model compared to the experimentally measured response.

Table 5.2: Constant coefficients for BV/TV-based Prony series (Manda et al., 2016b)

Function	Equation	Parameters		
Creep compliance function $D(t)$	Eq. 5.2	$A = 6.6 \times 10^{-4}$	$m = -1.033$	$m_t = -1.058$
		$\tilde{D}_1 = 0.026$	$\tilde{D}_2 = 0.071$	$\tilde{D}_3 = 0.093$
		$\tilde{\tau}_1 = 14.237$	$\tilde{\tau}_2 = 1.255$	$\tilde{\tau}_3 = 250.0$
Relaxation modulus function $E(t)$	Eq. 5.3	$B = 2043.0$	$p = 1.414$	$p_t = 1.014$
		$\tilde{E}_1 = 0.028$	$\tilde{E}_2 = 0.049$	$\tilde{E}_3 = 0.039$
		$\tilde{\rho}_1 = 8.828$	$\tilde{\rho}_2 = 0.929$	$\tilde{\rho}_3 = 133.23$

5.2.2 BV/TV-relaxation function

The creep compliance functions were converted to time-dependent relaxation functions using numerical interconversion methods (Park and Schapery, 1999). The long-term or equilibrium modulus (E_e) for all samples is shown in Table 5.1 and is in the range of 234.8-904.6 MPa; it was found to follow a

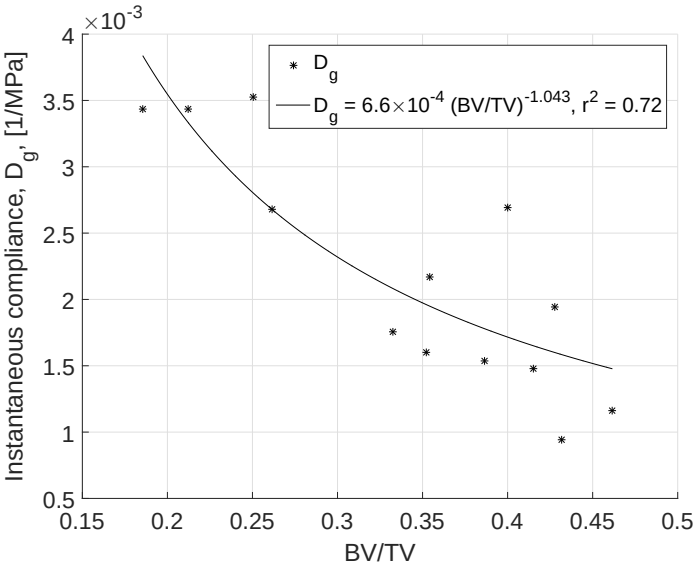

Figure 5.3: Instantaneous compliance (D_g) plotted against BV/TV with power law relationship ($r^2 = 0.72, p < 0.001$) (Manda et al., 2016b).

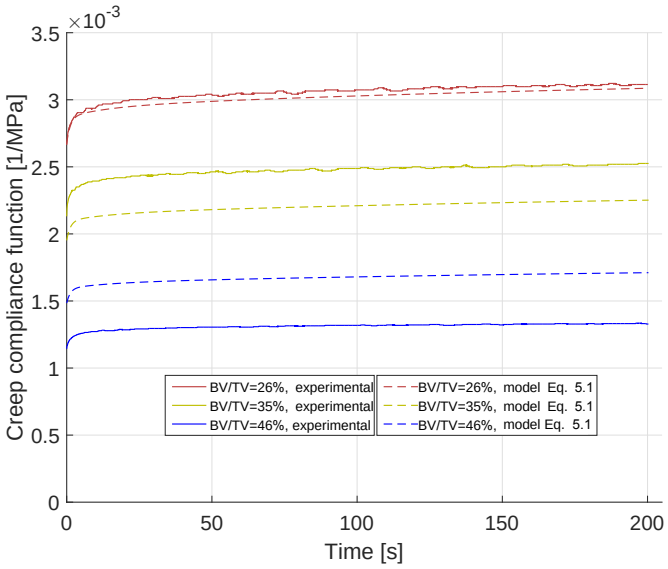

Figure 5.4: Predicted creep response from BV/TV-creep function prediction. It shows both experimental and predicted time-varying creep compliance ($\mathbf{C}_{cre}(t)$) from BV/TV-based Prony series for three typical samples (Manda et al., 2016b).

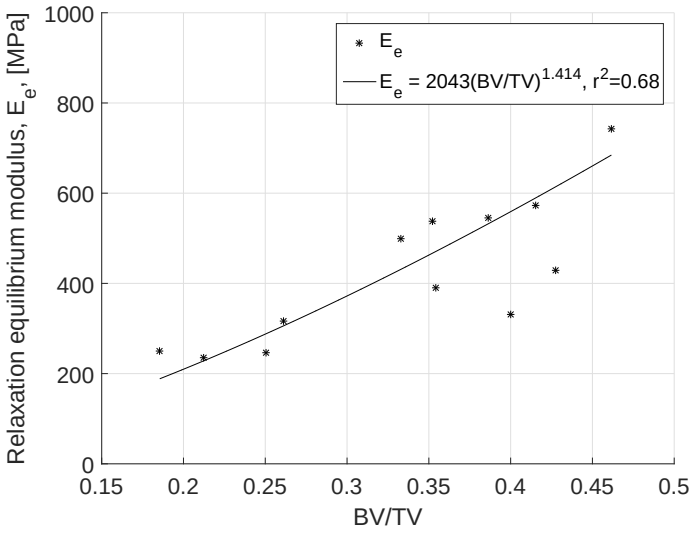

Figure 5.5: Equilibrium relaxation modulus, E_e plotted against BV/TV with power law relationship ($r^2 = 0.68, p < 0.001$) (Manda et al., 2016b).

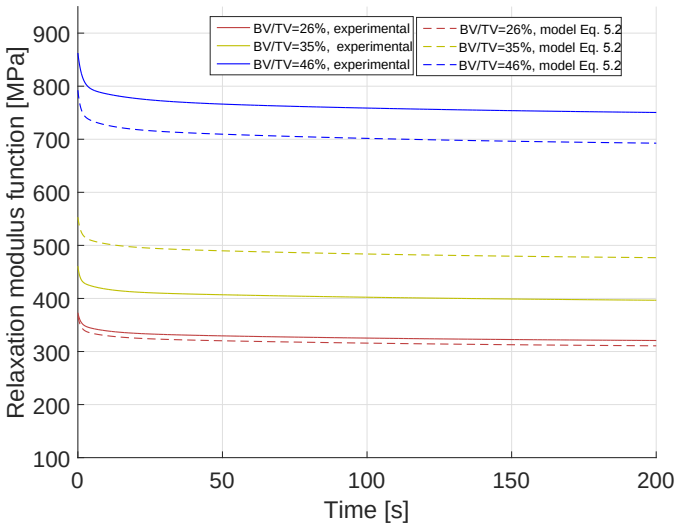

Figure 5.6: Accuracy of BV/TV-relaxation function prediction. Dotted lines with same colour show the predictions from regression model from Eq. 5.3 (Manda et al., 2016b).

power law relation with BV/TV as shown in Fig. 5.5 . Using an approach similar to that used for compliance functions, a relationship between time-dependent relaxation modulus function, $E(t)$, and BV/TV (ϕ) over time was found ($r^2 = 0.68, p < 0.001$) (Manda et al., 2016b).

$$E(t) = B\phi^p + B[\sum_{i=1}^{3} \tilde{E}_i exp(-t/\tilde{\rho}_i)\phi^{p_t}] \tag{5.3}$$

where $\tilde{E}_i$ represents the dimensionless transient moduli and are expressed as fractions of equilibrium modulus, $\tilde{\rho}_i$ are time coefficients, and B, ρ and ρ_t are constants. All evaluated parameters are reported in Table 5.2, and the resulting predicted viscoelastic response is shown in Fig. 5.6 for samples with BV/TV of 26%, 35% and 46%. For these three samples, the maximum errors between the measured and the predicted values from Eq. 5.3 were 3.1%, -20.3%, and 8.4% with BV/TV of 26%, 35% and 46%, respectively.

5.3 Nonlinear viscoelasticity (recovery part)

It is important to note that the unloading phase contains recoverable strain only, while the loading phase may consist of some irrecoverable strain. The recoverable strain response was found to be nonlinear with respect to the stress (see Sec. 4.6), therefore, Schapery's nonlinear model was employed. The linear viscoelastic parameters were obtained from its first cycle's unloading phase (which was assumed linear), then the nonlinear parameters can be determined from its higher unloading cycles. Three typical specimens' time-dependent response from unloading phase are shown in Fig. 5.7. These samples have significant different BV/TV of 25%, 33% and 46%. Amount of strain recovered increased with time for all stress levels. The first cycle's recovery behaviour was assumed as linear viscoelastic, and the 3-term Prony series was found to describe their time-dependent response well (Fig. 5.7). Linear Prony coeffi-

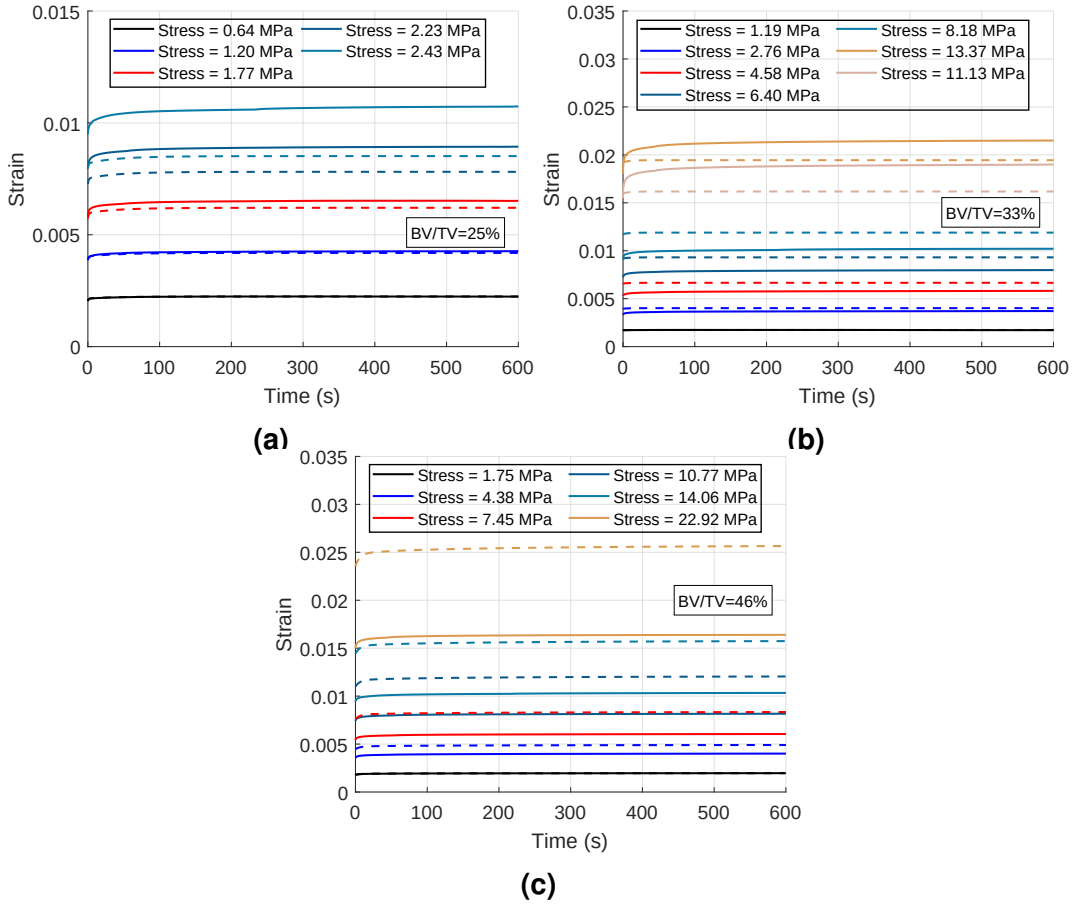

Figure 5.7: The recovery strain (unloading phase) of trabecular bone plotted against increased stress levels. BV/TV = 25% (a), BV/TV = 33% (b) and BV/TV = 46% (c). Dotted line are strain prediction for its higher stress levels by extrapolation from its first cycle's recovery behaviour.

cients at Cycle I are shown in Table 5.3 for all 19 samples.

If the material behaves in linear manner, then the strain response at the higher stress levels should be able to be described by Prony's parameters obtained from its first cycle. The experimental curves at the higher stress levels did not match with the linear extrapolation from its first cycle, which also implies that trabecular bone behaves in a nonlinear manner. For the most porous sample considered (Fig. 5.7a), the predicted strain was always smaller than experimental strain response, while for denser sample (Fig. 5.7c), the predicted strain was higher than the experimental strain response. For the samples with BV/TV in the middle (Fig. 5.7b), the predicted strain response was higher than experimental strain response at the lower stress levels and lower than experi-

mental curve at the higher stress level. As discussed in Chapter 4 (Sec. 4.5), the porous sample demonstrates softening from beginning (Fig. 5.7a), while dense sample demonstrates stiffening first and the softening only observed at higher stress level (Fig. 5.7c). This is also shown in Fig. 5.8. This indicated that a nonlinear constitutive model is needed.

The time-varying creep compliance ($\mathbf{C}_{cre}(t)$) is a measurement independent of applied stress level for linear viscoelastic material (as discussed in Sec. 3.4.1). It is clear that from experimental observations (Sec. 4.5) and Fig. 5.8, the time-varying recovery compliance for trabecular bone are not linear with stress levels. So, Schapery's nonlinear model was employed, and the nonlinear parameters obtained by nonlinear least square fitting of the experimental recovery curve with Eq. 3.35 and 3.36. All the nonlinear parameters are listed in Table 5.3.

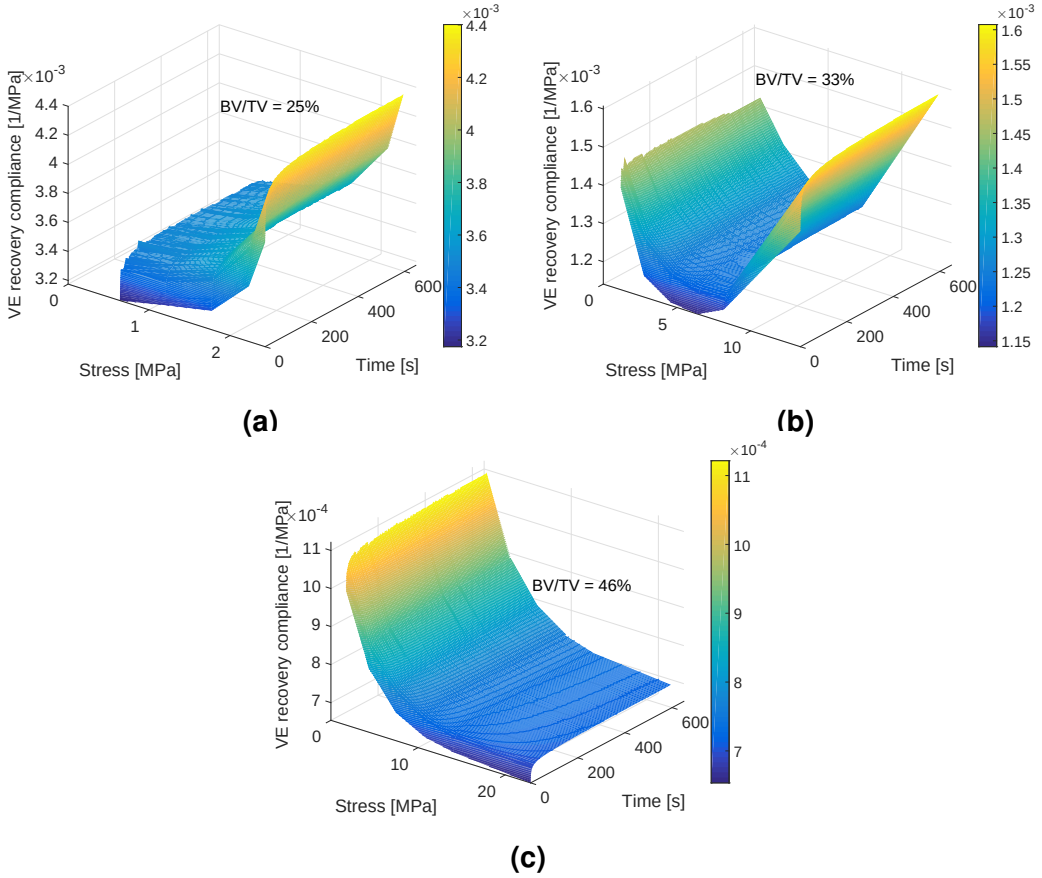

Figure 5.8: Experimental viscoelastic recovery compliance with the time and stress for three typical samples (Manda et al., 2016a).

Table 5.3: The nonlinear VE parameters along with linear Prony coefficients and irrecoverable strains at multiple stress levels for all 19 samples (Manda et al., 2016a)

BV/TV	Linear coefficients at Cycle I	Cycle No.	ε_l[%]	$\sigma^N[MPa]$	Nonlinear VE parameters				ε_{res}[%]
					g_0	g_1	g_2	a_σ	
0.15	$\begin{bmatrix} D_g \\ D_1 \\ D_2 \\ D_3 \\ \lambda_1 \\ \lambda_2 \\ \lambda_3 \end{bmatrix} = \begin{bmatrix} 6.40e-03 \\ 5.48e-04 \\ 3.24e-04 \\ 2.97e-04 \\ 8.64e-03 \\ 8.64e-01 \\ 9.31e-02 \end{bmatrix}$	I	0.20	0.36	1.00	1.00	1.00	1.00	0.041
		II	0.40	0.66	0.91	1.06	0.59	0.78	0.067
		III	0.60	0.94	0.94	1.03	0.67	0.82	0.104
		IV	0.80	1.17	0.99	1.01	0.82	0.85	0.158
		V	1.00	1.35	1.10	0.96	0.84	0.91	0.237
0.19	$\begin{bmatrix} D_g \\ D_1 \\ D_2 \\ D_3 \\ \lambda_1 \\ \lambda_2 \\ \lambda_3 \end{bmatrix} = \begin{bmatrix} 3.44e-03 \\ 1.85e-04 \\ 1.25e-04 \\ 2.47e-04 \\ 6.51e-01 \\ 4.12e-02 \\ 3.57e-03 \end{bmatrix}$	I	0.20	0.64	1.00	1.00	1.00	1.00	0.024
		II	0.40	1.24	0.89	0.85	0.94	0.88	0.045
		III	0.60	1.89	0.87	0.89	1.02	0.92	0.076
		IV	0.80	2.44	0.85	0.86	1.50	0.86	0.150
		V	1.00	2.74	0.90	0.85	1.51	0.90	0.230
0.21	$\begin{bmatrix} D_g \\ D_1 \\ D_2 \\ D_3 \\ \lambda_1 \\ \lambda_2 \\ \lambda_3 \end{bmatrix} = \begin{bmatrix} 3.42e-03 \\ 3.39e-04 \\ 3.29e-04 \\ 1.64e-04 \\ 6.20e-03 \\ 2.42e+00 \\ 1.12e-01 \end{bmatrix}$	I	0.20	0.60	1.00	1.00	1.00	1.00	0.026
		II	0.40	1.16	0.90	1.05	0.84	0.69	0.041
		III	0.60	1.73	0.87	1.06	0.82	0.69	0.062
		IV	0.80	2.38	0.85	1.05	0.91	0.73	0.099
		V	1.00	2.82	0.88	1.04	1.11	0.73	0.161
0.25	$\begin{bmatrix} D_g \\ D_1 \\ D_2 \\ D_3 \\ \lambda_1 \\ \lambda_2 \\ \lambda_3 \end{bmatrix} = \begin{bmatrix} 3.52e-03 \\ 1.31e-04 \\ 2.63e-04 \\ 1.30e-04 \\ 7.57e-02 \\ 6.44e-03 \\ 5.68e-01 \end{bmatrix}$	I	0.20	0.64	1.00	1.00	1.00	1.00	0.032
		II	0.40	1.20	0.90	1.02	0.82	0.79	0.049
		III	0.60	1.77	0.91	1.05	0.96	0.75	0.084
		IV	0.80	2.23	0.98	1.04	1.19	0.74	0.140
		V	1.00	2.43	1.06	1.01	1.44	0.81	0.209
0.26	$\begin{bmatrix} D_g \\ D_1 \\ D_2 \\ D_3 \\ \lambda_1 \\ \lambda_2 \\ \lambda_3 \end{bmatrix} = \begin{bmatrix} 2.68e-03 \\ 1.75e-04 \\ 1.33e-04 \\ 1.66e-04 \\ 7.77e-03 \\ 1.15e-01 \\ 1.06e+00 \end{bmatrix}$	I	0.20	0.80	1.00	1.00	1.00	1.00	0.057
		II	0.40	1.65	0.78	0.94	0.64	0.91	0.089
		III	0.60	2.48	0.77	0.99	0.71	0.88	0.116
		IV	0.80	3.28	0.81	0.90	0.65	0.96	0.142
		V	1.00	4.01	0.83	0.89	0.79	0.97	0.186
		VI	1.50	6.50	0.82	1.01	1.86	0.86	0.960
		VII	2.00	3.62	1.02	0.94	2.14	0.96	1.041

Continued on next page...

BV/TV	Linear coefficients at Cycle I			Cycle No.	ε_l[%]	$\sigma^N[MPa]$	Nonlinear VE parameters				ε_{res}[%]
							g_0	g_1	g_2	a_σ	
0.33	D_g	$=$	$1.75e-03$	I	0.20	1.19	1.00	1.00	1.00	1.00	0.065
	D_1		$7.46e-05$	II	0.40	2.76	0.66	0.93	0.84	0.98	0.076
	D_2		$1.11e-04$	III	0.60	4.58	0.63	0.94	0.74	0.99	0.083
	D_3		$6.68e-05$	IV	0.80	6.40	0.62	0.92	0.71	0.98	0.091
	λ_1		$9.87e-03$	V	1.00	8.18	0.62	0.95	0.67	0.99	0.100
	λ_2		$1.02e+00$	VI	1.50	13.37	0.75	0.92	1.32	0.95	0.442
	λ_3		$1.21e-01$	VII	2.00	11.13	0.78	0.92	1.53	0.96	0.526
0.35	D_g	$=$	$1.60e-03$	I	0.20	1.31	1.00	1.00	1.00	1.00	0.039
	D_1		$1.14e-04$	II	0.40	2.69	0.84	1.14	0.71	0.67	0.057
	D_2		$6.45e-05$	III	0.60	4.09	0.84	1.08	0.60	0.78	0.072
	D_3		$8.35e-05$	IV	0.80	5.59	0.82	1.00	0.57	0.87	0.075
	λ_1		$7.64e-03$	V	1.00	7.50	0.78	1.00	0.37	0.93	0.109
	λ_2		$9.41e-02$	VI	1.50	13.01	0.70	1.02	0.66	0.80	0.214
	λ_3		$7.05e-01$								
0.35	D_g	$=$	$2.16e-03$	I	0.20	0.94	1.00	1.00	1.00	1.00	0.047
	D_1		$1.41e-04$	II	0.40	2.16	0.70	1.02	0.84	0.84	0.077
	D_2		$1.43e-04$	III	0.60	3.46	0.67	1.03	0.80	0.85	0.097
	D_3		$1.11e-04$	IV	0.80	4.67	0.65	1.02	0.75	0.86	0.118
	λ_1		$6.41e-03$	V	1.00	6.04	0.63	1.02	0.72	0.87	0.135
	λ_2		$1.41e+00$	VI	1.50	10.67	0.62	1.04	0.82	0.80	0.406
	λ_3		$1.22e-01$	VII	2.00	11.83	0.62	1.03	0.94	0.79	0.522
0.36	D_g	$=$	$2.07e-03$	I	0.20	0.98	1.00	1.00	1.00	1.00	0.073
	D_1		$1.48e-04$	II	0.40	2.12	0.71	1.20	0.45	0.70	0.087
	D_2		$1.52e-04$	III	0.60	3.67	0.65	1.02	0.43	0.87	0.112
	D_3		$1.55e-04$	IV	0.80	5.28	0.62	0.95	0.41	0.93	0.128
	λ_1		$1.63e-01$	V	1.00	7.02	0.59	0.89	0.40	0.97	0.144
	λ_2		$1.07e-02$	VI	1.50	12.73	0.54	1.00	0.42	0.89	0.244
	λ_3		$1.75e+00$	VII	2.00	16.68	0.45	1.01	0.75	0.79	0.377
0.39	D_g	$=$	$1.53e-03$	I	0.20	1.33	1.00	1.00	1.00	1.00	0.058
	D_1		$1.07e-04$	II	0.40	2.92	0.76	0.83	0.76	0.97	0.066
	D_2		$1.07e-04$	III	0.60	4.79	0.67	1.02	0.78	0.83	0.076
	D_3		$8.45e-05$	IV	0.80	6.69	0.63	1.05	0.83	0.75	0.089
	λ_1		$6.37e-03$	V	1.00	8.53	0.65	1.07	0.64	0.79	0.111
	λ_2		$1.27e+00$	VI	1.50	14.81	0.66	1.02	0.56	0.86	0.288
	λ_3		$1.23e-01$	VII	2.00	17.19	0.60	1.04	1.01	0.77	0.458

Continued on next page...

BV/TV	Linear coefficients at Cycle I	Cycle No.	ε_l[%]	$\sigma^N[MPa]$	Nonlinear VE parameters				ε_{res}[%]
					g_0	g_1	g_2	a_σ	
0.40	$\begin{bmatrix} D_g \\ D_1 \\ D_2 \\ D_3 \\ \lambda_1 \\ \lambda_2 \\ \lambda_3 \end{bmatrix} = \begin{bmatrix} 2.88e-03 \\ 2.36e-04 \\ 5.01e-04 \\ 2.56e-04 \\ 1.12e-02 \\ 2.57e+00 \\ 1.54e-01 \end{bmatrix}$	I	0.20	0.71	1.00	1.00	1.00	1.00	0.127
		II	0.40	1.65	0.46	0.89	0.51	0.97	0.170
		III	0.60	2.95	0.44	0.87	0.41	0.96	0.201
		IV	0.80	4.32	0.43	0.90	0.40	0.98	0.220
		V	1.00	5.74	0.43	0.91	0.34	0.99	0.227
		VI	1.50	11.56	0.39	0.92	0.36	0.94	0.346
		VII	2.00	14.98	0.39	0.90	0.33	0.97	0.491
0.40	$\begin{bmatrix} D_g \\ D_1 \\ D_2 \\ D_3 \\ \lambda_1 \\ \lambda_2 \\ \lambda_3 \end{bmatrix} = \begin{bmatrix} 2.69e-03 \\ 9.10e-05 \\ 1.02e-04 \\ 1.26e-04 \\ 1.55e-01 \\ 9.68e-03 \\ 1.13e+00 \end{bmatrix}$	I	0.20	0.77	1.00	1.00	1.00	1.00	0.085
		II	0.40	2.13	0.52	0.85	0.73	0.96	0.109
		III	0.60	3.69	0.47	0.88	0.67	0.98	0.126
		IV	0.80	5.35	0.43	0.96	0.70	0.91	0.141
		V	1.00	7.11	0.43	0.88	0.60	0.98	0.160
		VI	1.50	13.69	0.37	0.99	0.69	0.89	0.295
		VII	2.00	17.41	0.38	1.01	0.95	0.87	0.550
0.42	$\begin{bmatrix} D_g \\ D_1 \\ D_2 \\ D_3 \\ \lambda_1 \\ \lambda_2 \\ \lambda_3 \end{bmatrix} = \begin{bmatrix} 1.47e-03 \\ 1.09e-04 \\ 8.72e-05 \\ 7.91e-05 \\ 2.81e+00 \\ 8.63e-03 \\ 1.76e-01 \end{bmatrix}$	I	0.20	1.37	1.00	1.00	1.00	1.00	0.037
		II	0.40	2.97	0.73	1.03	0.98	0.83	0.054
		III	0.60	4.74	0.71	1.04	0.86	0.82	0.059
		IV	0.80	6.57	0.69	1.04	0.82	0.84	0.079
		V	1.00	8.44	0.66	1.03	0.85	0.85	0.091
		VI	1.50	14.45	0.67	0.91	0.68	0.96	0.158
		VII	2.00	19.20	0.63	1.01	0.88	0.86	0.301
0.43	$\begin{bmatrix} D_g \\ D_1 \\ D_2 \\ D_3 \\ \lambda_1 \\ \lambda_2 \\ \lambda_3 \end{bmatrix} = \begin{bmatrix} 1.94e-03 \\ 1.19e-04 \\ 1.75e-04 \\ 9.27e-05 \\ 7.85e-01 \\ 7.38e-03 \\ 9.59e-02 \end{bmatrix}$	I	0.20	1.08	1.00	1.00	1.00	1.00	0.066
		II	0.40	2.39	0.67	1.09	0.60	0.74	0.096
		III	0.60	3.88	0.63	1.03	0.59	0.80	0.118
		IV	0.80	5.54	0.60	1.05	0.55	0.77	0.141
		V	1.00	7.22	0.61	0.89	0.52	0.96	0.146
		VI	1.50	13.04	0.57	1.01	0.42	0.84	0.268
		VII	2.00	16.91	0.55	1.00	0.51	0.85	0.406
		$VIII$	2.50	20.56	0.56	1.00	0.57	0.86	0.608
0.43	$\begin{bmatrix} D_g \\ D_1 \\ D_2 \\ D_3 \\ \lambda_1 \\ \lambda_2 \\ \lambda_3 \end{bmatrix} = \begin{bmatrix} 9.40e-04 \\ 3.67e-05 \\ 6.46e-05 \\ 6.43e-05 \\ 1.06e-01 \\ 6.74e-03 \\ 9.59e-01 \end{bmatrix}$	I	0.20	2.13	1.00	1.00	1.00	1.00	0.042
		II	0.40	4.75	0.74	1.09	0.70	0.73	0.057
		III	0.60	7.96	0.67	1.08	0.64	0.70	0.074
		IV	0.80	11.29	0.64	1.07	0.62	0.75	0.088
		V	1.00	14.65	0.61	1.06	0.68	0.78	0.102
		VI	1.50	24.26	0.66	1.04	0.75	0.72	0.180

Continued on next page...

BV/TV	Linear coefficients at Cycle I	Cycle No.	ε_l[%]	$\sigma^N[MPa]$	Nonlinear VE parameters				ε_{res}[%]
					g_0	g_1	g_2	a_σ	
0.46	$\begin{bmatrix} D_g \\ D_1 \\ D_2 \\ D_3 \\ \lambda_1 \\ \lambda_2 \\ \lambda_3 \end{bmatrix} = \begin{bmatrix} 1.16e-03 \\ 4.19e-05 \\ 5.82e-05 \\ 8.91e-05 \\ 6.99e-02 \\ 6.48e-03 \\ 6.75e-01 \end{bmatrix}$	I	0.20	1.75	1.00	1.00	1.00	1.00	0.037
		II	0.40	4.38	0.68	0.92	0.78	1.00	0.043
		III	0.60	7.45	0.61	0.89	0.69	0.97	0.049
		IV	0.80	10.77	0.57	0.88	0.62	0.97	0.056
		V	1.00	14.06	0.56	0.83	0.62	0.98	0.060
		VI	1.50	22.92	0.53	1.01	0.60	0.79	0.121
0.52	$\begin{bmatrix} D_g \\ D_1 \\ D_2 \\ D_3 \\ \lambda_1 \\ \lambda_2 \\ \lambda_3 \end{bmatrix} = \begin{bmatrix} 2.29e-03 \\ 1.74e-04 \\ 2.03e-04 \\ 1.60e-04 \\ 1.50e+00 \\ 6.85e-03 \\ 1.29e-01 \end{bmatrix}$	I	0.20	0.89	1.00	1.00	1.00	1.00	0.095
		II	0.40	2.25	0.48	1.13	0.63	0.66	0.138
		III	0.60	3.87	0.43	1.09	0.60	0.69	0.175
		IV	0.80	5.62	0.42	1.08	0.49	0.74	0.210
		V	1.00	7.54	0.43	0.76	0.50	0.97	0.239
		VI	1.50	15.62	0.36	1.05	0.41	0.76	0.364
		VII	2.00	20.88	0.36	1.03	0.32	0.82	0.447
		$VIII$	2.50	26.56	0.33	1.03	0.53	0.73	0.656
0.53	$\begin{bmatrix} D_g \\ D_1 \\ D_2 \\ D_3 \\ \lambda_1 \\ \lambda_2 \\ \lambda_3 \end{bmatrix} = \begin{bmatrix} 9.05e-04 \\ 4.26e-05 \\ 3.35e-05 \\ 4.21e-05 \\ 6.32e-01 \\ 6.40e-02 \\ 5.54e-03 \end{bmatrix}$	I	0.20	2.22	1.00	1.00	1.00	1.00	0.033
		II	0.40	5.03	0.79	0.81	0.95	0.92	0.048
		III	0.60	8.02	0.75	0.84	0.88	0.92	0.059
		IV	0.80	11.05	0.73	0.83	0.90	0.94	0.073
		V	1.00	14.10	0.71	0.87	0.91	0.96	0.085
		VI	1.50	23.66	0.67	1.00	1.07	0.78	0.174
		VII	2.00	30.13	0.75	1.01	0.90	0.86	0.310
0.54	$\begin{bmatrix} D_g \\ D_1 \\ D_2 \\ D_3 \\ \lambda_1 \\ \lambda_2 \\ \lambda_3 \end{bmatrix} = \begin{bmatrix} 1.36e-03 \\ 8.02e-05 \\ 6.44e-05 \\ 6.17e-05 \\ 8.56e-01 \\ 8.64e-03 \\ 9.62e-02 \end{bmatrix}$	I	0.20	1.49	1.00	1.00	1.00	1.00	0.050
		II	0.40	4.00	0.58	1.06	0.71	1.00	0.058
		III	0.60	7.38	0.50	1.11	0.48	1.00	0.061
		IV	0.80	11.01	0.45	0.90	0.60	0.98	0.065
		V	1.00	14.66	0.45	0.87	0.47	1.00	0.074
		VI	1.50	24.90	0.42	0.96	0.49	0.88	0.129

BV/TV is the bone volume fraction, D_g is the instantaneous compliance in $1/MPa$, D_n (n = 1, 2, 3) are transient compliance coefficients in $1/MPa$, and λ_n (n = 1, 2, 3) are reciprocal of nth retardation time in Prony series in s^{-1}, ε_l is the applied static strain in each loading cycle, σ^N is the stress corresponding to plateau stress in the Nth loading cycle in MPa. Parameters g_0, g_1, g_2, a_σ are stress-dependent nonlinear VE parameters and ε_{res} is the irrecoverable strain exist at the end of each loading cycle.

Parameters, g_0, g_1, g_2 and α_σ are the stress dependent nonlinear parameters used to describe the nonlinear behaviour of trabecular bone. The parameter g_0 is a nonlinear instantaneous compliance parameter, the transient nonlinear

parameter g_1 measures the nonlinearity effect in the transient compliance, and g_2 describes the effects of loading rate on the transient creep response and α_σ is the time-shift factor. Decreasing g_0 and g_1, g_2 (and product of $g_1 g_2$) indicate decrease of instantaneous and transient compliance, respectively, which also implies increase of modulus (elastic stiffening), while increase of these parameters implies decrease of modulus (elastic softening). As can be seen those parameters for Cycle I are unity as the Cycle I was assumed to be linear (Table 5.3).

Figure 5.9 shows the variation of the stress-dependent nonlinear viscoelastic parameters, g_0, g_1, g_2 and α_σ for two typical samples with BV/TV = 25% and 46%. The results show that for sample with smaller BV/TV the values of g_0, g_2 and a_σ first decrease and then increase with the stress level, whereas the value of g_1 first increases slightly and then decreases slightly with the stress level (Fig. 5.9a). The product of $g_1 g_2$ which affects the transient response was also found to first decrease and then increase. These observations indicated the choice of a second order polynomial function to represent the nonlinear viscoelastic parameters as functions of normalised effective stress. These second order functions produced coefficients of determination of r^2 = 0.97, 0.72, 0.98 and 0.69 for parameters g_0, g_1, g_2 and a_σ, respectively, as shown in Fig. 5.9a.

For sample with higher BV/TV, Fig. 5.9b, the parameters g_0, g_1, g_2 were found to decrease and then increase slightly with the stress level, and a_σ was almost constant (≈ 1) and then decreased in the last stress cycle. The second order polynomial functions of effective stress produced r^2 values of 0.83, 0.90, 0.92, and 0.93 for g_0, g_1, g_2 and a_σ , respectively for this typical sample. The increase in the values of g_0, g_1, g_2 or the product of $g_1 g_2$ essentially means that the trabecular bone material experiences elastic softening (reduction of stiffness) and decrease of these parameters imply that the material experiences stiffening.

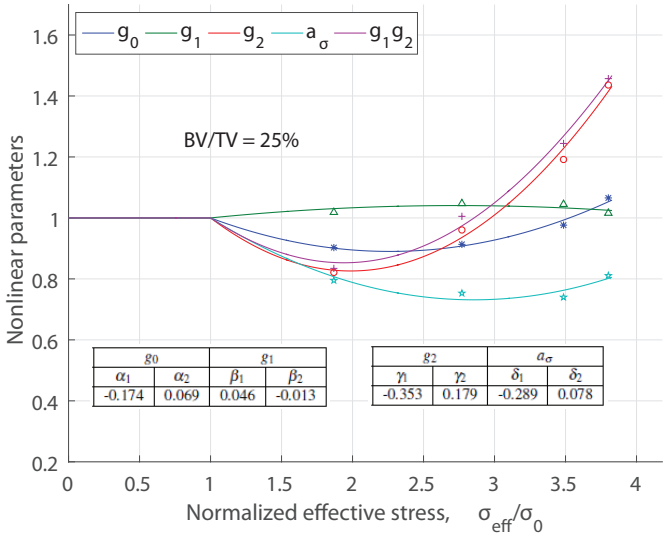

(a)

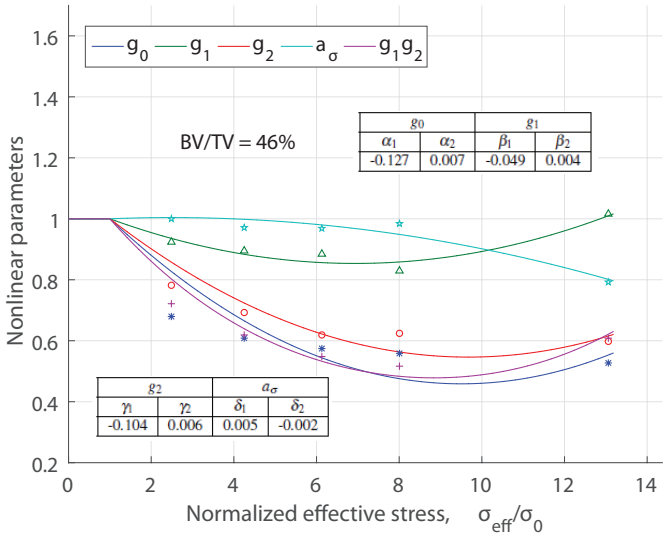

(b)

Figure 5.9: Nonlinear viscoelastic parameters, g_0, g_1, g_2 and α_σ, expressed as second-order polynomial function of normalised effective stress (σ_{eff}/σ_0): BV/TV = 25% (a) and BV/TV = 46% (b) (Manda et al., 2016a).

Figures 5.10a, 5.10b, 5.10c and 5.10d show the variation of nonlinear viscoelastic parameters, g_0, g_1, g_2 and α_σ,respectively, which were expressed as polynomial functions of effective stress, for all 19 samples. It can be seen that the variation described for two typical samples is largely followed by all.

The irrecoverable strain along with nonlinear viscoelastic (recoverable) strain response is shown in Figs. 5.11a and 5.11b. The figures also show the measured experimental strain response which comprises of the recoverable and

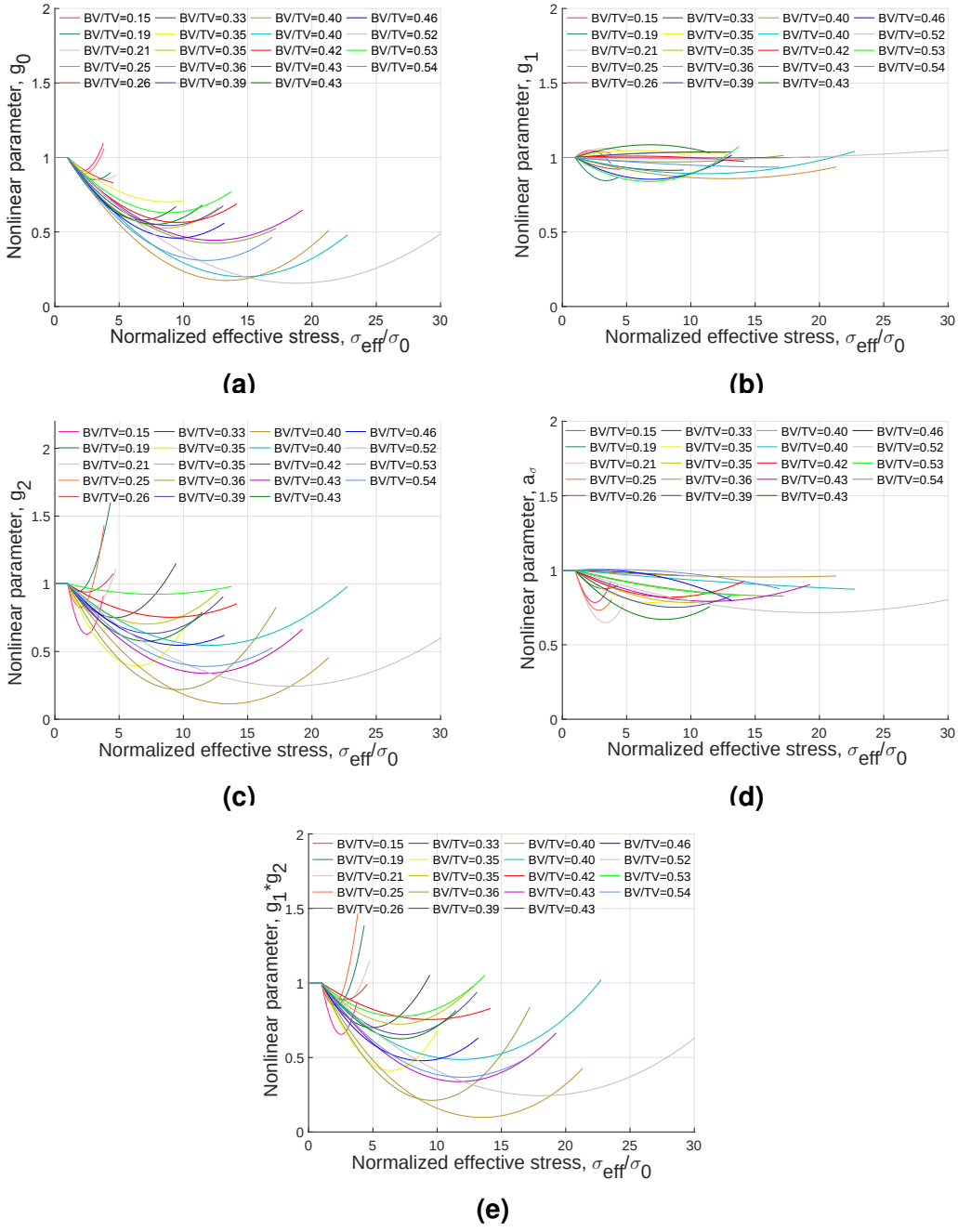

Figure 5.10: Nonlinear viscoelastic parameters, expressed as second order polynomial functions of effective stress, for all 19 samples are plotted against normalized effective stress. Parameter g_0 (a), parameter g_1 (b), parameter g_2 (c), parameter a_σ (d) and product of the parameters g_1 and g_2 (e) (Manda et al., 2016a).

irrecoverable strain components (Eq. 3.24). The viscoelastic strain was found to recover fully (to below 7 $\mu\varepsilon$) in under 10 minutes during the recovery phase of each loading cycle. Irrecoverable strains exist even at the end of the first loading cycle (stress level corresponding to apparent strain of 0.2%) and were

found to increase with stress. For sample with lower BV/TV, the irrecoverable strain increased to 0.20% by the end of cycle V from 0.03% in cycle I (Fig. 5.11a), whereas for sample with higher BV/TV, it increased to 0.12% by the end of loading cycle VI from 0.03% in cycle I (Fig. 5.11b).

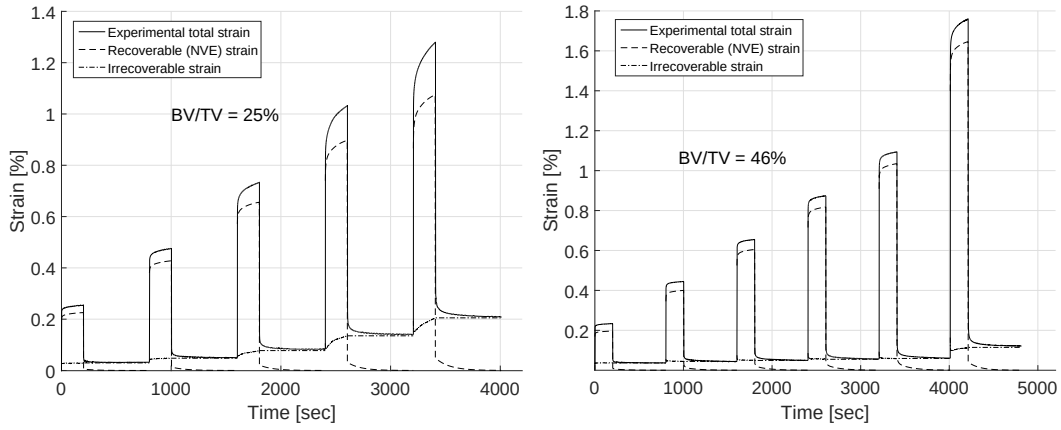

(a) **(b)**

Figure 5.11: Pure viscoelastic (recoverable) and the irrecoverable strain response are plotted along with the total creep strain response for two typical samples: BV/TV=25% (a) and BV/TV=46% (b) (Manda et al., 2016a).

5.4 Viscoplasticity

The irrecoverable strains after 600 s of recovery in each loading cycle for all 19 samples are shown in Fig. 5.12a. There were no significant correlations found between the irrecoverable strains and BV/TV in the loading cycles I-IV. However, a weak but significant power law correlation ($\varepsilon_{res} = 0.0757(\text{BV/TV})^{-0.61}$, $r^2 = 0.34$, $p < 0.001$) in the cycle V with BV/TV was found. At loading cycles at higher stresses or loading cycles, strong and significant power law relationships $y = 0.0177x^{-2.93}$ ($r^2 = 0.78$, $p < 0.001$) and $y = 0.0862x^{-1.78}$ ($r^2 = 0.73$, $p < 0.001$) were found between the irrecoverable strains and BV/TV in the cycles VI and VII, respectively. This irrecoverable strain was modelled as viscoplastic strain, which can be extracted by subtracting the nonlinear viscoelastic strain from the experimental total strain response at each stress levels (as

listed in Table 5.3). Here, two typical samples are selected and their viscoplastic parameters are determined (BV/TV = 15% and 35%).

The Drucker-Prager yield criterion in conjunction with Perzyna viscoplasticity model as discussed in Chapter 3 was employed. In this study, the friction angle θ and dilation angle θ' for the pressure-dependent Drucker-Prager yield criterion were assumed to be 46°and 0°, respectively, based on previous investigation on bone (Mercer et al., 2006). Shape parameter d was assumed to be 1 (Mercer et al., 2006). Consequently, α and β were equal to 1.035 and 0, respectively.

The conducted MLCUR experiments permitted evaluation of viscoplastic strain by subtracting the nonlinear viscoelastic strain from its total experimental strain response. Viscoplastic multiplier ($\Delta\gamma^{VP}/\Delta_t$, also called the viscoplastic strain rate) can be obtained by differentiating the viscoplastic strain with respect to time, as shown in Fig. 5.13 for two typical samples. Then, the viscoplastic parameters Γ, κ_0, κ_1, κ_2, N and σ_y^0 were obtained by minimising the error between experimental $\Delta\gamma^{VP}/\Delta_t$ and Eq. 3.39 at the specified stress level as shown in Fig. 5.13. The viscoplastic parameters were evaluated for the two samples, in cycle with plateau stress of 0.66 MPa and 1.20 MPa, respectively, and are show in Table 5.4.

Table 5.4: The values of the viscoplastic material parameters of two trabecular bone samples

BV/TV	α	β	$\Gamma(1/s)$	N	$\sigma_y^0(MPa)$	$\kappa_0(MPa)$	$\kappa_1(MPa)$	κ_2
15%	1.035	0.0	4.34×10^{-1}	3.0	3.38	2.42×10^{-3}	2.11	4.62×10^{2}
25%	1.035	0.0	4.91×10^{-3}	3.0	5.75	1.35×10^{-10}	4.11	3.50×10^{2}

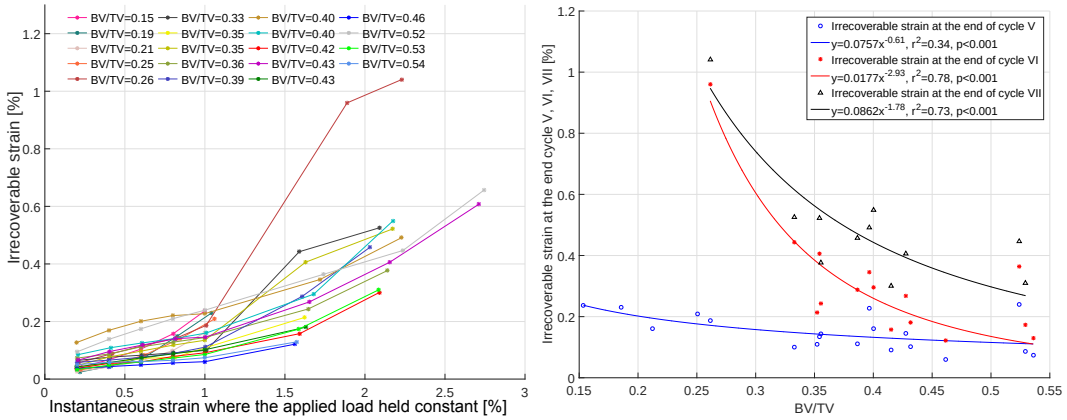

(a) (b)

Figure 5.12: Irrecoverable strain plotted against applied static strain and the BV/TV. Irrecoverable strains at the end of each loading cycle in each sample with the applied static strain (where plateau force was held constant during creep-recovery test) (a), irrecoverable strains in cycles V, VI and VII corresponding to static strains of 1.0, 1.5 and 2.0% are plotted against BV/TV of all samples (b). (Manda et al., 2016a)

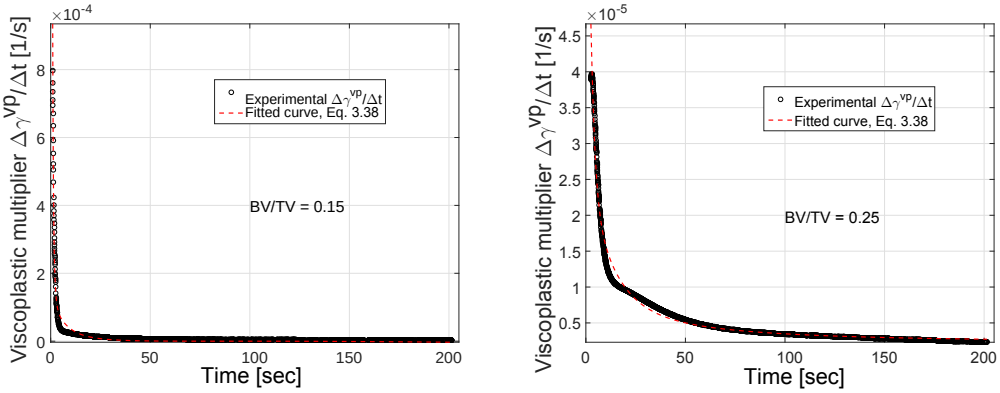

(a) (b)

Figure 5.13: The viscoplastic material parameter fitting results for two typical samples. BV/TV =15% (a) in a cycle with plateau stress of 0.66 MPa and BV/TV = 25% (b) in a cycle with plateau stress 1.20 MPa.

5.5 Validation of developed constitutive models

The nonlinear viscoelastic parameters ($D_g, D_n, \lambda_n, g_0, g_1, g_2$ and α_σ) and viscoplastic parameters (Γ, κ_0, κ_1, κ_2, N and σ_y^0) were determined from MLCUR experimental data. The numerical algorithm, described above was developed as a UMAT and used to simulate the MLCUR experiments in Abaqus.

The predicted FE responses, including total strain response (Fig. 5.14a, 5.14b), nonlinear viscoelastic strain response (Fig. 5.14c, 5.14d) and viscoplastic strain response (Fig. 5.14e, 5.14f) for two typical samples are shown (BV/TV = 15% and 25%). It is clear that the combined nonlinear viscoelastic-viscoplastic model predicts the total strain responses well in lower stress level cycles, but at higher stress levels the response was under predicted. At these higher stress levels the experimental response may not be purely composed of nonlinear viscoelasticity and viscoplasticity, but could include a possible damage, which is not included in the developed constitutive models. Although predicted nonlinear viscoelastic response was in excellent agreement with the measured response (Figs. 5.14c 5.14d), the predicted viscoplastic response was found to deviate a little from the measured viscoplastic response (Figs. 5.14e 5.14f).

5.6 Discussion

Trabecular bone had been investigated extensively for its mechanical properties, but its time-independent behaviour has received little attention (Bowman et al., 1994; Deligianni et al., 1994; Quaglini et al., 2009; Yamamoto et al., 2006). The popular FE based simulations mostly consider the trabecular bone as time-independent elastic material (Pankaj, 2013), but to predict the stability of joint replacement and fracture fixation implants, it is necessary to consider time-dependent properties for trabecular bone in FE simulations. Therefore, simple BV/TV-based viscoelastic constitutive model, as well as the nonlinear viscoelastic-viscoplastic constitutive models were developed.

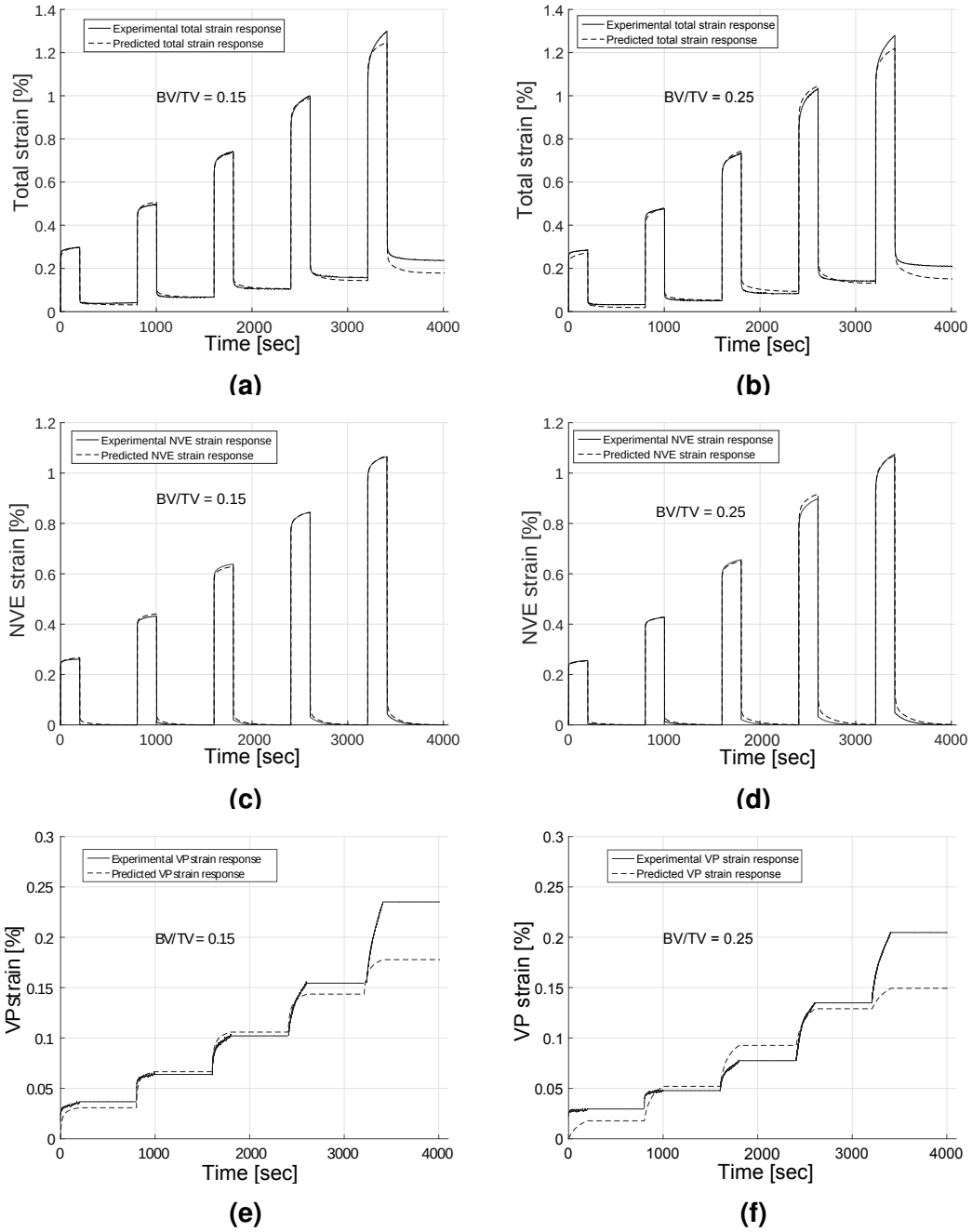

Figure 5.14: The predicted strain response from developed constitutive models along with experimental strain response. The comparison of experimental total strain response (a, b), nonlinear viscoelastic strain response (c, d) and viscoplastic strain response (e, f) from MLCUR and the predicted strain from Abaqus model for two trabecular bone samples.

5.6.1 BV/TV-viscoelastic

The Prony coefficients associated with linear viscoelastic response are determined from the loading phase at the small load levels (corresponding to 2,000 $\mu\varepsilon$). The relationships between time-independent elastic modulus and BV/TV (or density) have been reported extensively over the last two decades, but similar relationships of BV/TV with viscoelastic properties have not been previously investigated, to the best of author's knowledge. The results show that BV/TV can be significantly related to creep compliance functions with the coefficients of determination of r^2 =0.73 ($p < 0.001$), respectively. It is important to note that similar r^2 values have been previously reported by studies that relate bone density to time-independent elastic modulus (Morgan et al., 2003). In fact the instantaneous elastic compliance-BV/TV relationship from the creep experiments conducted in this study is similar to the relations reported in the literature (Zysset, 2003) with similar r^2 value.

Most commercial FE packages have viscoelastic modelling capabilities. With existing imaging capabilities subject-specific BV/TV values can be estimated permitting the application of viscoelastic properties based on the relationships developed in this study in finite element models if time-dependent behaviour of trabecular bone is of concern. Trabecular bone provides anchorage to orthopaedic implants, whose stability depends not only on bone quality but also on its relaxation or creep behaviour. The major role of trabecular bone is not only transferring the load but also to dissipate energy during daily activities thereby protecting the articular cartilage as well as the ends of long bones. So the developed BV/TV-based constitutive model can be easily used in FE simulations aimed at enhancing the understanding of clinically related problems.

5.6.2 Nonlinear viscoelasticity

The strain response from the unloading phase of the conducted experiments is viscoelastic, but it was found to vary nonlinearly with stress. Identification of the nonlinear parameters for trabecular bone can be classified as two-step process. The linear parameters (D_g, D_n, λ_n) can be obtained by fitting the unloading strain response with 3-term Prony series from its first loading cycle (equivalent to 2,000 $\mu\varepsilon$, assumed as linear). Bowman et al. (1994) experimentally observed the creep behaviour of trabecular bone until failure at different applied normalised stress levels (0.5% to 1% elastic strains) and concluded that the creep behaviour of trabecular bone is nonlinearly dependent on applied stress level. Since tests in this study were performed at relatively low stresses (maximum creep strain was under 0.26% from its first loading cycle, Fig. 5.2a) and the assumption of linear viscoelasticity appears to be valid.

In the second steps the linear viscoelastic response from the last step with additional appropriate nonlinear parameters is used to manipulate and match with experimental response at the higher stress levels. Thereby, the corresponding nonlinear parameters are evaluated at multiple stress levels.

All samples showed similar convex shape (Fig. 5.10a). For parameter g_0, which affects the instantaneous response, depending on their BV/TV with the coefficients of determination (r^2) of the polynomial functions were in the range of 0.18-0.99. The product of the parameters g_1 and g_2 which affects the transient response, Fig. 5.10e, produced the r^2 value in the range of 0.37-0.99. Some of the second-order polynomial functions of g_0 and $g_1 g_2$ for some samples were weakly correlated; however, all of the correlations were positive and showed an initially decreasing and then increasing trend, which implies decreasing and increasing trend in the instantaneous and transient responses (recoverable compliance), respectively, with increasing stress. These functions of stress-dependent parameters explain the stiffening-softening behaviour of

trabecular bone well under compressive creep loading. The change in parameter α_σ shows the nonlinearity in the time-shift factor as a function of stress. The approximations using second-order polynomial functions of stress were considered appropriate as the experiments provided only data points corresponding to 5-8 stress levels. The outstanding fact about these approximations is that all the functions revealed a stiffening-softening behaviour for all trabecular bone samples with varying degrees of success. With increasing stress the parameter g_0 and the product $g_1 g_2$ reduce to less than 1 indicating stiffening (or reduced compliance) followed by an increase beyond 1 indicating softening (or increased compliance) with the further increase in stress . This can be clearly seen from Fig. 5.10 and it can be observed that the viscoelastic response of samples with lower BV/TV was significantly different from samples with higher BV/TV. In general, for lower BV/TV samples, the parameters reach their minima and increase to greater than 1 rapidly, indicating quicker stiffening-softening behaviour with stress. For samples with higher BV/TV, the same behaviour was observed to vary more slowly with stress. From these results, it appears BV/TV is a good predictor of nonlinear stress-dependent viscoelastic response of the trabecular bone. Those results are consistent with the analysis undertaken using primarily experimental data in Chapter 4.

5.6.3 Viscoplasticity

One of the advantage of employing MLCUR experiment on investigation of time-dependent behaviour of trabecular bone, is that it allowed separation of viscoplastic and nonlinear viscoelastic strain from the total strain. This permits inclusion of viscoplasticity in modelling and a more realistic simulation of whole bone mechanics to address clinically relevant problems, and long-term creep simulation during ageing due to daily activities of life.

A constitutive model was developed to predict the complete time-dependent response of trabecular bone which always contains recoverable and irrecoverable responses. The numerical algorithm shows a good predictions of the time-dependent response of trabecular bone when subjected to different creep-recovery loading cycles. This model will be used at the later chapters to simulated the interfacial mechanics of a idealised bone-screw system under cyclic loading.

5.7 Limitation

The lower bond for the time range of retardation time (τ_n) for developed model was around 0.35 s. Since it is quite small and not too different to the loading time (with strain rate $0.01s^{-1}$, i.e. 0.2 s to reach 2,000 $\mu\varepsilon$ in the experiment), some creep strain may develop during the finite ramp loading. Further tests at the higher and lower strain rates are necessary to verify this.

5.8 Conclusions

- Time-dependent response of trabecular bone comprises of both recoverable and irrecoverable strain.
- Bone's mechanical response is BV/TV dependent, elastic stiffening followed by elastic softening is observed for relatively denser bone, while elastic softening may may start from very low load level for porous bone.
- Schapery's nonlinear viscoelastic constitutive model can predict the recovery behaviour well.
- Nonlinear viscoelastic-viscoplastic model is able to predict the creep-recovery behaviour of trabecular bone, which can be used in FE modelling to predict bone's mechanical behaviour more realistically.

"Each problem that I solved became a rule, which served afterwards to solve other problems."

Rene Descartes

6

Demineralised trabecular bone

Trabecular bone is a composite and consequently, it is important to understand the contribution of the constituents to its mechanical behaviour (Chapter 2). This Chapter examines the mechanical behaviour of demineralised trabecular bone, to understand the contribution of trabecular bone's organic phase to its overall behaviour.

Cyclic loading had been used to investigate the material properties of cortical (Caler and Carter, 1989) and trabecular bone (Cotton et al., 2005; Dendorfer et al., 2008), but these cited studies used constant amplitude rather than different amplitude. Cyclic loading with amplitude increased step-wise has been successfully used for biopolymer (Münster et al., 2013) and to limited extent on trabecular bone (Topoliński et al., 2011). Cyclic loading with increasing amplitude is capable of providing much greater information with shorter test duration (Topoliński et al., 2011).

To evaluate the mechanical behaviour of the organic phase, a number of previous studies have undertaken mechanical tests on demineralised bone; almost all of which have been on cortical bone (Bowman et al., 1999, 1996; Burstein et al., 1975; Catanese III et al., 1999; Novitskaya et al., 2011, 2013). Evaluation of elastic modulus and strength through monotonically increasing loading in tension (Bowman et al., 1996; Burstein et al., 1975; Catanese III et al., 1999) or compression (Novitskaya et al., 2011) has been the focus of most studies. Novitskaya et al. (2013) conducted cyclic loading tests on demineralised cortical bone in three different directions and showed that cortical bone has anisotropic cyclic behaviour with larger energy dissipation in transverse directions. Loading cycles in this cited study were confined to compression although the contribution of the organic phase to tension has been noted to be much more significant (Burstein et al., 1975). Studies conducted on the mechanical behaviour of demineralised trabecular bone are limited, confined to monotonic loading in compression and generally conducted with an aim to evaluate elastic modulus and strength (Chen and McKittrick, 2011). These limited studies indicate that there is considerable gap in understanding the mechanical behaviour of the organic phase of bone under cyclic loading at different load levels.

Therefore, the first part of this chapter aims to fill this gap by investigating the mechanical properties of demineralised trabecular bone (collagen matrix) by using reversed cyclic loading from tension to compression with load amplitude increasing stepwise. The objective is to investigate the differences in mechanical properties in tension and compression, and the influence of porosity. In the second part, the time-dependent behaviour of demineralised trabecular bone is investigated at varying stress levels by conducting tensile MLCUR experiments. The long-term creep behaviour of demineralised cortical bone had been previously examined, but only at a single stress level for each sample (Bowman et al., 1996).

6.1 Sample preparation

Fresh proximal tibia, from bovine (under 30 months old when slaughtered), were obtained from a local abattoir and stored at -20 $^{\circ}C$ until utilised. The bones were allowed to thaw at room temperature before bone cores were extracted along its principal axis, using diamond coring tools (Starlite, Rosement, IL, USA). A low speed rotating saw (Buehler, Germany) was used to create parallel sections and to trim growth plates if they were present. All coring and cutting were conducted in a water bath to avoid excessive heat generation. The cylindrical bone samples had a diameter of 10.6 $\pm$ 0.1 mm and mean height of 22.1 $\pm$ 0.7 mm.

Bone marrow was removed from each sample using a dental water jet (Interplak, Conair) with tap water at room temperature (Lievers et al., 2007). All the samples were then centrifuged at 2000 $r.p.m$ for 2 hours to remove any residual marrow (Sharp et al., 1990) at 37 $^{\circ}C$ and the samples were wrapped in PBS-soaked tissue paper.

6.2 μCT scanning

All the samples were scanned using μCT scanner (Skyscan 1172, Bruker, Kontich, Belgium) at a resolution of 17.22 μm. The system's software was used to evaluate BV/TV of the bone, which was found to be in the range 15.5 - 37.6%.

Scanning parameters used were: source voltage 54 kV, current 185 μA, exposure 885 ms with a 0.5 mm aluminium filter between X-ray source and the sample. The image quality was improved by using 2 frames averaging. It should be noted that the BV/TV mentioned in this Chapter relates to the BV/TV of its original sample (i.e. sample before demineralisation), because it is impossible to obtain the BV/TV for demineralised trabecular bone with μCT scanning.

6.3 Demineralisation

After scanning, demineralisation was conducted by submerging samples in 20 ml 0.6N hydrochloric acid (HCl) at room temperature with the assistance of a racking system. The solution was changed daily (Manilay et al., 2013) for two weeks after which the completeness of demineralisation was verified using μCT scanning. All samples were found to be fully demineralised in 2 weeks. It should be noted that although ethylenediaminetetraacetic acid (EDTA) solution has been previously used to demineralise bone, we used HCl because the process is much quicker and has been employed successfully in previous studies (Burstein et al., 1975; Castro-Ceseña et al., 2013; Chen and McKittrick, 2011; Chen et al., 2011).

Figure 6.1 shows a typical sample's μCT image before and after demineralisation. From visual inspection of sample's architecture, it is clear to see the architecture before demineralisation and is not after demineralisation.

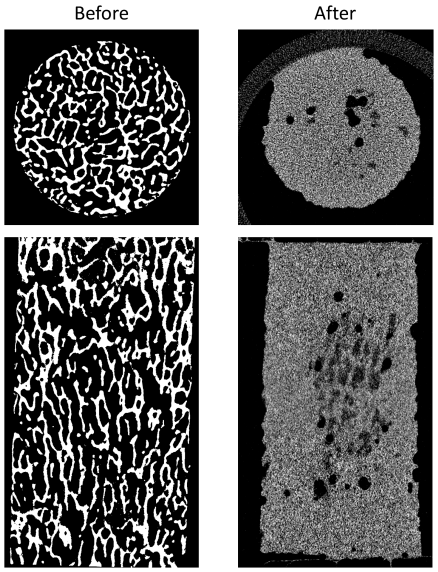

Figure 6.1: μCT images of trabecular bone sample before and after demineralisation. It shows the both top views (top images) and the side views (bottom images) of the cylindrical sample.

6.4 Experiment set-up

Samples were fixed into end-caps (Fig. 6.2) using bone cement (Simplex, Stryker, UK) with the assistance of a custom made alignment tool in order to minimise the end-artefacts during testing (Keaveny et al., 1997). The effective length (19.1 $\pm$ 0.7 mm) of each sample was calculated as the length of the sample between the end-caps plus half the length of the sample embedded within the end-caps (Keaveny et al., 1997). Each sample was placed in an epoxy tube filled with phosphate-buffered saline (PBS) to ensure that they remained hydrated at all stages of mechanical testing.

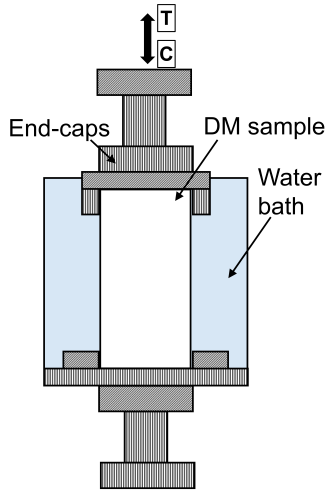

Figure 6.2: Schematic representation of loading set up. Sample is kept hydrated in the water bath throughout mechanical testing.

There were two different type of experiments conducted on demineralised trabecular bone samples. Five of them were subjected to fully-reversed tension-compression experiment and the other eight were subjected to tensile multiple-load-creep-unload-recovery (MLCUR) experiment.

Data related to Chapters 6 and 7 can be found at Edinburgh DataShare. It includes μCT images and experiment results and it entitled 'Characterisation of mechanical behaviour of demineralised and deproteinised trabecular bone samples' (http://dx.doi.org/10.7488/ds/2339).

6.5 Fully-reversed tension-compression experiment

6.5.1 Mechanical test

Each sample was subjected to reversible cyclic loading by means of an Instron material testing machine (50 N load cell, Model 3367). Samples were subjected to 5 loading cycles varying from tension to compression to the same axial force amplitude after which the load level was increased (Fig. 6.3). Five load levels were selected: 0.2, 0.4, 0.6, 0.8 and 1.0 N (corresponding to average axial stress varying from 2.27 to 11.33 kPa). The choice of 5 cycles at each load level was based on preliminary tests, which showed that most variation in strain (or displacement) response occurred in the first five cycles, after which this variation was very small. Preliminary tests also showed that initiating the first cycle in tension or compression made little difference to the strain response. Cyclic loads were applied under strain control, i.e. the strain was slowly increased till the required load level was achieved. A very slow 0.1 $\%/s$ strain-based loading rate was used to minimise the heat generation (e.g. demineralised samples took from 1 to 11 s to attain a load of 0.2 N).

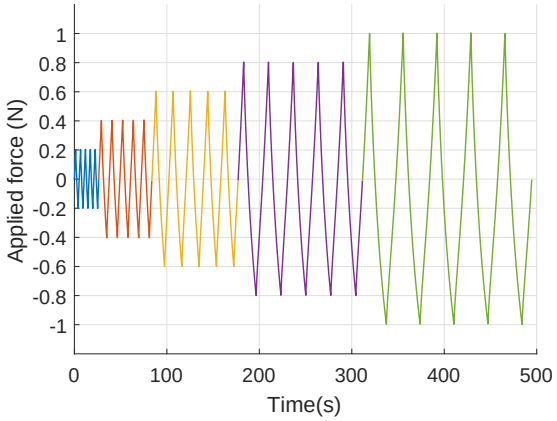

Figure 6.3: Load application of fully-reversed tension-compression cyclic loading experiment. Each sample is subjected to cyclic loading from tension to compression at five load levels from 0.2 N to 1 N with 0.2 N intervals, and 5 cycles to be applied to demineralised sample at each load level.

Ratcheting strain can be defined as the average of peak strain in tension (ε_t^{peak}) and compression (ε_c^{peak}) at the same load level (Fig. 6.4). A non-zero

ratcheting strain only occurs when the mechanical properties in tension and compression are different (Shariati et al., 2012). These were determined for the cyclic load tests. The secant moduli, defined as four different slopes for one complete cycle of loading and unloading in tension and compression as shown in Fig. 6.4 were evaluated. Dissipated strain energy density in tension (DSEDT) and compression (DSEDC), as shown in Fig. 6.4, was also determined for all load levels and for all samples.

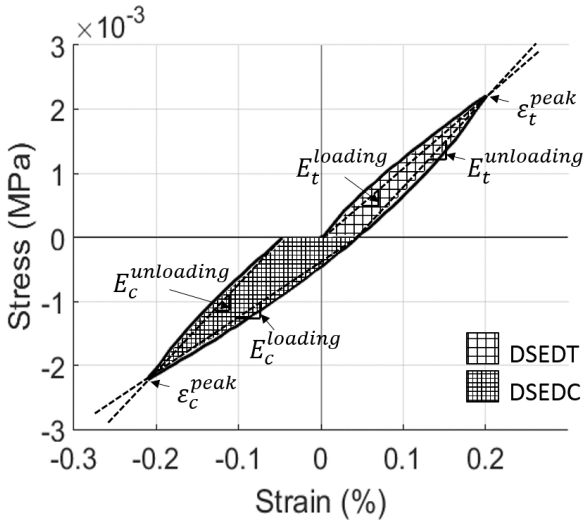

Figure 6.4: Definition of terms: ε_t^{peak} and ε_c^{peak} are the peak strains at the end of a loading cycle in tension and compression respectively. The secant moduli represent four different slopes for one complete cycle with subscripts 't' and 'c' denoting tension and compression respectively, and the superscripts representing loading and unloading branches. DSEDT and DSEDC represent dissipated strain energy density in tension and compression, respectively.

6.5.2 Results

The stress-strain curves for the first cycle at the lowest load level (0.2 N) and the highest load level (1.0 N) are shown in Fig. 6.5a and 6.5b, respectively. It is apparent that the resulting strain response is associated with the samples original BV/TV; samples with higher BV/TV experience much lower strain in comparison to the more porous samples. For example, the sample with BV/TV = 32% experienced only 0.14% strain in tension compared to 0.82% strain observed for sample with BV/TV = 21% (Fig. 6.5a). Comparing tension (taken

as positive) and compression for the first load cycle, it can be seen that the differences in axial strain magnitude is small for samples with higher BV/TV and the difference increases with increasing porosity and with increasing load level (Fig. 6.5b). It is clear that the mechanical behaviour of demineralised trabecular bone is strongly dependent on its original BV/TV.

This trend is consistent for all cycles and at all load levels. This is illustrated in Fig. 6.6a and 6.6b which show the cyclic loading history for two typical samples; the insets show load application. For clarity, only the first and fifth cycles for each load level are shown. Comparing Fig. 6.6a and 6.6b, it is apparent that the higher BV/TV sample experiences lower strains at the same load level (i.e. it is stiffer) for both tension and compression. Nonlinearity of the stress-strain response is also more pronounced for the lower BV/TV sample (Fig. 6.6a). This BV/TV dependence was observed with all the samples.

Another apparent observation from the shape of the curves in Fig. 6.6 is that the demineralised samples become stiffer with increasing stress in tension and exhibit stiffness reduction with increasing stress in compression; this was observed at all load levels, in all cycles and for all tested samples. More importantly, the transition from tension to compression is smooth for every load level (Fig 6.6a and 6.6b); this was observed for all the samples tested. Further examination of the loading and unloading curves in compression indicates that buckling is not entirely elastic. Figure 6.6 clearly indicates that the original BV/TV plays an important role in the cyclic response of demineralised trabecular bone. It is important to note that all samples were extracted in the same direction, from similar anatomical site, from cattle of about the same age and employing the same demineralisation process i.e. by using HCl solution.

Ratcheting strain

Ratcheting strain can be defined as the average of peak strain in tension (ε_t^{peak}) taken as positive and compression (ε_c^{peak}) taken as negative at the same load

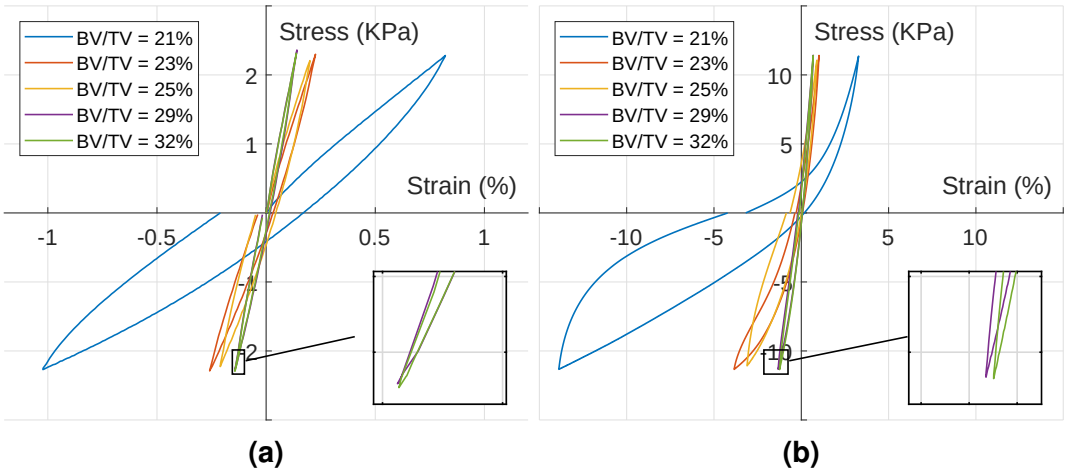

Figure 6.5: The stress-strain loops for demineralised trabecular bone samples under fully reversed tension-compression cyclic loading. Curves for samples tested at load level 1 (0.2 N) (a) and load level 5 (1 N) (b) for the first cycle of loading.

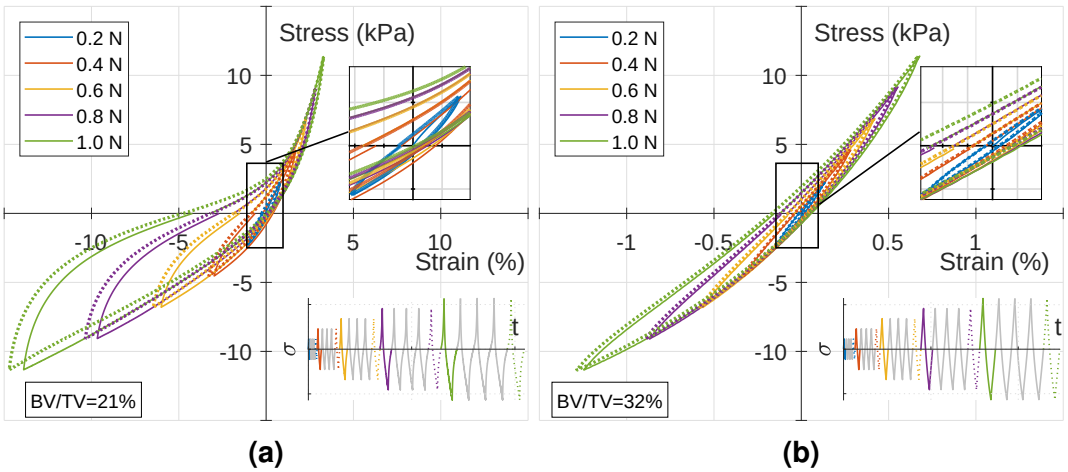

Figure 6.6: Comparison of all load levels for two typical samples under fully-reversed tension-compression cyclic loading. BV/TV = 21% (a) and BV/TV = 32% (b). For clarity, only the response to the first (solid line) and the fifth (dotted line) loading cycles are shown for each load level. Inset shows load application.

level (Fig. 6.4). A non-zero ratcheting strain only occurs when the mechanical properties in tension and compression are different (Shariati et al., 2012).

The most porous sample (with BV/TV of 21%) was considered first for demonstrating the variation in ratcheting strain (ε_r) in different cycles and at different load levels (Fig. 6.7a). Ratcheting strain was consistently negative, which implies that the demineralised samples experience larger strain in compression than in tension at the same load level (Fig. 6.7a). Even for this most porous sample the ratcheting strain only increases marginally with increasing

cycle number; while the increase with load level is nonlinear and much more significant. Next the ratcheting strain was considered for all 5 samples in the first load cycle for all load levels. As expected, the magnitude of ratcheting strains is much larger for samples with lower BV/TV (Fig. 6.7b). Also the ratcheting strains are consistently negative and their magnitude increases rapidly with load level (Fig. 6.7) indicating that the organic phase has a much better load bearing capability in tension without significant additional strains than in compression.

Dissipated strain energy density

DSEDT and DSEDC were calculated by integrating corresponding areas, as discussed and the results are shown in Fig. 6.8 for the first cycle for each load level. Both DSEDT and DSEDC increase with increasing load levels, and dissipated strain energy values and their rate of change increases with decreasing BV/TV (Fig. 6.8). Energy dissipation in compression was found to be consistently higher than in tension. This is because the samples experience not only lower strains in tension but also because tensile strains do not have large irreversible component. On the other hand, in compression the samples experience large strains and these include relatively large irreversible strains due to inelastic buckling of collagen struts.

Secant modulus

As discussed, four secant moduli were evaluated (Fig. 6.4): $E_t^{loading}$, $E_t^{unloading}$, $E_c^{loading}$ and $E_c^{unloading}$. These are illustrated for samples with the largest and smallest BV/TV in Fig. 6.9. As expected, the porous sample has smaller secant moduli in comparison to the denser sample (i.e. $E_t^{loading}$ = 0.28 MPa for BV/TV = 21% compared with 1.66 MPa for BV/TV = 32%). The unloading modulus is always higher than the loading modulus in both tension and compression.

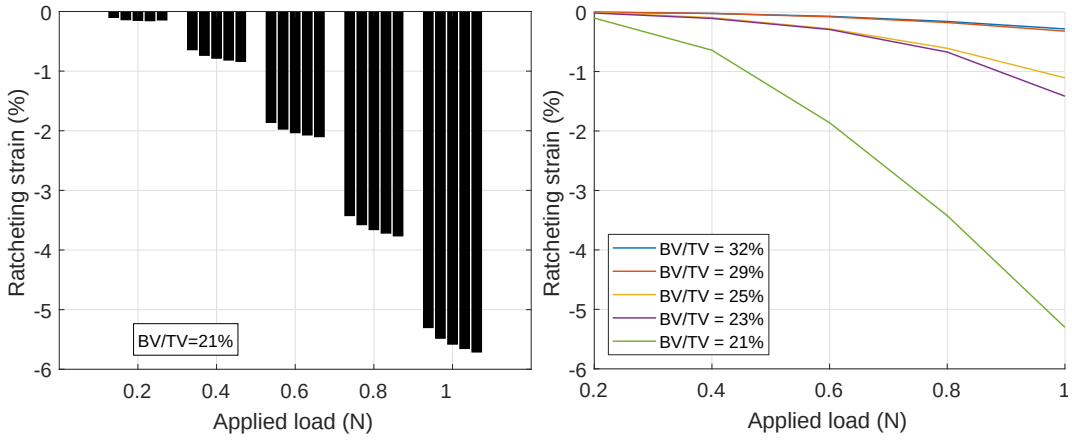

Figure 6.7: Ratcheting strain ($(\varepsilon_t^{peak}+\varepsilon_c^{peak})/2$), for all load levels and all cycles for a sample with BV/TV = 21% (a), and from cycle 1 for all samples at varying load levels (b).

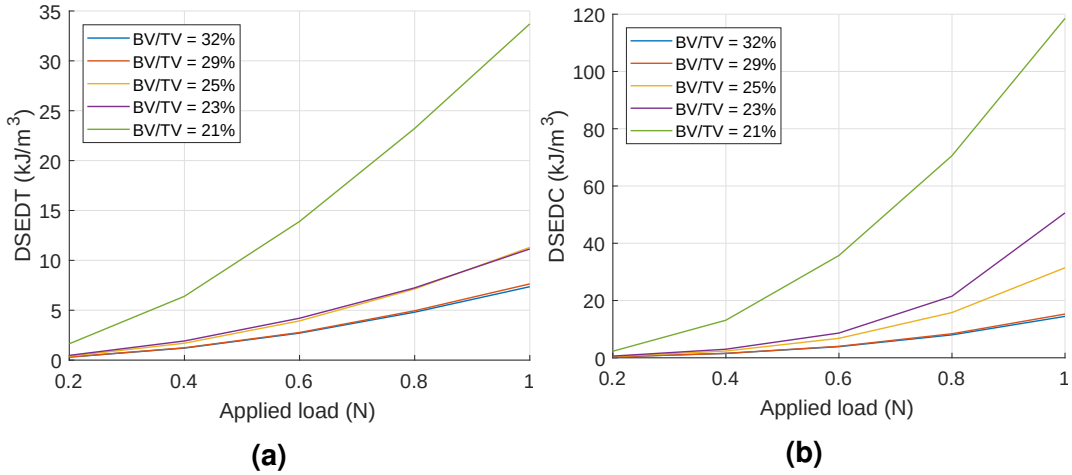

Figure 6.8: Dissipated strain energy density in tension and compression with varying load levels for all 5 samples; DSEDT (a) and DSEDC (b).

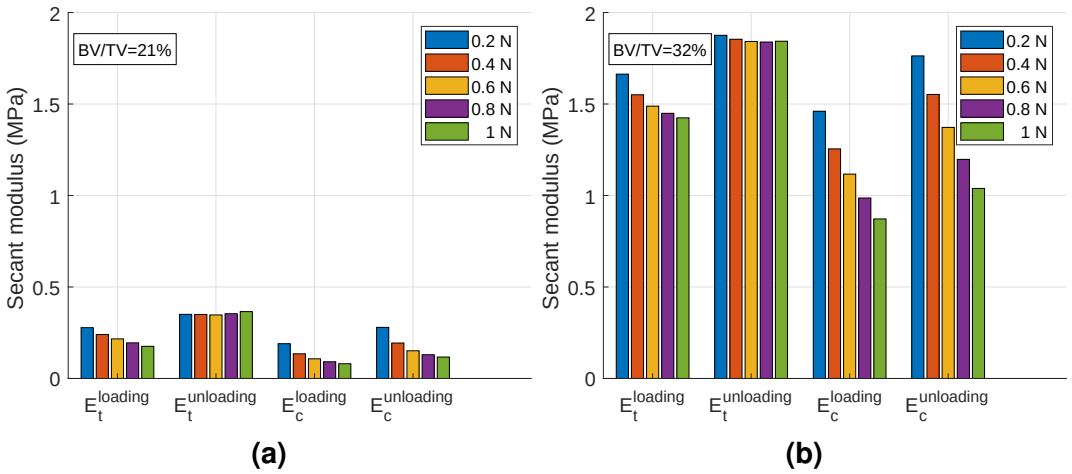

Figure 6.9: Secant moduli for two samples. BV/TV = 21% (a) and BV/TV = 32% (b).

With increasing load level, $E_t^{unloading}$ remains almost constant, while $E_t^{loading}$ decreases slightly. In contrast to tension, $E_c^{loading}$ and $E_c^{unloading}$ both decrease dramatically with increasing load level. This interesting trend, followed by all the samples, indicates that while compression leads to significant irreversible strain with increasing load in the demineralised microstructure of bone, this is relatively small in tension.

6.5.3 Discussion

This study considered fully reversible tension-compression cyclic loading tests on 5 demineralised trabecular bone samples with BV/TV ranging from 21% to 32%. Samples were subjected to five different load levels (0.2 to 1 N at 0.2 N interval denoted as load level 1 to 5), and 5 cycles were applied at each load level. The asymmetric responses of the organic phase of trabecular bone were found when it loaded cyclically from tension to compression. The study shows demineralised trabecular microstructure stiffens in tension and undergoes stiffness reduction in compression. The trend of the asymmetric mechanical response is associated to the original BV/TV.

In previous studies the shape of loading curve in compression for untreated trabecular bone have shown a reduced load carrying capacity with increasing load (Hansen et al., 2008; Kopperdahl and Keaveny, 1998; Matsuura et al., 2008) but unloading demonstrates that much of this is due to irrecoverable plastic strain (Keaveny et al., 1999; Moore and Gibson, 2002; Rapillard et al., 2006). It is perhaps not improper to infer that this is due to the damage and failure of the mineral phase. Stiffness reduction in compression has been previously observed for demineralised cortical bone (Novitskaya et al., 2013). For trabecular bone, however, the stiffness reduction is likely to be accentuated due to elastic and inelastic buckling of demineralised trabecular struts. Previous tests in tension on demineralised cortical bone have shown stiffening

with load increase (Bowman et al., 1996; Catanese III et al., 1999), similar to what was observed in this study. For untreated bone, however, it is stiffness reduction (rather than stiffness increase) that has been previously observed in tension as well (Kopperdahl and Keaveny, 1998), which can be attributed to failure of the mineral-collagen interface.

To the best of author's knowledge, there have been no previous tests on demineralised bone, cortical or trabecular, that have considered fully reversible cyclic loading. However, similar compression-softening and stretch-stiffening have been previously observed in semi-flexible biopolymers (van Oosten et al., 2016) where it has been suggested that this asymmetric response in tension and compression is caused by the bending and/or buckling stress in fibres under compression, force for which is much lower than the load required for straightening and stretching. This behaviour is akin to a rectangular steel frame braced along one diagonal and subjected to shear (Berman et al., 2005). When the diagonal brace is in tension the deformation of the frame is limited but when it is in compression its inelastic buckling results in larger deformation and residual deformations.

Observed irreversible strain, author believes, is due to inelastic buckling in compression as stated above and has implications for old/osteoporotic bone. Ageing bone not only leads to reduction in BV/TV but also relative increase in mineral to collagen ratio (Bailey et al., 1999). Consequently, there is increased reliance on the limited organic phase to provide ductility; the results show that the demand to sustain increasing magnitudes of strain by the organic phase increases dramatically in compression with decreasing BV/TV. At the macro scale the behaviour of bone in tension and its fracture toughness have been seen as key to bone fracture (Vashishth, 2007) while results from this section indicate that possible failure due to inelastic trabecular buckling in compression needs greater consideration. Mineral deposition increases the elastic modulus of bone and hence the buckling load, however once bucking is initiated

(which is more likely in low BV/TV bone) then it is likely to be inelastic due to limited contribution of mineral in tension. Buckling has been previously proposed as the probable cause of failure for vertebral trabecular bone (Bell et al., 1967; Snyder et al., 1993),. The results from this section demonstrated that this buckling of trabeculae could be initiated from organic phase of trabecular bone. This study also shows that the possibility of hip fractures in the elderly occurring due to normal physiological activities, such as level walking, resulting in the individual falling down (rather than the fracture being caused by a fall) does exist (Viceconti et al., 2012).

A few studies have attempted to develop predictive models of the mechanical behaviour of bone based on the properties of the mineral, organic phase and their interaction at either the solid phase level (Hamed et al., 2012b) or in terms of demineralised and deproteinised macro level (Lubarda et al., 2012). These cited studies have been limited to the prediction of elastic properties and have not distinguished between compression and tension. This study can help take these predictive models forward. It is important to note that many of the findings in this study were only made possible by the novel experimental protocol which permitted evaluation of demineralised samples at different load levels and in both tension and compression.

6.5.4 Limitations

This study suffers from a number of limitations. Firstly, all the tests were conducted at room temperature; creep behaviour has been reported to be temperature dependent (Bonfield and Li, 1968). Secondly, the stress-strain responses were measured directly from the machine rather than using extensometer, but the aim of the study is to compare the trends response to reversible cyclic loading from tension to compression and across samples with different BV/TV prior to demineralisation. Lastly, since only limited number of samples were

considered, a statistical analysis that considers the influence of different variables was not possible. These trends, author believes, are real despite the limitations.

6.6 Tensile MLCUR experiment

6.6.1 Mechanical test

Each sample was first preconditioned by subjecting it to 10 cycles of tensile loading with an amplitude of 0.1% apparent strain. The tensile multiple-load-creep-unload-recovery (MLCUR) experiment (Fig. 6.10) was conducted on 8 fully demineralised trabecular bone samples by using Instron material testing machine (50 N load cell, Model 3367).

Loading cycles comprise of load application corresponding to 0.6 $\%\varepsilon$, 0.8 $\%\varepsilon$, 1.0 $\%\varepsilon$, 1.5 $\%\varepsilon$, 2.0 $\%\varepsilon$, 2.5 $\%\varepsilon$, 3.0 $\%\varepsilon$, 3.5 $\%\varepsilon$, apparent static strains at the rate of 1.0 $\%\varepsilon/s$. While the first few strain levels are below the apparent yield strain for trabecular bone, the later ones are above it (Bayraktar et al., 2004). When the target strain was achieved the corresponding load was maintained for 400 s thereby permitting the sample to undergo creep. Each loading step was followed by an unloading step to a zero force at the same rate for loading (1.0 $\%\varepsilon/s$) and this force was maintained for 1000 s before proceeding to the next cycle. The durations for creep and recovery were determined after initial pilot tests which showed that 400 s and 1000 s were more than sufficient for the samples to achieve a constant creep rate and for recovery curves to reach a plateau, respectively.

6.6.2 Results

Without exception, each sample exhibited classical rapid primary and slow secondary regimes of creep behaviour across all stress levels and all 8 samples

could be subjected to the highest designated stress level, which corresponded to static strain of 3.5 $\%\varepsilon$, without tertiary creep.

Experiment observations

Figure 6.11a shows a strain response from tensile MLCUR experiment for one typical sample (medium porosity, BV/TV = 26.8 %). The stress levels were only 12.3 kPa and 106.9 kPa for achieving corresponding apparent static strain levels of 0.6 $\%\varepsilon$ and 3.5 $\%\varepsilon$, respectively. The time-varying compliance defined as the ratio between time-varying strain and its corresponding stress level, denoted as D_t^{cre} and D_t^{rec} for creep and recovery, respectively, were both found to increase with time for all stress levels as expected for viscoelastic material (Fig 6.11b and 6.11c). The compliances, D_t^{cre} and D_t^{rec}, for demineralised trabecular bone were also found to vary with stress levels, indicating a nonlinear viscoelastic response.

It can be seen that for this typical sample, the time-varying compliance decreases with increasing stress levels (i.e. the curves at lower stress levels were above those at the higher stress level), and this was true for both creep and recovery compliances (Fig 6.11b and 6.11c, respectively). This decreasing trend was followed by all the tested samples, which demonstrated elastic stiffening with increasing stress levels. It was also observed that the recovery compliance (D_t^{rec}) were slightly smaller than creep compliance (D_t^{cre}) at the same cycle (or at the same applied stress level). It was apparent that the creep compliance (D_t^{cre}) showed an increasing trend with time for every loading cycle, while recovery compliance (D_t^{rec}) reached a plateau after almost 400 s of recovery. This also reveals that irrecoverable strain develops in the loading and load holding phases, while viscoelastic strain recovers during unloading and recovery phases.

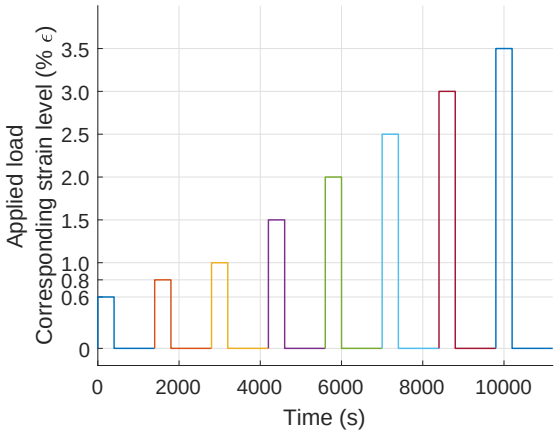

Figure 6.10: Load application of tensile multiple-load-creep-unload-recovery (MLCUR) experiment.

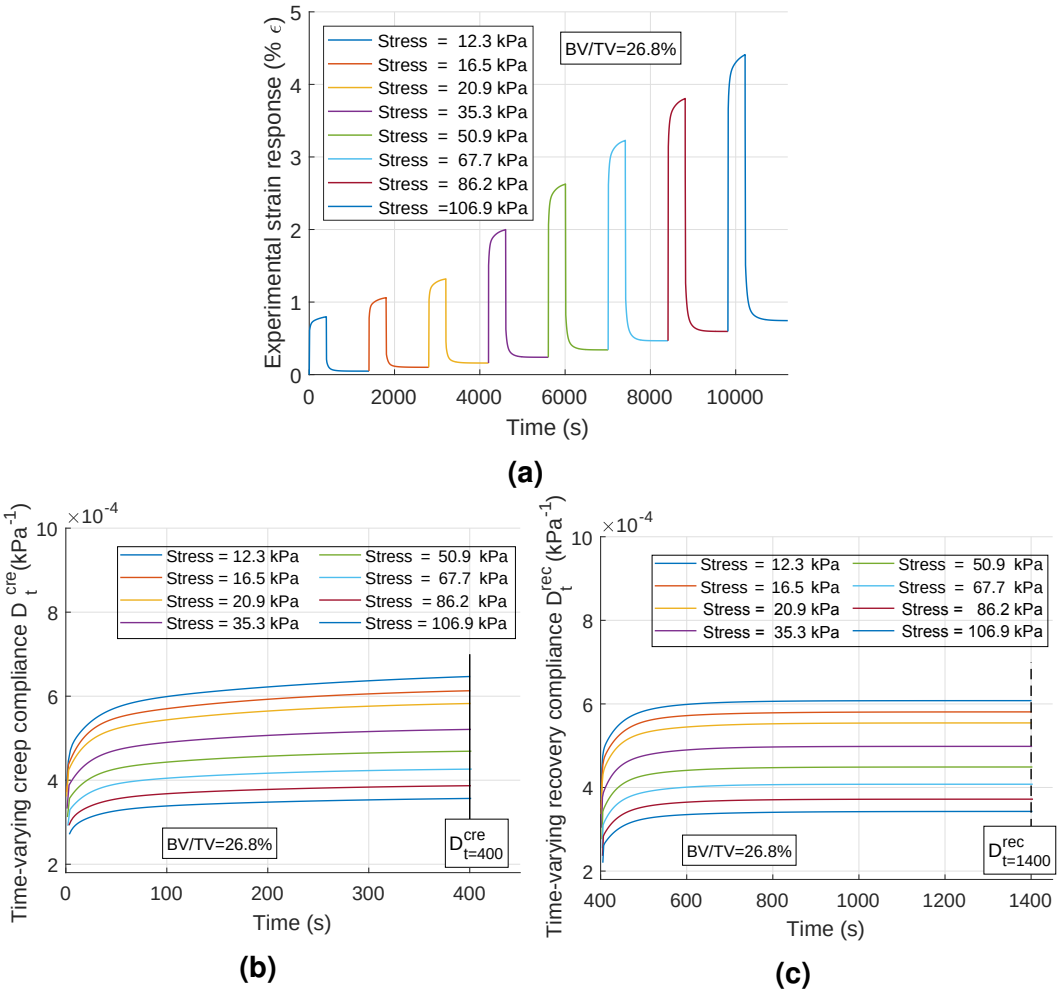

Figure 6.11: Experimental response and time-varying compliances for one typical sample. Experimental response of demineralised sample from tensile MLCUR test (a); experimental time-varying creep compliance (b) and recovery compliance (c) with varying stress levels.

Compliance at the end of creep (t = 400 s) and recovery (t = 1400 s) from every loading cycle are shown in Fig. 6.11b and 6.11c, denoted as $D^{cre}_{t=400}$ and$D^{rec}_{t=1400}$, respectively. Figure 6.12 shows both compliances plotted against normalised effective stress (σ/σ_0), for all tested samples. The normalised effective stress (σ/σ_0) defined as the stress in each cycle divided by the stress from its first cycle (Manda et al., 2016a).

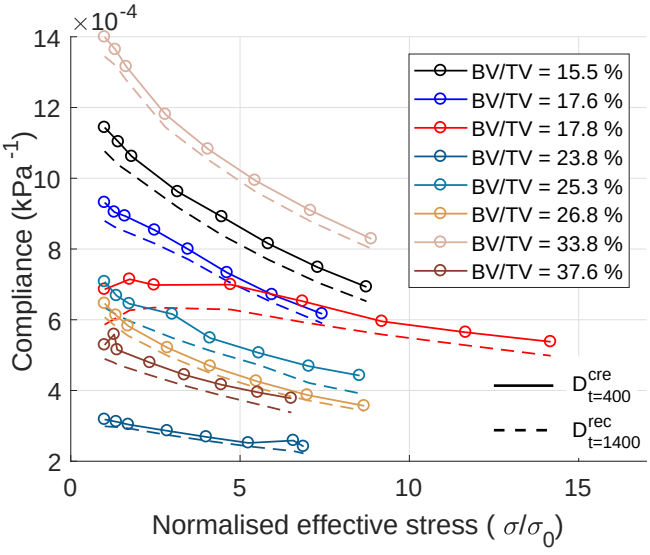

Figure 6.12: Compliances vs. normalised effective stress. Creep compliance at 400 s ($D^{cre}_{t=400}$) and recovery compliance at 1400 s ($D^{rec}_{t=1400}$) plotted against normalised effective stress for all 8 specimens.

The creep compliance at t = 400 s ($D^{cre}_{t=400}$) was in the range of 0.24×10^{-3} to 1.40×10^{-3} kPa^{-1}, and the recovery compliance at t = 1400 ($D^{rec}_{t=1400}$) was in the range 0.22×10^{-3} to 1.35×10^{-3} kPa^{-1} as shown in Fig. 6.12. The clear decreasing trend in compliances with increased normalised stress level was observed for almost all tested samples, except one sample with BV/TV = 17.8 % (in which the compliance slightly increased at first few cycles, but it decreased at the higher cycles). These results show that the samples with higher BV/TV have a lower compliance in comparison to samples with lower BV/TV (e.g. at Cycle I, the $D^{cre}_{t=400}$ is 1.14×10^{-3} kPa^{-1} for BV/TV of 15.5 % and reduced to 0.53×10^{-3} kPa^{-1} when BV/TV increased to 37.6 %). This BV/TV-based compliance dependence trend was largely followed by all samples, except two specimens (BV/TV = 33.8 % and 23.8 %). Decreasing compliance with stress level indicates that the demineralised trabecular bone behaves in nonlinear

viscoelastic manner and it stiffens with increasing stress levels. Therefore, the nonlinear constitutive model is required to describe time-dependent behaviour of demineralised trabecular bone.

The compliances from the recovery regimes become constant (recovery curve reach a plateau) in a short time, which indicates that the viscoelastic strain were recovered fully within this 1000 s of recovery time in each loading cycle. The strains at the end of each cycle were irrecoverable and it was found to exist even at the end of first loading cycle. Figure 6.13 shows the irrecoverable strain along with its applied apparent static strain for all the cycles and all the samples. A reasonable ($r^2 = 0.77$, $p<0.0001$) power law relationship was found between irrecoverable strain and applied static strain, whereas no significant correlation was found between the irrecoverable strain and its original BV/TV. It was clear that this irrecoverable strain increases with applied load level for all demineralised trabecular bone sample.

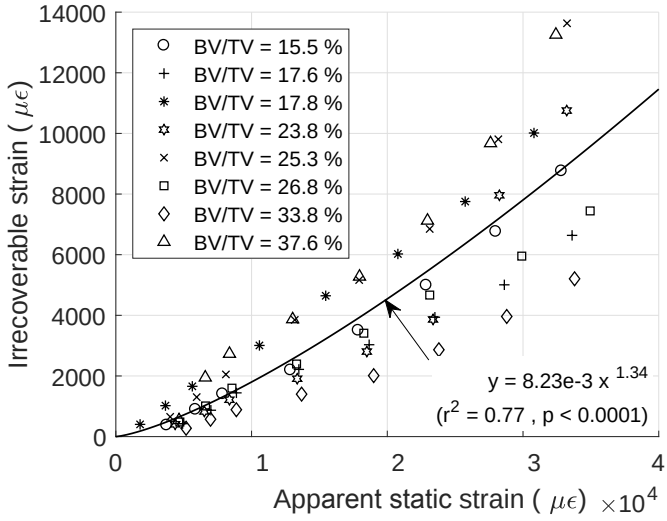

Figure 6.13: Irrecoverable strain vs. applied apparent static strain. Irrecoverable strain at the end of each loading cycle for all the specimens plotted against the applied apparent static strain (where plateau force was held constant during test) with a power law relationship (r^2 = 0.77 , $p<0.0001$).

Constitutive model

The linear and nonlinear Kelvin-Voigt model or Prony series were selected to describe time-dependent behaviour, described by Park and Schapery (1999) and discussed in Chapter 3. Some of equations are repeated here for convenience. The linear and nonlinear viscoelastic strain denoted as LVE and NVE

given by:

$$\varepsilon_{ve}(t) = D_g\sigma + \int_0^t \Delta D(t-\tau)\frac{d\sigma(\tau)}{d\tau}d\tau \tag{3.11}$$

and

$$\varepsilon_{nve}(t) = g_0 D_g\sigma + g_1\int_0^t \Delta D(\psi^t - \psi^\tau)\frac{d(g_2\sigma(\tau))}{d\tau}\tau \tag{3.20}$$

respectively. Following the approach used for untreated bone in the last Chapter, where the first cycle was assumed linear viscoelastic, so that glassy or instantaneous compliance (D_g), transient retardation strengths (ΔD) and retardation times (τ) can be evaluated by minimising the errors between experimental measurements and Eq. 3.11. Thereafter, the stress dependent nonlinear parameters g_0, g_1, g_2 and α_σ in Eq. 3.20 can be evaluated from higher loading cycles.

By fitting experimental curves from demineralised trabecular bone with LVE constitutive model, the instantaneous compliance (D_g) were found to be in the range 0.20 to 0.66 MPa^{-1} (Fig. 6.14). It was also found that D_g decreased with increasing BV/TV with a power law relationship, $D_g = 6.43 \times (\text{BV/TV})^{-0.87}$ ($r^2 = 0.55$, $p<0.0001$), as shown in Fig. 6.14.

As stated above, the demineralised trabecular bone response was in a nonlinear manner with respect to stress and stress-dependent nonlinear parameters were evaluated from higher loading cycles. Figure 6.15 shows a variation of these parameters for a typical sample with BV/TV = 26.8 %. It shows that

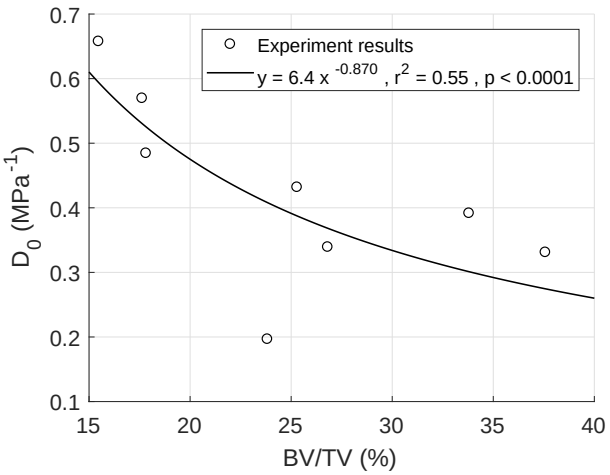

Figure 6.14: Instantaneous compliance (D_g) plotted against BV/TV for pooled data. Power law relationship was found, $D_g = 0.12 \times \text{BV/TV}^{-0.87}$ ($r^2 = 0.55$, $p<0.0001$).

for this typical sample, the values of g_0 and g_2 decrease with increasing normalised effective stress, whereas the values of g_1 and α_σ are almost constant (Fig. 6.15). The product of $g_1 g_2$, which affects the transient response was also found to decrease with increasing normalised effective stress. These observations lead to the choice of a second-order polynomial function to represent the nonlinear viscoelastic parameters as functions of normalised effective stress, which produced coefficients of determination of r^2 = 0.93, 0.84, 0.99 and 0.96 for parameters g_0, g_1, g_2 and α_σ, respectively, as shown in Fig. 6.15 for the selected typical sample. The decreasing trend of curves indicates that the demineralised trabecular bone stiffens with increased stress levels, and this elastic stiffening phenomenon were observed for all the samples tested.

The accuracy of linear viscoelastic (LVE) and nonlinear viscoelastic (NVE) constitutive model were compared with experimental strain response without considering residual strain (or irrecoverable strain) (Fig. 6.16a and 6.16b) and with residual strain in consideration (Fig. 6.16c and 6.16d) for two typical samples with BV/TV = 15.5% and 37.6%. These samples had the lowest and highest BV/TV. For clarity, only first 5 loading cycles are shown in Fig. 6.16.

It is important to reiterate that LVE and NVE constitutive models are based on recovery response which only comprises of viscoelastic response. Hence, the LVE and NVE prediction compared with experimental strain response without residual strain (Fig. 6.16a and 6.16b), i.e. in this case, the residual strain has been subtracted from each cycle. It is clear that the NVE constitutive model gives a more accurate prediction, whereas the LVE constitutive model gives a reasonable prediction at the lower loading cycle; it over-predicts the strain response at the higher cycles, which also indicates that the demineralised trabecular bone undergoes elastic stiffening with increased stress levels (Fig. 6.16a and 6.16b). This was found to be true for all the samples tested in this study.

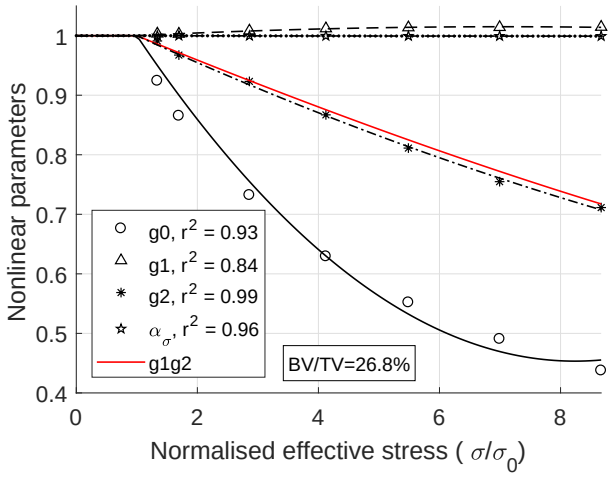

Figure 6.15: Nonlinear viscoelastic parameters for a typical demineralised sample. g_0, g_1, g_2, α_σ and $g_1 g_2$, are expressed as second-order polynomial functions of effective stress for a typical sample with BV/TV = 26.8 %.

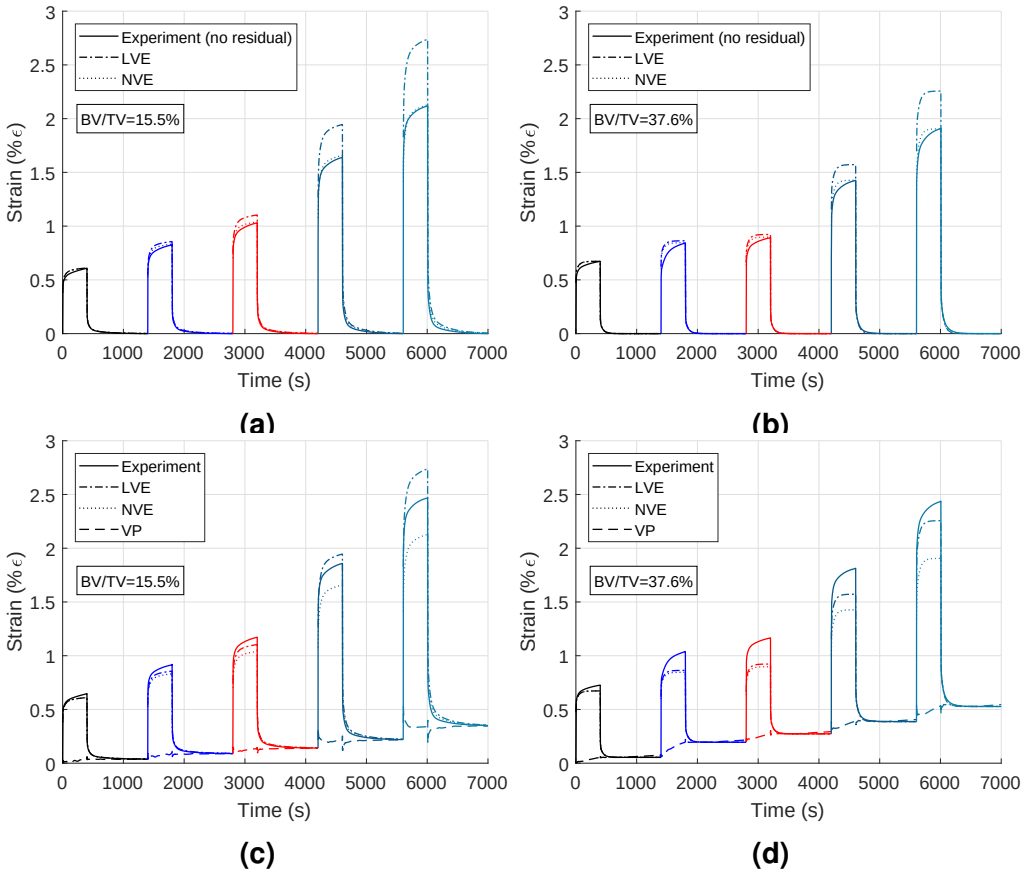

Figure 6.16: The comparison of experimental strain response and constitutive model predictions. Experiment response and the predicted LVE and NVE strain response when residual strain excluded (a and b), when residual strain included (c and d), for two samples with lowest and highest BV/TV.

The viscoplastic (VP) strain can be evaluated by taking the difference between creep (which include both viscoelastic and viscoplastic) and recovery curve (viscoelastic only), as shown in Fig. 6.16c and 6.16d. The accuracy of NVE model prediction is decreased when viscoplastic strain taking into account and as discussed earlier, this irrecoverable strain is not significantly related to bone's BV/TV (Fig. 6.13).

6.6.3 Discussion

This tensile multiple-load-creep-unload-recovery (MLCUR) experiment demonstrates that demineralised trabecular bone's response to mechanical forces is time-dependent and the strain always comprises of recoverable and irrecoverable components even at low stress levels. The results also showed that this time-dependent behaviour of demineralised trabecular bone varies nonlinearly with the applied stress, and it stiffens with increased stress levels.

The MLCUR experiment had been successfully conducted to investigate untreated trabecular bones time-dependent behaviour (Chapter 4 and 5). Therefore, this Chapter employed a similar MLCUR experimental protocol and similar analysis approaches to evaluate the time-dependent behaviour of demineralised trabecular bone. The 400 s for creep and 1000 s for recovery were chosen after number of preliminary studies, which showed that the steady state creep rate becomes constant in less than 400 s upon loading and the recovery curves reach a plateau in less than 1000 s. Previous studies have shown that the demineralised bone dose not yield up to an apparent yield of 10% in tension (Bowman et al., 1996). Therefore, the first strain level of 0.6 $\%\varepsilon$ can be considered still in the elastic range.

While untreated trabecular bone has been recognised as a time-dependent material, it is for the first time, the time-dependent behaviour of demineralised trabecular bone had been evaluated. The observed creep compliances for

demineralised trabecular bone in tension were in the range of 0.22×10^{-3} to $1.40 \times 10^{-3}\ kPa^{-1}$ while the creep compliance in compression for untreated bone was found to be in the range 1.08×10^{-3} to $4.17 \times 10^{-3}\ MPa^{-1}$ (Sec. 5.2). Those observations indicate that the demineralised trabecular bone is much more flexible than untreated bone. The decrease of modulus for bone after demineralisation has also been reported for cortical bone (Bowman et al., 1996; Burstein et al., 1975; Catanese III et al., 1999; Novitskaya et al., 2011) and trabecular bone (Chen and McKittrick, 2011), but limited to monotonic loading. There is only one study which conducted cyclic loading on demineralised cortical bone, and Novitskaya et al. (2013) reported that the demineralised sample has extremely low initial tangent modulus, below 5.1 MPa for its first loading cycle, for all three different anatomic directions.

Trabecular bone has been investigated extensively for its mechanical properties; the relationships between time-independent elastic modulus and BV/TV (or density) have been reported over last two decades (Currey, 1988). In Chapter 5 of this study (Sec. 5.2), a strong power law relationship between instantaneous creep compliance and BV/TV were found for untreated trabecular bone. In this Chapter, a similar relationship was found, not strong but significant, between instantaneous creep compliance (D_g) and BV/TV. Only a weak relationship ($r^2 = 0.55$) was observed; this possibly means that some other mechanisms are in play for demineralised trabecular bone, possibly at the nano-scale of organic phase of bone, which need further investigations.

Similar to untreated trabecular bone, the demineralised trabecular bone's time-dependent behaviour is nonlinearly related to its applied stress level and it stiffens with increased stress levels. This elastic stiffening behaviour has been observed from experimental observation, where the creep compliance at the lower stress levels are above those at the higher stress levels. This stiffening behaviour is also confirmed from the constitutive model study, the nonlinear parameters (g_0 and $g_1 g_2$) decrease with increasing normalised stress

levels. This elastic stiffening behaviour has been reported by a number of researches through compressive creep-recovery experiments on untreated bone (Kim et al., 2011) and demineralised bone (Bowman et al., 1996). The important role of sliding or reorganisation of collagen fibrils in the mechanical behaviour of bone had been pointed out by a number of studies (Bowman et al., 1998; Sasaki et al., 1993; Yamashita et al., 2001). After the mineral removal from bone, Bowman et al. (1996) found an initial nonlinear behaviour by conducting a tensile monotonic loading on demineralised cortical bone; a larger modulus was found at a higher strain range. This stiffening behaviour had also been observed by Schmoller et al. (2010), who conducted cyclic loading on actin networks. The consistent observation between current study and above cited studies all affirmed that the stiffening phenomena which is possibly due to reorganisation of collagen fibrils. The developed nonlinear time-dependent constitutive model can be incorporated together with properties of mineral to generate the composite model of bone. It will help provide a better understanding of this natural composite material.

The time-varying recovery compliance become constant in a short time, which indicates that the viscoelastic strain is recovered fully within 1000 s of recovery time in each loading cycle. This was also observed from its constitutive model prediction, the NVE prediction showed that the strain were recovered to zero within the designated 1000 s recovery time. This study also shows that there were strains at the end of each cycle which were irrecoverable.

By conducting uniaxial nano-mechanical compression on cylindrical samples, with diameters between 250 nm and 3,000 nm (nano- to micro-scale), Tertuliano and Greer (2016) proposed that inter-fibrillar sliding through shear of extra-fibrillar matrix was the mechanism of plasticity in bone, which is also reported by Gupta et al. (2006, 2005). Here, in this study, at the macro-scale, it is observed that some irrecoverable strain exists at the end of recovery. This irrecoverable strain could be also due to inter-fibrillar sliding at lower scale. This

irrecoverable deformation in collagen should be emphasised, as it is generally ignored in two-phase composite models of bone (Lubarda et al., 2012).

6.6.4 Limitations

This tensile MLCUR experiment suffers from a number of limitations, Firstly, all the test are conducted at room temperature; creep behaviour has been reported to be temperature dependent for untreated bone (Bonar and Glimcher, 1970; Bowman et al., 1998), so it is likely that the demineralised trabecular bone's viscoelastic behaviour is also temperature dependent. Secondly, it is not possible in practice to perform ideal creep-recovery experiments and in the tests conducted, the time interval to loading and unloading is finite (e.g. 1 s to reach 1% strain with the designated strain rate 1 $\%/s$). Small viscoelastic deformations are likely to occur during its loading and unloading. Lastly, this part only considered a limited number of samples, a statistical analysis that considers the influence variables was not possible.

6.7 Conclusions

6.7.1 Fully reversed tension-compression experiment

- The developed novel experimental protocol can evaluate the mechanical response of materials under cyclic loads of varying magnitudes ranging from tension to compression.
- Organic phase of trabecular bone exhibits tension-compression asymmetric and varies with load levels and porosity.
- Collagen struts stiffen in tension while they undergo stiffness reduction in compression.

- The organic phase exhibits inelastic buckling in compression, which is more apparent in porous samples. This may explain, at least partially, the reasons for non-traumatic fractures in the elderly.

- These finding will help in the development of composite models from the mechanical response of bone's constituents.

6.7.2 Tensile MLCUR experiment

- Organic phase of trabecular bone is much more flexible than untreated bone, with Young's modulus of a few MPa.

- The time-dependent behaviour of the organic phase of trabecular bone is nonlinearly related to its applied stress level - it stiffens with increased stress level.

- Irrecoverable strain exists even at the low stress level (corresponding to apparent static strain 0.6 $\%\varepsilon$).

- The nonlinear viscoelastic model give a good prediction of the time-dependent behaviour of the organic phase.

"An ounce of prevention is worth a pound of cure."

Benjamin Franklin

7

Deproteinised trabecular bone

Trabecular bone can be considered as a composite material consisting of interpenetrating mineral and organic phases. In the last Chapter, mechanical properties of demineralised trabecular bone were investigated. This Chapter considers the mechanical properties of deproteinised trabecular bone (mineral phase).

Although a few previous studies have attempted to understand the monotonic behaviour of deproteinised bone, they have been largely limited to cortical bone (Hamed et al., 2012b; Novitskaya et al., 2011) and to the author's knowledge there was only one study on trabecular bone (Chen and McKittrick, 2011). The apparent density (or BV/TV) had been successfully used as the predictor of mechanical behaviour of untreated bone, but the relationship between BV/TV and biomechanical properties of deproteinised bone remain unknown. This Chapter aims to fill this gap.

7.1 Sample preparation

Fresh proximal tibias from bovine (under 30 months old when slaughtered) were obtained from a local abattoir and were stored at -20 $^{\circ}C$ until utilised. The bones were allowed to thaw at room temperature before bone cores were extracted along its principle axis, using a 10.7 mm inner diameter diamond coring tools (Starlite, Rosement, IL, USA). A low speed rotating saw (Buehler, Germany) was used to create parallel section and to trim growth plates if they were present. All preparation processes, including coring and cutting, were conducted in a water bath to avoid excessive heat generated. The cylindrical bone samples, in total n = 9, were of mean length of 20.6 $\pm$ 0.6 mm.

Bone marrow was removed from each sample using a dental water jet (Interplak, Conair) with tap water at room temperature (Lievers et al., 2007). All the samples were then centrifuged at 2000 $r.p.m$ for 2 hours to remove any residual marrow (Sharp et al., 1990) and the samples were wrapped in PBS-soaked tissue paper.

7.2 μCT scanning

All the samples were scanned before any chemical treatment using micro-computed tomography (μCT) scanner (Skyscan 1172, Bruker, Kontich, Belgium) at a high voxel resolution of 17.22 μm. The following scan parameters were used: source voltage 54 kV, current 185 μA, exposure 885 ms with a 0.5 mm aluminium filter between X-ray source and the specimen. Image quality was improved by using two-frame averaging. The images were reconstructed with no further reduction in resolution using nRecon (V1.6.9.4, Bruker, Kontich, Belgium). Morphometric analysis was performed using CTan software (Bruker, Kontich, Belgium). By considering the whole volume of each specimen, the bone volume fraction (BV/TV) was found in the range of 15.5 - 37.6%.

7.3 Deproteinisation

Deproteinisation was accomplished by using mild bleach, 20 ml 6% sodium hypochlorite (NaOCl) at 37 $^{\circ}C$ water bath and the bleach solution subjected to change daily for 2 weeks (Manilay et al., 2013). To check the efficiency of deproteinisation, two samples were immersed in 0.6N HCl after deproteinisation, to remove the mineral. Visual examination found that there was no detectable dry material remains, indicating that the deproteinisation methodology is effective and the remaining 7 samples had been fully deproteinised (Chen et al., 2011). Figure. 7.1 shows a photography of deproteinised trabecular bone.

Figure 7.1: Photograph of deproteinised trabecular bone from bovine proximal tibia.

7.4 Compressive monotonic testing

A preliminary creep-recovery experiment conducted on deproteinised trabecular bone, there was no apparent time-dependent strain response observed when the constant force applied. Brittle nature of deproteinised samples prevented any cyclic loading experiment to be taken. Therefore, the tests conducted were limited to compressive monotonic testing.

Samples were glued into end-caps by using bone cement (Simplex, Stryker, UK) with the assistance of a custom made alignment tools to minimise the end-artefacts during testing (Keaveny et al., 1997). Effective length (17.6 $\pm$ 0.6 mm)

of each specimen was calculated as the length of the sample between the end-caps plus half the length of bone embedded within end-caps from each side (Keaveny et al., 1997). Each specimen was placed in an epoxy tube filled with phosphate-buffered saline (PBS), to ensure that the samples remain hydrated at all stages of testing. Seven DP samples were tested by compressive monotonic loading at loading rate of 0.5 $\%\varepsilon/s$ up to 20 $\%\varepsilon$ at room temperature using Zwick material testing machine (5 kN Load Cell, Model Z005/TH2A, Zwick Roell, Herefordshire, UK).

A number of output parameters were evaluated from the monotonic loading curve (Fig. 7.2): elastic modulus (E), stress at failure (σ_f) , corresponding strain at failure (ε_f) and toughness (W). Modulus (E) was obtained by taking the slope of stress-strain curve from the most linear part. Toughness (W) was determined by integrating the stress-strain curve, it is the energy of mechanical deformation per unit volume prior to fracture.

$$\boldsymbol{W = \int_0^{\varepsilon_f} \sigma d\varepsilon} \tag{7.1}$$

where σ, ε are stress and strain.

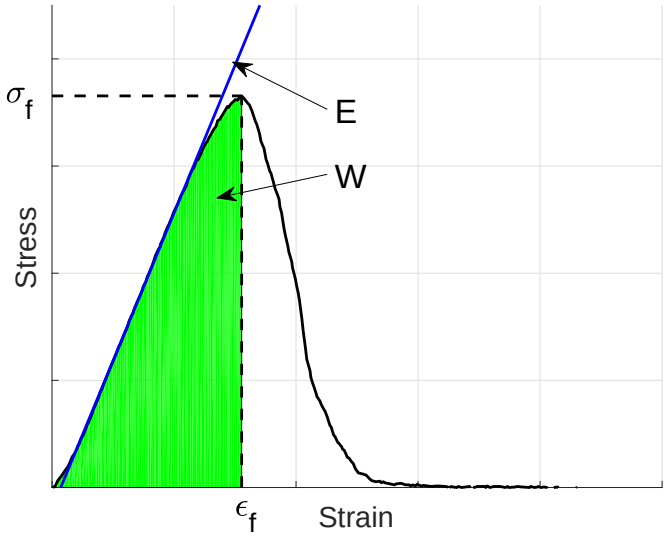

Figure 7.2: Definition of parameters defined from monotonic loading. The peak stress is σ_f and ε_f is corresponding strain. The enclosed area before peak point is W, and the slope of the initial $\sigma - \varepsilon$ curve is defined as E.

7.5 Results and discussion

Figure 7.3 shows cross-sectional and longitudinal images of untreated and deproteinised bovine tibia trabecular bone sample. It is apparent that they have similar structural morphology, and the μCT showed that there was almost no change in BV/TV of samples before and after the deproteinisation process.

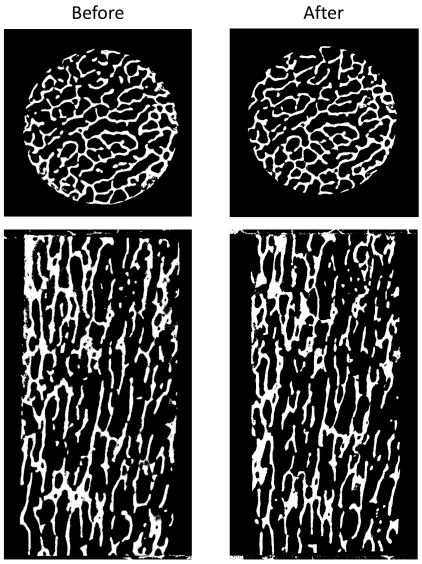

Figure 7.3: μCT image of the trabecular bone samples before and after deproteinisation. It shows both top views (top images) and side views (bottom images).

Six samples were successfully tested with monotonic experiments. The deproteinised trabecular bone samples were observed to be brittle, as the connecting and ductile collagen had been removed. One sample was damaged while being glued into the end-caps.

7.5.1 Phenomenological aspects

Figure 7.4a shows the stress-strain curve from compressive monotonic loading for all six deproteinised bovine tibia trabecular bone samples of different BV/TV. Four different regions can be observed: an initial linear-elastic regime that reaches a maximum stress followed by a rapid stress drop, and further followed by a plateau of roughly constant stress over a wide range of compressive strain of up to around 5%. At strains larger than 10% the stress rises due to densification. The enlarged loading curve within 2% of strain is shown in

Fig. 7.4b. The suddenly drop of stress from its peak point was observed for all deproteinised samples except one (BV/TV = 24.0%).

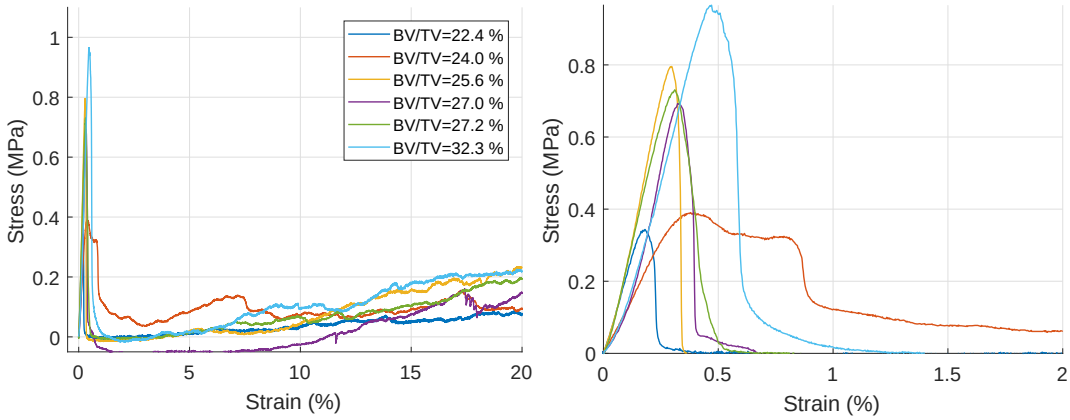

Figure 7.4: σ-ε curve from deproteinised trabecular bone samples when it was subjected to compressive monotonic loading. Stress-strain curve of deproteinised trabecular bone from bovine tibia with varying BV/TV (a); enlarged view of strain curve shows strain up to 2 % (b).

Figure 7.4b shows no apparent nonlinear behaviour before its peak point, although the deproteinised trabecular bone samples were loaded at such slow strain rate (0.005 ε/s). It is important to recall that the apparent initial nonlinear region could be seen from demineralised bone for both tension (Bowman et al., 1996; Burstein et al., 1975; Catanese III et al., 1999) and compression (Chen and McKittrick, 2011; Novitskaya et al., 2011, 2013). The fully reversed cyclic loading from tension to compression, performed in Chapter 6 also demonstrated that the biomechanics of organic phase is highly nonlinear.

In previous studies, the shape of loading curve for untreated trabecular bone shows reduced tangent modulus with increasing strain (Hansen et al., 2008; Keaveny et al., 1999; Kopperdahl and Keaveny, 1998; Matsuura et al., 2008; Moore and Gibson, 2002; Rapillard et al., 2006). It is fair to infer that the nonlinear response of bone is due to the nonlinear mechanical properties from bone's organic phase rather than the mineral phase.

7.5.2 Regression analysis

The samples were extremely fragile and fractured in a brittle mode, at very low compressive strength (<1.0 MPa) and failure strain (<0.5%) (Fig. 7.5a and 7.5b, respectively). Both σ_f and ε_f were found to be reasonably related with its BV/TV with a power law relationship (r^2 >0.65).

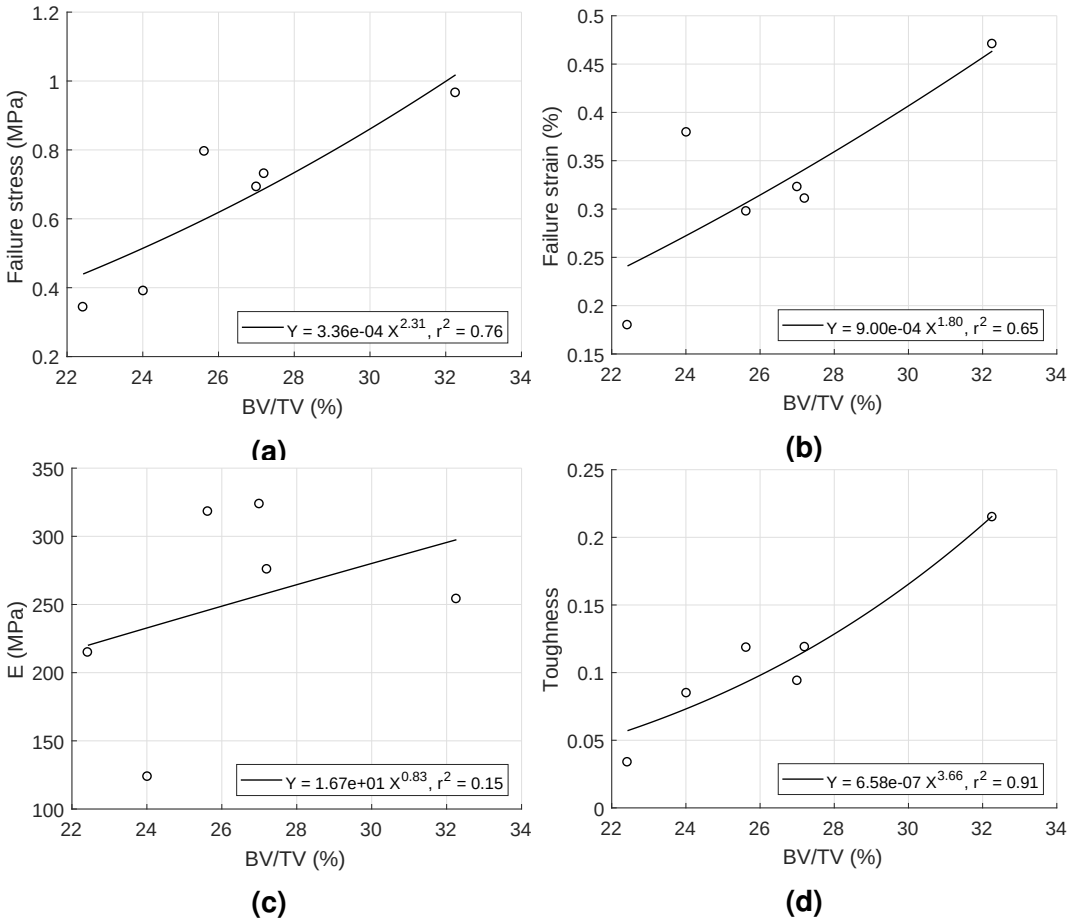

Figure 7.5: Regression analysis of some parameters from monotonic loading with changing BV/TV. Failure stress (a); failure strain (b); modulus (c) and toughness (d) plotted against BV/TV, and also their proposed power law fitting.

Chen and McKittrick (2011) reported that the deproteinised trabecular bone from bovine femur had strength of 0.48 ($\pm$ 0.36) MPa, while this study found the strength to be 0.65 ($\pm$ 0.24) MPa for deproteinised trabecular bone from tibia (the density of samples for above cited study and current study are taken before deproteinisation). It is worth noting that in Chen and McKittrick (2011)'s study, the reported apparent density was 0.23 g/cm^3, while the sample used in

this study had an average density of 0.60 g/cm^3, this might explain the larger strength or σ_f was found in this study. The ε_f was found in the range of 0.18 - 0.47% with mean value of 0.33% ($\pm$ 0.10%) and it increased with increasing BV/TV. Chen and McKittrick (2011) reported $\varepsilon_f < 1\%$.

The elastic modulus (E) is another important parameter to characterise the biomechanical properties of bone. Here, E was found between 123.74 - 323.68 MPa with a mean of 251.71 ($\pm$ 74.72) MPa while Chen and McKittrick (2011) reported a much smaller mean value of 43 MPa. Once again, part of this difference can be attributed to the difference in density of samples. While this study found E to increase with BV/TV, but the correlation was weak, with r^2 = 0.15.

Toughness (W) can be obtained by integrating the stress-strain curve until fracture and it was found to be related to BV/TV with r^2 = 0.91 and a positive power term. The results indicates that with increased BV/TV, as would be expected, W is increasing. It also reveals that the denser deproteinised trabecular bone has greater ability to absorb energy.

7.5.3 Cellular solids

The elastic modulus (E) (<350 MPa) and stress at failure (σ_f) (<1.0 MPa) are far lower compared to the solid phase of mineral which are 112 GPa and 800 MPa (Chen and McKittrick, 2011), respectively, this is due to its porous microstructure. The mechanical properties of trabecular bone can be modelled by using constitutive equations for cellular solids (Gibson and Ashby, 1999):

$$\begin{aligned} \frac{E^*}{E_s} &= C_1(\frac{\rho^*}{\rho_s})^n \\ \frac{\sigma^*}{\sigma_s} &= C_2(\frac{\rho^*}{\rho_s})^m \end{aligned} \tag{7.2}$$

where, superscript '*' and subscript '$_s$' represent the cellular and solid material, respectively. Solid phase elastic modulus (E_s), compressive strength (σ_s) and density (ρ_s) were assumed to be 112 GPa, 800 MPa and 3.15 g/cm^3, respectively (Chen and McKittrick, 2011).

Figure 7.6a and 7.6b show the relative elastic modulus (E^*/E_s) and relative compressive strength (σ^*/σ_s) as a function of relative density (ρ^*/ρ_s) plotted on a logarithmic scale. As one would expect from cellular materials, both E^*/E_s and σ^*/σ_s increase with increasing ρ^*/ρ_s.

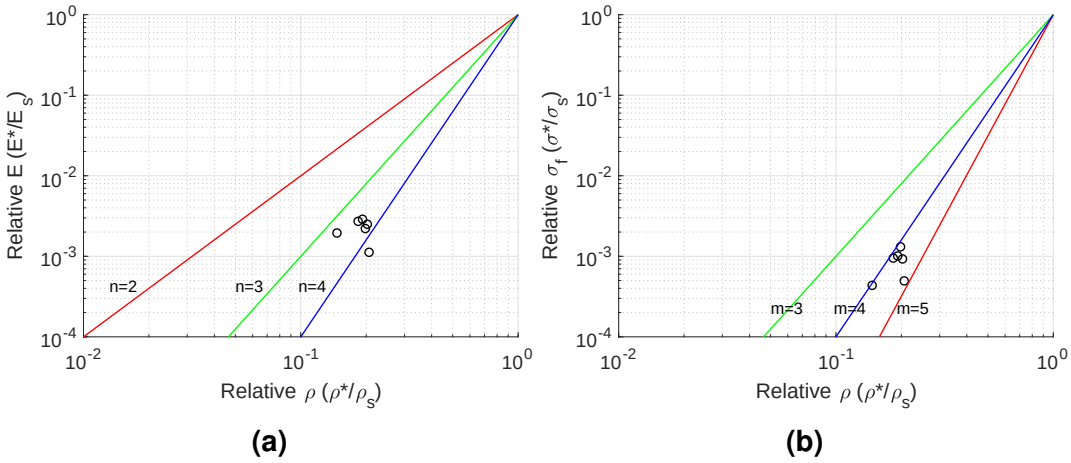

(a) **(b)**

Figure 7.6: Deproteinised trabecular bone sample modelled as cellular solids. Relative elastic modulus (a) and relative compressive strength (b) of deproteinised bovine tibia trabecular bone plotted against relative apparent density.

For E^*/E_s, the reported data on DP trabecular bone was found to fall between line of slope n = 3 and n = 4; while published study (Chen and McKittrick, 2011) reported that the data falls around the line of slop n=3 for deproteinised femur and between n = 2 and 3 for antler. The E is related to its density or BV/TV, and it also dependent on anatomic site (Morgan et al., 2003). Therefore, it is reasonable that these experimental data points fall at different location as they had different densities and were from different anatomic sites.

For σ^*/σ_s, the reported data was found to fall between line with slope m = 4 and m = 5, as shown in Fig. 7.6b; while Chen and McKittrick (2011) reported that it fall between m = 2 and 3 for both deproteinised femur trabecular bone

and deproteinised antler. This could also be due to these samples having different densities and from a different anatomic site compared to the published data.

7.6 Limitations

There were only a few trabecular bone samples from one anatomic site (i.e. bovine tibia), which were successfully tested under compressive monotonic loading until failure. More samples included in the analysis may give a better correlation.

7.7 Conclusions

- Deproteinised trabecular bone samples show a linear elastic behaviour up to its peak point, and a brittle behaviour with fracture strain of less than 1%.
- Mean modulus of 251.71 MPa was found, which is smaller than most reported values for untreated trabecular bone and it is associated with its BV/TV.
- Deproteinised bone has much smaller strength compared with untreated bone and it was found to be strongly related to its BV/TV.
- Toughness of deproteinised bone is strongly related to its BV/TV; denser bone has better ability to absorb energy compared to porous bone.
- The compressive mechanical properties of demineralised samples can be modelled as open-cell cellular solids; both relative elastic modulus and compressive strength increase with relative density.

Part II

Application of the Developed Models

"When you look at yourself from a universal standpoint, something inside always reminds or informs you that there are bigger and better things to worry about."

Albert Einstein

8

Linear viscoelastic analysis of a bone-screw system

One of the typical complications reported in the treatment of fractures using devices such as locking plates or unilateral fixators is loosening (Galbusera et al., 2015). Primary stability, before initiation of biological processes, is believed to be essential for the success of treatment (Taylor and Prendergast, 2015). It has been suggested that high strains in the bone at the bone-screw interface can initiate loosening (Sakaguchi and Borgersen, 1993) which can result in infection and further loosening (Clifford et al., 1987; Donaldson et al., 2012; Huiskes et al., 1985).

Trabecular bone is a time-dependent material as shown in previous Chapter. The displacement (or strain) response of bone is a function of cycles (i.e. bones cyclic loading history) (Bowman et al., 1998; Haddock et al., 2004;

Moore et al., 2004) and the loading frequency (Lafferty and Raju, 1979). Previous studies have considered the effect of: damage due to screw insertion (Steiner et al., 2016); screw threads (MacLeod et al., 2012; Steiner et al., 2017); screw tightening (MacLeod and Pankaj, 2014); insertion of a larger diameter screw in a small pilot hole (MacLeod et al., 2012); combined shear and pull-in/push-out forces (Donaldson et al., 2012); nonlinear material properties (Donaldson et al., 2012); and trabecular bone microarchitecture at the interface (Steiner et al., 2015). However, the effects of time-dependent behaviour on bone-screw interface mechanics at different loading frequencies has not been previously considered.

This chapter uses the bone volume ratio (BV/TV)-based linear viscoelastic constitutive model (Chapter 5) to evaluate the mechanical environment at the interface. The aim of this chapter is to evaluate effect of BV/TV, cyclic loading frequency and number of cycles on the interfacial deformations in an idealised bone-screw system.

8.1 Bone-screw system geometry

An idealised system, two-dimensional plane strain, construct with a screw and surrounding bone as shown in Fig. 8.1a was employed. It is clear that this is a simplification of reality as the screw is cylindrical whereas a plane strain representation implies a plate. However, since the plane-strain assumption provides confinement in the out-of-plane direction, it is expected to provide representative results in the plane of the model.

Exact fit between the screw and the bone was assumed along the length of the screw while a small gap was included between the screw end and the bone to avoid influence of any end shape effects and maintain simplicity. Screw threads were excluded. The screw was assumed to be unicortical and a 1 mm thick cortex was included in the model as shown in Fig. 8.1a.

The geometry was meshed using 4930 6-noded modified plain strain elements (CPE6M) in Abaqus 6.12 (Simulia, Providence, RI, USA). Mesh convergence studies were performed and they show that further mesh refinement resulted in an increase of maximum displacement of bone by less than 0.3%.

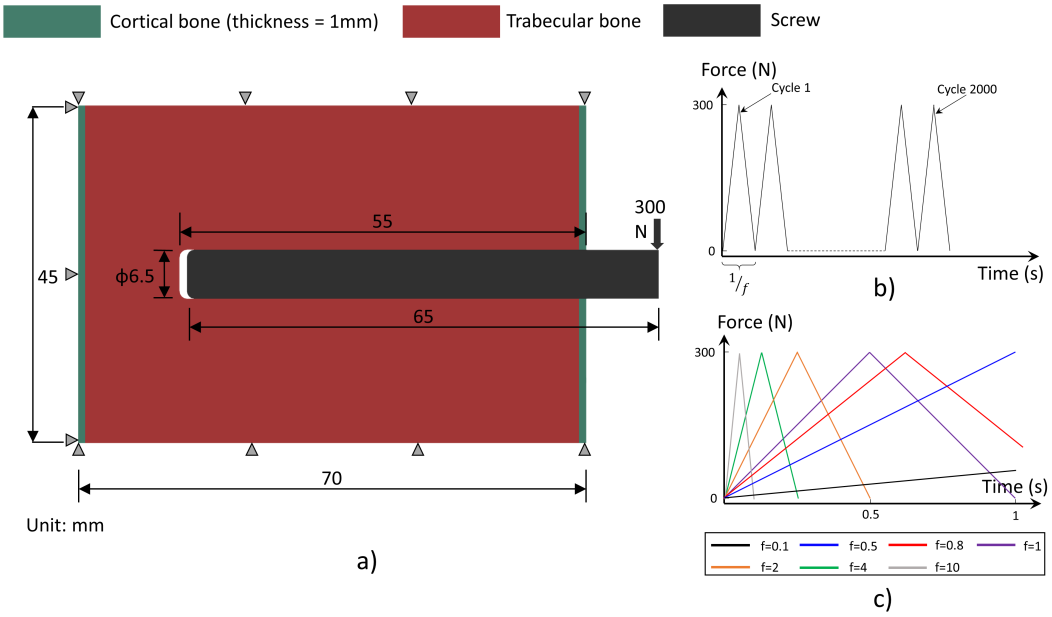

Figure 8.1: Schematic drawing of a bone-screw system and the load application. Idealised plain strain bone-screw system (a); cyclic loading for 2000 cycles (b); load applied at 7 different frequencies, Hz (c).

8.2 Material definition

The screw and cortical bone were assumed to be homogeneous, isotropic and time-independent materials, with Youngs modulus of 180 GPa and 20.7 GPa, respectively (MacLeod et al., 2012). BV/TV-based viscoelastic material properties were employed to define the time-dependent properties of trabecular bone in which the relaxation modulus function, $E(t)$ (developed in Sec. 5.2) is given by

$$E(t) = B\phi^p + B[\sum_{i=1}^{3} \tilde{E}_i exp(-t/\tilde{\rho}_i)\phi^{p_t}] \tag{8.1}$$

where ϕ is the BV/TV of trabecular bone, t is the time and $B, \rho, \rho_t, \tilde{E}_i$ and $\tilde{\rho}_i$ are constant material coefficients. Consequently, ϕ is the only variable in the

evaluation of relaxation modulus function. Three BV/TV values were selected: 15%, 25% and 35%. Poisson's ratio of ν=0.3 was applied to all the materials.

8.3 Loads and boundary conditions

A standard Coulomb friction coefficient of 0.3 was employed based on some of the recent studies (MacLeod et al., 2012, 2015), with surface-to-surface frictional contact assumed at the bone-screw interface. Translation degree of freedoms at all edges of bone section were constrained except at the edge with screw hole, as shown in Fig. 8.1a.

A 300 N concentrated triangular cyclic loading (Fig. 8.1b) was applied at the right end of the screw over a thickness of 3.25 mm (half diameter of screw) (Fig. 8.1a) with designated loading frequencies for 2000 cycles. One complete cycle includes a ramp loading and unloading. Seven loading frequencies, f, from 0.1 Hz to 10 Hz were investigated (Fig. 8.1c), which cover the physiological frequency range of normal human activities from slow walking to running (Abdel-Wahab et al., 2011).

8.4 Results

The displacements in trabecular bone were computed for 21 models: 3 BV/TV material models at 7 different loading frequencies. The displacement contours for BV/TV = 15%, at time points when the load is at its peak (loaded phase) and when the screw is completely unloaded (unloaded phase) are shown in Fig. 8.2 and 8.3, respectively for 8 selected cycles (cycle 1, 5, 10, 100, 500, 1000, 1500 and 2000 denoted as C1, C5, C10, C100, C500, C1000, C1500 and C2000, respectively). Similar contour plots for the other two BV/TV values are provided in Appendix (Fig. A.1 and A.2). For the above loading cycle numbers, the maximum displacements within trabecular bone were extracted and plotted

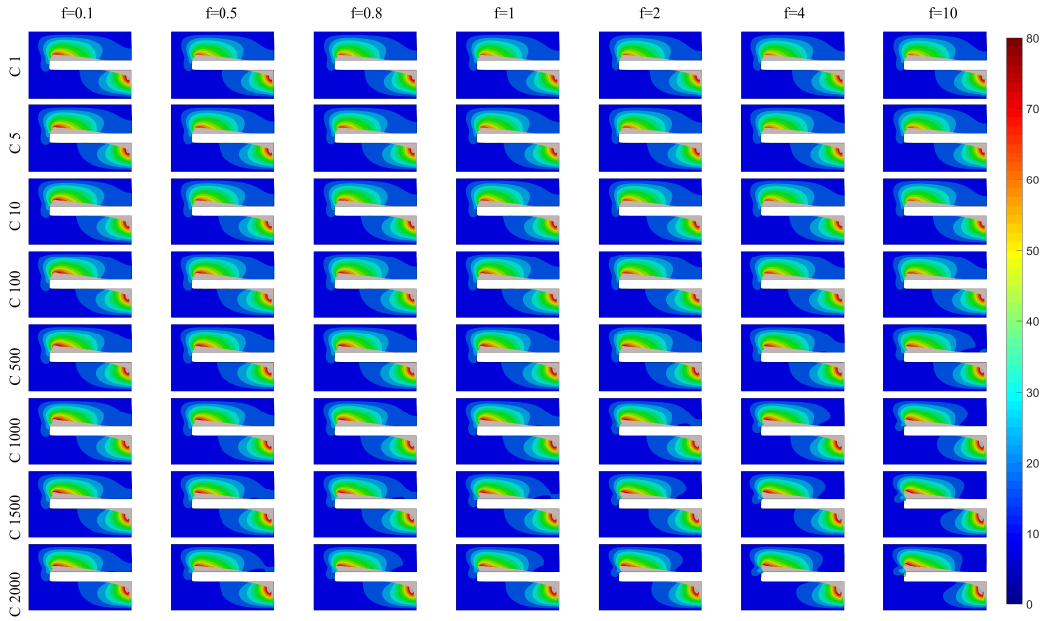

Figure 8.2: Displacement contours (μm) against loading frequencies at 8 selected cycles at the loaded phase for BV/TV = 15%. These displacement contours were superimposed over undeformed geometry and exaggerated by 50 times for better visualisation.

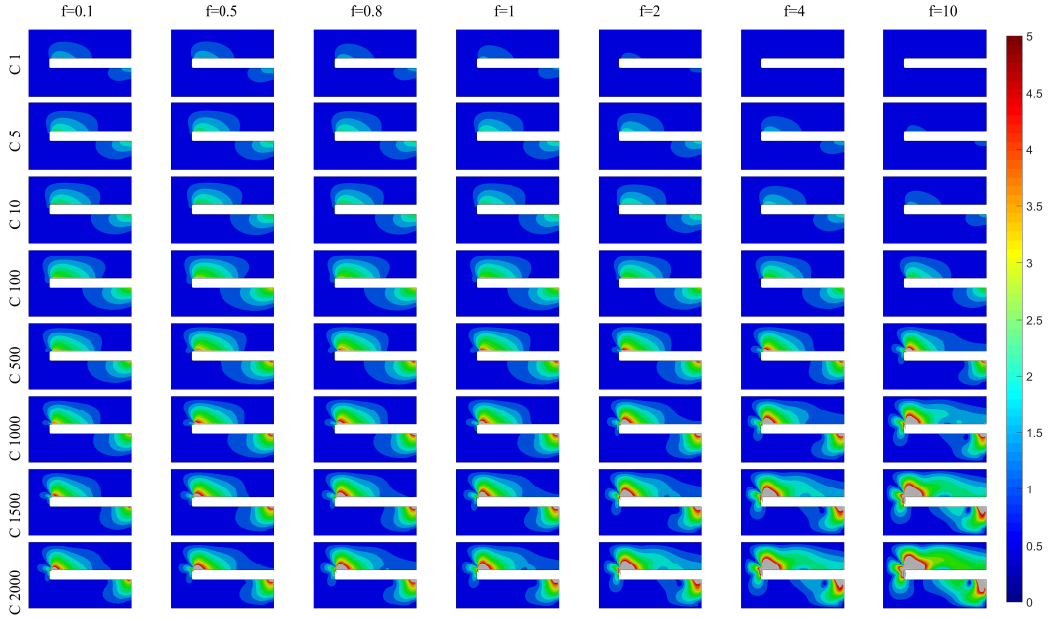

Figure 8.3: Displacement contours (μm) against loading frequencies at 8 selected cycles at the unloaded phase for BV/TV = 15%. These displacement contours were superimposed over undeformed geometry and exaggerated by 50 times for better visualisation.

against loading frequencies for all three BV/TV samples investigated in this chapter, these are shown in Fig. 8.4.

8.4.1 Loaded phase

The displacement contours at the loaded phase for BV/TV = 15% are shown in Fig. 8.2. These show similar displacement distributions at all frequencies considered. When the system has been subjected to a small number of loading cycles, a relatively larger displacement is observed for lower loading frequencies (e.g. at C1, f=0.1 Hz had relatively larger displacement compared to f = 10, as shown in Fig. 8.2). Small increase in displacement can be observed with increasing cycle numbers for each of the loading frequencies (e.g. for f=0.1 Hz , C2000 had relatively larger displacement compared to C1). With increasing loading cycles, relatively larger displacement was observed when bone-screw system was loaded at higher loading frequencies (e.g. at C2000, f=10 Hz case has relatively larger displacement compared to f=0.1 Hz case).

Maximum displacement of trabecular bone in the loaded phase, for all BV/TV values considered, was plotted against loading frequencies at selected cycles, and are shown in Fig. 8.4a, 8.4c and 8.4e. Observations from contour plots are confirmed from these maximum displacements plots. It is apparent that at C1 for BV/TV = 15% (Fig. 8.4a), f=0.1 Hz has the largest displacement compared to other loading frequencies. These plots also show that the maximum displacement reduces with increase in frequency in the initial loading cycles (e.g. Cycle 1 response in Fig. 8.4a reduces with frequency). However, higher maximum displacement is observed at higher loading frequencies after a number of loading cycles (e.g. $>$500 cycles). Rapid increase in displacement with increased cycle numbers was observed for higher loading frequency cases. At the end of C2000, the maximum displacement for f=10 Hz is much higher than maximum displacement observed in f=0.1 Hz case.

These observations were also found to be true for the other two samples (BV/TV = 25% and 35% considered in this investigation, and the results are shown in 8.4c and 8.4e for BV/TV = 25% and 35%. Additionally, if the bone-

screw system is loaded at the same frequency for the same number of cycles, then, as expected, higher maximum displacement is obtained with lower BV/TV (Fig. 8.4a, 8.4c and 8.4e).

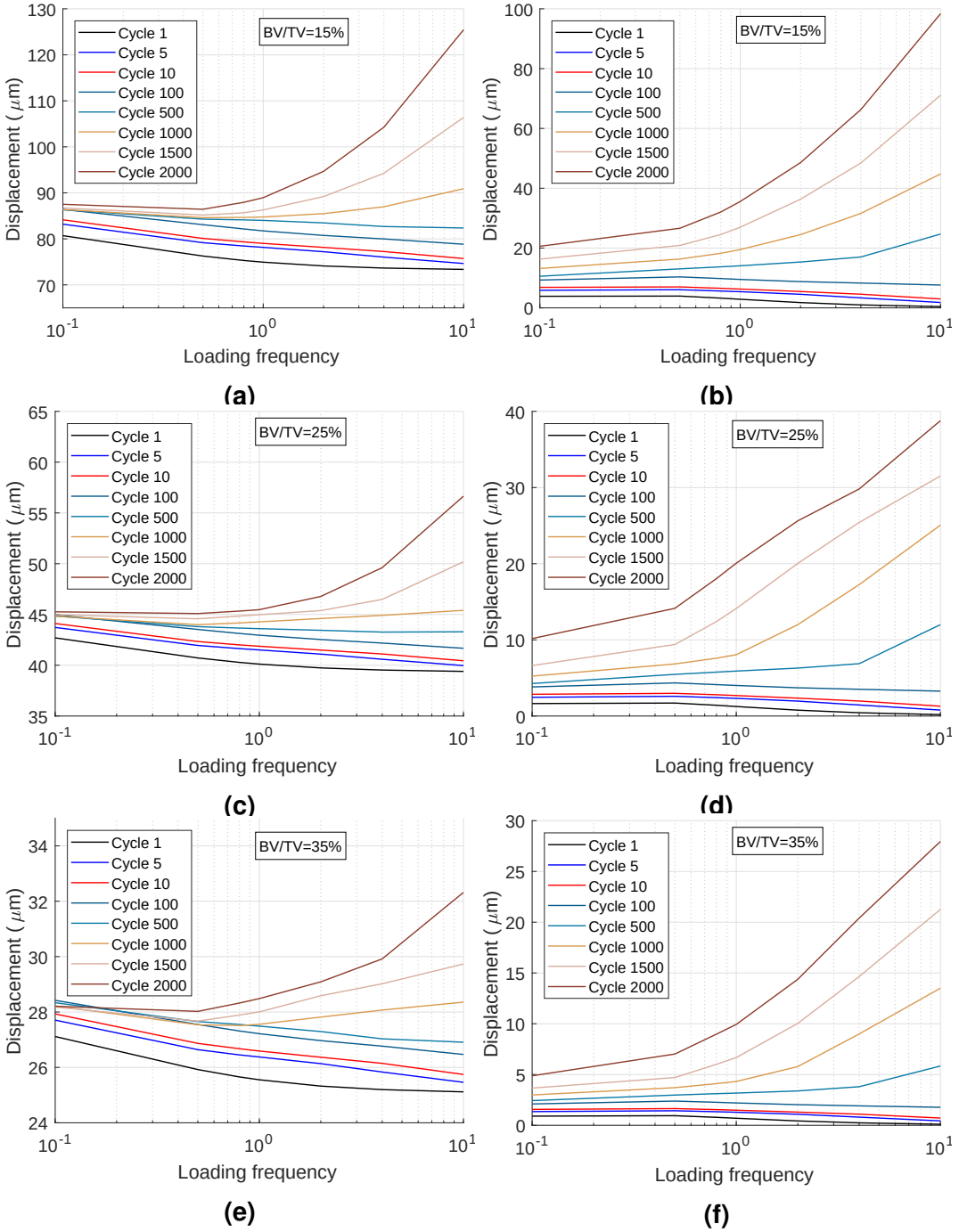

Figure 8.4: Maximum displacement of trabecular bone plotted against loading frequencies at 8 selected cycles: at the loaded ((a,c and e) and unloaded (b,d and f) phases for BV/TV = 15%, 25% and 35%.

8.4.2 Unloaded phase

As would be expected, majority of the displacements recover immediately upon unloading as shown in Fig. 8.3 (note that different scales are used in the contours for loaded and unloaded phases). There was negligible displacement remaining at the end of C1, especially for higher loading frequencies (e.g. f=10 Hz); while some displacement remained at C1 for lower frequencies (e.g. f=0.1 Hz). The displacement upon unloading accumulated significantly with increasing cycle numbers, which was true for all the loading frequencies. At C2000, the largest displacement was observed at higher loading frequencies (e.g. f=10 Hz), and it had the larger region with deformations in comparison to lower loading frequencies as shown in Fig. 8.3.

The maximum displacements of trabecular bone at the unloaded phase plotted against loading frequencies at 8 representative cycles, are shown in Fig. 8.4b, 8.4d and 8.4f for BV/TV = 15%, 25% and 35%, respectively. It is clear that the loading frequencies significantly affect the maximum displacement experienced by trabecular bone. For BV/TV = 15%, at lower cycles (i.e. below around C500), the maximum displacement was observed at low loading frequencies (Fig. 3). With further increase in cycle numbers, rapid increasing in maximum displacement with increased cycle numbers can be observed for higher loading frequencies. In other words, the displacement that remained at unloaded time points accumulated much faster at high loading frequencies, and this was found to be true for all the BV/TV samples examined in this simulation (Fig. 8.4b, 8.4d and 8.4f). At C2000, f=10 Hz had the largest maximum displacement and it was more than four times of maximum displacement observed for f=0.1 Hz (Fig. 8.3).

Displacement was related to BV/TV of bone; for trabecular bone with higher BV/TV lower displacement was observed, i.e. for the bone-screw system loaded at the same frequency for the same number of cycles, a much smaller

maximum displacement was observed when trabecular bone has higher BV/TV (Fig. 8.4b, 8.4d and 8.4f).

8.5 Discussion

This chapter shows that the displacements in trabecular bone due to cyclic loading applied to the screw in a bone-screw system are a function of loading cycles and loading frequencies. At the beginning of cyclic loading, lower loading frequencies result in higher displacement in trabecular bone for both loaded and unloaded phases; while with increased cycle numbers, higher displacements are observed at higher loading frequencies. In all cases displacements increase as BV/TV decreases. It is reasonable to assume that there are two linked mechanisms at play: effect of time-dependent material response and dynamic effect due to frequency of loading.

In the initial cycles higher frequency resulted in lower displacement response for both loaded and unloaded phases. This shows that the viscoelastic model used is able to capture the phenomenon observed in previous studies: higher strain rates result in higher effective stiffness (Hansen et al., 2008; Linde et al., 1991; Schaffler et al., 1989; Wallace et al., 2013). In the first few cycles, the lower loading frequency has a relatively longer loading time and relatively smaller loading rate. Therefore, larger displacement occurs when bone-screw system is loaded at a lower frequency during the loading and unloading phases as the bone is provided more time to deform or recover.

For a time-dependent material, the displacement increases with time when it is subjected to a constant force and recovery occurs upon force removal and again takes time. During cyclic loading, bone would only partially recover before it is subjected to the next cycle of loading. Consequently, the displacement accumulates with increasing number of cycles for all BV/TV samples and for all loading frequencies. This observation is consistent with previous experimental

studies (Basler et al., 2013; Bianco et al., 2016; Schüller et al., 2009), in which the displacement of bone in a bone-screw/implant system was found to be a function of number of loading cycles.

With increasing cycle numbers, the loading frequency starts playing a dominant role. When the bone-screw system is loaded at higher frequencies, the loading/unloading time is shorter (in comparison to lower frequency loading) and the bone is loaded again by the next cycle before it can recover from its last loading cycle. Therefore, the shift between the excitation force and displacement response occurs, which depends on the frequency of excitation. Recently, Sadeghi et al. (2017) suggested that to date, there is little data on the variation of mechanical properties of bone with increasing loading frequency. Lafferty and Raju (1979) reported that for the cortical bone, with increased loading frequencies (from 30 to 125 Hz), the number of cycles required to produce fracture decreases. Another indirect evidence is provided by Burr et al. (1996), who measured in vivo strains in the human tibia during walking and running, and reported that the strain experienced by bone was higher for running than walking, some of it is perhaps due to larger forces exerted during running. The viscoelastic model developed from experiments on trabecular bone and employed here for a bone-screw system is consistent with observations from previous studies. The effect of BV/TV is as expected with lower BV/TV giving higher deformations for all cycles and loading frequencies.

The aim of the current chapter was to develop trends how BV/TV effects accumulation of deformations under cyclic loads and what is the role of the loading frequency; these trends can only be evaluated by including time-dependent material models. To maintain focus and transparency of the simulations, the effect of damage due to screw insertion (Steiner et al., 2016), screw threads (MacLeod et al., 2012; Steiner et al., 2017), screw tightening (MacLeod and Pankaj, 2014) and local micro architecture (Steiner et al., 2015) was excluded. Screws experience combined shear, bending and axial forces

(Donaldson et al., 2012) – these too were not considered. All these phenomena will influence the mechanical environment at the interface, however their inclusion is unlikely to change the trends observed in this chapter.

The importance of viscoelastic behaviour of bone has been discussed in several contexts from material performance to links with microphysical processes (Lakes, 2001). In this chapter the context is implant loosening. The model provides a simple approach for inclusion of time-dependent behaviour in computational models. It can be used to evaluate implant performance and for providing post-operational rehabilitation advice to patients.

8.6 Limitations

This simulation has a few limitations. The experimental results used are from bovine trabecular bone, so they are not directly applicable to human bone. An idealised plane strain model was used which implies that the screw is essentially a plate inserted in a long block of bone. These simplifications are unlikely to change the trends with respect to loading frequencies and influence of number of cycles. The displacement response of bone follows a trend with respect to BV/TV; however, bone microstructure may have a role to play in addition to that of BV/TV as has been shown for time-independent properties (Steiner et al., 2015; Zysset, 2003).

8.7 Conclusions

- The importance of viscoelastic behaviour of bone has several contexts, this Chapter the context is implant loosening.
- The bone-screw interface mechanics are related to both BV/TV and loading frequencies.

- At initial cycle(s), lower loading frequencies result higher displacements for both loading and unloading phases.
- With increasing cycle numbers (e.g. $>$500), higher loading frequencies result higher displacement.
- The model provides a simple approach for inclusion of time-dependent behaviour in computational models, it can be used to evaluate implant performance and for providing post-operational rehabilitation advice to patients.

"Not everything that counts can be counted, and not everything that can be counted counts."

Albert Einstein

9

Nonlinear time-dependent analysis of bone-screw system

In computational modelling loosening at the interface has, in the past, been examined by evaluating strain level after employing time-independent elastic (MacLeod et al., 2016) or elastoplastic (Bianco et al., 2014; Donaldson et al., 2012) constitutive models for bone. While it is recognised that bone's response to loads is time-dependent (Bowman et al., 1994) and some permanent deformation arises even when bone is subjected to low strain levels ($<$ 3000 $\mu\varepsilon$) (Kim et al., 2011; Yamamoto et al., 2006). It has also been shown that, similar to time-independent material properties such as Young's modulus, time-dependent properties are also related to bone volume fraction (BV/TV) (Chapter 4 and 5). However, these time-dependent mechanical properties of bone are not generally incorporated in modelling (Pankaj, 2013).

The aim of this Chapter is to examine possible loosening due to cyclic loading in an idealised bone-screw system in which trabecular bone is assigned time-dependent (nonlinear viscoelastic and nonlinear viscoelastic-viscoplastic properties). The employed properties are based on the developed constitutive models in Chapter 5.

9.1 Bone-screw system geometry

To examine the response of bone at the bone-screw interface due to cyclic loading in conjunction with time dependent properties of trabecular bone, a simple geometrical model with a screw inserted in a block of bone was considered as shown in Fig. 9.1a, which also provides the dimensions. The dimensions for the screw are similar to that used in locking plates. Taking advantage of symmetry, only half of the bone block-screw system was modelled (Fig. 9.1b). Exact fit between the screw and the bone was considered at the screw circumference-bone interface; while a small gap was assumed between the screw end and bone to avoid influence of any end shape effects and maintain simplicity. Screw threads were excluded. The screw was assumed to be unicortical and a 1mm thick cortex was included in the model as shown in Fig. 9.1a.

The screw-bone system was modelled in Abaqus using 13182 three dimension finite elements (brick, C3D8 and tetrahedron, C3D10M). Mesh convergence studies were performed and they showed that further mesh refinement resulted in change of peak displacement of bone by less than 0.5%.

9.2 Material definition

The screw and the cortical bone were modelled as linear elastic time-independent materials, with Young's moduli of 180 GPa and 20.7 GPa, respectively (MacLeod

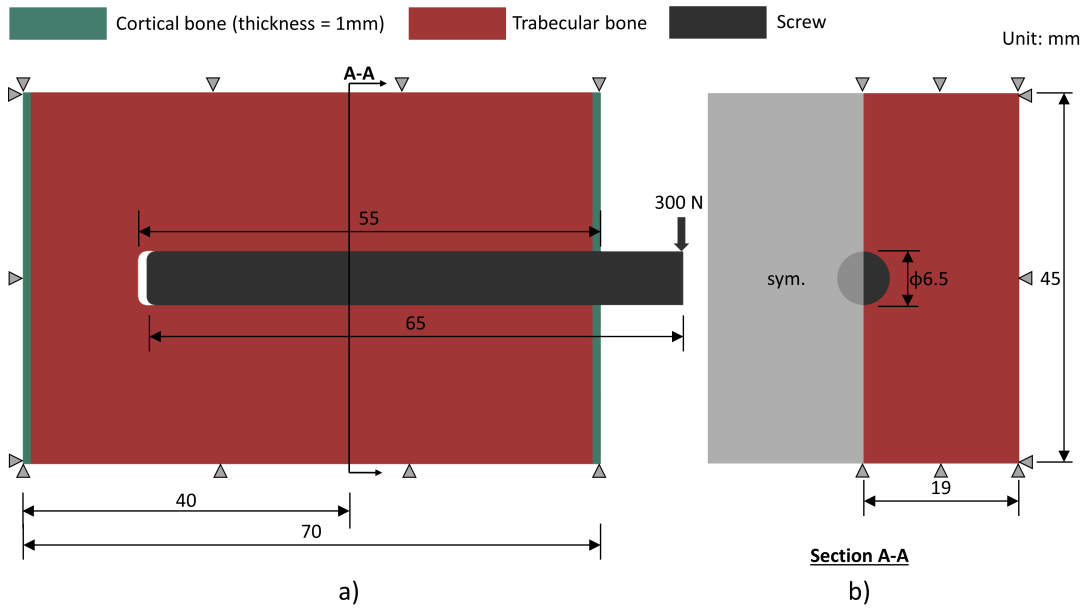

Figure 9.1: Schematic drawing of 3D bone-screw system. Symmetric surface (a); section A-A (b).

et al., 2012) and Poisson's ratio of 0.3.

Trabecular bone was modelled using two constitutive models: a nonlinear viscoelastic (VE) model; and a nonlinear viscoelastic-viscoplastic (VEP) model, which were developed in Chapter 5. For convenience, the evaluated nonlinear viscoelastic and viscoplastic parameters are shown in Table 9.1 and 9.2, respectively. These parameters were used as input to the user defined material (UMAT) for trabecular bone samples, which was implemented in Abaqus 6.12 (Simulia, Providence, RI, USA).

9.3 Loads and boundary conditions

All external faces of the block were assumed to be fully restrained except for the face with the screw hole and symmetry boundary conditions were applied at the symmetry surface (Fig. 9.1a, b). A frictional screw-bone interface was employed with a standard Coulomb friction coefficient of 0.3 (MacLeod et al., 2012, 2015). Triangular cyclic forces with an amplitude of 300 N and a frequency, f=1 Hz, as shown in Fig. 9.1c was applied to the external end of the

Table 9.1: The nonlinear viscoelastic parameters along with linear Prony coefficients and irrecoverable strains at multiple stress levels for three different BV/TV (Manda et al. 2016a)

BV/TV	Linear coefficients at Cycle I		Cycle No.	$\varepsilon_{static}(\%)$	σ^N	Nonlinear VE parameters				$\varepsilon_{irrec}(\%)$
						g_0	g_1	g_2	a_σ	
15%	$\begin{bmatrix} D_g \\ D_1 \\ D_2 \\ D_3 \\ \lambda_1 \\ \lambda_2 \\ \lambda_3 \end{bmatrix}$	$= \begin{bmatrix} 6.40\times10^{-3} \\ 5.48\times10^{-4} \\ 3.24\times10^{-4} \\ 2.97\times10^{-4} \\ 8.64\times10^{-3} \\ 8.64\times10^{-1} \\ 9.31\times10^{-2} \end{bmatrix}$	I	0.20	0.36	1.00	1.00	1.00	1.00	0.041
			II	0.40	0.66	0.91	1.06	0.59	0.78	0.067
			III	0.60	0.94	0.94	1.03	0.67	0.82	0.104
			IV	0.80	1.17	0.99	1.01	0.82	0.85	0.158
			V	1.00	1.35	1.10	0.96	0.84	0.91	0.237
25%	$\begin{bmatrix} D_g \\ D_1 \\ D_2 \\ D_3 \\ \lambda_1 \\ \lambda_2 \\ \lambda_3 \end{bmatrix}$	$= \begin{bmatrix} 3.52\times10^{-3} \\ 1.31\times10^{-4} \\ 2.63\times10^{-4} \\ 1.30\times10^{-4} \\ 7.57\times10^{-2} \\ 6.44\times10^{-3} \\ 5.68\times10^{-1} \end{bmatrix}$	I	0.20	0.64	1.00	1.00	1.00	1.00	0.032
			II	0.40	1.20	0.90	1.02	0.82	0.79	0.049
			III	0.60	1.77	0.91	1.05	0.96	0.75	0.084
			IV	0.80	2.23	0.98	1.04	1.19	0.74	0.140
			V	1.00	2.43	1.06	1.01	1.44	0.81	0.209
35%	$\begin{bmatrix} D_g \\ D_1 \\ D_2 \\ D_3 \\ \lambda_1 \\ \lambda_2 \\ \lambda_3 \end{bmatrix}$	$= \begin{bmatrix} 1.60\times10^{-3} \\ 1.14\times10^{-4} \\ 6.45\times10^{-5} \\ 8.35\times10^{-5} \\ 7.64\times10^{-3} \\ 9.41\times10^{-2} \\ 7.05\times10^{-1} \end{bmatrix}$	I	0.20	1.31	1.00	1.00	1.00	1.00	0.039
			II	0.40	2.69	0.84	1.14	0.71	0.67	0.057
			III	0.60	4.09	0.84	1.08	0.60	0.78	0.072
			IV	0.80	5.59	0.82	1.00	0.57	0.87	0.075
			V	1.00	7.50	0.78	1.00	0.37	0.93	0.109
			VI	1.50	13.01	0.70	1.02	0.66	0.80	0.214

BV/TV is the bone volume fraction, D_g is the instantaneous compliance in $1/MPa$, D_n (n = 1, 2, 3) are transient compliance coefficients in $1/MPa$, and λ_n (n = 1, 2, 3) are reciprocal of nth retardation time in Prony series in s^{-1}, ε_{static} is the applied static strain in each loading cycle, σ^N is the stress corresponding to plateau stress in the N^{th} loading cycle in MPa. Parameters g_0, g_1, g_2, a_σ are stress-dependent nonlinear VE parameters and ε_{irrec} is the irrecoverable strain exist at the end of each loading cycle.

Table 9.2: The values of the viscoplastic parameters for three different BV/TV

BV/TV	α	β	N	Γ (s^{-1})	κ_0 (MPa)	κ_1 (MPa)	κ_2	σ_y^0 (MPa)
15%	1.035	0	3	4.34 $\times10^{-2}$	2.42 $\times10^{-3}$	2.11	4.62 $\times10^{2}$	3.38
25%	1.035	0	3	4.91 $\times10^{-3}$	1.35 $\times10^{-10}$	4.11	3.50 $\times10^{2}$	5.75
35%	1.035	0	3	5.35 $\times10^{-2}$	4.03 $\times10^{-1}$	10.40	5.00 $\times10^{2}$	26.70

BV/TV is the bone volume fraction, α is a pressure-sensitivity parameters related to friction angle, β is a parameter related to dilation angle, σ_y^0 and N are material constant, Γ is a viscosity parameter, κ_0 is the initial yield stress, κ_1 is the saturated stress for the fully-hardened material, κ_2 is the the transition rate between κ_0 and $\kappa_0 + \kappa_1$.

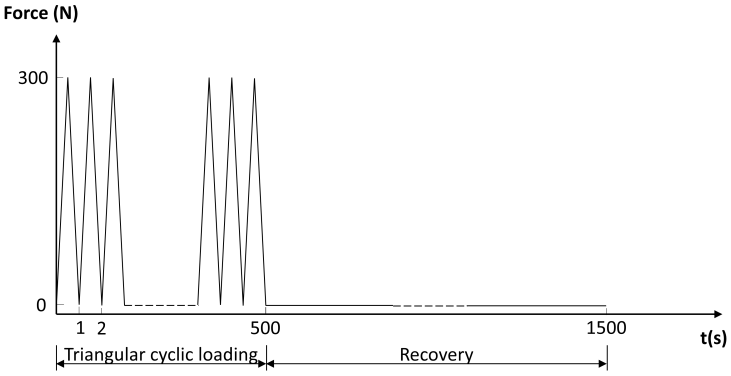

Figure 9.2: Load application. Each model was subjected to 500 triangular cyclic load up to 300 N, and followed by 1000 s of recovery.

screw (Fig. 9.1a). The models were permitted 1000 s of recovery time after 500 complete cycles as shown in Fig. 9.2. 500 cycles were selected as this study was largely interested in evaluating the trends, though this choice was also partly dictated by the computational resources required for this highly nonlinear problem.

9.4 Results

Trabecular bone displacements and strains in the region around the screw were compared at three stages for different cycles: time points when the load is at its peak (300N); time points when the load is zero; and at the end of the recovery (at the end of 1000 s after cyclic loading is stopped). In Fig. 9.3, the rows present displacement contours at different stages and at different cycles. The columns are for different bone samples (the numerals indicate BV/TV percentage of the samples used) and for the two time-dependent material models used (VE=nonlinear viscoelastic; VEP=nonlinear viscoelastic-viscoplastic). For each case, contours along the length of the screw (Fig. 9.1a) and at the symmetry surface, section A-A (Fig. 9.1b) are shown in Fig. 9.2. They were exaggerated by 150 times, and the section plots are superimposed with undeformed geometry for better comparison with its original shape. Seven

representative cycles (cycle 1, 5, 10, 50, 100, 300 and 500) were selected for examining displacement variation.

In all cases, the peak trabecular bone displacements occurred at the interface in the middle region of the screw hole at the top, and entrance of screw hole at the bottom for all three stages. The peak displacements of trabecular bone at section A-A at selected cycles for all 6 models were extracted and are shown in Fig. 9.3.

The maximum and minimum principal strain contours are shown in Fig. 9.5 for VEP models at 7 representative cycles. Additional information on contact opening contours are shown in Appendix (Fig. B.1).

9.4.1 Peak loading time points

At the peak loading points, the difference in displacements between the samples with different BV/TV is apparent. It is clear that the lower BV/TV samples undergo larger interfacial displacements than higher BV/TV samples. This is apparent from the displacement contours (Fig. 9.3a), peak displacements (Fig. 9.4a) and principal strain contours (Fig 9.5a , 9.5b).

At peak loading time points, similar displacement contours were observed for models which included viscoplasticity (VEP) and those that were modelled using nonlinear viscoelasticity alone (VE). Small differences were, however, observed after the samples had experienced relatively larger number of cycles and for trabecular bone with low BV/TV (e.g. 15VEP had slightly higher displacement compared to the 15VE case). These differences between VE and VEP models were negligible at the highest BV/TV considered in the study (e.g. between 35VE and 35VEP). As expected, Fig. 9.4a shows that the maximum displacement experienced by trabecular bone increases with the number of cycles, however this increase was found to be small; the largest increase for the lowest BV/TV sample with VEP model was 15%. Lower BV/TV in conjunction

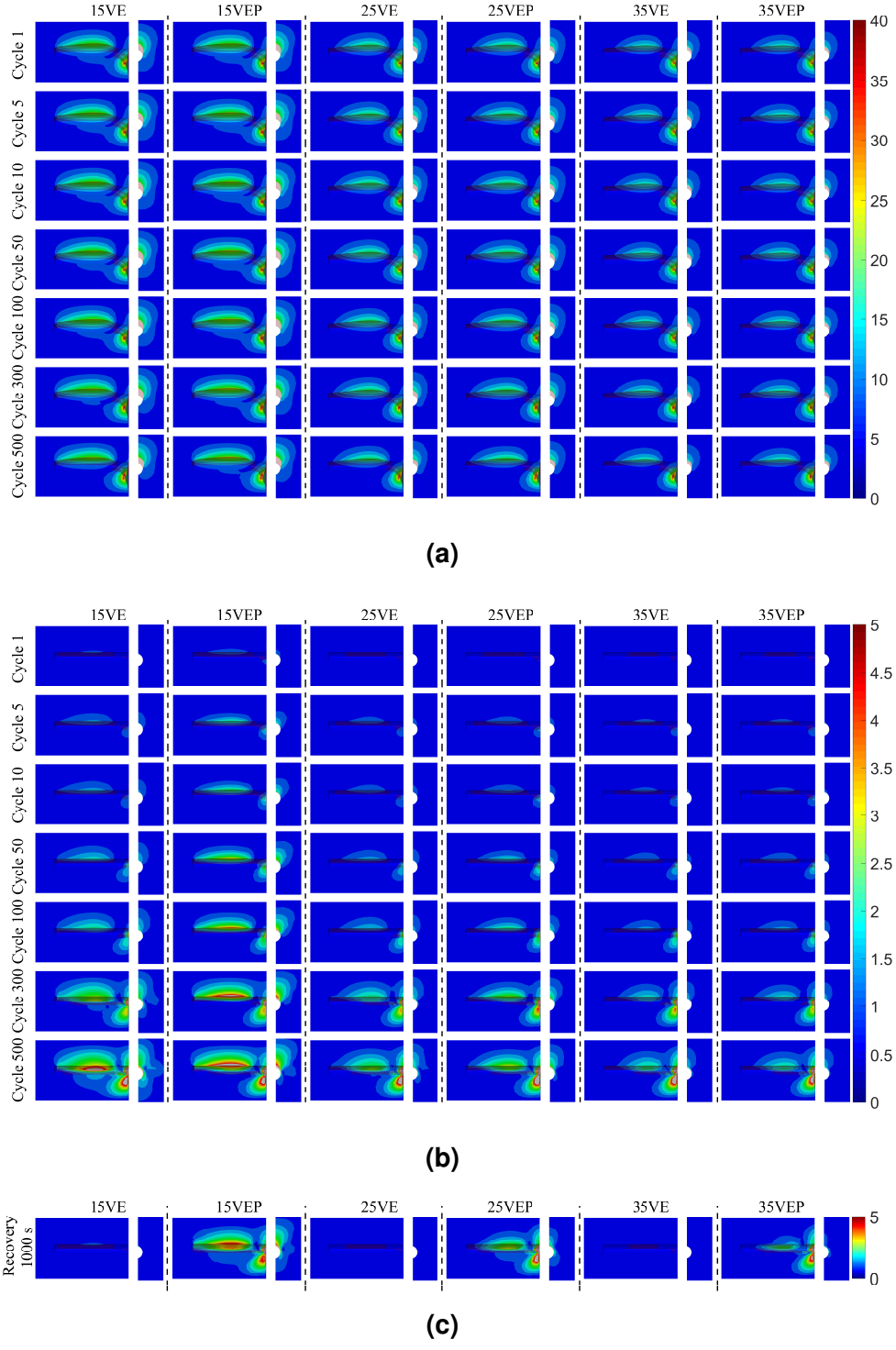

Figure 9.3: Displacement (μm) contours at symmetry surface and section A-A for 7 representative cycles: at the time points when load at its peak (300N) (a); at the time points when load is zero (b) and recovery after 1000 s (c). They are exaggerated by 150 times, and the section plots are superimposed with undeformed geometry for better comparison with its original shape.

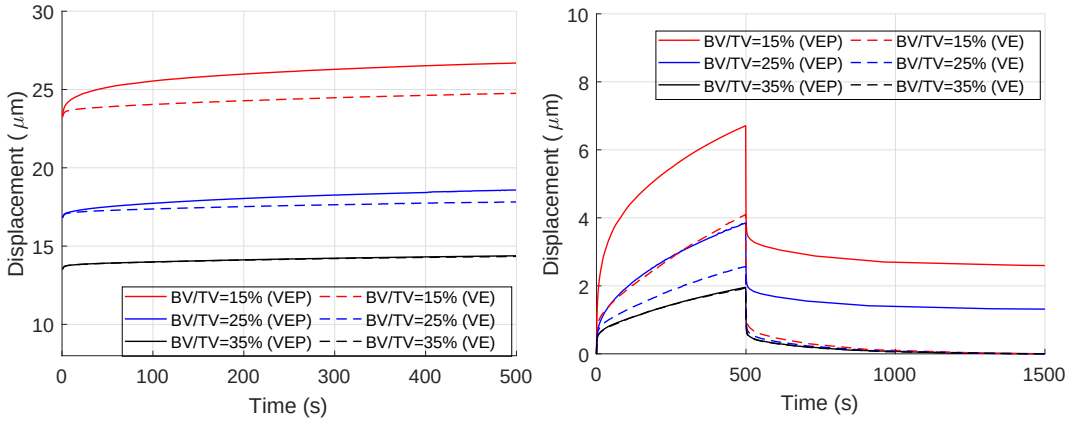

Figure 9.4: Peak displacement experienced of trabecular bone at section A-A for both VE and VEP models: at the time points when load is at its peak (300N) (a); at the time points when load is zero and after 1000 s recovery (b).

with viscoplasticity produced larger maximum displacements.

By examining the maximum (Fig 9.5a) and minimum (Fig 9.5c) principal strain contours, it can be seen that the strain experienced by trabecular bone increases with the number of cycles. It is worthy noting, that in the current study the magnitude of strains in bone during loading phase were generally below 0.5% and 0.7% for tension and compression, respectively, which are the typically reported yielding strains in literature (Bayraktar and Keaveny, 2004; Levrero-Florencio et al., 2016; Morgan and Keaveny, 2001). Another apparent observation is that the trabecular bone experiences higher strain in compression than in tension (Fig. 9.5a , 9.5b). Similar to observation from displacements, strain magnitude increases with decrease in BV/TV of trabecular bone.

9.4.2 Zero loading time points

In the initial cycles, most of the deformation is recovered upon unloading (Fig. 9.3b), however, as the number of cycles increase, deformations accumulate with increasing number of cycles at zero load time points. This indicates development of a gap between the screw and the bone. This is also demonstrated when comparing peak displacements as shown in Fig. 9.4b. As expected,

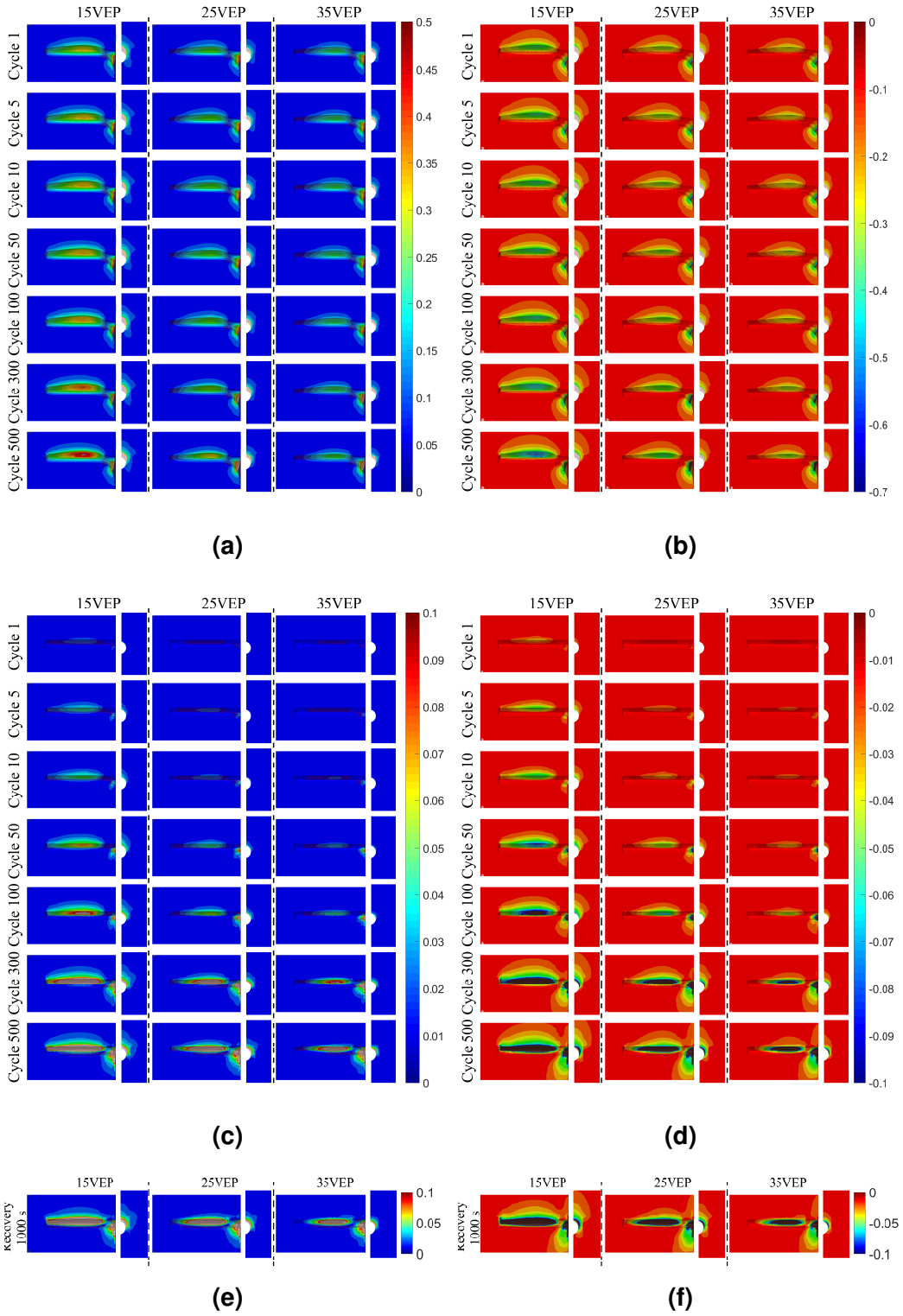

Figure 9.5: Maximum principal strain (a, c, e) and minimum principal strain (b, d, f) contours at symmetry surface and section A-A for 7 representative cycles: at the time points when load at its peak (300N) (a, b); at the time points when load is zero (c, d) and recovery after 1000 s (e, f). strain is expressed as percentage.

the VEP models have much larger peak deformation upon unloading compared to VE models, especially for lower BV/TV samples (Fig. 9.4b). Similar to the loading phase, the displacements of trabecular bone at zero loading time points were related to trabecular bone's BV/TV, the deformations were found to increase with decrease in BV/TV. The largest increase for the lowest BV/TV sample with VEP model (15VEP) was more than 700% from cycle 1 to 500. It is important to note that at zero load time points, there are residual bone displacements not only when using viscoplastic models but also when employing viscoelastic models; displacements cannot be obtained if time-independent elastic material properties are used which require that the deformation to recover instantaneous upon unloading.

Figure 9.5c and 9.5d show the maximum and minimum principal strain upon unloading with increased cycle number for VEP models. The majority of strain is recovered upon unloading (note the difference in scale of the contour plots for peak loading time points and zero loading time points), but residual strains accumulate with cycle numbers and these residual strains are associated with bone's BV/TV. This study also found that the accumulation of principal strains, both maximum and minimum, is more rapid for bone with lower BV/TV.

9.4.3 Recovery

All the six models investigated in this study were allowed to recover for 1000 s under zero force condition after 500 cycles of loading. As expected, the VE models show almost complete recovery of displacement, whereas there is residual displacement with VEP models (Fig. 9.3c). These irrecoverable deformations were found to be related to BV/TV (Fig. 9.3c); irrecoverable deformations increased with decreasing BV/TV. The highest irrecoverable deformation was found for the bone with lower BV/TV and irrecoverable deformation was found to be negligible for bone with the highest BV/TV considered (Fig. 9.4b).

This is also apparent from principal strain contours in Fig 9.5e and 9.5f. Sample with lower BV/TV experiences the relatively higher irrecoverable minimum and maximum principal strain. This observation shows that the viscoplasticity plays an important role.

9.5 Discussion

This study employed nonlinear viscoelastic and nonlinear viscoelastic-viscoplastic models for trabecular bone in a bone-screw system in which cyclic loading was applied to the screw. Three trabecular bone samples with different BV/TV were selected and their time dependent properties based on tests conducted therein were employed. The study finds that, in a bone-screw system subjected to cyclic loading, inclusion of time-dependent properties for trabecular bone causes separation between the screw and the bone which increases with the increase in cycle number. Incorporation of viscoplasticity results in larger deformation, some of which is irrecoverable. Interfacial deformation was found to follow a trend based on BV/TV with porous bone experiencing larger deformations (or separation between the screw and the bone).

9.5.1 Cycle dependent deformation

Numerical simulation of loosening due to mechanical forces in a bone-screw system subjected to cyclic loading has not been possible previously, as time-dependent material constitutive model of bone has not been included before. The MLCUR experiment (Chapter 4) followed by development of time-dependent constitutive models (Chapter 5) for trabecular bone has permitted their use in this clinically relevant study. A number of previous studies, both clinical (Born et al., 2011) and experimental (Basler et al., 2013), have reported that the migration of implant or loosening of screw is a function of time or cycle numbers.

Taylor and Tanner (1997) suggested that the migration of implant is a mechanical phenomenon or at least mechanically triggered, rather than a biological process. As demonstrated by previous in vitro studies simulations undertaken here show that deformation is a function of cycle numbers for both loading and unloading phases. Inclusion of time-dependent properties implies that deformation accumulates with increased cycle numbers, in contrast to conventional time-independent FE analyses, in which the deformation or strain remains unchanged with increasing number of cycles.

Inclusion of time dependent properties implies that upon unloading although significant proportion of deformation is recovered, residual deformations do exit. So while the screw returns to its undeformed and unstrained configuration, the bone's deformation recovery lags behind and this lag increases with each loading cycle. As would be expected, inclusion of viscoplasticity results in the unloaded deformations being larger due to a proportion being irrecoverable. The latter is apparent when deformations following 1000 s of recovery are compared in which the deformations with the nonlinear viscoelastic model recover almost entirely.

During the loading phase the deformations in the bone are forced to follow those of the screw. Consequently, bone deformations only show a small increase with increasing number of cycles as the time lag between the bone response and the instantaneous screw response increases. At the peak loading time point in the first cycle there is no difference between deformations from VE and VEP models (Fig. 9.4), however, with increasing number of cycles the differences start emerging. Thus, the study shows that the inclusion of viscoplasticity not only produces larger deformations in the unloaded phase but also at the peak loading time points.

9.5.2 Bone volume fraction

The strong positive relationship between trabecular bone's BV/TV and its time-independent properties has been previously reported (Levrero-Florencio et al., 2016; Zysset, 2003). In general, bone with higher BV/TV has a larger stiffness and yields at larger loads, though it is recognised that the bone's microstructure also has an important role. In other words, the denser trabecular bone has a better ability to resist the applied forces and undergoes lower deformations. This trend was consistently observed with the three samples considered in this Chapter. The deformations at different stages followed a clear trend based on trabecular bone's BV/TV; porous bone (lower BV/TV) experiences higher deformation in comparison to less porous bone. This is true for loading and unloading time points and even for recovery modelled using viscoplasticity. It has also been reported in a number of studies that the bone with low-density (e.g. due to osteoporosis) is at higher risk of implant instability; these studies include in vitro experiments (Basler et al., 2013; Johnston et al., 2006; Zhu et al., 2000), FE simulations (Donaldson et al., 2011; Wirth et al., 2012) and clinical findings Galbusera et al. (2015). Basler et al. (2013) found that the displacement was strongly correlated to initial BV/TV (r^2= 0.95) which implies that it is also related to implant migration (Basler et al., 2013). Consistent results are observed in the current study; a low BV/TV bone not only experiences higher interfacial deformation (i.e. is at higher risk of screw instability) in comparison to denser bone, but also the deformation increases more rapidly with increasing cycle number.

9.5.3 Displacement magnitude

This Chapter considers primary stability soon after the operation and before any biologically driven bone remodelling has occurred in a manner similar to several previous computational (Bianco et al., 2014; MacLeod et al., 2016)

and in vitro (Basler et al., 2013; Bianco et al., 2016) studies. Primary stability relies on interlocking and frictional bone-screw contact phenomena. The cycle-dependent deformation results in the screw hole becoming enlarged and that will cause the frictional resistance at the bone-screw interface to reduce with increasing loading cycles. Donaldson et al. (2012) reported that in unilateral external fixators there exist push-in and pull-out forces that accompany axial loading. These push-in and pull-out forces in conjunction with increasing screw hole diameter and decreasing frictional resistance can result in increased risk of loosening particularly in low BV/TV bone.

It has been suggested that bone ingrowth/ongrowth occurs if the micromotions are less than 40-50 $\mu\varepsilon$ (Taylor and Prendergast, 2015). If physiological loads give rise to bone-implant relative micro-movements of the order of 100 - 200 $\mu\varepsilon$ then they inhibit bone in-growth, resulting in the formation of a fibrous tissue layer around the prosthesis (Pilliar et al., 1986), and eventual loosening of the implant (Viceconti et al., 2000). Some previous experiments conclude that the threshold value of micromotion for osseointegration is between 30 and 150 $\mu\varepsilon$ (Kadir, 2013). Although this study considers an idealised system, with a screw inserted in a block of bone, it is tempting to examine quantitative values of the interfacial motions; they are smaller than the threshold value of micromotion required in the formation of a fibrous tissue layer. However, it is important to note that in the idealised system used in this study, the offset at which the load is applied is perhaps similar to that in a locking plate; devices with larger offset (e.g. unilateral fixators) will result in much larger forces at the bone-screw interface. Moreover it has been previously shown that deformations increase nonlinearly as the external plate/frame bends (MacLeod et al., 2016), a phenomenon not included in this study. Only 500 cycles were applied (as nonlinear simulation takes considerable computational resources), however the trends show the separation continues to increase. While the maximum and minimum principal strains are generally lower than the typically reported values of yield

they are not too far from yield values after 500 cycles of load application, particularly for the lowest BV/TV sample considered. It is also important to note that while minimum principal strain occurs primarily in the direction radial to the screw that maximum principal strain is in the hoop direction. Steiner et al. (2016) reported that bone damage may occur due to the screw insertion process itself, and the most bone damage occurs within a 300μm radial distance of the screws. In this study, it is assumed that the screw is inserted into bone without any damage. Consequently, this study is valid with respect to trends rather than actual quantitative values.

Current study is more advanced compared to conventional FEA on bone-screw interface mechanics in which only time-independent material properties that are either elastic (Goffin et al., 2013; MacLeod et al., 2012) or inelastic (Donaldson et al., 2012; Pankaj, 2013) are assigned to bone. However, it does not consider a full bone fixator construct or the influence of healing. Importance of time-dependent effects at bone-screw interface was discussed at least a couple of decades ago (Taylor and Tanner, 1997), but these have not been previously included in models due to lack of experimental data and absence of time dependent constitutive models for bone. The developed nonlinear viscoelastic-viscoplastic constitutive models permit simulation of time and cycle dependent response to be included in the analysis of bone screw systems.

9.6 Limitations

This study has a few limitations. A single frequency of 1 Hz was used. It shows that the quantitative results will vary with the choice of frequency from Chapter, however, the trends in the frequency range that are not too dissimilar to the one selected here are likely to be maintained. A clear trend was found with variation in BV/TV, but only three samples were considered. So while it is expected that

the trend to be generally followed we deliberately did not develop a relationship with respect to BV/TV. Previous studies on time-independent mechanical properties of bone have shown that in addition to BV/TV, microstructure plays an important role. Microstructure may have a role in time-dependent properties as well (Steiner et al., 2015; Zysset, 2003). As the focus of this study was to examine the radial separation at the bone-screw interface and not slippage due to pull-out forces, screw threads were not included. Screw threads are likely to reduce loosening due to slippage when pull-out or push-in forces are applied. One the other hand, they generate stress/strain concentrations at the interface which will may also accentuate loosening. Only 500 cycles were applied, larger number of cycles will increase the predicted separation. Lastly, in this study, time-independent elastic material properties were employed for cortical bone and screw; the time-dependent effect on screw is negligible, but cortical bone too will have time-dependent behaviour. Inclusion of time-dependent behaviour for cortical bone is likely to accentuate screw loosening even further.

9.7 Conclusions

- The developed nonlinear viscoelastic-viscoplastic constitutive models (for trabecular bone in this thesis) permit simulation of time and cycle dependent response to be included in the analysis of bone screw systems.
- Bone-screw system interfacial deformation in the bone increases with cycle number.
- The use of nonlinear viscoelastic-viscoplastic model results in larger deformations, some of which are irreversible.
- Interfacial deformations increase with increasing bone porosity indicating that osteoporotic patients are at a greater risk of loosening of implants.

“Isn’t it a pleasure to study and practice what you have learned?”

Confucius

10

Conclusions and recommendation for future work

The primary aims of this study were to evaluate the mechanical properties of trabecular bone and its constituents, in particular their time-dependent behaviour. It considered creep and recovery behaviour of untreated and demineralised bone, cyclic behaviour for both tension and compression for demineralised bone and the monotonic behaviour of deproteinised bone. Later, the developed time-dependent constitutive models for trabecular bone were used to examine the mechanical environments of bone-screw interface when a cyclic loading subjects to idealised bone-screw system.

10.1 Untreated trabecular bone

The deformation of bone when subjected to loads is not instantaneous but varies with time. To investigate this time-dependent behaviour, trabecular bone specimens were subjected to compressive loading, creep, unloading and recovery at multiple load levels corresponding to apparent strains of 2,000-25,000 $\mu\varepsilon$. It is found that: the time-dependent response of trabecular bone comprises of both recoverable and irrecoverable strain; the strain response is nonlinearly related to applied load levels; and the response is linked to bone volume fraction. Although majority of strain is recovered after load-creep-unload-recovery cycle, some residual strain always exists even after loading and unloading at low stress (or corresponding strain) level. The analysis of results indicates that trabecular bone becomes stiffer initially and then experiences stiffness reduction with increasing load levels. Steady state creep rate was found to be dependent on applied stress level and bone volume fraction with a power law relationship.

The first cycle of MLCUR experiment was assumed to be linear viscoelastic, and the corresponding parameters were obtained by fitting the experimental creep strain response to a generalised Kelvin-Voigt rheological model. Its time-dependent response was found to vary nonlinearly with stress and consequently the Schapery's nonlinear viscoelastic constitutive model was employed to describe the nonlinear behaviour of trabecular bone. Viscoplastic models were used to describe the irrecoverable strain. These parameters, including linear viscoelastic, nonlinear viscoelastic and viscoplastic parameters, incorporated in a finite element program by coding a user defined material (UMAT) subroutine. The comprehensive nonlinear viscoelastic-viscoplastic model for the trabecular bone allows more realistic simulation of whole bone finite element models to address clinically relevant problems.

10.2 Demineralised trabecular bone

Trabecular bone is a cellular composite material comprising primarily of mineral and organic phases with their content ratio known to change with age. Therefore, the contribution of the constituents on bones' mechanical behaviour, in tension and compression, at varying load levels and with changing porous structure (which deteriorates with age) is of great interest, but remains unknown.

Firstly, the mechanical response of demineralised bone was investigated by subjecting samples to fully-reversed cyclic tension-compression at varying load levels. It was found that the tension to compression response of the organic phase of trabecular bone is asymmetric; it stiffens in tension and undergoes stiffness degradation in compression. The results indicate that demineralised trabecular bone struts experience inelastic buckling under compression while irreversible strains are less visible in tension. Further, the trend of the asymmetric mechanical response is associated to the original BV/TV. It is anticipated that this study will help in the understanding of non-traumatic fractures in the elderly.

Although it has been reported that its organic phase contributes to time-dependent behaviour of bone, but the insight on time-dependent behaviour of organic phase is limited, especially for trabecular bone. The time-dependent response of demineralised trabecular bone was investigated by subjecting it to tensile MLCUR loading. It is clear that demineralised trabecular bone possesses time-dependent behaviour and it is nonlinearly related to its applied stress levels. It also stiffens with increased stress levels. The results also indicated that its time-dependent behaviour is reasonably associated to its original bone volume fraction (BV/TV); while irrecoverable strain exists even at the low strain levels, but they are not associated with BV/TV. Further, it is also found that the nonlinear viscoelastic model can accurately predict time-dependent

behaviour of bones organic phase, which can be incorporated together with properties of mineral to generate the composite model of bone. It will help and provide the better understanding of this natural composite material.

10.3 Deproteinised trabecular bone

Deproteinised trabecular bone shows a linear elastic behaviour up to its peak stress when it is loaded monotonically, and it shows brittle failure with failure strain less than 1%. The elastic modulus of deproteinised trabecular bone is smaller than untreated trabecular bone and it is reasonably well related to its BV/TV. The toughness is strongly related to its BV/TV and denser bone has better ability to absorb energy.

The compressive mechanical properties of demineralised samples can be modelled using the Gibson's constitutive equations for open-cell cellular solids; both relative elastic modulus and compressive strength increase with relative density.

10.4 Application of the developed models

The developed time-dependent constitutive models were assigned to the trabecular bone in an idealised bone-screw system, which was subjected to triangular cyclic loading at designated loading frequencies.

It is clear that the deformation at the bone-screw interface is a function of loading cycles; the deformation increases with increasing cycle numbers, which might accentuate screw loosening. When the bone-screw system is loaded at the different loading frequencies, the time-dependent effect dominates in the initial cycles with larger displacements at lower loading frequencies. With increasing loading cycles, dynamic effects dominate, higher loading frequencies result in higher displacement at the interface; this is true for both

loading and unloading phases, and the displacement is accumulated with loading cycles.

When the trabecular bone defined as nonlinear viscoelastic-viscoplastic material in a bone-screw system, bone displacement is a function of cycles and interfacial displacement is highly related to bones BV/TV for loading, unloading and recovery phases. Bone accumulates more plastic deformation if it has lower BV/TV, which will cause the screw hole size to increase with increasing loading cycles and the increase in deformation is larger for more porous bone. The results indicated that the patients with porous bone (e.g. due to osteoporosis) are at a higher risk of screw loosening. This finding is likely to apply to a range of orthopaedic implants and is not limited to bone-screw systems.

10.5 Future work

- Further experimental tests on trabecular bone at the higher and lower strain rate are necessary to calibrate the strain development during loading phase in a MLCUR testing protocol. Moreover dynamic tests will help calibrate behaviour at difference.

- The current study considered the relationships between time-dependent properties and BV/TV. Previous studies have shown that time-independent properties, such as elastic modulus, are not only based on BV/TV but other indices of microstructure. So further studies should explore relationships between time-dependent properties and a wider spectrum of microstructural indices. It is very likely that time-dependent response will have elements on anisotropy which this exploration will reveal.

- Tests that explore demineralised and deproteinised bone at their solid phase constituent level will help complement tests conducted in this study and further development of composite models.

- Time-dependent models developed in this study were employed for an idealised screw-bone system. Their application to bone-implant systems, for both fracture-fixation and joint replacement, should be explored. Further, the current models ignore any changes occurring at the interface due to biological processes. Incorporation of biology in the current models will lead to a comprehensive approach that includes mechanics and biology.

References

Abdel-Wahab, A. A., Alam, K., and Silberschmidt, V. V. (2011). Analysis of anisotropic viscoelastoplastic properties of cortical bone tissues. *Journal of the Mechanical Behavior of Biomedical Materials*, 4:807–820.

Alves, J. M., Xu, W., Lin, D., Siffert, R. S., Ryaby, J. T., and Kaufman, J. J. (1996). Ultrasonic assessment of human and bovine trabecular bone: a comparison study. *IEEE Transactions on Biomedical Engineering*, 43:249–258.

Bailey, A. J., Sims, T. J., Ebbesen, E. N., Mansell, J. P., Thomsen, J. S., and Mosekilde, L. (1999). Age-related changes in the biochemical properties of human cancellous bone collagen: Relationship to bone strength. *Calcified Tissue International*, 65:203–210.

Basler, S. E., Traxler, J., Müller, R., and van Lenthe, G. H. (2013). Peri-implant bone microstructure determines dynamic implant cut-out. *Medical Engineering and Physics*, 35:1442–1449.

Bayraktar, H. H. and Keaveny, T. M. (2004). Mechanisms of uniformity of yield strains for trabecular bone. *Journal of Biomechanics*, 37:1671–1678.

Bayraktar, H. H., Morgan, E. F., Niebur, G. L., Morris, G. E., Wong, E. K., and Keaveny, T. M. (2004). Comparison of the elastic and yield properties of human femoral trabecular and cortical bone tissue. *Journal of Biomechanics*, 37:27–35.

Bell, G. H., Dunbar, O., Beck, J. S., and Gibb, A. (1967). Variations in strength of vertebrae with age and their relation to osteoporosis. *Calcified Tissue Research*, 1:75–86.

Berman, J. W., Celik, O. C., and Bruneau, M. (2005). Comparing hysteretic behavior of light-gauge steel plate shear walls and braced frames. *Engineering Structures*, 27:475–485.

Bianco, R.-J., Arnoux, P.-J., Wagnac, E., Mac-Thiong, J.-M., and Aubin, C.-É. (2014). Minimizing pedicle screw pullout risks: A detailed biomechanical analysis of screw design and placement. *Clinical spine surgery*, 30:226–232.

Bianco, R.-J., Aubin, C.-E., Mac-Thiong, J.-M., Wagnac, E., and Arnoux, P.-J. (2016). Pedicle screw fixation under nonaxial loads: A cadaveric study. *Spine*, 41(3):124–130.

Bonar, L. C. and Glimcher, M. J. (1970). Thermal denaturation of mineralized and demineralized bone collagens. *Journal of ultrastructure research*, 32:545–548.

Bonfield, W. and Li, C. H. (1968). The temperature dependence of the deformation of bone. *Journal of biomechanics*, 1:323–329.

Born, C. T., Karich, B., Bauer, C., Von Oldenburg, G., and Augat, P. (2011). Hip screw migration testing: First results for hip screws and helical blades utilizing a new oscillating test method. *Journal of Orthopaedic Research*, 29:760–766.

Bowman, S. M., Gibson, L. J., Hayes, W. C., and McMahon, T. A. (1999). Results from demineralized bone creep tests suggest that collagen is responsible for the creep behavior of bone. *Journal of biomechanical engineering*, 121:253–258.

Bowman, S. M., Guo, X. E., Cheng, D. W., Keaveny, T. M., Gibson, L. J., Hayes, W. C., and McMahon, T. A. (1998). Creep contributes to the fatigue behavior of bovine trabecular bone. *Journal of biomechanical engineering*, 120:647–654.

Bowman, S. M., Keaveny, T. M., Gibson, L. J., Hayes, W. C., and McMahon, T. A. (1994). Compressive creep behavior of bovine trabecular bone. *Journal of Biomechanics*, 27(3):301–310.

Bowman, S. M., Zeind, J., Gibson, L. J., Hayes, W. C., and McMahon, T. A. (1996). The tensile behavior of demineralized bovine cortical bone. *Journal of Biomechanics*, 29(11):1497–1501.

Bredbenner, T. L. and Davy, D. T. (2006). The effect of damage on the viscoelastic behavior of human vertebral trabecular bone. *Journal of biomechanical engineering*, 128(4):473–480.

Burr, D. B., Forwood, M. R., Fyhrie, D. P., Martin, R. B., Schaffler, M. B., and Turner, C. H. (1997). Bone Microdamage and Skeletal Fragility in Osteoporotic and Stress Fractures. *Journal of Bone and Mineral Research*, 12(1):6–15.

Burr, D. B., Milgrom, C., Fyhrie, D., Forwood, M., Nyska, M., Finestone, A., Hoshaw, S., Saiag, E., and Simkin, A. (1996). In vivo measurement of human tibial strains during vigorous activity. *Bone*, 18(5):405–410.

Burstein, A. H., Zika, J. M., Heiple, K. G., and Klein, L. (1975). Contribution of collagen and mineral to the elastic-plastic properties of bone. *The Journal of bone and joint surgery. American volume*, 57:956–961.

Caler, W. E. and Carter, D. R. (1989). Bone creep-fatigue damage accumulation. *Journal of biomechanics*, 22(6/7):625–635.

Castro-Ceseña, A. B., Novitskaya, E. E., Chen, P. Y., Hirata, G. A., and McKittrick, J. (2011). Kinetic studies of bone demineralization at different HCl concentrations and temperatures. *Materials Science and Engineering: C*, 31:523–530.

Castro-Ceseña, A. B., Sánchez-Saavedra, M. P., Novitskaya, E. E., Chen, P.-Y., Hirata, G. A., and McKittrick, J. (2013). Kinetic characterization of the deproteinization of trabecular and cortical bovine femur bones. *Materials Science and Engineering: C*, 33:4958–4964.

Catanese III, J., Iverson, E. P., Ng, R. K., and Keaveny, T. M. (1999). Heterogeneity of the mechanical properties of demineralized bone. *Journal of Biomechanics*, 32:1365–1369.

Charlebois, M. (2008). *Constitutive Law for Trabecular Bone in Large Strain Compression*. PhD thesis, Technische Universitat Wien.

Chen, P. Y. and McKittrick, J. (2011). Compressive mechanical properties of demineralized and deproteinized cancellous bone. *Journal of the Mechanical Behavior of Biomedical Materials*, 4:961–973.

Chen, P. Y., Toroian, D., Price, P. A., and McKittrick, J. (2011). Minerals form a continuum phase in mature cancellous bone. *Calcified Tissue International*, 88:351–361.

Christensen, R. M. (1980). Nonlinear theory of viscoelasticity for application to elastomers. *Journal of Applied Mechanics, Transactions ASME*, 47:762–768.

Ciarelli, M. J., Goldstein, S. A., Kuhn, J. L., Cody, D. D., and Brown, M. B. (1991). Evaluation of orthogonal mechanical properties and density of human trabecular bone from the major metaphyseal regions with materials testing and computed tomography. *Journal of Orthopaedic Research*, 9(5):674–682.

Clifford, R. P., Lyons, T. J., and Webb, J. K. (1987). Complications of external fixation of open fractures of the tibia. *Injury*, 18(3):174–176.

Conlisk, N., Howie, C. R., and Pankaj, P. (2016). An efficient method to capture the impact of total knee replacement on a variety of simulated patient types: A finite element study. *Medical Engineering and Physics*, 38:959–968.

Cotton, J. R., Winwood, K., Zioupos, P., and Taylor, M. (2005). Damage rate is a predictor of fatigue life and creep strain rate in tensile fatigue of human cortical bone samples. *Journal of biomechanical engineering*, 127(2):213–219.

Cowin, S. C. (2001). *Bone mechanics Handbook*. CRC Press, second edition.

Currey, J. D. (1964). Three analogies to explain the mechanical properties of bone. *Biorheology*, 2:1–10.

Currey, J. D. (1988). The effect of porosity and mineral content on the Young's modulus of elasticity of compact bone. *Journal of Biomechanics*, 21(2):131–139.

Currey, J. D., Brear, K., and Zioupos, P. (1996). The effects of ageing and changes in mineral content in degrading the toughness of human femora. *Journal of Biomechanics*, 29(2):257–260.

Deligianni, D. D., Maris, A., and Missirlis, Y. F. (1994). Stress relaxation behavior of trabecular bone specimens. *Journal of Biomechanics*, 27(12):1469–1476.

Dempster, W. T. and Liddicoat, R. T. (1952). Compact bone as a non-isotropic material. *American Journal of Anatomy*, 91(3):331–362.

Dendorfer, S., Maier, H. J., Taylor, D., and Hammer, J. (2008). Anisotropy of the fatigue behaviour of cancellous bone. *Journal of Biomechanics*, 41:636–641.

Donaldson, F. E., Pankaj, P., Cooper, D. M. L., Thomas, C. D. L., Clement, J. G., and Simpson, A. H. R. W. (2011). Relating age and micro-architecture with apparent-level elastic constants: a micro-finite element study of female cortical bone from the anterior femoral midshaft. *Proceedings of the Institution of Mechanical Engineers Part H-Journal of Engineering in Medicine*, 225(H6):585–596.

Donaldson, F. E., Pankaj, P., and Simpson, A. H. R. W. (2012). Bone properties affect loosening of half-pin external fixators at the pin-bone interface. *Injury*, 43(10):1764–1770.

Findley, W. N., Lai, J. S., and Onaran, K. (1976). *Creep and relaxation of nonlinear viscoelastic materials, with an introduction to linear viscoelasticity*. North-Holland series in applied mathematics and mechanics. North-Holland Pub. Co.

Fondrk, M., Bahniuk, E., Davy, D., and Michaels, C. (1988). Some viscoplastic characteristics of bovine and human cortical bone. *Journal of Biomechanics*, 21(8):623–630.

Fratzl, P., Gupta, H. S., Paschalis, E. P., and Roschger, P. (2004). Structure and mechanical quality of the collagen-mineral nano-composite in bone. *Journal of Materials Chemistry*, 14:2115–2123.

Galbusera, F., Volkheimer, D., Reitmaier, S., Berger-Roscher, N., Kienle, A., and Wilke, H.-J. (2015). Pedicle screw loosening: a clinically relevant complication? *European Spine Journal*, 24:1005–1016.

Gibson, L. J. (2003). Cellular Solids. MRS Bulletin.

Gibson, L. J. and Ashby, M. F. (1999). *Cellular solids: structure and properties*. Cambridge university press.

Goffin, J. M., Pankaj, P., and Simpson, A. H. (2013). The importance of lag screw position for the stabilization of trochanteric fractures with a sliding hip screw: A subject-specific finite element study. *Journal of Orthopaedic Research*, 31(4):596–600.

Gorczyca, J. T., McKale, J., Pugh, K., and Pienkowski, D. (2002). Modified tibial nails for treating distal tibia fractures. *Journal of Orthopaedic Trauma*, 16(1):18–22.

Goulet, R. W., Goldstein, S. A., Ciarelli, M. J., Kuhn, J. L., Brown, M. B., and Feldkamp, L. A. (1994). The relationship between the structural and orthogonal compressive properties of trabecular bone. *Journal of biomechanics*, 27(4):375–389.

Guedes, R. M., Simões, J. A., and Morais, J. L. (2006). Viscoelastic behaviour and failure of bovine cancellous bone under constant strain rate. *Journal of Biomechanics*, 39:49–60.

Gupta, H. S., Seto, J., Wagermaier, W., Zaslansky, P., Boesecke, P., and Fratzl, P. (2006). Cooperative deformation of mineral and collagen in bone at the nanoscale. *Proceedings of the National Academy of Sciences*, 103(47):17741–17746.

Gupta, H. S., Wagermaier, W., Zickler, G. A., Raz-Ben Aroush, D., Funari, S. S., Roschger, P., Wagner, H. D., and Fratzl, P. (2005). Nanoscale deformation mechanisms in bone. *Nano Letters*, 5(10):2108–2111.

Haddock, S. M., Yeh, O. C., Mummaneni, P. V., Rosenberg, W. S., and Keaveny, T. M. (2004). Similarity in the fatigue behavior of trabecular bone across site and species. *Journal of Biomechanics*, 37(2):181–187.

Hall, R. H. (1951). Variations with pH of the tensile properties of collagen fibres. *J. Soc. Leather Trades Chem.*, 35:195–210.

Hambli, R. and Barkaoui, A. (2012). Physically based 3D finite element model of a single mineralized collagen microfibril. *Journal of Theoretical Biology*, 301:28–41.

Hamed, E., Jasiuk, I., Yoo, A., Lee, Y., and Liszka, T. (2012a). Multi-scale modelling of elastic moduli of trabecular bone. *Journal of The Royal Society Interface*, 9:1654–1673.

Hamed, E., Novitskaya, E., Li, J., Chen, P.-Y., Jasiuk, I., and McKittrick, J. (2012b). Elastic moduli of untreated, demineralized and deproteinized cortical bone: Validation of a theoretical model of bone as an interpenetrating composite material. *Acta Biomaterialia*, 8:1080–1092.

Hansen, U., Zioupos, P., Simpson, R., Currey, J. D., and Hynd, D. (2008). The effect of strain rate on the mechanical properties of human cortical bone. *Journal of Biomechanical Engineering*, 130:1–8.

Helgason, B., Perilli, E., Schileo, E., Taddei, F., Brynjólfsson, S., and Viceconti, M. (2008). Mathematical relationships between bone density and mechanical properties: A literature review. *Clinical Biomechanics*, 23:135–146.

Hellmich, C., Barthélémy, J.-F., and Dormieux, L. (2004). Mineral-collagen interactions in elasticity of bone ultrastructure - A continuum micromechanics approach. *European Journal of Mechanics, A/Solids*, 23:783–810.

Hibbitt, Karlson, and Sorenson (2012). Abaqus Theory Manual, Abaqus Analysis User's Manual. *ABAQUS Version (6.12-4), ABAQUS Inc.:*.

Hildebrand, T., Laib, A., Müller, R., Dequeker, J., and Rüegsegger, P. (1999). Direct three-dimensional morphometric analysis of human cancellous bone: microstructural data from spine, femur, iliac crest, and calcaneus. *Journal of Bone and Mineral Research*, 14(7):1167–1174.

Hollister, S. J., Fyhrie, D. P., Jepsen, K. J., and Goldstein, S. A. (1991). Application of homogenization theory to the study of trabecular bone mechanics. *Journal of Biomechanics*, 24(9):825–839.

Huang, C.-W., Abu Al-Rub, R. K., Masad, E. A., Little, D. N., and Airey, G. D. (2011). Numerical implementation and validation of a nonlinear viscoelastic and viscoplastic model for asphalt mixes. *International Journal of Pavement Engineering*, 12(4):433–447.

Huiskes, R., Chao, E. Y. S., and Crippen, T. E. (1985). Parametric analyses of pin-bone stresses in external fracture fixation devices. *Journal of Orthopaedic Research*, 3(3):341–349.

Johnston, T. L., Karaikovic, E. E., Lautenschlager, E. P., and Marcu, D. (2006). Cervical pedicle screws vs. lateral mass screws: uniplanar fatigue analysis and residual pullout strengths. *Spine Journal*, 6:667–672.

Kadir, M. R. A. (2013). *Computational biomechanics of the hip joint*. Springer Science & Business Media.

Keaveny, T. M., Guo, X. E., Wachtel, E. F., McMahon, T. A., and Hayes, W. C. (1994a). Trabecular bone exhibits fully linear elastic behavior and yields at low strains. *Journal of Biomechanics*, 27(9):1127–1136.

Keaveny, T. M., Morgan, E. F., Niebur, G. L., and Yeh, O. C. (2001). Biomechanics of trabecular bone. *Annual Review of Biomedical Engineering*, 3:307–333.

Keaveny, T. M., Pinilla, T. P., Crawford, R. P., Kopperdahl, D. L., and Lou, A. (1997). Systematic and random errors in compression testing of trabecular bone. *Journal of Orthopaedic Research*, 15:101–110.

Keaveny, T. M., Wachtel, E. F., Ford, C. M., and Hayes, W. C. (1994b). Differences between the tensile and compressive strength of bovine tibial trabecular bone depend on modulus. *Journal of Biomechanics*, 27(9):1137–1146.

Keaveny, T. M., Wachtel, E. F., and Kopperdahl, D. L. (1999). Mechanical behavior of human trabecular bone after overloading. *Journal of Orthopaedic Research*, 17:346–353.

Kelly, P. (2013). Solid mechanics part I: An introduction to solid mechanics. The University of Auckland lecture notes.

Kim, D. G., Navalgund, A. R., Tee, B. C., Noble, G. J., Hart, R. T., and Lee, H. R. (2012). Increased variability of bone tissue mineral density resulting from estrogen deficiency influences creep behavior in a rat vertebral body. *Bone*, 51:868–875.

Kim, D.-G., Shertok, D., Ching Tee, B., and Yeni, Y. N. (2011). Variability of tissue mineral density can determine physiological creep of human vertebral cancellous bone. *Journal of Biomechanics*, 44:1660–1665.

Knauss, W. G. and Emri, I. J. (1981). Non-linear viscoelasticity based on free volume consideration. *Computers and Structures*, 13:123–128.

Kopperdahl, D. L. and Keaveny, T. M. (1998). Yield strain behavior of trabecular bone. *Journal of Biomechanics*, 31:601–608.

Lafferty, J. and Raju, P. V. V. (1979). The Influence of Stress Frequency on the Fatigue Strength of Cortical Bone. *Journal of Biomechanical Engineering*, 101:112–113.

Lakes, R. (2001). Viscoelastic Properties of Cortical Bone. In *Bone mechanics handbook*. CRC Press, second edition.

Lakes, R. S. (2009). *Viscoelastic materials*. Cambridge University Press.

Levrero-Florencio, F., Margetts, L., Sales, E., Xie, S., Manda, K., and Pankaj, P. (2016). Evaluating the macroscopic yield behaviour of trabecular bone using a nonlinear homogenisation approach. *Journal of the Mechanical Behavior of Biomedical Materials*, 61:384–396.

Li, B. and Aspden, R. M. (1997). Composition and mechanical properties of cancellous bone from the femoral head of patients with osteoporosis or osteoarthritis. *Journal of bone and mineral research*, 12(4):641–651.

Lievers, W. B., Lee, V., Arsenault, S. M., Waldman, S. D., and Pilkey, A. K. (2007). Specimen size effect in the volumetric shrinkage of cancellous bone measured at two levels of dehydration. *Journal of Biomechanics*, 40:1903–1909.

Linde, F. and Hvid, I. (1989). The effect of constraint on the mechanical behaviour of trabecular bone specimens. *Journal of biomechanics*, 22(5):485–490.

Linde, F., Norgaard, P., Hvid, I., Odgaard, A., and Soballe, K. (1991). Mechanical properties of trabecular bone. Dependency on strain rate. *Journal of Biomechanics*, 24(9):803–809.

Linde, F. and Sørensen, H. C. F. (1993). The effect of different storage methods on the mechanical properties of trabecular bone. *Journal of Biomechanics*, 26(10):1249–1252.

Liu, S., Qi, W., Zhang, Y., Wu, Z.-X., Yan, Y.-B., and Lei, W. (2014). Effect of bone material properties on effective region in screw-bone model: an experimental and finite element study. *Biomedical engineering online*, 13:1–13.

Lou, Y. C. and Schapery, R. A. (1971). Viscoelastic characterization of a nonlinear fiber- reinforced plastic. *Journal of Composite Materials*, 5:208–234.

Lubarda, V. A., Novitskaya, E. E., McKittrick, J., Bodde, S. G., and Chen, P. Y. (2012). Elastic properties of cancellous bone in terms of elastic properties of its mineral and protein phases with application to their osteoporotic degradation. *Mechanics of Materials*, 44:139–150.

MacLeod, A. and Pankaj, P. (2014). Computer Simulation of Fracture Fixation Using Extramedullary Devices: An Appraisal. In Doyle, B., Miller, K., Wittek, A., and Nielsen, P. M. F., editors, *Computational Biomechanics for Medicine: Fundamental Science and Patient-specific Applications*, pages 87–99. Springer, New York, NY.

MacLeod, A. R., Pankaj, P., and Simpson, A. H. R. W. (2012). Does screw-bone interface modelling matter in finite element analyses? *Journal of biomechanics*, 45:1712–1716.

MacLeod, A. R., Simpson, A. H. R., and Pankaj, P. (2016). Age-related optimization of screw placement for reduced loosening risk in locked plating. *Journal of Orthopaedic Research*, 34:1856–1864.

MacLeod, A. R., Simpson, A. H. R. W., and Pankaj, P. (2015). Reasons why dynamic compression plates are inferior to locking plates in osteoporotic bone: a finite element explanation. *Computer Methods in Biomechanics and Biomedical Engineering*, 18(16):1818–1825.

Manda, K., Wallace, R. J., Xie, S., Levrero-Florencio, F., and Pankaj, P. (2016a). Nonlinear viscoelastic characterization of bovine trabecular bone. *Biomechanics and Modeling in Mechanobiology*, 16:173–189.

Manda, K., Xie, S., Wallace, R. J., Levrero-Florencio, F., and Pankaj, P. (2016b). Linear viscoelasticity - bone volume fraction relationships of bovine trabecular bone. *Biomechanics and Modeling in Mechanobiology*, 15(6):1631–1640.

Manilay, Z., Novitskaya, E., Sadovnikov, E., and McKittrick, J. (2013). A comparative study of young and mature bovine cortical bone. *Acta Biomaterialia*, 9:5280–5288.

Maquer, G., Musy, S. N., Wandel, J., Gross, T., and Zysset, P. K. (2015). Bone volume fraction and fabric anisotropy are better determinants of trabecular bone stiffness than other morphological variables. *Journal of Bone and Mineral Research*, 30(6):1000–1008.

Marques, S. P. and Creus, G. J. (2012). *Computational viscoelasticity*. Springer Science & Business Media.

Matsuura, M., Eckstein, F., Lochmüller, E. M., and Zysset, P. K. (2008). The role of fabric in the quasi-static compressive mechanical properties of human trabecular bone from various anatomical locations. *Biomechanics and Modeling in Mechanobiology*, 7:27–42.

Mauch, M., Currey, J. D., and Sedman, A. J. (1992). Creep fracture in bones with different stiffnesses. *Journal of Biomechanics*, 25(1):11–16.

Mercer, C., He, M. Y., Wang, R., and Evans, A. G. (2006). Mechanisms governing the inelastic deformation of cortical bone and application to trabecular bone. *Acta Biomaterialia*, 2:59–68.

Michel, M. C., Guo, X.-D. E., Gibson, L. J., McMahon, T. A., and Hayes, W. C. (1993). Compressive fatigue behavior of bovine trabecular bone. *Journal of biomechanics*, 26(4/5):453–463.

Moore, T. L. A. and Gibson, L. J. (2002). Microdamage accumulation in bovine trabecular bone in uniaxial compression. *Journal of biomechanical engineering*, 124:63–71.

Moore, T. L. A., O'Brien, F. J., and Gibson, L. J. (2004). Creep does not contribute to fatigue in bovine trabecular bone. *Journal of biomechanical engineering*, 126:321–329.

Morgan, E. F., Bayraktar, H. H., and Keaveny, T. M. (2003). Trabecular bone modulus-density relationships depend on anatomic site. *Journal of Biomechanics*, 36:897–904.

Morgan, E. F. and Keaveny, T. M. (2001). Dependence of yield strain of human trabecular bone on anatomic site. *Journal of Biomechanics*, 34:569–577.

Morgan, E. F., Yeh, O. C., Chang, W. C., and Keaveny, T. M. (2001). Nonlinear behavior of trabecular bone at small strains. *Journal of biomechanical engineering*, 123:1–9.

Mullins, L. P., Bruzzi, M. S., and McHugh, P. E. (2009). Calibration of a constitutive model for the post-yield behaviour of cortical bone. *Journal of the Mechanical Behavior of Biomedical Materials*, 2(5):460–470.

Münster, S., Jawerth, L. M., Leslie, B. a., Weitz, J. I., Fabry, B., and Weitz, D. a. (2013). Strain history dependence of the nonlinear stress response of fibrin and collagen networks. *Proceedings of the National Academy of Sciences*, 110(30):12197–202.

Nicholson, P. H. F., Haddaway, M. J., Davie, M. W. J., and Evans, S. F. (1993). Vertebral deformity, bone mineral density, back pain and height loss in unscreened women over 50 years. *Osteoporosis International*, 3:300–307.

Novitskaya, E., Chen, P. Y., Lee, S., Castro-Ceseña, A., Hirata, G., Lubarda, V. A., and McKittrick, J. (2011). Anisotropy in the compressive mechanical properties of bovine cortical bone and the mineral and protein constituents. *Acta Biomaterialia*, 7:3170–3177.

Novitskaya, E., Lee, S., Lubarda, V. A., and McKittrick, J. (2013). Initial anisotropy in demineralized bovine cortical bone in compressive cyclic loading-unloading. *Materials Science and Engineering: C*, 33:817–823.

Novitskaya, E., Zin, C., Chang, N., Cory, E., Chen, P., D'Lima, D., Sah, R. L., and McKittrick, J. (2014). Creep of trabecular bone from the human proximal tibia. *Materials Science and Engineering: C*, 40:219–227.

Nyman, J. S., Roy, A., Shen, X., Acuna, R. L., Tyler, J. H., and Wang, X. (2006). The influence of water removal on the strength and toughness of cortical bone. *Journal of Biomechanics*, 39:931–938.

Odgaard, A., Kabel, J., Van Rietbergen, B., Dalstra, M., and Huiskes, R. (1997). Fabric and elastic principal directions of cancellous bone are closely related. *Journal of Biomechanics*, 30(5):487–495.

Olszta, M. J., Cheng, X., Jee, S. S., Kumar, R., Kim, Y.-Y., Kaufman, M. J., Douglas, E. P., and Gower, L. B. (2007). Bone structure and formation: A new perspective. *Materials Science and Engineering: R: Reports*, 58:77–116.

Pankaj, P. (2013). Patient-specific modelling of bone and bone-implant systems: the challenges. *International Journal for Numerical Methods in Biomedical Engineering*, 29:233–249.

Park, S. and Schapery, R. (1999). Methods of interconversion between linear viscoelastic material functions. Part I - a numerical method based on Prony series. *International Journal of Solids and Structures*, 36:1653–1675.

Perzyna, P. (1971). Thermodynamic Theory of Viscoplasticity. *Advances in Applied Mechanics*, 11(C):313–354.

Pilliar, R. M., Lee, J. M., and Maniatopoulos, C. (1986). Observations on the Effect of Movement on Bone Ingrowth into Porous-Surfaced Implants. *Clinical Orthopaedics and Related Research*, 208:108–113.

Pollintine, P., Luo, J., Offa-Jones, B., Dolan, P., and Adams, M. A. (2009). Bone creep can cause progressive vertebral deformity. *Bone*, 45:466–472.

Quaglini, V., Russa, V. L., and Corneo, S. (2009). Nonlinear stress relaxation of trabecular bone. *Mechanics Research Communications*, 36:275–283.

Rapillard, L., Charlebois, M., and Zysset, P. K. (2006). Compressive fatigue behavior of human vertebral trabecular bone. *Journal of Biomechanics*, 39:2133–2139.

Rimnac, C. M., Petko, A. A., Santner, T. J., and Wright, T. M. (1993). The effect of temperature, stress and on the creep of compact bovine bone. *Journal of Biomechanics*, 26(3):219–228.

Roylance, D. (2001). Engineering Viscoelasticity. MIT lecture notes.

Ruffoni, D. and van Lenthe, G. (2017). 3.10 Finite Element Analysis in Bone Research: A Computational Method Relating Structure to Mechanical Function. In *Comprehensive Biomaterials II*, pages 169–196.

Sadeghi, H., Espino, D. M., and Shepherd, D. E. (2017). Fatigue strength of bovine articular cartilage-on-bone under three-point bending: the effect of loading frequency. *BMC Musculoskeletal Disorders*, 18:142:1–8.

Sakaguchi, R. L. and Borgersen, S. E. (1993). Nonlinear finite element contact analysis of dental implant components. *The International Journal of Oral & Maxillofacial Implants*, 8(6):655–661.

Sasaki, N., Nakayama, Y., Yoshikawa, M., and Enyo, A. (1993). Stress relaxation function of bone and bone collagen. *Journal of Biomechanics*, 26(12):1369–1376.

Sasaki, N. and Odajima, S. (1996). Elongation mechanism of collagen fibrils and force-strain relations of tendon at each level of structural hierarchy. *Journal of Biomechanics*, 29(9):1131–1136.

Schaffler, M. B., Choi, K., and Milgrom, C. (1995). Aging and matrix microdamage accumulation in human compact bone. *Bone*, 17(6):521–525.

Schaffler, M. B., Radin, E. L., and Burr, D. B. (1989). Mechanical and morphological effects of strain rate on fatigue of compact bone. *Bone*, 10(3):207–214.

Schapery, R. A. (1969). On the characterization of nonlinear viscoelastic materials. *Polymer Engineering & Science*, 9(4):295–310.

Schmoller, K. M., Fernández, P., Arevalo, R. C., Blair, D. L., and Bausch, A. R. (2010). Cyclic hardening in bundled actin networks. *Nature communications*, 1:134.

Schoenfeld, C. M., Lautenschlager, E. P., and Meyer, P. R. (1974). Mechanical properties of human cancellous bone in the femoral head. *Medical & biological engineering*, 12(3):313–317.

Schüller, M., Drobetz, H., Redl, H., and Tschegg, E. K. (2009). Analysis of the fatigue behaviour characterized by stiffness and permanent deformation for different distal volar radius compression plates. *Materials Science and Engineering: C*, 29:2471–2477.

Schüller, M., Herndler, S., Weninger, P., Jamek, M., Redl, H., and Tschegg, E. K. (2008). Stiffness and permanent deformation of extra-articular distal tibia fractures treated with unreamed small diameter intramedullary nailing. *Materials Science and Engineering: C*, 28:1209–1216.

Seeman, E. and Delmas, P. D. (2006). Bone quality - the material and structural basis of bone strength and fragility. *The New England journal of medicine*, 354(21):2250–2261.

Shariati, M., Hatami, H., Yarahmadi, H., and Eipakchi, H. R. (2012). An experimental study on the ratcheting and fatigue behavior of polyacetal under uniaxial cyclic loading. *Materials and Design*, 34:302–312.

Sharp, D. J., Tanner, K. E., and Bonfield, W. (1990). Measurement of the density of trabecular bone. *Journal of Biomechanics*, 23(8):853–857.

Shultz, T. R., Blaha, J. D., Gruen, T. A., and Norman, T. L. (2006). Cortical bone viscoelasticity and fixation strength of press-fit femoral stems: a finite element model. *Journal of biomechanical engineering*, 128:7–12.

Snyder, B. D., Piazza, S., Edwards, W. T., and Hayes, W. C. (1993). Role of trabecular morphology in the etiology of age-related vertebral fractures. *Calcified Tissue International*, 53(Supplement 1):14–22.

Steiner, J. A., Christen, P., Affentranger, R., Ferguson, S. J., and van Lenthe, G. H. (2017). A novel in silico method to quantify primary stability of screws in trabecular bone. *Journal of Orthopaedic Research*, 35(11):2415–2424.

Steiner, J. A., Ferguson, S. J., and van Lenthe, G. H. (2015). Computational analysis of primary implant stability in trabecular bone. *Journal of Biomechanics*, 48:807–815.

Steiner, J. A., Ferguson, S. J., and van Lenthe, G. H. (2016). Screw insertion in trabecular bone causes peri-implant bone damage. *Medical Engineering and Physics*, 38(4):417–422.

Taylor, M., Cotton, J., and Zioupos, P. (2002). Finite Element Simulation of the Fatigue Behaviour of Cancellous Bone. *Meccanica*, 37:419–429.

Taylor, M. and Prendergast, P. J. (2015). Four decades of finite element analysis of orthopaedic devices: Where are we now and what are the opportunities? *Journal of Biomechanics*, 48:767–778.

Taylor, M. and Tanner, K. E. (1997). Fatigue failure of cancellous bone: a possible cause of implant migration and loosening. *The Journal of Bone and Joint Surgery. British volume*, 79-B(2):181–182.

Tertuliano, O. A. and Greer, J. R. (2016). The nanocomposite nature of bone drives its strength and damage resistance. *Nature Materials*, 15:1195–1202.

Topoliński, T., Cichański, A., Mazurkiewicz, A., and Nowicki, K. (2011). Study of the behavior of the trabecular bone under cyclic compression with stepwise increasing amplitude. *Journal of the Mechanical Behavior of Biomedical Materials*, 4:1755–1763.

Tschegg, E. K., Herndler, S., Weninger, P., Jamek, M., Stanzl-Tschegg, S., and Redl, H. (2008). Stiffness analysis of tibia-implant system under cyclic loading. *Materials Science and Engineering: C*, 28:1203–1208.

Turner, C. H. and Burr, D. B. (1993). Basic biomechanical measurements of bone: a tutorial. *Bone*, 14:595–608.

Turner, C. H., Chandran, A., and Pidaparti, R. M. V. (1995). The anisotropy of osteonal bone and its ultrastruetural implications. *Bone*, 17(1):85–89.

van Oosten, A. S. G., Vahabi, M., Licup, A. J., Sharma, A., Galie, P. A., MacKintosh, F. C., and Janmey, P. A. (2016). Uncoupling shear and uniaxial elastic moduli of semiflexible biopolymer networks: compression-softening and stretch-stiffening. *Scientific reports*, 6:1–9.

Vashishth, D. (2007). The role of the collagen matrix in skeletal fragility. *Current Osteoporosis Reports*, 5(2):62–66.

Viceconti, M., Muccini, R., Bernakiewicz, M., Baleani, M., and Cristofolini, L. (2000). Large-sliding contact elements accurately predict levels of bone-implant micromotion relevant to osseointegration. *Journal of Biomechanics*, 33:1611–1618.

Viceconti, M., Taddei, F., Cristofolini, L., Martelli, S., Falcinelli, C., and Schileo, E. (2012). Are spontaneous fractures possible? An example of clinical application for personalised, multiscale neuro-musculo-skeletal modelling. *Journal of Biomechanics*, 45:421–426.

Wähnert, D., Hoffmeier, K. L., von Oldenburg, G., Fröber, R., Hofmann, G. O., and Mückley, T. (2010). Internal fixation of type-C distal femoral fractures in osteoporotic bone. *The Journal of Bone & Joint Surgery*, 92:1442–1452.

Wallace, R. J., Pankaj, P., and Simpson, A. H. R. W. (2013). The effect of strain rate on the failure stress and toughness of bone of different mineral densities. *Journal of Biomechanics*, 46(13):2283–2287.

Wang, X. and Nyman, J. S. (2007). A novel approach to assess post-yield energy dissipation of bone in tension. *Journal of Biomechanics*, 40:674–677.

Wang, X., Shen, X., Li, X., and Mauli Agrawal, C. (2002). Age-related changes in the collagen network and toughness of bone. *Bone*, 31(1):1–7.

Wang, X. D., Masilamani, N. S., Mabrey, J. D., Alder, M. E., and Agrawal, C. M. (1998). Changes in the fracture toughness of bone may not be reflected in its mineral density, porosity, and tensile properties. *Bone*, 23(1):67–72.

Weiner, S. and Wagner, H. D. (1998). The material bone: structure-mechanical function relations. *Annual Review of Materials Science*, 28:271–298.

Wirth, A. J., Müller, R., and Harry van Lenthe, G. (2012). The discrete nature of trabecular bone microarchitecture affects implant stability. *Journal of Biomechanics*, 45:1060–1067.

Wirth, A. J., Müller, R., and van Lenthe, G. H. (2010). Computational analyses of small endosseous implants in osteoporotic bone. *European Cells and Materials*, 20:58–71.

Wright, T. M., Vosburgh, F., and Burstein, A. H. (1981). Permanent deformation of compact bone monitored by acoustic emission. *Journal of Biomechanics*, 14(6):405–409.

Yamamoto, E., Crawford, R. P., Chan, D. D., and Keaveny, T. M. (2006). Development of residual strains in human vertebral trabecular bone after prolonged static and cyclic loading at low load levels. *Journal of Biomechanics*, 39:1812–1818.

Yamashita, J., Furman, B. R., Rawls, H. R., Wang, X., and Agrawal, C. M. (2001). The use of dynamic mechanical analysis to assess the viscoelastic properties of human cortical bone. *Journal of Biomedical Materials Research Part A*, 58(1):47–53.

Zhu, Q., Lu, W. W., Holmes, A. D., Zheng, Y., Zhong, S., and Leong, J. C. Y. (2000). The effects of cyclic loading on pull-out strength of sacral screw fixation. *Spine*, 25(9):1065–1069.

Zilch, H., Rohlmann, A., Bergmann, G., and Kölbel, R. (1980). Material properties of femoral cancellous bone in axial loading. Part II: Time dependent properties. *Archives of orthopaedic and trauma surgery*, 97:257–262.

Zysset, P. K. (2003). A review of morphology-elasticity relationships in human trabecular bone: Theories and experiments. *Journal of Biomechanics*, 36:1469–1485.

A

Linear viscoelastic analysis of bone-screw system

The displacement contour plots for BV/TV = 25% & 35 % are shown in Fig. A.1 and A.2. Those displacement contour plots were superimposed with undeformed geometry and exaggerated by 50 times for better visualisation.

It is clear that the observations from BV/TV = 15 % were true for other two BV/TV investigated, including 25 % and 35 %. Additionally, if the bone-screw system to be loaded at the same frequencies for same cycles, obviously, the lower peak displacement was observed in the model with higher BV/TV for both loading and unloading phases.

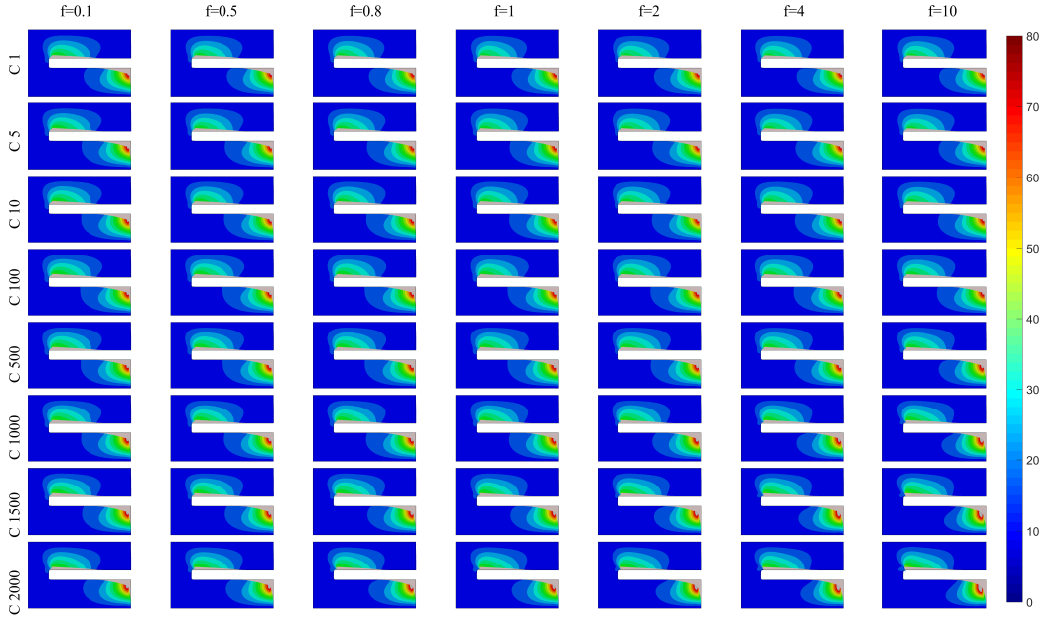

(a)

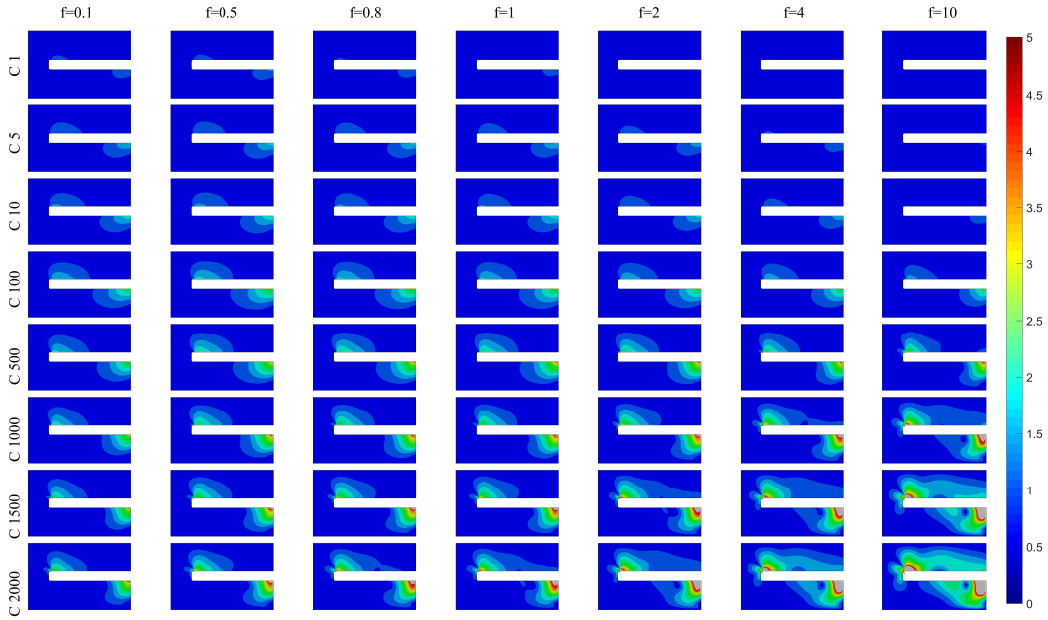

(b)

Figure A.1: Displacement contours (μm) against loading frequencies at the loaded (a) and unloaded (b) phase for BV/TV = 25%.

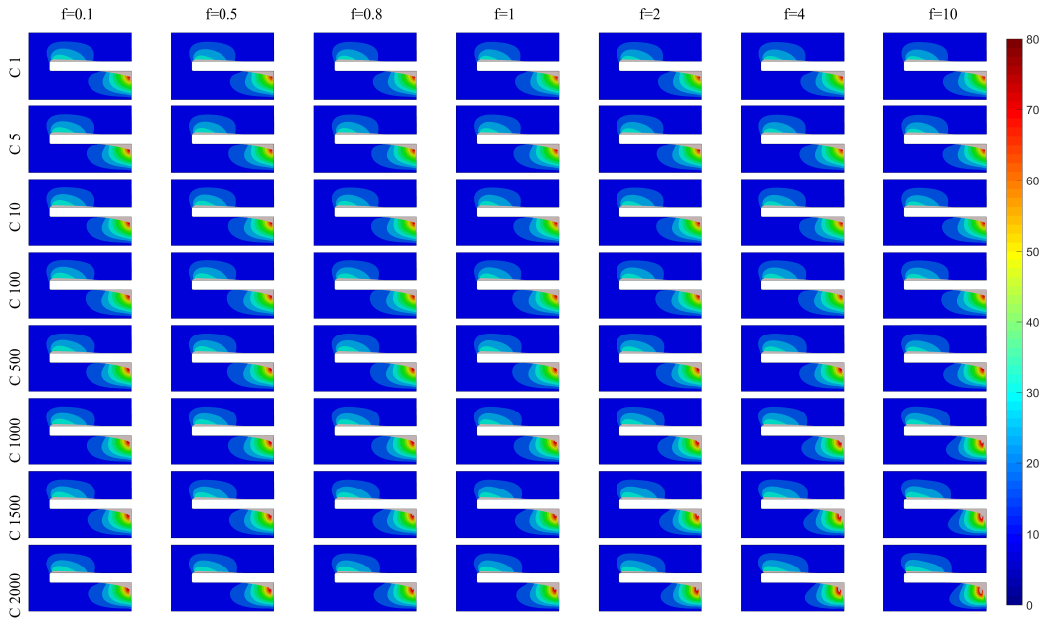

(a)

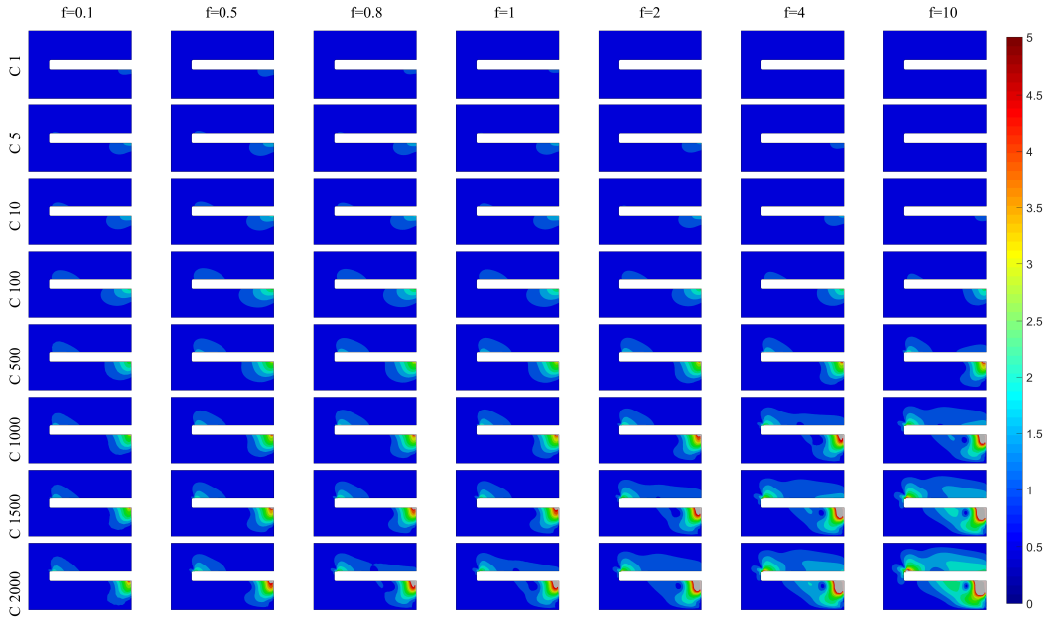

(b)

Figure A.2: Displacement contours (μm) against loading frequencies at at the loaded (a) and unloaded (b) phase for BV/TV = 35%.

B

Nonlinear time-dependent analysis of bone-screw system

Contact opening contours for all 6 models at peak loading time point (Cycle 500), zero loading time point (Cycle 500) and recovery after 1000 s are shown in Fig. B.1, which can help understand the separation events at the bone-screw interface after the system is subjected to cyclic loading.

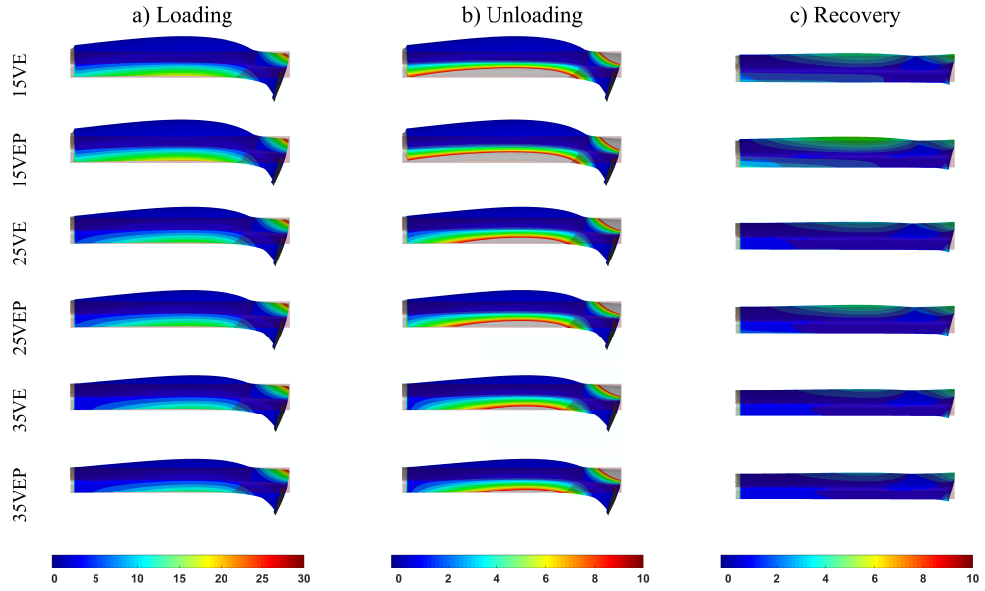

Figure B.1: Comparison of contact opening contours (μm) for all 6 models at peak loading time point (Cycle 500) (a), zero loading time point (Cycle 500) (b) and recovery after 1000 s (c).

C

Scientific production

C.1 Conference podium presentations and poster

1. Manda, K., **Xie, S.**, Wallace, R., Sales, E., Levrero-Florencio, F., & Pankaj, P. (2015). Identification of nonlinear viscoelastic parameters for bovine trabecular bone from creep-recovery experiments. 6^{th} *International Conference on Computational Bioengineering*, Barcelona, Spain. Podium presentation.

2. Manda, K., Wallace, R., **Xie, S.**, Sales, E., Levrero-Florencio, F., & Pankaj, P. (2015). A combined nonlinear viscoelastic-viscoplastic model for trabecular bone. 21^{st} *Congress of the European Society of Biomechanics*, Prague, Czech Republic. Podium presentation.

3. **Xie, S.**, Manda, K., Wallace, R., Sales, E., Levrero-Florencio, F., Simp-

son, H., & Pankaj, P. (2015). Experimental Investigation of Creep-Recovery Behaviour of Trabecular Bone. *British Orthopaedic Research Society 2015 Annual Meeting*, Liverpool, United Kingdom. Podium presentation.

4. **Xie, S.**, Manda, K., Wallace, R., Levrero-Florencio, F., Simpson, H., & Pankaj, P. (2016). Creep-recovery behaviour investigation on trabecular bone at varying stress levels. 22^{nd} *Congress of the European Society of Biomechanics*, Lyon, France. Podium presentation.

5. **Xie, S.**, Wallace, R., Manda, K., & Pankaj, P. (2017). Demineralised trabecular bone stiffens with increasing load levels. 23^{th} *Congress of the European Society of Biomechanics*, Seville, Spain. Podium presentation.

6. **Xie, S.**, Manda, K., & Pankaj, P. (2018). Bone's time-dependent behaviour accentuates loosening in fracture fixation using bone-screw systems. 8^{th} *World Congress of Biomechanics*, Dublin, Ireland.

C.2 Peer-reviewed journal papers

1. Manda, K., **Xie, S.**, Wallace, R. J., Levrero-Florencio, F., & Pankaj, P. (2016). Linear viscoelasticity - bone volume fraction relationships of bovine trabecular bone. *Biomechanics and Modeling in Mechanobiology*, 15(6): 1631-1640. https://doi.org/10.1007/s10237-016-0787-0

2. Levrero-Florencio, F., Margetts, L., Sales, E., **Xie, S.**, Manda, K., & Pankaj, P. (2016). Evaluating the macroscopic yield behaviour of trabecular bone using a nonlinear homogenisation approach. *Journal of the Mechanical Behavior of Biomedical Materials*, 61: 384-396. https://doi.org/10.1016/j.jmbbm.2016.04.008

3. Manda, K., Wallace, R. J., **Xie, S.**, Levrero-Florencio, F., & Pankaj, P. (2016). Nonlinear viscoelastic characterization of bovine trabecular bone.

Biomechanics and Modeling in Mechanobiology, 16(1): 173-189. https://doi.org/10.1007/s10237-016-0809-y

4. **Xie, S.**, Manda, K., Wallace, R. J., Levrero-Florencio, F., Simpson, A. H. R. W., & Pankaj, P. (2017). Time dependent behaviour of trabecular bone at multiple load levels. *Annals of Biomedical Engineering*, 45(5): 1219-1226. https://doi.org/10.1007/s10439-017-1800-1

5. **Xie, S.**, Wallace, R. J., Callanan, A., & Pankaj, P. (2018). From tension to compression: Asymmetric mechanical behaviour of trabecular bone's organic phase. *Annals of Biomedical Engineering*, 46: 801. https://doi.org/10.1007/s10439-018-2009-7

6. **Xie, S.**, Manda, K., & Pankaj, P. (2018). Bone's time-dependent behaviour accentuates loosening in fracture fixation using bone-screw systems. *Bone & Joint Research* (Accepted)

7. **Xie, S.**, Manda, K., & Pankaj, P. (2018). Effect of loading frequency on deformations at bone-implant interface. *Medical Engineering & Physics* (Accepted)

8. **Xie, S.**, Wallace, R. J., Manda, K., & Pankaj, P. Demineralised trabecular bone stiffens with increasing load levels. (In preparation)

9. Manda, K., Levrero-Florencio, F., **Xie, S.**, Wallace, R. J., & Pankaj, P. A nonlinear viscoelastic-viscoplastic constitutive model of trabecular bone. (In preparation)